Title of thesis

Synthesis and Pulsed Laser Deposition of Lead-based cuprate Superconducting Materials.

Syed Haider Hussain Naqvi

A thesis submitted to the University of London in fulfilment for the degree of Doctor of Philosophy.

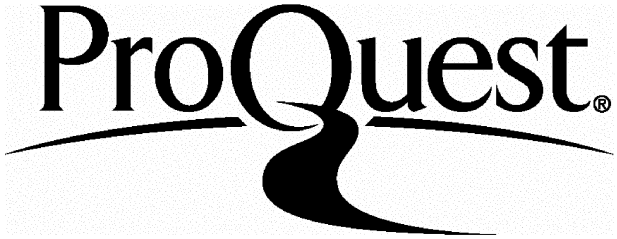

Dedicated to my mother

Abstract

The search for the synthesis, and the characterisation of new superconducting materials such as the Y-Ba-Cu-O, Tl-Ba-Ca-Cu-O, Bi-Sr-Ca-Cu-O, Pb-Sr-Y-Ca-Cu-O systems have initiated an almost unparalleled degree of activity during the past several years because of their various possible technological applications. Different existing techniques of synthesis have been applied or modified for the fabrication of these superconducting copper oxide materials (cuprate), with the motive of obtaining single phase and better superconducting properties.

The bulk synthesis and reproducibility of lead-cuprates are not straightforward because of the formation of complex co-existing phases, the volatile nature of lead and the required oxygen adjustment in the structure to obtain good superconducting properties. Usually, different superconducting phases give rise to different superconducting transition temperatures which are also modified by the cationic ratios (Pb:Sr:(Y,Ca):Cu) of the constituent elements of lead-cuprates. The synthesis of various cationic ratios of lead-based materials have been performed through a two-step ceramic technique or in a single-step with some modifications in synthesis procedure and optimisation, and characterised using EDX, XRD, resistive and diamagnetic transition temperature measurement. The different cationic ratios of Pb:Sr:(Y,Ca):Cu such as Pb-2213, (Pb,Cu)-1212, Pb-1213, Pb-1313, and Pb-3324 have been proposed, and those are shown to exhibit superconducting properties at various temperatures up to 83K.

The pulsed laser deposition technique (PLD) has been used for the synthesis and fabrication of cuprate superconducting thin layers since the discovery of the Y-Ba-Cu-O system. This technique enables very precise and stoichiometric evaporation from an irradiated target due to its pulsed nature. It also allows thin layers of complex materials to be produced. This thesis also reports on the growth and synthesis of single phase $Pb_2Sr_2(Y_{0.5}Ca_{0.5})Cu_3O_8$ layers using PLD and the highest transition temperature achieved so far in this material by any technique. The synthesis of (Pb,Cu)-1212 phase layers on MgO substrates has also been demonstrated using PLD multi-layering of nonsuperconducting $Sr_2(Y_{0.5}Ca_{0.5})Cu_3O_8$, and PbO targets. Ex-situ annealing of these structures in air provided superconducting (Pb,Cu)-1212

phase layers. Ex-situ and in-situ thin film growth of the Pb-2213 phase on MgO substrate by PLD are also reported, whereby the growth parameters such as annealing temperature and duration are optimised. The superconducting properties of the thin films are found to be sensitive to the annealing period at certain temperatures in a nitrogen ambient. In-situ oxygen-adjustment and minimisation of lead loss with high substrate temperature are shown to be excessively difficult task. In-situ adjustment of the oxygen in nitrogen ambient after deposition has been demonstrated with maximum onset transition temperature of 79K and zero resistance at 63K. Layers prepared by both annealing routes are found to be highly c-axis oriented.

Uniformity and large area deposition are inherently serious problems with PLD. A simple approach to understanding and alleviating these difficulties using a four sided substrate holding geometry is presented. A substrate holder placed inside, mid way, and along the forward motion of plume at certain inclinations enable the main problem of droplets, non-uniformity and large-area deposition without any scanning of laser beam, target or substrate rotation to be minimised. A slight variation in superconducting transition temperature in 7X7mm samples deposited at distances from 3 to 12 cm from the target is demonstrated after ex-situ annealing.

The critical current density is an important parameter for the potential use of any superconducting material. This was found to vary with oxygen content in the thin $Pb_2Sr_2(Y_{0.5}Ca_{0.5})Cu_3O_8$ layers. Different reduction periods provided variations in the critical currents. The critical current density in $Pb_2Sr_2(Y_{0.5}Ca_{0.5})Cu_3O_8$ was found to be as high as $0.32x10^6 A/cm^2$ in zero field and $0.5x\ 10^4 A/cm^2$ in 1Tesla applied field at 55K. These values are much higher than for the bulk where a critical current density value of typically $5.5A/cm^2$ in zero field and $0.6A/cm^2$ in 2 Tesla field at 65K was found. The bulk (Pb, Cu)-1212 compositions with some impurity phases showed its highest onset transition temperature of 82K and $T_{c,\ zero}$ of 76K without the requirement of high pressure oxygen anneal. The critical current density was found to be as high as $130A/cm^2$ at 50K in zero field. The bulk composition $Pb_3Sr_3(Y_{0.5}Ca_{0.5})_2Cu_4O_z$ has shown maximum $T_{c,onset}$ of 81.5K, $T_{c,\ zero}$ of 74K and a critical current density as high as $75A/cm^2$ in zero field and $1.2A/cm^2$ in 1 Tesla at 60K.

Acknowledgements

First of all I would like to thank The Ministry of Education, Government of Pakistan, Islamabad, whose award and support made the work of this thesis possible.

I would like to convey my sincere gratefulness to my supervisor, Prof. I. W. Boyd for his advises and supports towards the completion of the project.

Through out the course of this work, a number of people have been helpful and provided their possible support. They deserve many thanks for it.

Most of the x-ray diffraction measurements were performed at the Department of Crystallography, Birkbeck College, London. I would like to thank Dr.P.Barnes for allowing the use of equipment and specially, Mr.Martin Vickers for his encouragement and help.

I am also thankful to Dr. David Caplin for allowing me to access his cryogenic equipments and arrangement of training at Imperial College, London. I am also obliged to Dr. Leslie Cohen and Mr.Gary Perkins for the critical current measurements and their help.

Many thanks to Dr.F.Saba, Department of Material Science, Imperial College, for the Energy Dispersive X-ray analysis, and Mr.K.Reeves and Dr.Dafydd Griffiths, Institute of Archeology, UCL, for EDX, Electron-probe micro-analysis and reading some part of my thesis.

I am also thankful to the member of workshop team, at the department, Mr. M.Gillet, A.Gorrod, T.Hamer and A.Dury for the job done for laser ablation equipment.

Many thanks for Mrs.Mavis Small, Mrs. Maureen Goldstein, Mrs. Manju Karia as a supporting secretarial team at the department for their kindness and help.

I am also grateful to my colleagues and friends for their support, guidance and encouragements. Many thanks to Dr.G.C.Tyrell, for the help in mass spectroscopic measurements. I am also thankful to Dr. Frank Beech, Dr.Valentin Craciun and Dr. Simon King for their assistance, encouragement and supports during the experimental or suggestion during writing work.

I am deeply grateful to my mother for her patient, support and encouragements that let me to complete my training.

Contents **page**

Chapter 1

Introduction

The superconducting state is achieved only when electric resistance becomes zero and magnetic fields are expelled from the material where the transition state of matter does not follow the Ohm's law and the quantum properties of electrons adopt a 'new order.' High electric currents flowing without losses and strong magnetic repulsion are the concerned properties for future applications. Because of the synthesis and the maximum current flowing capacity are closely related to how these ceramic materials are fabricated to minimise impurity phases, weak-links and vortex movement for the applications in high magnetic fields. In this thesis, various syntheses and processing methodologies used for the preparation of bulk or thin layers of superconducting materials are described. Besides the common ceramic method, other techniques such as coprecipitation and precursor techniques, the sol-gel method, the alkali flux method, the combustion method and the shock-wave synthesis have been applied by a large number of research groups for the fabrication of superconducting cuprates. In case of lead based cuprates, improvements in the superconducting properties have been achieved by changing preparation conditions such as high oxygen pressure, low oxygen ambient or partial melt processing [1, 2, 3, 4, 5].

Mainly, the research work on the Y-Ba-Cu-O family has been performed during past several years due to non-toxic and non-volatile Ba, Cu and Y cations. World wide research has also been performed to raise the superconducting transition temperature (T_c) that has resulted the discovery of the bismuth, thallium and mercury based superconducting materials. Among bismuth (Bi), thallium (Tl) and mercury (Hg) based cuprates, Tl and Hg are very toxic and need special treatments during the synthesis whereas each of three cations is multivalent and volatile in nature that generates impurity phases and micro-inhomogeneity.

Soon after the discovery of bismuth and thallium based superconductors, attempts were made in several laboratories to synthesise lead-based superconducting cuprate [3, 4, 6], because of low cost of the lead and the similarity in oxidation states with bismuth and

thallium (such as Pb^{+2} and Pb^{+4}). It was also observed that the cations Pb^{+2} and Pb^{+4} substitute for Bi^{+3} and Tl^{+3} ions respectively in the bismuth and thallium cuprates. Therefore, in search of a material with higher transition temperature, critical current and magnetic field, it was considered that the lead based material could be showing better performance as a HTSC material similar to chevrel phases ($PbMo_6S_8$, 15K, 60Tesla) among conventional low temperature superconductors. The synthesis and reproducibility of lead-based superconductors have not proved any straightforwardness because of the volatile nature of lead, impurity forming ability and required oxygen adjustment to achieve better superconducting properties. At the time of my joining of UCL, London, other students were already investigating the suitable materials present at that time. However, there were few materials showing higher superconducting transition temperature but the toxicity, safety regulations and available facilities were not feasible to investigate them. The choice was the only newly reported $Pb_2Sr_2(R_{1-x}Ca_x)_{n-1}Cu_{n+1}O_{2n+4}$, (where R is the rare earth element) lead cuprate, commonly known as Pb-2213 phase [3], renamed as PSYCCO.

A variety of lead cuprates have been synthesised and some of them exhibited superconductivity. A large number of reports regarding various compositions in lead cuprate have been published such as $Pb_2Sr_2(R_{1-x}Ca_x)_{n-1}Cu_{n+1}O_{2n+4}$ or (Pb-2213), $(Pb,Bi)_2Sr_{2-x}La_xCu_2O_{6+\delta}$ or Pb-2202, $(Pb,Cu)Sr_2(Y,Ca)Cu_2O_7$ or Pb-1212, $(Pb,Cu)(Sr,Pr)_2Pr_2Cu_2O_9$ or Pb-1222, $Pb(Ba,Sr)_2(Ln,Ce)_2Cu_3O_9$ or Pb-2222, and $Pb_2Sr_2(Ln,Ce)_nCu_3O_z$ or Pb-22n3, (where n=3,4,..)[3, 6, 7, 8, 9, 10, 11]. Among all these phases, the most considerable and investigated phases are Pb-2:2:1:3 and Pb-1:2:1:2, because they exhibited higher transition temperature than the other phases that ranges from 70K to 80K and 40K to 65K respectively [1, 2, 3, 4, 5]. These lead cuprates have crystallographic structures similar to those of Bi- and Tl-based superconducting materials. The structure of Pb-1212 phase resembles that of $TlBa_2CaCu_2O_7$ that has a $YBa_2Cu_3O_7$-like arrangement of metal cations. In both phases, common charge reservoir block consisting of 1 to 3 atomic layers usually made of Pb, M (Cu, Sr, Ce or Ca) and oxygen, replaces the known charge reservoirs such as Bi_2O_2, Tl_2O_2 and TlO in the Bi- or Tl-based cuprates [1, 2, 3, 6, 7,10].

Usually, variations by the cationic ratios of the constituent elements in any system provide changes in properties such as Y:Ba:Cu: has 1:2:3, 2:4:8, 2:4:7 compositions

with the transition temperatures of 90K, 80K, and 40K with optimum oxygen values. Similarly, the Bi:Sr:Ca:Cu system has 2:2:0:1, 2:2:1:2, 2:2:2:3 compositions and T_c of 20K, 80K and 110K respectively where the transition temperature increases up to three CuO_2 planes and then it saturates [12]. However, the structure of the lead cuprates have similarity with Bi- and Tl-based systems but the transition temperatures are low enough, and vary significantly due to variations of M in the charge reservoir (Pb, M)-O, or Ca in (R, Ca)-O or oxygen in Cu-O_δ layers in the Pb-1212 or Pb-2213 phases, and converting the material from insulating→semiconducting→superconducting phases. Therefore, reproducibility of the results is arduous task where the synthesising procedure and environment can induce different transition temperatures in lead cuprates.

To check the possibility of enhancement in superconducting transition temperature, synthesis of various cationic ratios of lead cuprate has been performed through optimisation efforts during annealing and characterisation. Different compositions such as (Pb, Cu)-1212, Pb-1213, Pb-2213, Pb-1313 and Pb-3324 have been checked. All of them exhibited superconducting properties whenever the compositions were annealed in nitrogen. Through the minimisation of synthesising durations most of the lead-based materials were synthesised and have exhibited better superconducting properties than the other reports if those are present in the literature.

The thin layers of superconducting materials are important in terms of superconducting devices and to learn more about the fundamental properties of superconducting cuprates. It has easier mode of elimination of the weak links in between the grains as compared to bulk ceramic synthesis. Weak links and amorphous filling between crystallites cause a rapid deterioration of the transport critical currents as the applied magnetic field increases. This difficulty of synthesis could be controlled easily in the thin layers using substrate induced synthesis that is not possible perfectly in case of the bulk processing. Similar to bulk synthesis, variations in processing parameters and compositions can also alter the superconducting properties of thin films. The technique of pulsed laser-ablation deposition (PLD) has been studied extensively during the present decade that started just after the discovery of $YBa_2Cu_3O_7$ material in 1986 [13]. The research up to now has developed the most of the avenues of this technique but the studies vary from material to material due to sensitivity of different laser

parameters with the chemical, optical and mechanical properties of material, deposition and growth parameters. One can modify the properties of thin layers by controlling them. The deposition and growth parameters of great interest are:

i) In case of pulsed laser-ablation-deposition (PLD), the deposition rate is greatly concerned with the parameters of laser pulses, material, properties of pellet, and position of substrate with respect to plume.
ii) The deposition temperature of the substrate during ablation of material, annealing temperature after deposition and cooling rate of the substrate.
iii) The partial pressure of the gas present in the chamber during ablation also determines the plume size, roughness and the stoichiometry of the deposited layers.
iv) The quality of the substrate with respect to structural properties of the deposited material that is very effective to grow high quality textured or epitaxial layer on single-crystal substrate.

The most of the efforts were devoted to grow single phase textured thin solid $Pb_2Sr_2(Y_{0.5}Ca_{0.5})Cu_3O_8$ films so that it could be used both for fundamental studies and to check the possibilities of formation of devices where the width of superconducting transition temperature should be as narrow as possible. The chapters of this thesis highlighted as follows:

Chapter two includes a brief discussion of the various synthesising techniques used to fabricate superconducting materials during present decade. Description also includes hot-pressing and melt texturing of bulk cuprates to minimise grain boundaries and enhancing the critical currents.

Chapter three starts a short introduction to conventional superconductors, its history of developments and BCS theory. It includes the common properties of cuprate superconductors. Among the various lead based superconductors, the structural properties of main two phases are called Pb-2213 and Pb-1212 have been described. Atomic oxygen ordering, charge localisation and its transfer to CuO_2 sheets in Pb-2213 phase structure have been discussed.

Chapter four describes various techniques which use substrate-induced synthesis to fabricate thin superconducting layers. It follows a brief description regarding laser-ablation-deposition (PLD), laser-pulse-target interaction and plasma formation, PLD advantages and disadvantages. Long duration laser-target-interaction creates cones and segregates the surface of target. The cone formation model and roughness of deposited layer have been described in detail. It also includes the basic processes on the substrate surface, the crystallinity and orientation of thin layers.

Chapter five describes the experimental set-up to synthesise superconducting thin layers using single or multitarget holder and Nd:YAG laser. It includes the details of processing furnace, techniques used to analyse and characterise the bulk and thin layers after processing.

Chapter six includes the results obtained during the course of research on lead-based bulk materials and their synthesis. The ceramic synthesis technique used to induce superconductivity through various attempts such as modification in usual processing and in different cationic ratios through the adjustment of oxygen stoichiometry.

Chapter seven deals with the substrate-induced synthesis of Pb-2213 phase material. It includes ex-situ annealing and in-situ processing. For ex-situ growth, the parameters such as annealing temperature and durations, deposition temperature and stoichiometry, variations in superconducting transition temperature with lead content were considered. The technique of in-situ growth of Pb-2213 layers was developed to control the oxygen related superconductivity in this phase, and results are presented. Novel multilayering technique was used to synthesise Pb-1212 phase thin layers and Bi-Sr-Ca-Cu-O/Pb-Sr-(Y, Ca)-Cu-O/MgO multilayered structure. Topics relating the effects of annealing temperature, oxygen partial pressure and microstructure have been presented. Atmosphere and water can deteriorate most of the HTSC material. An attempt has been made to demonstrate the environmental and water effects on Pb-2213 phase thin layers through XRD and resistive transition temperatures.

Chapter eight includes a discussion related to the problem of droplet formation and elimination during PLD processing. It describes an attempt to deposit large and smooth area films. It also includes the variations in droplets and the surface smoothness of thin

layers. Pressing forces of pellets also affect the mass ablation and smoothness of deposited surface. One topic includes the results which belong to pulsed-laser-mass-ablation of HTSC materials. The energy of ablated particles using mass-spectrometry and related experimental arrangements are described. It also shows the effects of partial pressure of oxygen and annealing on uniformity. Other topics describe a simple approach to deposition using a four sided substrate holding geometry, droplets minimisation techniques and larger average area without substrate rotation or scanning of laser-beam or target.

Chapter nine describes critical current measuring technique, vortex pinning, description of Bean model, vibrating-sample magnetometer (VSM) and SQUID magnetometer, The experimental results regarding critical currents flowing in Pb-2213 phase film, and in Pb-2213, Pb-1212 and Pb-3324 (Y=1, Ca=1) phase bulk compositions were described and at the end a conclusion was included.

Chapter ten ends up with the conclusions regarding bulk synthesis of the lead based materials, the thin film preparation using PLD technique and future work to enhance the superconducting transition temperature and critical currents in the lead-based system.

References

[1] T.Rouillon, J.Provost, M.Hervieu, D.Groult, C.Michel and B.Raveau, Physica C 159, 201 (1989).

[2] X.X.Tang, D.E.Morris and A.P.B.Sinha, Phys.Rev.B 43, 7936 (1991).

[3] R.J.Cava, B.Batlogg, J.J.Krajewski, L.W.Rupp, L.F.Schneemeyer,T.Siegrist, R.B.vanDover, P.Marsh, W.F.Peck Jr., P.K.Gallagher, S.H.Glarrum, J.H.Marshall, R.C.Farrow, J.B.Waszczak, R.Hull and P.Trevor, Nature 336, 211 (1988).

[4] M.A.Subramanian, J.Gopalakrishnan, C.C.Torardi, P.L.Gai, E.D.Boyes, T.R.Askew, R.B.Flippen, W.E.Farneth and A.W.Sleight, Physica C 157, 124 (1989).

[5] M.Masuzawa, T.Noji, Y.Koike and Y.Saito, Jpn. J. Appl. Phys. 28, L1524 (1989).

[6] H.W.Zandbergen, W.T.Fu, J.M.van Ruitenbeek, L.J.de Jongh, G. van

Tendeloo, and S.Amelinckx, Physica C 159, 81-86 (1989).

[7] J.Y.Lee, L.S.Swinnea and H.Steinfink, J.Mater Res. 4, 763 (1989).

[8] S.Adachi, O.Inoue, S.Kawashima, H.Adachi, Y.Ichikawa, K.Setesune, and K.Wasa, Physica C 168, 1 (1990).

[9] A.Tokiwa, T.Oku, M.Nagoshi, D.Shindo, M.Kikuchi, T.Oikawa, K.Hiraga and Y.Syono, Physica C 172, 155(1990).

[10] T.Mochiku, M.Osawa and H.Asano, Jpn. J. Appl. Phys.29, L1406(1990).

[11] A.Tokiwa, T.Oku, M.Nagoshi, and Y.Syono, Physica C 181, 311(1991).

[12] T.Kawai, M.Kanai, T.Matsumoto, H.Tabata, K.Horiuchi, and S.Kawai, E-MRS, ICAM-91, Symposium A-1, V1-2, (1991).

[13] H.M.Smith and A.F.Turner, Appl. Opt., 4, 147 (1965).

Chapter 2

Various Techniques of Bulk Synthesis

There are various processing methodologies which have been adopted or could be used in the synthesis of copper oxide superconductors (cuprates) in general, and lead cuprates in particular. In this chapter, the different synthesising techniques, and their effects on superconducting properties are reviewed. Other than the generally used ceramic method, different techniques such as coprecipitation and the precursor technique, the sol-gel method, the alkali flux method, the combustion method, the shock-wave synthesis and high-pressure annealing have been utilised during last several years by different research groups in the fabrication of superconducting ceramics. Through a series of efforts by different researchers [1,2,3,4], improvement in superconducting properties has been obtained by varying preparation conditions such as high oxygen pressure, low oxygen ambient and melt-texture processing.

2.1 Ceramic method

The so-called 'ceramic method' or 'solid-state reaction method' is the most common technique of preparing oxide superconductors. This involves the reaction at elevated temperature (above 750°C) of the constituent oxides, carbonates or nitrates in appropriate stoichiometric amount. However, it is difficult to obtain reproducible homogeneous material using this technique, particularly, when one or two small elemental fractions are present as in some electroceramics or HTSC cuprates whose properties are often controlled by grain boundary phases containing minute quantities of additives.

If all the starting materials are solids, the preparation-technique is called the 'ceramic method'[5]. Usually, the starting materials such as metal oxides, nitrates, carbonates or other salts, are mixed, thoroughly homogenised (it may take hours) and are placed to calcine in a suitable crucible, made from, e.g., platinum, silica (SiO_2), zirconia oxide

(ZrO_2) or alumina (Al_2O_3). Commonly, the powder is homogenised, pressed in the form of a tablet, and placed inside a furnace, in a suitable container. Because of the reactivity of the materials one must be careful in selecting the type of container used to heat at a sufficient temperature and time to complete reaction. The material is heated several times for different periods and reground to ensure the most complete reaction to occur. Once the reaction is completed, sintering or densification is performed where particles join together, and bring about a volume reduction, decrease in porosity and increase in grain size. The phase distribution or microstructure within the ceramic is developed during sintering.

A slight alteration of the method is that the metal oxides /carbonates are dissolved in concentrated nitric acid (HNO_3). The obtained solution is heated to dryness in argon or nitrogen (inert) ambient. Usually, carbon dioxide is released during the reaction of carbonates with nitric acid but if there is small amount, the heating process in nitrogen enables the decomposition of carbonates at lower temperature (~500°C) and also allows the evolved carbon dioxide to be flushed out effectively.

A product fabricated by the ceramic method depends on the nature of the starting compounds (the choice of oxides, carbonates or nitrates), the homogeneity of the mixture of the powders, the rate of the heating as well as the reaction temperature, duration and number of grinding and heating cycles.

The main disadvantages of this technique are:

i) The starting materials are inhomogeneous at the atomic level.

ii) When no melt is formed during the reaction, the entire reaction has to take place in the solid state, first by a phase boundary reaction at the points of contact between the components and later by the diffusion of the constituents through the product phase. With the progress of the reaction, diffusion paths become longer and the reaction rate slower; the reaction rates can be increased to some extent by regrinding and heating procedure.

iii) To obtain a homogeneous product with perfect stoichiometry is difficult due to loss of components during firing at high temperature. This is very common in cuprates, particularly in case of any volatile element with lower melting point compared to other such as Pb, Bi, Tl and Hg. The difficulties in maintaining chemical homogeneity is a serious problem and has a bad effect on electrical properties of the ceramic. Usually, an excess amount of volatile reactants (Pb, Bi, Tl, Hg, etc) is required to maintain

perfect stoichiometry. For example, loss of copper even occurs at high temperature processing (1000°C). Therefore, a slightly excess amount of copper can provide cuprates (Y-Ba-Cu-O) with a sharper transition [6].

iv) There is no simple way of finding the progress of the reaction. It is just the trial and error method that one finds the suitable conditions required for the completion of the reaction. Because of this difficulty, with the ceramic method one often ends up with mixtures of reactants and products. Separation of the desired products from such mixtures is difficult, if not impossible. Barsoum et al. [7] found the repulsion of a superconductor by a strong magnetic field (Meissner effect) could be used to separate the desired phase from non-superconducting phases. For example, $YBa_2Cu_3O_{7-\delta}$ powder sealed in a glass tube, cooled to liquid nitrogen temperature and was drawn over a magnetic pole to use Meissner effect. The superconducting phase was found to move away from the applied magnetic field, while the other non-superconducting phases remained stationary. Unfortunately, this process is not suitable to separate various co-existing superconducting phases with a smaller difference in superconducting properties (such as 123-, 124- or 247-YBaCuO, Bi-2212, -2223, -2213 or Pb-2213, Pb-1212 phases).

2.2 Co-precipitation and precursor method

This process involves the separation of a solid from a solution, containing different chemically bound ionic species. The metal salt solutions are combined in stoichiometric proportions that results in mixing of metal ions on the atomic scale. Therefore, a co-precipitation process can result in the development of homogeneous crystalline or amorphous solids.

The steps involved in the chemical routes are shown in *figure 2.1.*

Co-precipitation of well-defined stoichiometry concerning the metal ions is obtained only when the following requirements are satisfied:

i) The precipitation agent is a multivalent organic compound that can co-ordinate with more than one metal ion, and the precipitation rate is fast.

ii) The solid precipitating out of the solution should be completely insoluble in the mother liquor.

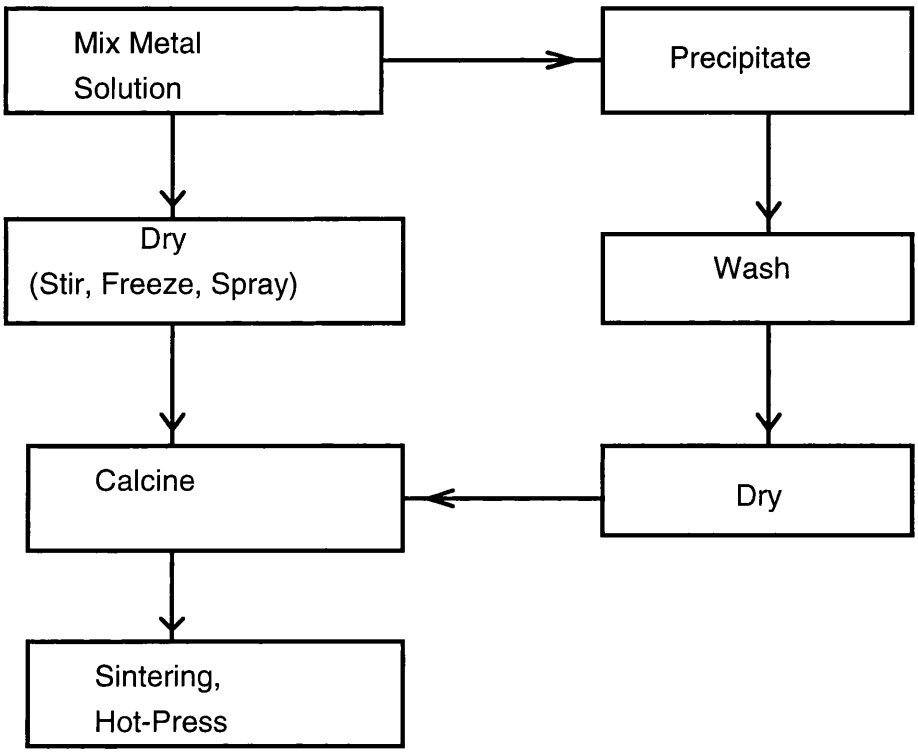

Figure 2.1. *Different steps involved in the chemical routes to fabricate layered copper oxide materials.*

The anion generally preferred for co-precipitation of oxidic materials are carbonates, oxalates, citrates, etc. For cuprate superconductors, preferential solution route is through nitrate salts, noting that bismuth nitrate requires a moderately strong nitric acid addition to render it soluble in water. The precipitates in some instances could be genuine precursors or solid solutions [8]. It is well known that precursor solid solutions drastically bring down diffusion distances for the cations and facilitate reactions in the solid state. The precipitates (carbonate, oxalate etc.) are heated at required temperatures in a suitable atmosphere to obtain the desired material. Different methods of conversion of the atomically-mixed solutions are used to the desired atomically mixed solids. Fast evaporation of the solvent (water) by spray on hot plate, stirring and evaporating of solvent [9] and freeze-drying that also depends on spraying an atomised solution. Tretyakov [10] has sprayed solution into acetone at -40°C to assist with water removal, and has also utilised cold concentrated ammonia or non-aqueous liquids to produce "cryoprecipitation".

Carbonate co-precipitation is suitable for the synthesis of Pb-2213 and Pb-1212 phases [11]. Co-precipitation as carbonate has been achieved by adding the nitrate solution of the constituent metal ions to an aqueous solution of sodium carbonate (in excess) under constant stirring. The carbonate precipitates thus obtained are washed and dried. The

decomposed powder is heated in the form of pellets around 880°C in a suitable atmosphere. Pb-2213 phase obtained by this method after heating for four hours in nitrogen containing 1% O_2 showed Pb-2213 as a major phase ($T_{c,onset}$ 70K) with impurities such as Y_2O_3 and CuO. This technique has the advantage of single heating rather than the multi-step procedures required in the other techniques. Some of the advantages of the co-precipitation over the ceramic method are an homogeneous distribution of components, a decrease in the reaction temperatures and of the duration of annealing, a high density and lower particle size of the final product. The main disadvantage of this route is the control over the stoichiometry of the product that is important factor in obtaining right superconducting properties.

2.3 Sol-gel process

Sol-gel processing of alkoxides has been intensively used during last 20 years, because it offers non-melt routes to high purity glasses and crystalline ceramics. In 1932, Kistler first time developped a technique named as the sol-gel that involves the synthesis of inorganic oxides from inorganic or organo-metallic precursors called alkoxides [12]. In its broad sense the term "sol-gel" refers to the preparation of inorganic oxides by wet chemical methods, irrespective of the final form of the product, either powder, crystalline or amorphous. The metal alkoxides $[M(OR)_x]_n$, where M is a metal of valency x and R is an alkyl group, are excellent precursor molecules for the deposition of metal oxides by MOCVD or sol-gel bulk synthesis. These alkoxides can be synthesised by the direct-reaction between alkali, alkaline earth's or divalent/trivalent metals and alcohol but some time the use of catalyst (either I_2 or $HgCl_2$) is also required to initiate the reaction [13,14,15]. The suitable ternary and quaternary alkoxides can be prepared by various methods of which the simplest one is to combine the binary alkoxides in correct proportions or using a metal chloride and a ternary or even higher metal alkoxide to get hetero-metal alkoxides MM'..M" $(OR)_x$[16].

Sol-gel as a multistep technique is involving chemical and physical processes associated with hydrolysis, polymerisation, drying and densification [17]. The sol-gel process is used in order to get homogeneous mixing of cations on an atomic scale. The

solid state reaction is completed in a shorter period and at the lowest possible temperature due to atomically mixed starting materials. The term sol often refers to a suspension or dispersion of discrete colloidal particles, while gel represents a colloidal or polymeric solid containing a fluid component which has the internal network structure where both the solid and the fluid components are highly dispersed.

In the sol-gel process a concentrated sol of the reactant oxides or hydroxides is converted to a semi-rigid gel by removing the solvent. The dry gel is heated at an appropriate temperature to obtain the product. Most of the reactions in the sol-gel process occur through hydrolysis and ploycondensation. Some necessary descriptions of the steps involved in sol-gel ceramic preparation are [18]:

i) hydrolysis: a process may start with a mixture of metal alkoxide and water in solvent (usually alcohol) at ambient or slightly higher temperature. Acid or base catalyst are usually employed to speed up the reactions;

ii) polymerisation: condensation reactions occur between adjacent molecules in which H_2O and OH are eliminated and metal oxide linkages are formed. Polymer networks grow to colloidal dimensions in the liquid and colloidal dispersion is named as sol;

iii) gelation: polymer network link up to form a three dimensional network throughout the liquid. The system becomes rigid. Solvent and the products of the condensation reactions, water and alcohol, remain in the pores of the gel;

iv) drying: water and alcohol are removed from the system at moderate temperature (<100°C), leaving a highly hydroxylated metal oxide with some residual organic content. The solvent may be removed supercritically;

v) dehydration: the reasonable high temperatures, 400-800°C, are required to drive off the residual organics and chemically bound water, yielding a glassy metal oxide;

vi) densification: temperatures typically in excess of 1000°C cause elimination of porosity and formation of a dense compacts.

Two different routes for the sol-gel process are usually described in the literature for the synthesis of cuprate materials[19]:

i) Via molecular precursors (e.g. metal alkoxides) in organic medium;

ii) Via ionic precursors in aqueous medium (citrate gel process).

The phase purity, microstrusture and physical properties of the product are controlled by varying the precursor, solvent, pH, firing temperatures and heating atmosphere.

Following advantages offered by the use of sol-gel techniques in the preparation of ceramic and glasses have been included by different authors [20, 21]:

i) better homogeneity compared to commonly used ceramic method;

ii)lower temperature processing and crystallisation is possible;

iii)more uniform phase distribution in multicomponent systems;

iv)better size and morphological control in powder synthesis.

Some of the main disadvantages of sol-gel method are:

i) undesirable or incomplete reactions of precursor may result in by-products. Also, the presence of residual carbon due to incomplete removal of the organic content can exist during sintering;

ii) there remain challenges in the area of health and fire safety. Special protection is required for the handling of certain precursors, and volatile products evolved during processing can be poisonous or flammable:

iii) the starting raw materials, for example, the metal alkoxides for sol-gel processing are several times costly than mineral-based inorganic salts and mineral powders.

Horowitz et al. [16] has used hydrolysable organo-metallic compounds, including alcohol-soluble Cu alkoxides, and aqueous metal hyponitrites to prepare the $YBa_2Cu_3O_{7+\delta}$. They first prepared the tetragonal phase of $YBa_2Cu_3O_{7+\delta}$ at only ~ 650°C in an inert ambient and then converted it to the orthorhombic phase by heating in oxygen at 400°C. This synthesising temperature is much lower than the temperature used in solid state technique to achieve similar properties of the product.

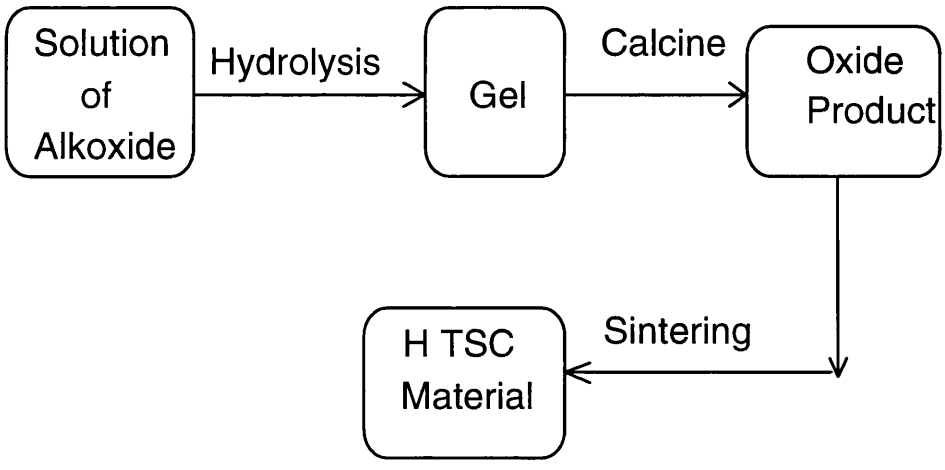

Figure 2.2. *Outline of the sol-gel process for cuprate superconductors.*

2.4 Citrate gel process

One basic method is to start with the mixed-metal nitrate solution and then to form a complex by adding citric acid. The viscosity of the mixture can be increased as desired by adding ethylene glycol. This technique was developed by Marcilly & co-workers in 1970. In order to form an organo-metallic complex, they added citric acid to the combined zerconyl and Gd(iii) nitrate solutions (acid and metal mole ratio=2:1) whose pH had been increased with NH_4OH to among 6 and 7.5. Other organic acids containing at least one hydroxyl and one carboxylic group such as tartaric, lactic and glycollic acid can be used.

Several authors have used the citrate gel process [22, 23] in the fabrication of compositions $YBa_2Cu_3O_{7-\delta}$ and $La_{1.7}Sr_{0.15}Ba_{0.15}CuO_4$ in order to achieve greater homogeneity, and reproducibility for the cuprates than is achievable by mixing powders in ceramic method. Lead-based HTSC have also been successfully synthesised by mixing the nitrate solution of the relevant cations in the required molar ratio. A mixture of citric acid and ethylene glycol in the molar ratio 1:4 was added slowly to the nitrate solution under constant stirring. The clear blue solution obtained is concentrated at 100-200°C in order to obtain gel. The gel is then decomposed by heating at 500°C for 5 hours in air and the ash coloured crystalline powder thus formed is subjected to different heat treatments in 1% O_2 in nitrogen or oxygen ambient depending on whether the cuprate is Pb-2213 or 1212 phase. The Pb-2213 phase obtained from this process shows a sharp transition at 60K when the fine powders were pressed in a form of pellet and heated in a flowing 1% O_2 at 800°C for 10 hours, however, $(Pb_{0.7}Cu_{0.3})Sr_2(Y_{0.6}Ca_{0.4})Cu_2O_7$ phase is semiconducting and $Pb_{0.5}Cu_{0.5}SrBaY_{0.75}Ca_{0.25}Cu_2O_7$ is superconducting with a T_c midpoint of 50K [24].

More recently, synthesis of lead based $Pb_2Sr_{0.8}La_{1.2}Cu_2O_{6.1+\delta}$ superconductor has also been demonstrated by Wang et al.[25] using a polymeric citrate precursor. Metal nitrates of the nominal compositions were used as the starting materials. After pyrolysis of the gel-like polymeric citrates, the precursor obtained was calcined at

800°C for 4 hour, and sintered at 790°C for 6 hours in a flowing nitrogen ambient followed by furnace cooling. Their XRD pattern has shown the presence of a little coexisting phase of $La_{2-x}Sr_xCuO_4$. The $T_{c,onset}$ and $T_{c,zero}$ were 36K and 9.3K, respectively. Here, again a broad superconducting transitional width is indicating the some inhomogeneity, could be due to oxygen distribution that is common in lead based materials. They claimed that the citrate precursor method has the shorter processing period than the ceramic method [26, 27].

2.5 Alkali-flux method

This method, either in the form of solid carbonate fluxes, molten hydroxides or highly concentrated alkali solutions can be used for the synthesis of cuprate superconductors. The alkali flux method takes advantage of both the moderate temperatures of the molten media (180-400°C) as well as of the acid-base characteristics of molten hydroxides to simultaneously precipitated oxides or oxide precursors such as hydroxides or peroxides of the constituent metals. The method stabilises higher oxidation states of the metal by providing an oxidising ambient. This technique does not require several grindings and heating cycles during processing. Furthermore the technique is efficient and lowers the cost of synthesising compared to other processing techniques.

2.6 Combustion methods

Solid combustion synthesis (SCS) or self-propagating high temperature synthesis (SHS) first developed by Merzhanov and Borovinskaya [8], provides a simple and fast method of preparing inorganic materials. The combustion method is based on the principle that the heat energy liberated by many exothermic non-catalytic solid-solid or solid-gas reactions can self-propagate throughout the sample at a certain rate. This process can therefore occur in a narrow zone that separates the starting substances and reaction products. Traditionally, combustion chemistry deals with reactions of thermal dissociation and oxidation of different fuels: natural and synthetic, organic or inorganic, solid, liquid, and gaseous. The selection of combustible systems is based on the choice of chemical which burn to release as much energy as possible that is used to form a material. Usually, the chemical energy of fuels is released as thermal energy, which is transformed into other kinds of energy in well-known manners. Reactions of elemental

synthesis are the most extensively studied part of SHS reactions in which the metal acts as a fuel and nonmetal as an oxidant[28].

The simplest way of ignition is local heating of a powder compact when the enthalpy of reaction is exothermic enough to start a steady state reaction. Using this technique, the mixture of elements to be combined is surrounded by another mixture of highly reactive materials. The reaction inside the outer layer of material gives a burst of heat to the inner part that reacts and adds its own heat to that of the oven [29]. The thermal explosion mode consists of heating the elemental blended powders at a constant rate until they react. The reaction is quick and a cast-product may be obtained [29, 30].

The synthesis of almost all families of cuprate superconductors involve the addition of an appropriate fuel to a solution containing the metal nitrates in the proper stoichiometry. The ratio of the metal nitrates to the fuel is such that when the solution is dried at around 150°C, the solid residue undergoes flash combustion, giving an ash containing the mixture of oxides in the form of very fine particles (0.3-0.5 μm) [31]. The ash is then given the appropriate heat treatment under the desired atmosphere to obtain the cuprate. The small particle size of the ash facilitates the reaction between the metal oxides due to smaller diffusion distances between the cations. Fuels such as urea [32], glycine [33], and tetraformal triazine (TFTA) [34], are generally utilised for synthesising copper oxide superconductors. Some of the new materials have been prepared by this route include $La_{2-x}Sr_xCuO_4$ (T_c=35K), $YBa_2Cu_3O_7$ (90K), $Bi_2CaSr_2Cu_2O_8$(T_c=85K), $Pb_2Sr_2Ca_{0.5}Y_{0.5}Cu_3O_8$ (T_c=60K) and $Nd_{2-x}Ce_xCuO_4$ (T_c=30K) [35]. SHS is a very interesting mode with such advantages as short synthesis times, low energy consumption, simplicity in process organisation and high quality products are obtained in optimum conditions, compared with other advanced techniques. It has a serious puzzle that the most of the product is porous and the impossibility of sustaining endothermic reactions.

2.7 Shock-wave synthesis

The use of shock-waves as an ultrafast synthesising technique for cuprates (i.e., in a few microseconds) has been demonstrated by several research groups [36, 37, 38]. The shock-wave can be produced by a confined explosive blast in a variety of geometries or

the impact of a high velocity projectile in a gun barrel arrangement. A generated dynamic pressure ranging from about 1 to a few hundred GPa can be achieved using gun barrel arrangement; along with intergranular temperatures of up to a few thousand degrees for a very short period. By controlling the packing density, the size of the particles and their distributions in the precursor powder, and detonation or projectile velocity at the shock front, it is possible to obtain a solid body compacted to high density as a result of enter particle welding. At the microscopic level, a variety of dislocation, defects are introduced into the cuprates. The shock pressure and its duration are the main processing parameters that dictate the optimum solidification of the powder and tailoring of the properties of the compacted materials. The shock-pressure and shock-duration obviously control the degree of solidification and the density of microscopic defects.

As mentioned earlier, the shock-pressure can be generated by direct contact with explosive or by impact from a plate accelerated either by compressed gas in a gun or by explosives. One of the most commonly used systems are the 12-capsule plate impact system. The arrangement consists of 12 capsules containing the powder in a target plate that is backed by a momentum trapping plate of similar thickness. A plane-wave lens arrangement contains the explosive that, on detonation, accelerates the plate to impact against the capsules; the speed of the impact plate is monitored by a high speed camera. 10-100 GPa pressures can be generated in this apparatus to give cylindrical samples about 12mm in diameter and 5mm thick. At a time, 12 different compositions, one in each capsule, can be subjected to identical shock conditions. A lower range of shock pressures in the range of 0.1 to 5 GPa can be generated by a gas gun arrangement described by Nellis et al.[39].

The first shock-wave synthesises of cuprate superconductor were performed by Graham et al. [37] and Miller et al. [38]. These groups used a flyer plate's set-up and $La_{2-x}Sr_xCuO4$ and $YBa_2Cu_3O_{7-\delta}$ compounds. Mixed oxide powder precursors corresponding to the stoichiometry of $La_{1.85}Sr_{0.15}CuO_4$, were prepared by co-precipitating the metal nitrates by adding a sodium carbonate precipitate was calcined for 2hrs at 825°C to give a precursor material consisting primarily of the oxides and lanthanum oxicarbonates. Under shock conditions using the flyer plate geometry with estimated peak pressure in the range of 17-22GPa and peak temperature among 800°C

to 900°C, it was possible to obtain a surprisingly high yield (85-90%) of the $La_{2-x}Sr_xCuO_4$ compound in the correct K_2NiF_4 phase. XRD patterns of the shock-synthesised La-Sr-Cu-O compound, obtained as highly dense cylinders, showed some line broadening indicative of residual strain. Some unidentified phases were found other than the unreacted oxides. The $T_{c,onset}$ of 15K was reported but an anneal for 1hour in air at 1100°C provided single phase bulk superconductivity with a $T_{c,onset}$ near 40K. This indicates that the correct oxygen content and lattice parameters are only obtained by subsequent annealing.

Morosin [40] and Miller [38] attempted to synthesise a good percentage of $YBa_2Cu_3O_{7-\delta}$ by using shock wave pressures of 22GPa but they had some success only when using BaO_2 instead of BaO in the precursor under the similar conditions. This shows that the higher oxygen contents are more suitable for shock-synthesis. The reported $T_{c,onset}$ of 14K is too small to compare with other techniques.

The preparation of Bi-based superconductors was also attempted using shock-wave techniques by Yoshimoto et al.[41]. They could not produce any of the desired crystalline phases even at very high shock pressures (>30GPa). It appears that the kinetics for the formation of the Bi-based superconductors is slow and this probably precludes the synthesis of these phases using this technique.

Attempts at shock synthesising the Tl-based (Tl-2212, Tl-2223) cuprate have been made by Iqbal et al. [42] at 20 GPa and Yoshimoto et al.[41] up to 30GPa. Iqbal used a precursor consisting of Tl_2O_3 and a pre-fired (at 850°C) precursor of nominal composition $Ba_2Ca_2Cu_3O_x$ in the 2223 & 1223 stoichiometric ratio, while Yoshimoto used only the metal oxides as a mixed powder. Using XRD data, it was reported that small amounts of materials in the Tl-2212 structure are obtained. However, Yoshimoto et al. reported the formation of a small fraction of a superconducting phase but, in contrast to the results of Iqbal et al., their samples showed a weak diamagnetic signal with a $T_{c,onset}$ at 75K.

Summarising, it is clear from the attempts made till now that shock synthesis with sizable superconducting product, has been successful only for $La_{1.75}Sr_{0.15}CuO_4$ and $Tl_2Ba_2CuO_6$ with superconductivity present in the as-recovered state only in the Tl-deficient version of the latter phase. The slow kinetics for the formation of the double and triple-CuO_2 layered Bi- and Tl-based compounds exclude the use of shock-wave synthesis. Suitable precursor powders and optimisation of shock conditions are the requirement to enhance yield fractions of cuprate superconductors. However, lead based materials need a reduced oxygen ambient for superconductivity to occur but have not been tried by this technique.

The shock technique may therefore provide a relatively cheap and fast means to safely produce single CuO_2 layered superconducting ceramics such as Tl-based cuprates because the toxicity of T_2O_3 vapours would preclude their large scale production by furnace-processing technique.

2.8 Hot-pressing

In shock-wave synthesis, virtually no temperature rise above ambient is used, thereby preventing oxygenation, and crystallisation relies only on pressure (several GPa). Hot-pressing is a complex and very slow operation compared to sintering and shock-compaction but has produced better results. However, hot pressing is inappropriate for 123 bulk samples for the reason that porosity is necessary to achieve oxygenation in the interior of the material.

Hot-pressing is used in normal ceramic processing to produce a denser material at the lowest possible temperature. The use of pressure during sintering forces the reacting components together and increases the inter-granular reaction rate. The advantage of using the lowest possible reaction temperature is that grain growth can be minimised. This increases thermal shock resistance and the percentage of grain boundaries in the solid.

2.9 Melt-texture processing

Critical current depends on the microstructure of the materials and varies with the fabrication process and weak-links at the grain boundaries.

The main cause for the low critical current (J_C) behaviour is the presence of weak-links in the polycrystalline cuprate superconductors [43]. The disorientation angle between the adjacent grains influences the current carrying capability at the grain boundary [44]. Across most of the large-angle grain boundaries, the flow of the transport electrical current is severely limited, particularly in the presence of a magnetic field. The weak-link problem in these materials can be greatly reduced by elimination or minimisation of large-angle grain boundaries in the path of the transport current. It is well known that the preferential crystallographic alignment of grains parallel to the a-b conduction planes (CuO_2) in cuprates can provide the best results. Different approaches to this end have been reported in literature are:

i) melt-texture processing, using directional crystallisation of the copper oxide materials,

ii) magnetic field alignment, using the anisotropic paramagnetic susceptibility of the cuprate particles,

iii) substrate-induced texturing using either epitaxial growth or the interaction of the superconductor with the substrate that provides oriented deposition under certain conditions.

Each of the above techniques has advantages and some limitations. Only approaches (i) and (ii) have been discussed here whereas the third forms a major section within a separate chapter, being is of the main topics of this thesis. Melt processing [45,46] is basically a directional solidification from the melt or partial melt state. The process is performed in several steps from the peritectic temperature to the temperature for nucleation and growth, followed by additional slow cooling (2-10°C/hour) to lower temperatures where oxygenation or reduction is required. Grain alignment by melt texture processing can be accomplished in at least four ways: (i) continuous cooling of a stationary sample maintaining the temperature gradient [45] (ii) continuous zone melting by a moving hot zone [47] (for example, by IR lamps, laser or electrical heating), (iii) zone melting by slowly and continuous pulling the sample rod through a

temperature gradient, and (iv) melt-texture processing, without a temperature gradient, of prealigned precursor wire [48].

Many possible variations in the melt-texture technique have been used initially in the processing of bulk $YBa_2Cu_3O_{7-\delta}$. Enhanced T_c of 96K with a sharp transition and strong pinning (7Tesla, 77K) in melt-processed $NdBa_2Cu_3O_{7-d}$ superconductors has recently been demonstrated by Yoo et al. [49]. They used 0.1% O_2 in Ar during the melt processing and a subsequent long term oxygen annealing period (100hrs) at 600-350°C.

Jin [45] reported that oriented polycrystalline $YBa_2Cu_3O_{7-\delta}$ can be produced by the melt-texture growth method (MTG) with a high J_c of $10^4 A/cm^2$ at 77K and in a magnetic field of 1Tesla. Melt textured Bi-Sr-Ca-Cu-O (2212 phase) material can possibly be obtained as a weak-link free superconductor with J_c up to $10^5 A/cm^2$ at 4.2K in a magnetic field of several Tesla [50, 51].

Tachikawa[52] and Morita[53] have produced pseudo-single-crystalline bulk $YBa_2Cu_3O_{7-\delta}$ samples by the quench and melt growth (QMG) technique. In the first step, YBaCuO (123) powder is melted at 1400°C for 5 minutes in a platinum container and quenched to a plate shape. At this stage, the material transforms into Y_2O_3 grains and liquid phase mixture of $BaCuO_2$ and CuO. In the second step, the plates were reheated at about 1200°C on a platinum net and cooled to 1000°C within 10hours then from 1000°C to 950°C with a cooling rate of 30°C /hour. In the fourth step, the material was slowly cooled from 950°C to room temperature at the rate of 100°C /hour. They obtained the samples containing Y_2BaCuO_5(211) phases along with the $YBa_2Cu_3O_{7-\delta}$ phase but got throughout grain boundary a region of 1.2cm in the a-b direction along the length of the sample. The heating pattern of the QMG process is shown in *figure 2.3* that illustrate the four steps involved in processing.

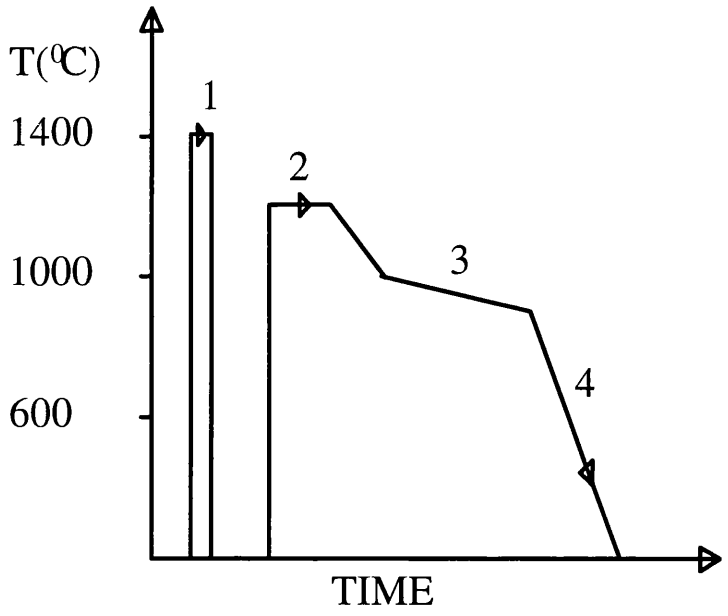

Figure 2.3 *The heating pattern of the quench and melt growth process showing the following steps:*

(1)decomposition of $YBa_2Cu_3O_{7-\delta} \rightarrow Y_2O_3 + L\ (BaCuO_2 + CuO)$

(2) $Y_2O_3 + L \rightarrow Y_2BaCuO_5$ *(or 211) + L,*

(3) $211 + L \rightarrow 123 + 211$ *and*

(4) 123 tetragonal → 123 orthorhombic transformation

Kim et al.[54] have also reported similar work in which they pressed bar samples of $Y_2BaCuO_5/BaCuO_2$ + CuO mixtures: these bars were pulled through a high temperature zone to produce growth of grains of the 123 phase with a high degree of preferred orientations. The textured samples were then reheated to provide further oxygenation. Similarly, Zhou et al. [55] have utilised Y_2BaCuO_5 + BaCuO mixtures in the correct stoichiometries ratio to obtain textured samples by partial melting at 1040°C, where the samples were moved through the hot zone and then passed into a severe temperature gradient. After cooling to 500°C, the samples were oxygenated and J_c values of 10800A/cm^2 at 77K in a magnetic field of 1Tesla were obtained.

2.10 Magnetic field alignment

This technique uses anisotropic paramagnetic susceptibility of the cuprate materials. Fine particles of superconductor are dispersed in a liquid medium such as heptane, and a strong magnetic field of 1-8 Tesla is applied [56,57], 123-YBCO plate-shaped grains are aligned with their c-axis parallel to the applied field direction. After the aligned

particles settle, the heptane is allowed to evaporate. The dried cake is then sintered in oxygen and slowly cooled. A strong (00l) texture was obtained in the 123 superconductor prepared by this technique [57]. However, the field alignment (e.g., c-axis alignment) does not differentiate between the a and b orientations. As a result, many of the in-plane aligned, plate like grains tend to have a twist relationship (rotation of grains around the c axis) relative to each other, producing a considerable number of large-angle grain boundaries. For efficient grain alignment by the field alignment technique, one has to be sure that the most of the superconductor particles are single crystalline, to avoid internal large-angle grain boundaries, and preferably have a plate-shaped geometry to exploit the possible mechanical alignment factor during gravitational settlement of the particles. Unless the a, b misorientation (in-plane twist) is reduced by some means, it may be hard to completely eliminate large-angle (weak link) grain boundaries by this technique.

2.11 Other techniques

Along with the various techniques discussed above, a few other methods such as spray drying [58, 59], freeze drying [60, 61], and electrochemical methods [62, 63] have also been utilised for the preparation of bulk superconductors. Making use of electrochemical oxidation at room temperature, the $La_2CuO_{4+\delta}$ (214 phase) with a T_c of 44K has also been prepared which is otherwise possible only by the use of high oxygen pressures [64].

2.12 Summary

Some of the important bulk properties of superconductors depend fundamentally on different processing routes other than their intrinsic properties. The large-grained and highly oriented materials are required to maximise critical current density, J_c, whereas very-fine-grained compacts favour mechanical properties but make it difficult to oxygenate the inside of the pellet. In this chapter, various synthesising techniques used to fabricate superconducting cuprate materials were described in detail with their advantages and disadvantages.

References

[1] A.W.Sleight, Science, 242, 1519 (1988).

[2] C.N R.Rao, Chemistry of High Temperature Superconductors (Singapore, World Scientific), 1991.

[3] C.N.R. Rao, Phil. Trans. R.Soc., A336, 595 (1991].

[4] M.Morita, K.Miyamoto, K.Doi, M.Murakami, K.Sawano, and S.Matsuda, Physica C 172, 383 (1990).

[5] C.N.R.Rao and J.Gopalakrishnan , New Directions in Solid State Chemistry Cambridge University Press (1989).

[6] A.M.Umarji and K.S.Nanjundaswamy, Pramana- J.Phys.29, L611 (1987).

[7] M.Barsoum, D.Patten and S. Tayagi, Appl. Phys. Lett. 51, 1954 (1987).

[8] A.G.Merzhanov and I.P.Borovinskaya, Dokl.Acad.Nauk. 204, 366(1972).

[9] F.V.Shaw, Amer.Ceram.Soc.Bull., 69, 1484 (1990).

[10] Yu. D. Tretyakov, Abstract B1.2B-LO1, 7th Cimtec World Cerams Congress, Montecatini Terme, Italy, (1990).

[11] R.A.Mohan Ram and A.Clearfield, Chem.Mater. 3, 313 (1991).

[12] S.S.Kistler, J.Phys.Chem. 36, 52 (1932).

[13] Chemical synthesis of advanced ceramic materials by David Segal, (1989).

[14] Ultra structure Processing of Advanced Materials edited by Donald, R.Uhlman and Donald R. Ulrich (1992), Part-1, Precursors, Chemistry and Structure Development in Ultra structure Processing, pp.2-25.

[15] D.C.Bradley, R.C.Mehrotra and D.P.Gaur, Metal Alkoxides, Academic Press, London-Newyork (1978) D.C.Bradley, Chemical Rev; 89, 1317(1989).

[16] H.S. Horowitz, S.J. McLain,A.W.Sleight, J.D.Druliner, P.L.Gai, M.J.VanKavelaar J.L.Wagner, B.D.Biggs and S.J.Poon, Science,243, 66 (1989).

[17] L.C.Klein (Ed.): In: Sol-gel Technology for Thin Films, Fibers, Preforms, Electronics and Specialty Shapes, Noyes Publications, New Jersey (1988).

[18] L.Y.Hench and J.K.West, Chem. Rev. 90, 33 (1990).

[19] J.L.Woodhead, Key Eng.Materials, 72-74, 447 (1992).

[20] J.D.MacKenzie, J.Non-Cryst Solids 48, 1-10 (1982).

[21] D.R.Uhlmann, B.J.Zelinski and G.E.Wnek, In: C.J.Brinkler, D.E.Clark and D.R.Ulrich (Eds), Better Ceramics Through Chemistry, North-Holland, New York, 59 (1984).

[22] Y.Tang, B.Ling, W.Zhang, Z.Lui, X.Zheng, N.Wu, M.Shao, C.Li, K.Chen, and J.Li, Preparative and structural studies on the superconducting $YBa_2Cu_3O_{7-\delta}$ phase In the proceeding of the Beiging, 22June-1July, 1987, ed. Z.Z.Gan, G.J.Cui, G.Z.Yang and Q.S.Yang, pp. 129-44 (1987). Singapore: World Scientific Co. Ltd.

[23] F.Mahloojchi, F.R.Sale, J.W.Ross & N.J.Shah (1987), Oxide Superconductors produced by the citrate gel process. Paper number P18, at The First European Workshop on HTC Superconductors and Potential Application, Genoa, Italy, 1July(1987).

[24] R.Mahesh, R.Nagarajan and C.N.R.Rao, J. Sold. State Chem., 96, 2 (1992).

[25] C.M.Wang, T.P.Wei and H.C.I.Kao, Physica B 194-196, 2169 (1994).

[26] H.W.Zandbergen, W.T.Fu, J.M.van Ruitenbeek, L.J.de Jongh, G.van Tendeloo and S.Amelinckx, Physica C 159, 81 (1989).

[27] N.H.Wang, C.M.Wang, H.C.I.Kao, D.C.Lin, H.C.Ku and K.H.Lii, Jpn.J.Appl.Phys.28, L1505 (1989).

[28] J.C.Gachon, Pure & Appl. Chem. 66, 1823 (1994).

[29] Z.A.Munir, Ceramic Bull., 67 (2), 342 (1988).

[30] H.C. Yi and J.J.Moore, J.Matl.Sci., 24, 3456 (1989).

[31] R.Mahesh,V.A.Pavate, Om Prakash and C.N.R.Rao, Supercond. Sci. Technol 5, 174 (1992).

[32] H.Varma, K.G.Warrier and A.D.Damodaran, J.Am. Ceram. Soc.73, 3103 (1990).

[33] L.R.Pederson, G.D.Maupin, W.J.Weber, D.J.McReady and R.W.Stephens, Mater.Lett.10, 437 (1991).

[34] S.S.Manoharan, V.Prasad, S.V.Subramanyam and K.C.Patil, Physica C 190, 225 (1992).

[35] R.Mahesh, A.P.Vikram, Om Prakash and C.N.R.Rao, Supercond. Sci. Technol. 5, 174, (1992).

[36] L.E.Murr, A.W.Hare and N.G.Eror, Nature, 329, 37 (1987).

[37] R.A.Graham, E.L.Venturini, B.Morosin and D.S.Ginley, Phys., Lett. A123, 87 (1987).

[38] S.C.Schmidt, J.N.Johnson and L.W.Davison, Editors, Shock Compression of Condensed Mater, North Holland (1989).

[39] W.J.Nellis, M.B.Maple and T.H.Geballe, Proc. SPIE 878, 2 (1988).

[40] B.Morosin, E.L.Venturini, R.A.Graham and D.S.Ginley, Synthetic Metals 33, 185 (1989).

[41] M.Yoshimoto, H.Yamamoto, H.Koinuma and A.B.Swaoka, in Proc., 2nd Workshop on Industrial Application Feasibility of Dynamic Compaction Technology, Tokoyo, Japan, pp84 (1988).

[42] Z.Iqbal, N.N.Thadhani, K.V.Rao, R.Puzniak, R.Sharma, B.L.Ramakrishna, H.Eckhardt and F.J.Owens, Proc. Int.Conf., on Superconductivity, Bangalore, India,1990-Bull. Material Science14, 135 (1991).

[43] J.W.Ekin, Adv.Ceram.Mater., 2, 586 (1987).

[44] D.Dimos, P.Chaudhari, and J.Mannhart, Phys.Rev.B, 41, 4038(1990).

[45] S.Jin, T.H.Tiefel, R.C.Sherwood, M.E.Davis, R.B.van Dover, G.W.Kammlott, R.A.Fastnacht, and H.D.Keith, Appl. Phys. Lett.52, 2074 (1988).

[46] S.Jin, R.C.Sherwood, E.M.Gyorgy, T.H.Tiefel, R.B.van Dover, S.Nakahara, L.F.Schneemeyer, R.A.Fastnacht and M.E.Davis, Appl. Phys. Lett., 54, 584 (1989).

[47] P.J.McGinn, W.Chen, N.Zhu, U.Balachandran and M.T.Lanagam Physica C, 165, 480 (1989).

[48] R.L.Meng, C.Kinalidis, Y.Y.Sun, L.Gao, Y.K.Tao, P.H.hor, and C.W.Chu, Nature 345, 326 (1990).

[49] S.I.Yoo, M.Murakami, N.Sakai, T.Higuchi and S.Tanaka, Jpn.J.Appl.Phys., 33, L1000-1003 (1994).

[50] K.Heiner, J.Tenbrink, and M.Thoner, Appl. Phys. Lett.55, 2441 (1989).

[51] S.Elschner and J.Bock, Adv. Mater.4, 242 (1992).

[52] K.Tachikawa, K.Togano: Proc. IEEE, 77, 1124 (1989).

[53] M.Morita, K.Miyamoto, K.Doi, M.Murakami, K.Sawano and S.Matsuda, Physica C, 172, 383 (1990).

[54] K.No, D.S. Chung and J.M.Kim, J.Mater.Res., 5, 2610 (1990).

[55] L.Zhou, P.X.Ziang, P.Ji, K.Wang, J.R. and X.Wu, Supercon.Sci. Technol.,3, 490 (1990).

[56] D.E.Farrel, B.S.Chandrashekher, M.R.DeGuire, M.M.Fang, V.G.Kogan, J.R.Klem, and D.K.Finnemore, Phys.Rev.B, 36,4025(1987).

[57] R.H.Arendt, A.R.Gaddipati, F.E.Luborsky and L.L.Schilling, in M.R.Brodsky, R.C.Dynes, K.Kitazawa and H.L.Tuller (eds.), High-Temperature

Superconductors,Materials Research Society, Pittsburgh, PA, 203 (1988).

[58] K.Kourtakis, M.Robbins and P.K.Gallagher, J.Solid State Chem. 82, 290 (1989).

[59] T.Tomizawa, H.Matsunaga, M.Fujishiro and H.Kakegawa, J.Solid State Chem.89, 212 (1990).

[60] J.Horn, H.Borner, H.C.Semmelhack, B.Lippold, J.Herman, M.Wurlitz, M,Krotzsch, U.Boehnke, F.Schlenkrich and Ch. Frenzel, Solid state Commun. 79, 483 (1991).

[61] K.H.Song, H.K.Liu, S.Dou, and C.C. Sorrell, J.Am.Soc. 73,1771(1990).

[62] J.C.Grenier, A.Wattiaux, N.Lagueyte, J.C.Park, E.Marquestaut, J.Etourneau and M.Pouchard, Physica C173, 139 (1991).

[63] J.C.Bennett, M.Olfert, A.C.Scholz and F.W.Bosewell, Phys.Rev.B 44, 2727 (1991).

[64] Y.Koike, M.Msuzawa, T.Noji, H.Sunagawa, H.Kawabe, N.Kobayashi and Y.Saito, Physica C 170, 130 (1990).

Chapter 3

Conventional superconductivity and cuprate superconductor

There is no comparison of the era in which Onnes was in Leiden with the present period, where technologically enhanced knowledge could be applied to create new superconducting materials. Only one thing is common that both periods could not explain perfectly the phenomenon of superconductivity. This chapter is concerned with the common properties of conventional superconductors, which follow the well-known BCS theory and the materials that are in doubt due to their normal and superconducting properties. The structural and superconducting properties of lead cuprates are briefly described.

3.1 Historical introduction

The phenomenon known as superconductivity was discovered in 1911 at 4.2K in mercury by H.Kamerlingh Onnes in Leiden, just three years after he had first liquefied helium [1]. Within few years it was discovered that several other metallic elements exhibit superconductivity below liquid helium temperature. Among those metals, Nb was discovered in 1930 as a pure element with highest superconducting transition temperature of 9.25K. In 1935, the number of known superconductors was about eighty, and later it was increased slightly over one hundred. Up to 1964, at least twenty-five elements entered into the superconducting state and a large number of intermetallic alloys had shown superconductivity [2].

In 1933, W. Meissner discovered first niobium oxide (NbO) superconductor [3], and since then to 1986, a large number of oxide systems have displayed superconductivity at lower temperatures, ranging from 0.6K to 13.7K such as Rb_xWO_3 [4], Cs_xWO_3 [5], $LiTi_2O_4$ [6,7], and $Ba(Pb_{1-x}Bi_x)O_3$ [8].

In 1933, Meissner and Oschsenfeld discovered another fundamental property of superconductors, that is perfect diamagnetism [9] and later called as Meissner effect. They found that magnetic flux is expelled from the interior of the sample below the critical temperature in weak applied magnetic fields. In 1934, soon after the discovery of the Meissner effect, F.London and H. London proposed a simple two fluids model in which one has to modify the Ohm's law. London model explained the Meissner effect and predicted the penetration depth, λ, that is a characteristic length of penetration of the static magnetic flux into a superconductor, while the interior of a pure superconducting metal expels the magnetic flux. The static flux remains within a depth of λ, at the surface of the sample and the value of the penetration depth decreases exponentially towards the core of the superconductor [10].

In 1950, V.L.Ginzburg and L.D.Landau proposed a phenomenological macroscopic theory of superconductivity [11]. In 1957, A.Abrikosov [12] studied the behaviour of superconductors in an external magnetic field and discovered that one can distinguish two types of superconductors called as type-1 and type-11. Type-1 expels magnetic flux completely while type-11 does it completely only at small magnetic fields, but partially in higher applied fields.

In 1957, J.Bardeen, L.Cooper and R.Schrieffer [13] proposed a complete microscopic theory of superconductivity and later known as the BCS theory. The BCS theory involves a loose association of electrons into pairs through exchange of phonons, known as Cooper pair, carries twice of electronic charge, zero spin similar to Boson. These pairs are supposed to move co-operatively through the lattice in such a manner that electron-phonon collisions are avoided, so that there is no heat dissipation due to scattering of electron.

In 1962, B.D.Josephson proposed an interesting quantum tunnelling effect that should occur when supercurrent tunnels through an extremely thin layer of an insulator. The voltage drop across the insulating thin layer is zero when condensed electron pair (Cooper pair) tunnels through it. His predictions were confirmed within a year and the effects are now known as the Josephson effects [14, 15].

In 1971, there was discovery of a new class of ternary molybdenum chalcogenides of the type $M_xMo_6X_8$, where M stands for large atomic number of metals and rare earth›s and x for the chalcogens; S, Se or Te. The highest T_c in the series is obtained in $PbMo_6S_{7.2}$, whose value is 14.5K and has also an unusual high critical field (H_{c2}, 0K) of 58Tesla [16]. The large values of the upper critical field as compared with Nb_3Sn and NbTi make these materials interesting for making wires and critical currents as high as $3x10^5 A/cm^2$ at 4.2K [17].

An historical excitement also exist in the era of 1980, when first organic superconductor was reported with T_c<1K, where charge transfer occurs between an organic cation molecule and an inorganic anion complex. The π orbitals in the cations are responsible for the metallic conductivity. Now, there are many organic superconductors, showing anisotropic behaviour similar to cuprate, among them few conduct only along one direction and many have conductivity in plane only. The excitement was enhanced with the discovery of K_3C_{60} 'fullerance', initially a term used for C_{60} molecule doped with K and has a structure similar to soccer ball with carbon atoms on a truncated icosahedron, with T_c of 18K [18] and later was increased by 31.3K in Rb_2CsC_{60} [19]. In 1973, before the recent discovery of HTSC materials, the record highest superconducting phase transition temperature (T_c) was 23.2K for Nb_3Ge [20]. In 1986, G.Bednorz and K.A.Muller [21] found superconducting ceramic oxides, closed to 35K ($La_{2-x}Sr_xCuO_4$). They had taken the point of view that higher T_c values might be found in materials in which the Jahn-Teller effect could enhance the electron-phonon coupling parameter.

In1987, Paul Chu [22] designed an exciting and excellent superconducting ceramic ($YBa_2Cu_3O_7$) with T_c~92K, as the first superconductor above liquid nitrogen temperature. Only a year later, early 1988, Bi- and Tl- cuprate oxides [23, 24] were discovered with T_c~110 and 125K respectively. All these cuprates are anisotropic and hole doped where mainly CuO_2 planes are responsible for superconducting transition temperature.

In 1989, Tokura et al. discovered the first electronic HTSC, $Nd_{2-x}Ce_xCuO_{4-\delta}$ among the oxide cuprates with superconducting transition temperature of 24K [25]. The majority carriers are electrons rather than holes and for this reason the cuprate is termed as n-type. In this material the reducing ions Ce^{4+} can add electrons to the copper

atoms, driving the valence from 2+ to 1+, that is essential for n-type copper-oxide plane in cuprate. More recently, mercury cuprate, $HgBa_2Ca_2Cu_3O_{8+\delta}$ (Hg-1223), a layered structure with three CuO_2 sheets has been synthesised under extremely high oxygen pressure (at 238Kbar) with T_c of 157K [26, 27].

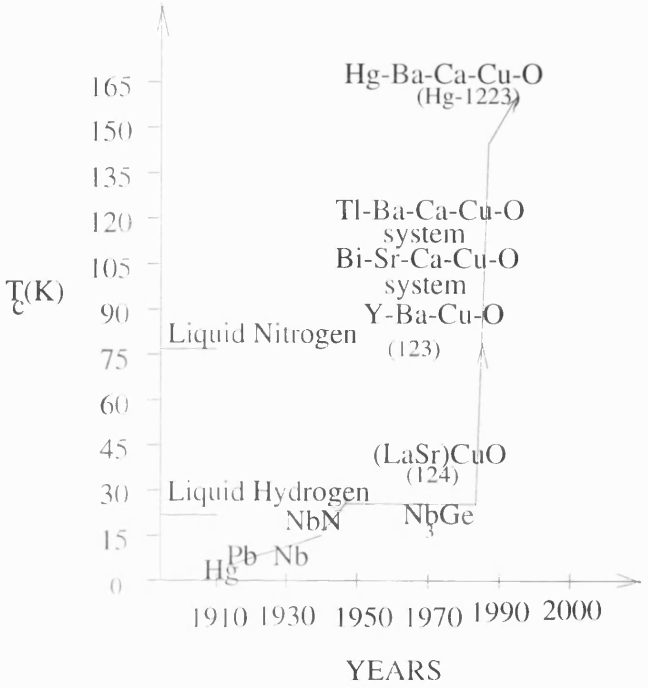

Figure 3.1. *The evolution of superconducting transition temperature.*

At the time of discovery of superconductivity, there was not any theory to explain even metallic character in solids, and it was not surprising that the phenomenon could not be explained. However, although quantum mechanics has found a satisfactory explanation for most metallic phenomena and even for conventional superconductors (low T_c, before 1986), but the superconductive and normal state properties of high HTSC cuprate are still in the second stage of debate, whereas superconducting transition temperature is unpredictable at what level it will reach. *Table 3.1* shows different oxides superconducting materials discovered up to 1993.

3.2 The superconducting properties

There are six properties of conventional superconductors [33] that must be satisfied by any proposed theory and it is necessary to demonstrate main features for any kind of superconductor as a zero resistance ($\rho=0$ for all $T < T_c$) plus perfect diamagnetism ($B=0$, inside the superconductor).

TABLE 3.1. *Some of the old and new oxide superconductors, their maximum transition temperature, author of paper and year of discovery.*

System/ Notation	Year of discovery	T_c(K)	Author / Reference
NbO	1933	1.2-1.5	Meissner/ [3]
$SrTiO_{3-\delta}$	1964	0.7	Schooley/ [28]
$Li_{1+x}Ti_{2-x}O_4$	1973	13	Johson/ [29]
$Ba(Pb_{1-x}Bi_x)O_3$	1975	13	Sleight/ [8]
$(La_{1-x}A_x)_2CuO_{4+\delta}$ A=Ba, Sr / 214	1986	35	Bednorz/ [21] First HTCS
$RBa_2Cu_3O_{7-\delta}$, R=Y,La,Nd,Sm,Eu,Gd,Dy,H0,Er,Tm,Yb, and Lu/ 123	1987	95	Wu/ [22], superconductor above liquid nitrogen.
$Ba_{1-x}K_xBiO_3$	1988	30	Mattheis/ [30]
Bi-Sr-Ca-Cu-O/ Bi-2201,-2212, Bi-2223	1988	115	Maeda/ [23]
Tl-Ca-Ba-Cu-O / Tl-2021,-1122,-1223, Tl-1324	1988	125	Sheng/ [24]
$Pb_2Sr_2(R_{1-x}Ca_x)Cu_3O_8$ / Pb-2213, Pb-1212	1988	70	Cava/ [31]
$Ln_{2-x}Ce_xCuO_{4-\delta}$/ Ln-214, Ln=Pr, Nd, Sm	1989	24	Tokura/[25], first n-type cuprate
$(La_{1-x}Sr_x)_2CaCu_2O_6$	1990	60	Cava/ [32]
$HgBa_2Ca_2Cu_3O_{8+\delta}$/Hg-1223	1993	133-150	Antipov and Chu/ [26, 27]

3.2.1. Zero resistance

At the superconducting transition temperature, T_c, the material displays zero resistance to direct currents (DC) as well as low frequency alternating currents. A typical superconductor loses its resistivity as frequencies enter the microwave regions. There is a limit on a current density for a particular superconductor below T_c, that keeps the sample in superconducting state and above that limit, the sample returns to normal state known as critical current density J_c.

3.2.2. Meissner effect

The discovery made by Meissner and Ochsenfeld is related to a zero resistivity and formation of a magnetic field that converts the superconductor as a perfect diamagnetic material. It implies that in a magnetic field, superconductors develop surface currents that give rise to magnetic fields that exactly cancel the applied magnetic field, leaving a field free bulk. This shows that the exclusion of the magnetic field from the interior of a superconducting specimens is direct evidence that the superconducting state is not simply one of zero resistance that could be achieved from the perfect conductivity but would not show any diamagnetism. The superconductor has a magnetic moment (M) (related to the surface screening currents) that equals and opposes the applied magnetic field. The applied field can not exceed a limit called a critical magnetic field, H_c, at certain temperature below a superconducting transition temperature, the sample otherwise returns to normal state. The reduction of the applied field or the temperature to below their critical values can change the status of the phase transition.

3.2.3. Specific heat

Cooling a superconductor below its critical temperature without the influence of a magnetic field increases the specific heat of the metal without formation of latent heat. If the same superconductor is forced back into a normal state through the introduction of a magnetic field, the lattice specific heat does not change, but the conduction electrons are altered. A similar specific heat anomaly occurs when liquid helium ($^2He_4$) becomes superfluid. For a metal in the normal state, the total specific is the sum of the term arising from the lattice vibrations (the Debye's law term) and one directly proportional to

the absolute temperature representing the temperature-dependence of energy for a Fermi-electron gas.

3.2.4 Isotope effect

This effect was first time reported by Reynolds et al. in 1950 [34]. They found that the superconducting transition temperature for the isotopes is inversely proportional to the square root of the mass of isotope, M, of the same element ($T_c \propto M^{0.5}$). This effect is generally regarded as the important measure of the electron-phonon interaction. One conclusion from this observation is that the crystal lattice structure determines the properties of the electrons or holes found in these elemental isotopes and superconductivity is connected with phonon mediated electron interactions. In some cuprate superconductors such as $La_{2-x}Ba_xCuO_4$, the isotope effect is sufficiently large to indicate that the phonons play major mediating role in the attractive interactions between electrons [35]. The isotope effect in the $Ba_{1-x}KBi_xO_3$ and K_3C_{60} systems suggesting phonon mediated mechanism whereas this mechanism for Y-Ba-Cu-O and Bi-Sr-Ca-Cu-O systems is very small for oxygen isotopes, and electron-phonon mechanism alone is not successful to explain this effect [36].

3.2.5. Coherence length

In 1950, Ginzburg-Landau introduced a theory in which a complex pseudo-wave function, $\psi(r)$, is related to the local density of ordered electrons $n_s \equiv N_s/V = |\psi(r)|^2$. They introduced a temperature dependent coherence length, $\xi(T)$, that is the shortest distance within that there may be an remarkable change in pair wave function. It can vary with the impurity content of the superconductor, related to the scattering of electrons by the impurities that shortens the coherence length and also increases the normal resistivity. In 1953, Pippard reported that the superconducting wave function should have a characteristic length, ξ_0, that plays a role analogous to an electron mean free path, *l*, in a normal metal where it varies rapidly with alloying and causes an increased electron-impurity scattering. It was defined as

$$\xi_0 = \alpha \hbar V_F/(k_B T_c) \qquad (3.1)$$

where, V_F= Fermi velocity, k_B= Boltzmann's constant, $\hbar = h/2\pi$, h= Plank's constant,

$\alpha = -(e\hbar H_{c_2})/m$ where 'm' is the mass of electron and H_{c_2}=upper critical fields.

The BCS theory that will be described in detail in section 3.3.2, defines a temperature

independent coherence length, ξ_0, as the length over which the electrons in a Cooper pair remains correlated and could be considered as a kind of microscopic dimension of a pair presented by following equation

$$\xi_0 = hV_F/\pi\Delta(0) \qquad (3.2)$$

where h, V_F, and $\Delta(0)$ are the Fermi velocity, Plank's constant and gap parameter at absolute temperature respectively. It is an intrinsic property of the material and one can estimate ξ_0 by tunnelling or optical absorption.

3.3.1 Type-I and type-II superconductors

Abrikosov [12] classified the superconducting materials as type-1 and type-11, according to their magnetic behaviour. The type-1 expels the applied magnetic flux completely from their interior, while type-11 does it completely only at small fields, and partially in higher applied fields.

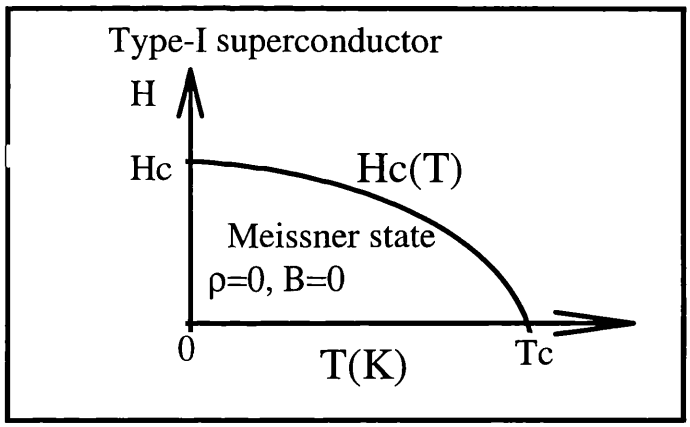

Figure 3.2. *Schematic diagram of H_c (T) for type-1 superconductor.*

In type-II superconductors, one is lower critical field H_{c1} below which a complete flux exclusion is observed and other is upper critical field H_{c2}. At fields above H_{c1} the flux partially penetrates into the material until the upper critical field and the superconductivity is destroyed. A type-II superconductor has also zero resistivity in between H_{c1} and H_{c2}, although it consists of a mosaic of vortices of normal and superconducting regions.

For a type-I superconductor, the wave-functions are coherent over much larger distances than the penetration depth, and it takes less energy to create a single external barrier between the magnetic field and the superconductor than it does to permit a

filamentary structure. Interface energy decays into the superconductor over a penetration depth (λ) while the superconducting wave function falls to zero at the surface over a coherence length (ξ). Penetration depth (λ) can be defined in simple way as the distance in which B decreases by a factor of 1/e (where e is the base of the natural logarithm $\approx$ 2.71828). The ratio of λ to ξ is known as Ginzburg-Landau constant, $K = \lambda/\xi$. At a critical field H_c the magnetic energy is equal to the condensation energy so that the perfect diamagnetism is not energetically favourable. The superconducting sample becomes normal and the magnetic force fully penetrates the sample. The variation of the critical field with the temperature for type-I superconductor is approximately parabolic (figure 3.2) and often referred to as Tuyn's law:

$$H_c = H_0 [1 - (T/T_c)^2] \qquad (3.3)$$

where H_0 is the extrapolated value at T=0.

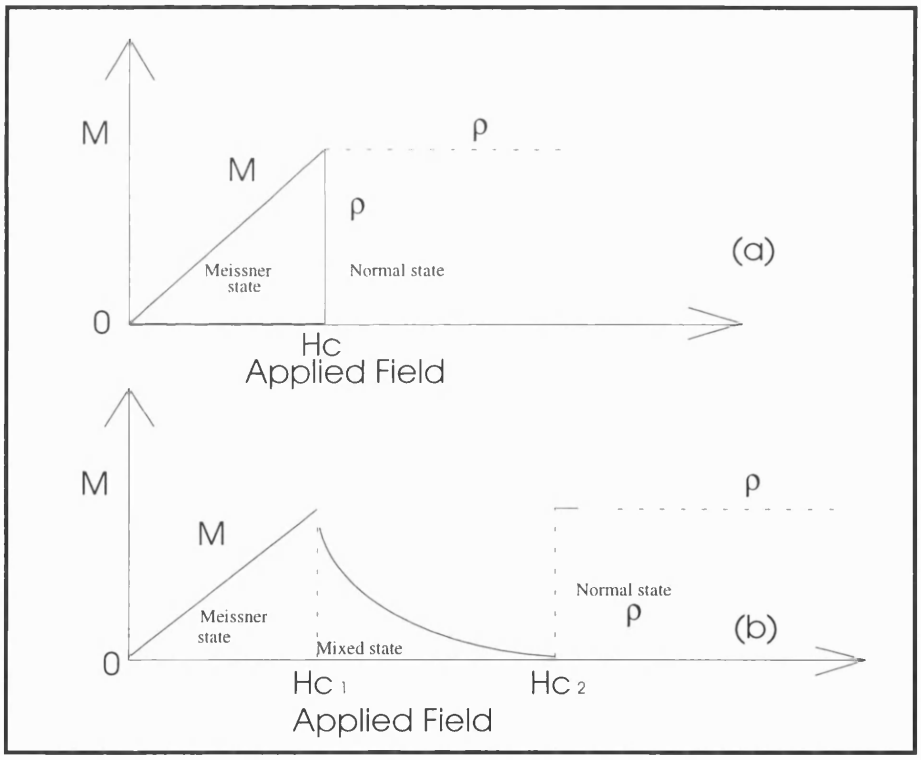

Figure 3.3. *Variation of magnetisation (-M) and resistivity (ρ) of an (a) type-I and (b) type-II superconductor as a function of the applied magnetic field (H).*

In type-II superconductors where ξ is less than λ, the interaction energy of the normal-tubes or filaments lead to mutual repulsion, ensuring that in a perfectly crystalline solids they would take up a regular array, equally spaced on a triangular lattice, whose spacing is a function of applied field. Each filament carries a magnetic flux Φ_0=

$h/2e=2.067x10^{-15}$ Weber, where h is the Plank's constant and e is the charge of the electron. The magnetic induction is directly related to the number of vortices per square meter. The differences in magnetic behaviour between type-I and type-II superconductors are presented in figure 3.3, showing the superconductor's magnetisation, M, and resistivity, ρ, versus applied field intensity, H.

3.3.2 BCS theory

In 1957, Bardeen, Cooper and Schrieffer [37] presented a theory known as BCS theory on the ground of Frolich's idea about the electron-phonon interaction in a periodic lattice to couple two electrons together. The coupled electrons behave in such a way that there is a direct interaction between them through the transmission of phonon in the presence of lattice ion. One electron emits a phonon that is then immediately absorbed by another. Cooper [38] went on to show that if two electrons are added to a metal at absolute zero, an attractive interaction between them, however weak, will result in the formation of an electron pair whose total energy is less than twice of the Fermi energy ($2E_F$) so that they can follow the Pauli's principle. This reduction in energy is maximised if the pairing occurs between electrons with equal and opposite momenta as well as spins are termed as Cooper's pair. This reduction of potential energy due to pairing exceeds the amount by which the kinetic energy is in excess of $2E_F$.

Bardeen, Cooper and Schrieffer postulated mainly two points to apply Cooper's results to many interacting electrons:

i) only Cooper pair interactions are significant in a superconductors,

ii) all non Cooper pair electrons in a superconductor only serve as limiters on the states into which the interacting pair can be scattered.

There is a limit to a number of electrons that can be raised from $\mathbf{p}<\mathbf{p}_F$ to form Cooper pairs. In order that a pair of electrons may be scattered from $(\mathbf{p}_i\uparrow,-\mathbf{p}_i\downarrow)$ to $(\mathbf{p}_j\uparrow,-\mathbf{p}_j\downarrow)$ where $\mathbf{p}_x$ corresponds to electron with momentum $\mathbf{p}$ in state x and arrows denote spin up or down of the electrons, the dispersion requires that the states $(\mathbf{p}_i\uparrow,-\mathbf{p}_i\downarrow)$ must be occupied and the states $(\mathbf{p}_j\uparrow,-\mathbf{p}_j\downarrow)$ must be empty. As the electrons form the Cooper pairs, the probability that the $(\mathbf{p}_j\uparrow,-\mathbf{p}_j\downarrow)$ will remain empty becomes increasingly small. Thus the scattering process becomes limited and the negative potential energy

decreases. Finally, a level is reached where the potential energy can not offset the kinetic energy and the total energy will not be lower by forming Cooper pairs. There is an optimum arrangement that gives the lowest overall energy and this can be described by the probability h_i of the pair state ($\mathbf{p}_i\uparrow,-\mathbf{p}_i\downarrow$) being occupied and given by

$$h_i = 1/2\ [1-(E_i-E_F)/\{(E_i-E_F)^2 + \Delta^2\}^{1/2}] \quad (3.4)$$

where $E_i=\mathbf{p}_i^2/2m$. The quantity Δ which has the dimensions of the energy is given by,

$$\Delta = 2hV_L \exp[-\{N(E_F)V\}^{-1}] \quad (3.5)$$

where V_L is the average vibrational frequency of the lattice, $N(E_F)$ is the density of the states for electrons at the Fermi energy and V is the strength of the (lattice mediated) attractive electron-electron interaction. Thus the state of lowest energy or ground state occurs when all electrons with a given momenta are bound in Cooper pairs with opposite momentum and spins. This kind of ground state is called condensed state.

Cooper pairs have lower energy than two corresponding single electrons. Thus Cooper pair formation results in the lowering of the energy of the overall system by an amount equal to the binding energy of condensed pair. This leads to the formation of an energy gap in the electronic energy spectrum of a superconductor by an amount denoted by 2Δ. If the superconductor is excited to a higher state, by raising the temperature or by electromagnetic radiation of an appropriate wave length, energy is imparted to the Cooper pairs, and the minimum amount of energy used to break up a Cooper pair is 2Δ, known as the energy gap. At 0K the energy gap is at its maximum value, denoted by $2\Delta(0)$. As the temperature is increased towards T_c, the break-up of Cooper pairs increases and thus reducing the energy gap. The energy gap falls to zero at the critical temperature, T_c. A relationship between the energy gap T_c and at 0K can be written by :

$$E_g(0)=2\Delta(0) \quad (3.6)$$

or

$$3.5k_BT_c=2hV_L \exp[-\{N(E_F)V\}^{-1}]$$

The temperature variation of the energy gap predicted from BCS theory is shown in figure 3.4.

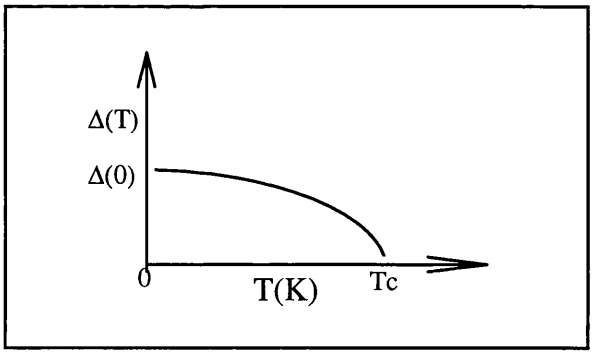

Figure 3.4. Temperature versus superconducting energy gap Δ(T).

3.4.1 Common properties of high temperature superconductors (HTSC)

All the superconducting cuprates have the most significant common properties which differ from conventional superconductors. Among them, a very small coherence length and anisotropic behaviours in normal and superconducting states are prominant. The conventional superconductors have ξ~500Å to 10,000Å while cuprate superconductors have ξ~12Å to 17Å along CuO_2 planes whereas along c-axis of crystals it is only 2Å to 5Å that is even smaller than the interplane distances. In metals the magnetic susceptibility and the Hall coefficient are temperature independent. In the normal state the conductivity is much higher in CuO_2 planes or sheets along the a- or b-axis of the cuprate-crystals than it is perpendicular to the planes (along c-axis). One can also observes the anisotropy in supercurrent-transport, penetration depth, λ, and critical magnetic fields. The value of the H_{c2} is much higher for cuprates than any other kind of superconductors [39, 40]. Now, it is well known that HTSC cuprates exhibit bulk superconductivity over a limited compositional range. At optimal stoichiometry, materials can be single phase, but as one moves away from the optimum, microscopic inhomogenieties are induced, and further deviation from optimum leads to phase separation. Such inhomogeniety can cause a reduction in mean free path 'l', thereby moving the material closer to the 'dirty limit' [41]. From the brief survey of the crystal structures of the most commonly known families of new superconductors, it is found that these materials crystallise with (intergrowth) an alternating sequence of layers of different crystallographic structure that have an epitaxial matching of bond lengths across the interlayer interfaces. Tokura et al.[42] proposed that the superconducting CuO_2 planes or sheets are separated by charge reservoir layers that act to control the charge on the superconducting planes (through the chemical substitution) either

through insertion of holes or electrons. It is now well known that the most fundamental structure for the production of superconductivity in the cuprate is CuO_2 plane (or sheets if the planes are buckled) with 180° Cu-O-Cu bonds. In between the CuO_2 layers there are other metal-oxide isolation layers (also called charge reservoirs), more or less ionic in nature, where the commonly used metal atoms are La, Sr, Ba, Y, Tl, Pb, Bi or Hg. There is not any direct relationship of transition temperature and carrier concentration in the cuprate superconductors. For example, the Tl-Ba-Ca-Cu-O and Bi-Sr-Ca-Cu-O materials with three CuO_2 layered structures, show T_c around 110 to 125K respectively, whereas LaSrCuO material has very low T_c~40K but has almost the same number of charge carriers per copper atom (0.15-0.2). From the literature survey it is found that the T_c for each material maximising for three CuO_2 layers. The single CuO_2 layer cuprate support a T_c of around 40K, the double CuO_2 layers 80-90K and three CuO_2 layers cuprates 110-125K. Aside from the demonstrated correlation with the number of copper-oxygen planes in the structure where T_c first increases before plateauing and then decreases in Bi-Sr-Ca-Cu-O and Tl-Ba-Ca-Cu-O systems [46], the most clearly established correlation is between T_c and the carrier concentration with in the material [47]. Shafer and Penney demonstrated that although there are distinct T_c versus hole relationships for each cuprate, a broad maximum at around 0.20 holes per copper plane is obtained for all the systems such as La-214, Sr-214, Y-123, and Bi-2122 [47]. The most common features are given as:

i) all cuprate superconductors can be considered to be a result of the intergrowth of perovskite layers of $ACuO_{3-x}$ with AO-type rock-salt layers leading to the general formula $[ACuO_3]_n[AO]_{n'}$. However, $YBa_2Cu_3O_{7-\delta}$ compound has not rock-salt layers and may be considered as the $n'=0$ member of this general family.

ii) all the cuprates possess CuO_2 plane or sheet that is responsible of superconductivity, and sandwiched between certain charge reservoirs block or layers(e.g. BiO, PbO, CaO, TlO).

iii) The Cu-O bonds in the cuprates are highly covalent. There is sufficient experimental evidence to believe that the Cu(3d)-O(2p) hybridisation is strong while the Cu-O charge-transfer energy is small. The CuO_2 sheets have high electronic polarizability.

iv) The parent materials in all superconducting ceramic families exhibit antiferromagnetic non-metalic behaviour. For example, La_2CuO_4, $YBa_2Cu_3O_6$, Nd_2CuO_4, $Pb_2Sr_2YCu_3O_{8+\delta}$ are parent non-metals of $La_{2-x}Sr_xCuO_4$, $YBa_2Cu_3O_7$ and $Nd_{2-x}Ce_xCuO_{4-\delta}$, $Pb_2Sr_2(Y_{1-x}Ca_x)Cu_3O_{8+\delta}$ superconductors.

v) All the cuprates have mixed valent copper, and oxygen stoichiometry, homogeneity and disorder play an important role in superconducting properties.

3.4.2 Granularity and weak links

The critical current density of any material is one of the most important parameters for technical applications. The HTSC materials exhibit high values of critical current ($\sim 10^7 A/cm^2$) in single crystals or oriented films. But, almost all the families of cuprate superconductors exhibit some degree of granularity in bulk shapes where inter-grain contacts are formed. These contacts or weak-links behave like Josephson junctions. This is considered due to random orientation of the crystals in bulk cuprates and responsible of lowering critical current in polycrystalline materials than that with in a single crystals or oriented textured layers. Therefore, the problem of weak-links in these materials can be solved using grain alignment parallel to the a-b CuO_2 planes in cuprates through substrate-induced texturing or melt-texture solidification under temperature gradient. Till now, the exact nature of the grain boundary weak-links is not too obvious. However, initially it was considered because of the presence of amorphous layers at the grain boundary or microcracks [43]. More recently published reports suggested the existence of cation compositional deviation and oxygen non-stoichiometry at the grain boundaries as one of the main reasons of weak-link behaviour [44, 45].

3.4.3 Substitutional chemistry of cuprates

All the copper oxide superconductors have parent structures with antiferromagnetic (CuO_2) sheets; the superconductors have a mixed valence in the CuO_2 sheets. This means there is an antiferromagnetic ordering of the localised spins on the copper atoms of the CuO_2 layers. The oxygen co-ordination at a copper atoms may vary from 2 to 6. Linear two fold co-ordination or tetrahedral four fold co-ordination are commonly

associated with Cu(I). The copper(II) ion is found in the structure of cuprate superconducting materials in the form of square-coplanar, square pyramidal or octahedral, with a Jahn-Teller distortion. Oxidation of the CuO_2 sheets provides p-type superconductivity while reduction of the CuO_2 sheets gives n-type superconductivity. As the charge carriers are introduced, the long range antiferromagnetic order is destroyed and metallic regime entered. At low temperature it is this metallic phase that enters the superconducting state. Whether the (CuO_2) sheet can be oxidised or reduced sufficiently to become superconductive appears to be controlled principally by the Cu-O bond length and the oxygen co-ordination number of the copper atoms, both of which are strongly influenced by the non-superconductive intergrowth that stabilizes the parent structure. The mechanism by which the induction of charge carriers occurs varies from system to system. In an intergrowth structure, the oxidation or reduction of the CuO_2 sheets can be achieved in several manners such as aliovalent substitution, cation deficiency and increasing or decreasing anions. For example:

i) aliovalent cation substitution in the inactive layers as in $La_{2-x}Sr_xCuO_4$ [48] or $Nd_{2-x}Ce_xCuO_4$ [25].

ii) aliovalent anion substitution in the inactive layers as in $Nd_xCuO_{4-x}F_x$ [49].

iii) insertion of excess oxygen into the inactive layers; as in $La_2CuO_{4+\delta}$ [50] $YBa_2Cu_3O_{6+\delta}$ [48], or $Bi_2Sr_2Ca_{n-1}Cu_nO_{2n+4+n}$ [52, 53, 54];

iv) aliovalent cation substitution for non-copper cations in the superconductive layers as in $Sr_{1-x}Nd_xCuO_2$ or $Sr_{1-x}Ca_xCuO_2$ [55]; and

v) overlap of a conduction band or a redox level in the non-superconducting layer with the Cu(III/II) redox band in the superconducting layer, which results in an internal redox reaction as in $Tl_2Ba_2Ca_{n-1}Cu_nO_{2n+4-\delta}$ [56, 57, 58].

The easiest mode to change the carrier concentration is just changing the oxygen content where the superconductivity is destroyed either by having few holes ($P<0.05$ per CuO_2 plane) or too many ($p> 0.27$ per CuO_2 plane) in most of the cuprates. The advantage of this technique is that the carrier content can be varied in the same sample simply by heat treatments under different oxygen partial pressures or annealing in inert ambient [59]. When the valence of copper is +2, the electrons are localised in a copper-oxygen bond. In some cases, when additional oxygen atoms are present in the compound further electrons can be pulled away from the copper atoms, pushing the average valence of copper ions towards 3+, where the formation of Cu ions with the

valence greater than 2 (oxidation of Cu) implies the addition of a positive charge carrier (hole). The reverse process can create deficiency of the oxygen atoms and reduction of some Cu atoms that can adjust the carrier concentration necessary for optimised superconducting properties of the materials such as $Pb_2Sr_2(Y_{1-x}Ca_x)Cu_3O_{8+\delta}$.

3.5 Lead cuprate superconductors

In this section a review of the structural and electronic properties of $Pb_2Sr_2(Y_{1-x}Ca_x)Cu_3O_{8+\delta}$ and $[Pb_{1-y}(Cu,Sr)_y]Sr_2(Y_{1-x}Ca_x)Cu_2O_{7-\delta}$ phases is presented, with the object of assessing the inherent difficulties in obtaining optimum superconducting transition temperature and minimal transitional width.

3.5.1 $Pb_2Sr_2(Y_{1-x}Ca_x)Cu_3O_{8+\delta}$ phase

Structural Properties

A property common to all the copper oxide superconductors (cuprate) is the high covalency of the Cu-O bonds and two-dimensional character of the copper-oxygen framework closely related to that of the perovskites. Thus a large family of layered cuprates with the general formula $[ACuO_{3-x}]_m.[AO]_n$ can be considered. Such a class of oxides corresponds to the intergrowth of multiple oxygen-deficient perovskite layers $[ACuO_{3-x}]$, with rock-salt-type layers AO[60]. They can be represented by the symbol [m, n], where m and n denote the number of copper layers and [AO] layers in the perovskite and rock-salt slab respectively. Divalent lead, $Pb^{2+}$is similar to Bi(111) and Tl(I), in the respect that it has a $6s^2$ lone pair and is a potential cation for the generation of layered-structures [61]. Thus it is interesting in the synthesis of cuprates for which two dimensional property of the structure appears as an important factor for superconductivity. Cava et al.[64] utilised this idea by the synthesis of the $Pb_2Sr_2Ln_{1-x}Ca_xCu_3O_{8+\delta}$ (Ln=Y, or rare earth elements) superconductor. The structure of this phase consists of double pyramidal layers $[(CuO_{2.5})_2]_\infty$ interfaced with calcium and yttrium ions, as already observed in the bismuth and thallium oxides and in $YBa_2Cu_3O_7$, associated with single rock-salt-type layers $[(Sr, Pb)_1 O]_\infty$ similar to those observed in La_2CuO_4-type oxides. The rock-salt layers are themselves connected through layers of monovalent copper, with Cu(1) in two-fold co-ordination,

showing a great resemblance with $YBa_2Cu_3O_6$. *Figure 3.5.a,* shows the $Pb_2Sr_2YCu_3O_8$ structure which consists of double oxygen-deficient perovskite layers and single perovskite layers intergrown with single rock-salt-type layers $[(Pb, Sr)_1 O]_\infty$. The sequence of layers is -(Y)o-(CuO_2)c-(SrO)o-(PbO)c-(Cu)o-(PbO)c-(SrO)o-(CuO_2)c-(Y)o-, where the subscript o and c indicate whether the cation is at the origin or at the center of the mesh, respectively.

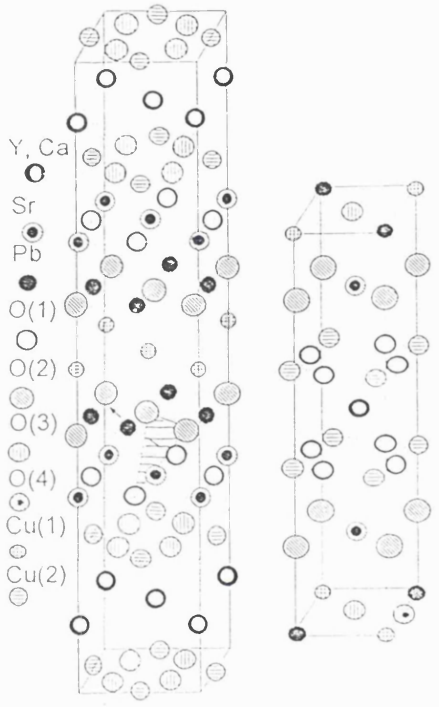

(a) Layering sequence of Pb-2213 phase **(b)1212-PSYCCO**

Figure 3.5. a) *The structure of $Pb_2Sr_2YCu_3O_8$ showing the sequence of layers perpendicular to the c-axis (adapted from [62]). b) The elementary cell of $(Pb_{1-y}Cu_y)Sr_2(Y_{1-z}Ca_z)Cu_2O_7$ where oxygen O(4) is the site of the excess oxygen (adapted from [63]).*

All oxygen atoms are absent in the (Y) and (Cu) layers. The (CuO_2) (SrO) blocks create pyramidal CuO_5 layers which represent one of the common features for most of the cuprate superconductors. The Sr ions are surrounded by 9 oxygen atoms similar to the La-polyhedron in La_2CuO_4. The Y cations are surrounded by 8 oxygen atoms forming a prismatic polyhedron common to all cuprates containing the (CuO_2)-(Ln)-(CuO_2) blocks in which Ln is either a rare-earth element or Ca. The Pb cations are surrounded by 5 oxygen atoms arranged as pyramid. The Pb-O distances vary over a large range with three short distances forming a triangle and two long ones, that is due

to the 'lone pair' of electrons of Pb^{2+}. The copper cations of the oxygen-deficient Cu layer inserted between PbO layers exhibit the stick (linear) co-ordination that may not be linear because of the oxygen disordering exists in the PbO layers. It is worth pointing out that such an oxide can be obtained as a superconductor when it is synthesised in a reducing ambient or either at higher temperature (920°C) where oxygen soaking is very small to keep the Cu as monovalent in PbO-Cu-PbO layer.

Table-3.2. *A comparison of the calculated and observed x-ray spectra of* $Pb_2Sr_2(Y_{0.5}Ca_{0.5})Cu_3O_{8+\delta}$ *material (After P.Goodman et al.[67]).*

h k l	$d_{obs.}$(Å)	$I_{(calc.)}$	$I_{(obs.)}$	h k l	$d_{obs.}$(Å)	$I_{(calc.)}$	$I_{(obs.)}$
0 0 1	15.82	31.9	28.1	2 0 2	2.56	9.0	2.7
0 0 2	7.91	6.5	14.1	2 0 3	2.40	10.19	1.4
0 0 3	5.27	5.6	9.4	0 2 4	2.25	4.7	3.6
0 0 4	3.95	2.9	12.5	2 0 4	2.24	4.6	0.7
1 1 0	3.82	11.0	9.8	1 1 6	2.17	10.9	11.6
1 1 1	3.72	19.7	21.4	0 2 5	2.09	5.4	1.1
0 0 5	3.15	17.5	17.0	2 0 5	2.06	5.4	16.1
1 1 3	3.10	11.8	11.6	0 0 8	1.91	8.7	10.7
1 1 4	2.74	100.0	100.0	2 2 0	1.97	31.8	32.1
2 0 0	2.71	35.2	32.1	1 3 4	1.59	16.8	15.2
				3 1 4	1.57	16.6	17.0
0 2 1	2.69	6.6	28.6				
2 0 1	2.67	6.5	2.7				
0 0 6	2.63	1.8	5.4				

Neutron diffraction techniques also show that the Pb_2Sr_2 $(Y_{1-x}Ca_x)$ $Cu_3O_{8+\delta}$ (Pb-2213 phase) has an orthorhombic unit cell [64, 65], and is more complex than the earlier known materials due to the intermediary PbO-CuOδ-PbO layer. The compound deviates slightly from tetragonal symmetry, (space group: Cmmm) with lattice parameters a=0.53933(2), b=0.54311(2), and c=1.57334(6)nm [62]. The origin of the orthorhombic symmetry distortion of these materials is evidently caused by the disordering in the a-b plane of the oxygen atoms of the PbO layers over the general position (0, 0, z) of the space group with x = 0.0275(5) and y = 0.0402(5)nm. This disorder is considered to be due to the lone-pair of the electrons associated with the

Pb^{2+} cations which repel the oxygen atoms in the PbO layers away from their symmetric position, leading to the orthorhombic distortion. Two opposite basal oxygen atoms of the pyramid, surrounding the Pb^{2+} move closer to the cation while the other two move further away. This arrangement satisfies the irregular co-ordination requirement of the Pb^{2+}(lone-pair) ion within its square pyramidal oxygen environment [62, 66] (See for example *figure 3.5.a*). As oxygen level in the structure increasing in Pb-2213 phase to $O_{9.47}$, disordering increases due to oxidation of $Pb^{2+}$to Pb^{4+} and also the disordered oxygen induces changes in the co-ordination of all cations [67]. In these layers of the Pb-2213, the Pb is in a divalent state, and the oxygen non-stoichiometry has a value of $\delta \cong 0$ in the superconducting state. In this phase, the electronically active double CuO_2 pyramidal layers are separated by more than 1.5nm, making the material highly two dimensional from a structural point of view, and further can be increased by the substitution of Ca for Y as a bigger cation. A comparison of the experimental and calculated powder x-ray diffraction pattern (XRD) is given in *table 3.1.*

Table 3.3. *XRD data for a $Pb_2Sr_2(Y_{0.6}Ca_{0.4})Cu_3O_{9-\delta}$ phase obtained on powder ground from a single crystal (After J.S.Xue et al.[68]).*

h k l	d(Å)	h k l	d(Å)	h k l	d(Å)	h k l	d(Å)
0 0 2	7.906	0 0 6	2.628	3 1 0	1.703	2 3 5	1.355
0 0 3	5.254	0 0 7	2.254	3 1 1	1.694	4 0 0	1.345
0 0 4	3.947	0 2 4	2.233	1 1 9	1.593	4 1 3	1.268
1 1 0	3.822	1 1 6	2.165	0 0 10	1.576	1 1 12	1.242
1 1 1	3.716	0 2 5	2.005	1 3 4	1.572	1 3 9	1.225
1 1 2	3.440	2 0 5	2.047	3 1 4	1.563	2 4 0	1.211
1 1 3	3.093	0 0 8	1.971	2 2 6	1.545	4 2 0	1.205
1 1 4	2.745	2 2 0	1.910	2 2 7	1.456	4 1 7	1.130
0 2 0	2.710	0 0 9	1.752	2 3 3	1.444		
2 0 0	2.692	0 2 7	1.732	0 0 11	1.433		
0 2 1	2.672	2 2 4	1.719	2 2 8	1.371		
2 0 1	2.654	1 3 0	1.713	0 2 10	1.363		

Divergence between these results arise from (i) a possible preferred orientation effects in the sintered pellet used and

(ii) from the assumption made in the calculations of a random distribution of species within the Ca-Y plane. The XRD data for the $Pb_2Sr_2(Y_{0.6}Ca_{0.4})Cu_3O_{9-\delta}$ material obtained from powder (ground single crystals) has also been included with the lattice

parameters a=5.383(1)Å, b=5.423(1)Å and c=15.765(2)Å in table 3.3. Scanning electron microscopy of polycrystalline samples and single crystals of the Pb-2213 phase generally show a plate-like morphology [64]. High resolution electron microscopy (HREM) analysis of this compound by means of multislice image match confirmed the structure model of Cava et al., and also provided the c-axis value of 1.58nm [67]. The investigation was carried out using a JEOL 40000EX electron microscope operated 400kV and fitted with a top-entry stage, which had a capability of lattice resolution of 0.12nm and point-to-point resolution of 0.14nm. The preparation of samples was performed by crushing under a mixture of ethanol and liquid nitrogen to make a suspension which was dried onto holey carbon films. It has also been shown that these compounds are not c-centred. Weak, but sharp reflections violating c-centring were observed, indicating long-range ordering of oxygen in the PbO layers. It is also pointed out that this material is the most stable i.e. never degrades with time, in the 400kV electron beam than other cuprate superconductors [67].

3.5.2 Atomic ordering and charge localisation

The $Pb_2Sr_2Y_{1-x}Ca_xCu_3O_{8+\delta}$ structure exhibits one way in which local charge distribution controls the electronic properties of layered cuprate superconductors. To show the local charge distribution, one can rewrite the formula as $Sr_2(Y,Ca)Cu_2O_6[Pb_2CuO_{2+\delta}]$; where the structural component in square brackets acts as a charge reservoir which controls the charge on the superconducting Cu-O planes. When x=0 and δ=0 the material is an antiferromagnetic semiconductor in which Pb is in a divalent state, the copper between the PbO layers is monovalent and in-plane copper atoms are divalent. The PbO-CuO_δ-PbO sandwich can accommodate a significant charge density (5 electronic charges per formula unit) by the oxidation of the Cu^{1+} to Cu^{2+} and Pb^{2+} to Pb^{4+}[68]. Chemical analysis of the Pb-2213 phase by the selective dissolution method and the inductively coupled plasma technique as well as by NMR have confirmed that the average valence of all the copper atoms increases up to +2.0 with increasing δ for $0.5 \leq \delta \leq 1.8$ [69, 70].

On the basis of the chemical analysis and Hall effect measurements [68], it has also been shown that holes introduced by extra oxygen first enter the CuO_δ layer and then the PbO layer only after the average valence of the copper changes to +2. This charge remains locked and never gets transferred to the CuO_2 layers whilst the divalent

calcium is absent [64, 71]. However, when the trivalent Y cation between the CuO_2 planes is partially substituted by Ca the material becomes superconducting. In this case, the charge modification is accommodated by the oxidation of the CuO_2 layers, directly adjacent to the Y/Ca planes, thereby producing charge neutrality on a local scale. However, more recently, Jorgensen et al.[72] have shown from calculations of bond-valence sums by following the procedure of Brown and Altermatt [73], and powder neutron diffraction data for $Pb_2Sr_2Y_{1-x}Ca_xCu_3O_8$ samples (for x=0, 0.5) that the Ca doping causes a positive charge transfer to the CuO_2 as well as to the PbO sheets. The bond-valence sum for the Cu ions in the CuO_2 sheet increases as a function of doped value of calcium, whereas for the Pb ions it increases to x=0.4 and then saturates. The axial Cu(2)-O(1) and Cu(2)-C(2) distances are the sensitive probes of the charge state of the C(2) ions. The distance between the Cu(2) ions in the CuO_2-(Y, Ca)-CuO_2 sandwich is increased by 0.14Å when x changes from x=0.0 to x=0.5 [72]. Therefore, it is important to note that the charge transfer process in Pb-2213 phase is an interplay between the oxidation of Cu(2) and Pb ions.

Superconducting behaviour is observed when the average valence of the copper in each CuO_2 plane reaches 2.25+ (i.e. it is oxidised), while the copper and lead remain in the reduced condition in the sandwich layers[71]. The mixture of oxidised and reduced cations in the same crystallographic unit cell creates much difficulty in synthesising the superconducting phase, requiring low pressure oxygen ambients at high temperature to keep the PbO-Cu-PbO sandwich reduced while simultaneously oxidising the planar copper atoms. When established, the balance between the oxidised and reduced states can occasionally be intentionally modified in such a way as to alternatively expel and re-establish the superconducting properties. For example, when the superconducting phase is heat-treated at low temperature (300-500°C) in O_2 or in air it exhibits behaviour similar to the undoped compound [66, 74]. The superconductivity can be re-established by heating the samples in an oxygen-free ambient around the same temperature [74].

3.5.3 Oxygen stoichiometry

The $Pb_2Sr_2YCu_3O_{8+\delta}$ material can be oxidised in oxygen or air within only a few hours at temperatures around 500°C, where $\delta \cong 1.9$ as determined by thermogravimetric analysis (TGA). This oxygen soaking induces some changes in the lattice parameters and a change in symmetry from orthorhombic to tetragonal [66]. *Table 3.4* shows the lattice parameters obtained with different oxygen values in Pb-2213 phase.

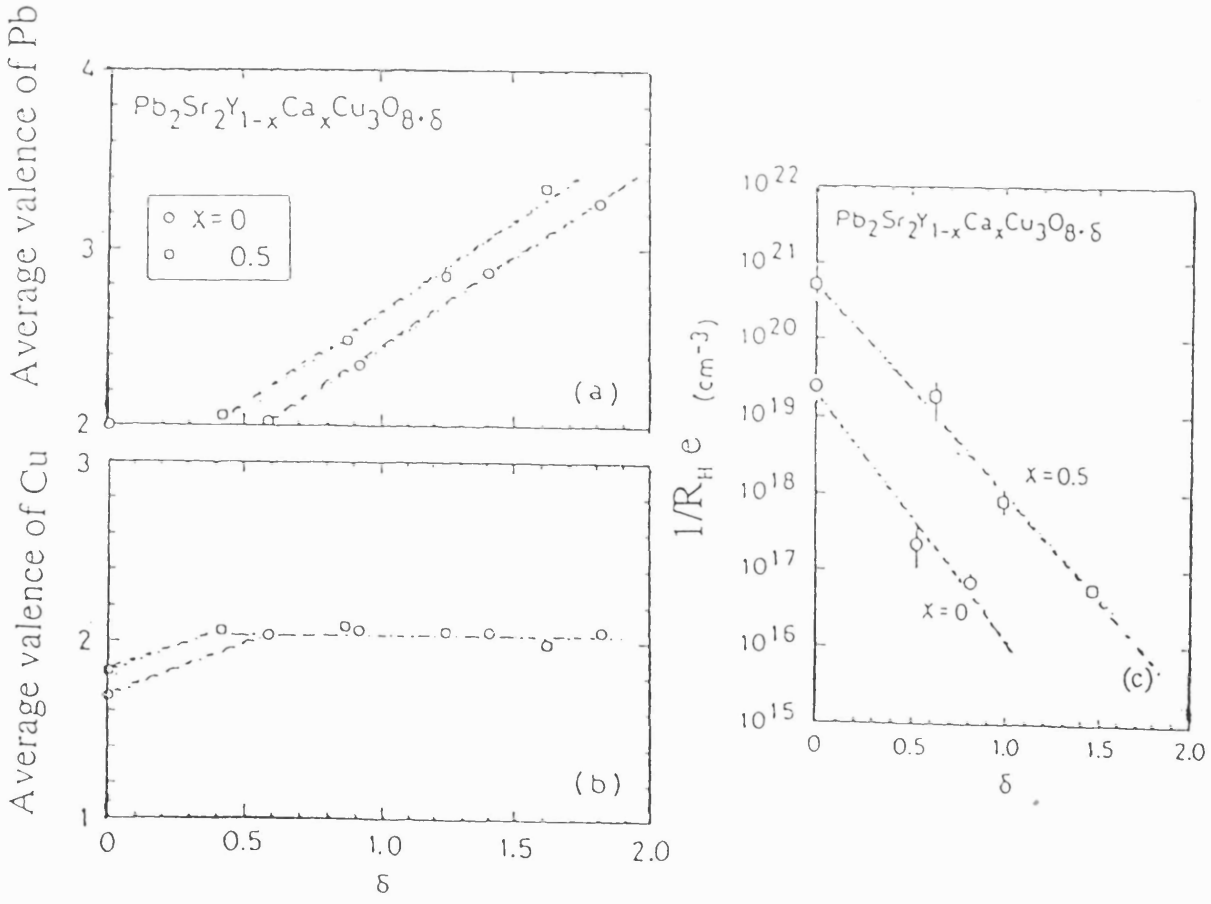

Figure 3.6. Dependence on δ of the average valence of a) Pb, b) Cu and c) the hole concentration ($1/R_H.e$) at 300K [75].

Table 3.4 Lattice parameters for samples with different oxygen stoichiometry[66].

$\delta=0$, $a=\sqrt{2}xa_p$ a_p is the simple perovskite parameter.	$\delta=1.4$, 450°C in O_2 $a\approx b\approx a_p$	$\delta=1.37$, 500°C in O_2 $a\approx b\approx a_p$
a=5.389(3)Å	a=3.838(2)Å	a=3.848(3)Å
b=5.428(3)Å	b=3.870(2)Å	b=3.848(3)Å
c=15.717(8)Å	c=15.845(8)Å	c=15.822(8)Å

Oxygen stoichiometry has a dramatic effect on the superconducting properties of lead-based $Pb_2Sr_2Y_{1-x}Ca_xCu_3O_{8+\delta}$. As discussed earlier, this system shows a wide range of oxygen take-up although the maximum superconducting transition temperature, T_c, is observed only when δ is close to zero. With increasing δ the resistivity tends to increase, the hole concentration decreases, and the superconductivity is suppressed in samples where $0 \leq x \leq 0.5$ [75]. From the chemical analysis, it is observed that the average valence of Cu increases up to +2.0 with increasing δ for $0 \leq \delta \leq 0.5$, and is almost constant for $0.5 \leq \delta \leq 1.8$ value [75].

3.6.1 $[Pb_{1-y}(Cu,Sr)_y]Sr_2(Y_{1-x}Ca_x)Cu_2O_{7-\delta}$ phase

Subramanian et al. [65], Lee et al. [76], and Rouillons et al. [77] independently discovered the $[Pb_{1-y}(Cu \text{ or } Sr)_y]Sr_2(Y_{1-x}Ca_x)Cu_2O_{7-\delta}$ lead cuprates. Those groups [65,76] analysed the crystallographic structure using single crystals of those compounds by XRD and concluded that the compounds had the same structure as $TlBa_2CaCu_2O_7$ that is known as Tl-1212 phase which has a $YBa_2Cu_3O_7$-like arrangement of cations. Because of the similarity in structure, lead cuprate is referred to as the Pb-1212 phase. Here, mixed lead-strontium infinite (∞) monolayers $[Pb_{0.5}Sr_{0.5}O]_\infty$ or lead-copper monolayers $[Pb_{1-x}Cu_xO]_\infty$ replace the $[TlO]_\infty$ monolayers in the double rock-salt slabs.

Figure 3.5-b shows the tetragonal elementary cell of the space group P4/mmm of Pb-1212 phase [63, 76]. It differs slightly from the $YBa_2Cu_3O_7$, in that a (Pb,Cu)-O plane replaces the Cu-O chain commonly found in the YBaCuO family. The central core consisting of CuO_2-(Y,Ca)-CuO_2 layers is the same but Sr replaces Ba. Lee et al. [76] reported the lattice constants as a=3.8027(4)Å and c=11.826(1)Å in the $(Pb_{0.71}Cu_{0.29})Sr_2(Y_{0.73}Ca_{0.27})Cu_2O_7$ phase. The Pb-O bond lengths involving the two oxygen ions above and below the Pb plane are 1.9681(4)Å. The Cu ion, displaced from the origin, can be considered as tetrahedrally co-ordinated. The four Cu-O bond distances in the CuO_2 plane are 1.917(6)Å and the bond length to the fifth oxygen atom is 2.304(14) Å at the apex of the square-based pyramid. The Y and Ca atoms occupy the same site and are in cubic co-ordination. The compound with Ca and without Y ions does not posses a Pb-1212 phase [76].

In the case of the $(Pb_{0.5}Sr_{0.5})Sr_2(Y_{0.5}Ca_{0.5})Cu_2O_7$ phase, the first report [77] appeared in the literature concerning the structure determined by XRD refinement technique and the proposed structure was subsequently confirmed by high resolution electron microscopy (HREM) investigations showing the characteristic contrast expected for the Pb-1212 phase, with the two triple rows of alternated white spots. The first triple point row is brighter and can be associated with the layering sequence 'SrO-(Sr, Pb)O-SrO' whereas the second one is weaker (less brighter) and corresponds to the sequence 'CuO_2-(Y,Ca)-CuO_2 [77].

Another composition has recently been analysed by the Rietveld method for XRD data where the (Pb,Cu)-O sheet was replaced by $(Pb_{0.5}Cd_{0.5})$-O. The samples containing Ca=0.0, 0.4 & 0.5 values were studied. Both Cd and Pb ions are displaced from their ideal sites. Other cations such as Sr^{2+}, Cu^{2+} and Cd^{2+} can occupy the (Pb, Cd) sites for those samples. They also reported that as the calcium content increases, O(2) atoms move closer to the CuO_2 planes and far from the (Pb, Cd) sheets which obviously increases the hole concentration to the superconductive copper oxide sheets [78].

The lead in this compound was shown to be present as Pb^{4+}. When the sample was dissolved in HCl and then reacted with KI, the titer value was about 3.5e per mole, of which 2.5e is from the transfer of 2.5 Cu^{2+} and 1e from the transfer of 0.5 Pb^{4+} into $0.5Pb^{2+}$[79]. From XRD analysis it was also found that the ionic radii of the Pb^{4+}

was 0.0775nm, which is closer to the radii of Cu^{2+}ions (0.073nm) [63, 76]. Therefore, the ions in the (Pb,Cu)-O layers are considered to be present in the tetravalent state.

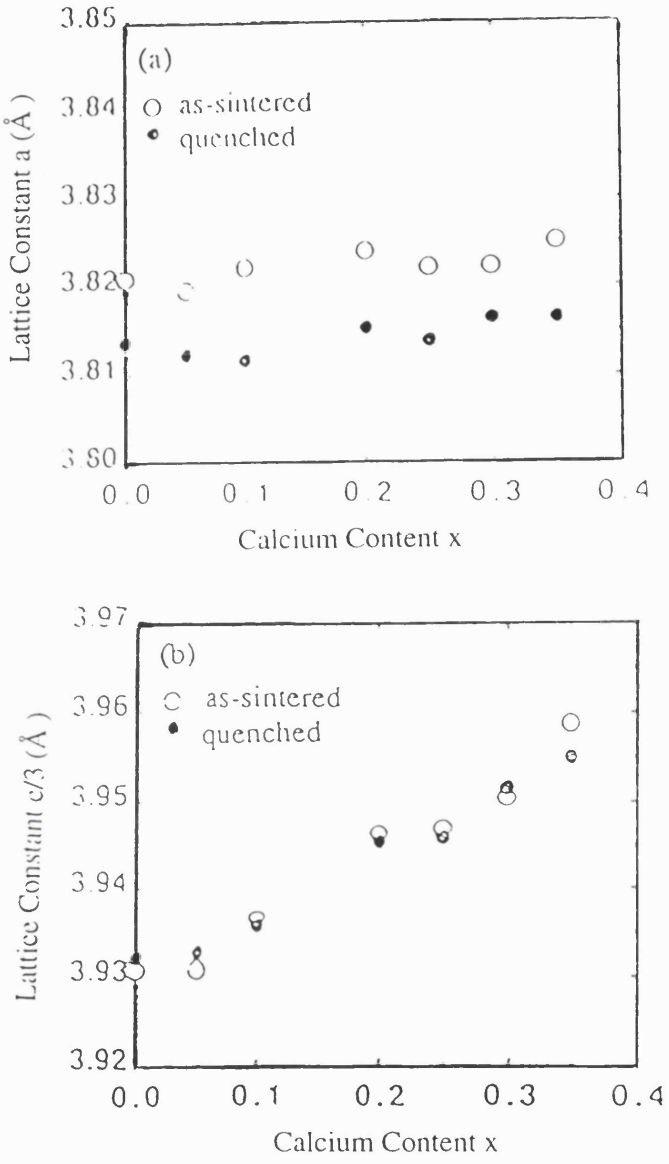

Figure 3.7. The Ca-content, x, dependence of the lattice constants of (a)a and (b) for both samples slowly cooled and quenched (adopted from[63]).

3.6.2 The oxygen stoichiometry

Thermogravimetry (TG or TGA) experiments in which the mass of a specimen is measured as a function of temperature (or time) as a specimen is heated under a controlled temperature program show a weight loss of this phase in air. However, this was small and corresponds to about 0.1 oxygen atoms, i.e., from O7 to $O_{6.9}$ [75]. The loss rate increases between 470°C and 600°C and then decreases to 800°C. Cooling in air from 800°C to room temperature shows the reversible process.

3.6.3 Superconductivity among the (Pb, M)-1212 family

The (Pb, M)-1212 phase, where M denotes divalent cations, was expected to be superconducting with T_c>80K because of its structural similarity with Tl-1212. However, in the first two reports [65,76], the compositions $(Pb_{0.69}Cu_{0.31})Sr_2(Y_{0.85}Ca_{0.15})Cu_2O_{6.8}$[65] and $(Pb_{0.71}Cu_{0.29})Sr_2(Y_{0.73}Ca_{0.27})Cu_2O_7$ [76] studied were found to be nonsuperconducting. Subsequently, Ono and Uchida [80] investigated a wide range of compositions and were able to form single-phase compounds for a Ca content $0<x<0.35$ and a Pb content $0.6\leq(1-y)\leq0.80$. When the sample with x=0.30, y=0.35 was annealed in air at 860°C for 1hour and then quenched in liquid nitrogen, a T_c of 17K was achieved. On the other hand, furnace cooled samples from 860°C to 300°C in air and then quenched in liquid nitrogen did not show superconductivity down to 4.2K. It was also observed that this phase does not superconduct unless Ca-ions are doped into the host material resulting in a $T_{c,zero}$ change from zero to 80K in thin films and to 74K in bulk [81, 82, 83]. However, Hughes et al.[81] found higher superconducting transition temperature with a high degree of orientation demonstrated through XRD patterns of 15 thin layer samples but impurity or unidentified phases were 40% in their thin layers. It was concluded that the relatively low T_c was due to difficulty in obtaining the correct formal copper valence and oxygen site distribution [80, 83].

The $(Pb_{0.5}Sr_{0.5})Sr_2(Y_{0.5}Ca_{0.5})Cu_2O_{6.8}$ material [65] exhibited a $T_{c,\,onset}$ of 100K whereas $T_c(0)$ varied from 45 to 53K depending upon the thermal treatment that relates the oxygen adjustment and compositional inhomogeneity [77]. Another substitution in the (Pb, M)-O layers was performed by several authors [84, 85] by using Cd^{2+} for M. The $(Pb_{0.5}Cd_{0.5})Sr_2(Y_{1-x}Ca_x)Cu_2O_7$ phase had a transition temperature [$T_c(0)$] ranging from 45 to 60K.

The parent material $(Pb_{0.5}Cu_{0.5})Sr_2YCu_2O_7$ has also been investigated by Koriyama et al. [86] by using substitutional chemistry. When Sr was substituted by Ba, the superconducting transition did not exist down to 4.2K. They further showed that the superconductivity does not exist in Ba-free samples with various Ca contents. However, Hall coefficient was positive and decreased with Ba concentration. This

shows that the holes are created in the ($Pb_{0.5}$ $Ba_{0.2}Cu_{0.3}$) layer but are not in sufficient amount to form the CuO_2 as a superconducting-sheet. However, keeping Ba=0.2 and increasing the calcium content, substitutes the Y ion and closer to CuO_2, the resistivity decreases. For Ca=0.1, a resistive transition appears, and increases to 25K (onset transition temperature) for Ca=0.2. This implies that bond lengths play an important role in dictating the superconducting properties in the cuprate materials.

3.7 Summary

Historical development from dream to reality of achieving 150K superconducting transition temperature and other properties associated with conventional superconductors were introduced in this chapter. A simple out line of the BCS theory was included to describe the quantum properties of electrons into superconducting state that lead to a pair formation. The common features of layered high temperature superconductors, HTSC, were briefly described. In HTSC, the charge carriers could be positively charged holes or negatively charged electrons and paired species are known to exist but the mechanism responsible for their formation has not yet been fully explained. Much work has to be performed to develop new formulas of HTSC materials through chemical substitutions with in the structure to improve T_c. Among all the cuprate families, the lead cuprates are the most complex family because of the structure and oxygen sensitive behaviour towards the superconducting properties. The structural and electronic properties of Pb-2213 and Pb-1212 phases were described.

References

[1] K.Onnes, Leiden Comm., 122b (1911).

[2] B.W.Roberts, Progr. Cryog., 4, 161 (1964).

[3] W.Meissner, H.Fraz and H.Westerhoff, Ann.Phys.,17, 593 (1933).

[4] R.K.Stanley, R.G.Morris and W.G.Moulton, Phys.Rev., B20, 1904(1979).

[5] M.R.Stokan, W.G.Moulton and R.C.Morris, Phys.Rev., B20, 3670(1979).

[6] A.Deschanvres, B.Raveau and Z.Sekkal, Mat.Res.Bull., 6, 699 (1971).

[7] D.C.Johnston, H.Prakash, W.H.Zachariasen and R.Viswanathan, Mat.Res.Bull., 8, 777 (1973).

[8] A.W.Sleight, J.L.Gillson and F.E.Bierstedt, Solid State Commun. 17, 27(1975).

[9] W.Meissner and Oschsenfeld, Naturwissenschaften, 21, 787 (1933).

[10] F.London and H.London, Proc.Roy.Soc., A149, 71 (1935).

[11] V.L.Ginzburg and L.D.Landau, Zh.Eksperim. I Teor.Fiz. 20, 1064(1950).

[12] A.A.Abrikosov, Zh.Eksperim. i Teor.Fiz. 32, 1442 (1957).

[13] J.Bardeen, L.N.Cooper, and J.R.Schrieffer, Phys. Rev. 108, 1175(1957).

[14] B.D.Josephson, Phys.Letters 1, 251 (1962).

[15] B.D.Josephson, Rev.Mod.Phys. 36, 216 (1964).

[16] J.Cors, D.Cattani, M.Decroux, A.Stettler and φ. Fischer, Physica B, 165 and 166, 1521 (1990).

[17] R.Schollhorn, In Inclusion Compounds (eds. J,L,Atwood, J.E.D.Davies and D.D.Mac Nicol) Vol. 1, p. 249, Academic Press, London (1984).

[18] A.F.Hebard, M.J.Rosseinsky, R.C.Haddon, D.W.Murphy, S.H.Glarum, T.T.M.Plastra, A.P.Ramirez and A.R.Kortan, Nature, 350, 600 (1991).

[19] K.Tanigaki, T.W.Ebbesen, S.Saito, J.Mizuki, J.S.Tsai, Y.Kubo, and S.Kuroshima, Nature, 352, 222 (1991).

[20] J.R.Gavaler, Appl.Phys.Lett. 23, 480 (1973).

[21] J.P.Bednorz and K.A.Muller, Z.Phys.B, 64, 189 (1986).

[22] M.K.Wu, J.R.Ashburn, C.J.Torng, P.H.Hor, R.L.Meng, L.Gao, Z.J.Huang, Y.Q.Wang and C.W.Chu, Phys.Rev.Lett., 58, 908, (1987).

[23] H.Maeda, Y.Tanaka, M.Fukutomi and T.Asano, Jpn. J. Appl.Phys., 27, L206(1988).

[24] Z.Z.Sheng and A.M.Herman, Nature, 332, 55 (1988).

[25] Y.Tokura, H.Takagi and S.Uchida, Nature, 337, 345 (1989).

[26] S.N.Putilin, E.V.Antipov, O,Chmaissem, and M.Marezio, Nature362, 226 (1993).

[27] C.W.Chu, L.Gao, F.Chen, Z.J.Huang, R.L.Meng and Y.Y.Xue, Nature 365, 323 (1993).

[28] J.F.Schooly, W.R.Hosler and M.L.Cohen, Phys.Rev.Lett., 12, 474(1964).

[29] D.C.Johnson, H.Prakash, W.H.Zachariasen and R.Viswanathan, Matr.Res.Bull., 8, 777 (1973).

[30] L.F.Mattheiss, E.M.Gyorgy and D.W.Johnson Jr., Phys.Rev. B, 37, 3745 (1988).

[31] R.J.Cava, B.Batlogg, J.J.Krajewski, L.W.Rupp, L.F.Schneemeyer, T.Siegrist, R.B.Van Dover, P.Marsh, W.F.Peck, P.K.Gallagher, S.H.Glarum, J.H.Marshall, R.C.Farrow, J.V.Waszscak, R.Hull and P.Trevor, Nature, 336, 211 (1988).

[32] R.J.Cava, B.Batlogg, R.B.Van Dover, J.J.Krajewski, J.V.Waszscak, R.M.Fleming,W.F.Peck Jr., P.Marsh, A.C.W.P.James and L.F.Schneemeyer, Nature, 345, 602 (1990).

[33] A.C.Rose-Innes and E.H.Rhoderick, 'Introduction to Superconductivity', IS in Solid State Physics, vol.6, Pergammon Press, Oxford, U.K.

[34] Reynolds, Serin, Wright and Nebitt, Phys.Rev.78, 487 (1950).

[35] T.A.Faltens, W.K.Ham, S.W.Keller, K.J.Leary, J.N.Michaels, A.M.Stacey, H.C.zurLoye, D.E.Morries, T.W.Barbee III, L.C.Bourne, M.L.Cohen, S.Hoen and A.Zettl, Phys.Rev.Lett. 59, 915 (1987).

[36] D.R.Harshman and A.P.Mills, Jr., Phys.Rev. B, 45, 10684 (1992).

[37] J.Bardeen, L.N.Cooper and J.R.Schrieffer, Phys. Rev., 108, 1175(1957).

[38] L.N.Cooper, Phys.Rev, 104, 1189 (1956).

[39] Elbio Dagotto, 'corrolated electrons in high-temperature superconductors', Review of Modern Physics, 66, 763 (July 1994).

[40] G.Burns, 'High-Temperature Superconductivity', Academic Press, USA,(1992).

[41] D.R.Harshman, G.Aeppli, B.Batlogg, G.P.Espinoso, R.J.Cava, A.S.Cooper, L.W.Rupp, E.J.Ansaldo, and D.Li. William, Phys. Rev.Lett. 63, 1187 (1989).

[42] Y.Tokura, H.Takagi, S.Ushida, Nature 337, 345 (1989).

[43] S.E.Babcock, and D.C.Larbalestier, Appl.Phys.Lett. 55, 393 (1989).

[44] M.Kawasaki, P.Chaudhri and A.Gupta, Phys.Rev.Lett. 68, 1065(1992).

[45] M.S.Osofsky, J.L. Cohen, E.F.Skelton, M.Miller, R.J.Soulen, S.A.Wolf Jn., and T.A.Vanderalu, Phys. Rev. B45, 4916

[46] A.W.Sleight, M.A.Subramanian and C.C.Torardi, Mat.Res.Bull., 14, 45 (1989).

[47] M.W.Shafer and T.Penney, Eur.J.Solid State Inorg. Chem., 27, 191(1990).

[48] I.S.Shaplygin, B.R.Kakhan and V.B.Lazarev, Russ.J.Inorg.Chem.24, 820, (1979).

[49] A.C.W.P.James, S.M.Zahurak and D.W.Murphy, Nature 338, 240 (1989).

[50] C.Chaillout, S.W.Cheong, Z.Fisk, M.S.Lehman, M.Mrezio, B.Morosin and J.E.Schirber, Physica C158, 183 (1989).

[51] A.Manthiram, J.S.Swinnea, Z.T.Sui,H.Steinfink and J.B.Goodenough, J.Am.Chem.Soc. 109, 6667 (1989).

[52] C.C.Torardi, J.B.Parise, M.A.Subramanian, J.Gopalakrishnan and A.W.Sleight, Physica C157, 115 (1989).

[53] A.Manthiram and J.B.Goodenough, Appl.Phy.Lett.53, 420(1988).

[54] J.Ren, D.Jung, M.H.Whangbo, J.M.Trascon, Y.LePage, W.R.McKinnon and C.C.Torardi, Physica C 159, 151 (1989).

[55] M.G.Smith, A.Manthiram, J.Zhou, J.B.Goodenough and J.T.Markert, Nature 351, 549 (1991).

[56] A.Manthiram, M.Paranthaman and J.B.Goodenough, Physica C 171, 135(1990).

[57] M.Paranthaman, A.Manthiram and J.B.Goodenough, J.Solid State Chem. 87, 479, (1990).

[58] S.Nakajima, M.Kikuchi, T.Oku, N.Kobayashi,T.Suzuki, K.Nagase, K.Hiraga, Y.Muto and Y.Syono, Physica C160, 458 (1989).

[59] M.R.Presland, J.L.Tallon, R.G.Buckley, R.S.Lui and W.E.Flower, Physica C, 176, 95 (1991).

[60] A.Santaro, F.Beech, M.Marazio and R.J.Cava, Physica C 156, 693(1988).

[61] B.Raveau, Reviews on Silicon, Germanium, Tin and Lead Compounds 6, 287 (1982).

[62] R.J.Cava, M.Marezio, J.J.Krajewski, W.F.Peck Jr., A.Santoro, and F.Beech, Physica C, 157, 272 (1989).

[63] T.Maeda, K.Sakuyama, Shin-ichi Koriyama, H.Yamauchi, and S.Tanaka, Phys.Rev.B, 43, 7866 (1991).

[64] R.J.Cava, B.Batlogg, J.J.Krajewski, L.W.Rupp, L.F.Schneemeyer, T.Siegrist, R.B.vanDover, P.Marsh, W.F.Peck, Jr, P.K.Gallagher, S.H.Glarum, J.H.Marshall, R.C.Farrow, J.V.Waszczak, R.Hull and P.Trevor, Nature 336, 211 (1988).

[65] M.A.Subramanian, J.Gopalakrishnan, C.C.Torardi, P.L.Gai, E.D.Boyes, T.R.Askew, R.B.Flippen, W.E.Farneth, and A.W.Sleight, Physica C 159, 124(1989).

[66] M.Marizio, A.Santoro, J.J.Caponi, E.A.Hewat, R.J.Cava and F.Beech, Physica C, 169, 401 (1990)

[67] P.Goodman, D.G.Jensen and T.J.White, Physica C 158, 173(1989).

[68] J.S.Xue, M.Reedyk, Y.P.Lin, C.V.Stager, and J.E.Greenman, Physica C 166, 29 (1990).

[69] M.Namiki, K.Hirokawa and Fresenius, J.Anal.Chem., 338, 296(1990).

[70] O.Okada, T.Oashi, K.Kumagai, T.Noji, Y.Koike and Y.Saito, Physica C 185-189,1075 (1991).

[71] R.J.Cava, Science 247, 656 (1990).

[72] J.E.Jorgensen and N.H.Anderson, Physica C218, 43-50 (1993).

[73] I.D.Brown and D.Altermatt, Acta crystallogr. B41, 155 (1985).

[74] S.H.H.Naqvi, F.Beech, I.W.Boyd, Elect. Lett., 27, 430 (1991).

[75] Y.Koike, H.Sunagawa, T.Noji, M.Masuzawa, N.Kobayashi, M.Namiki, K.Hirokawa and Y.Saito, Physica C 171, 331 (1990).

[76] J.Y.Lee, J.S.Swinnea and H.Steinfink, J.Mater.Res. 4, 763 (1989).

[77] T.Rouillons, J.Provost, M.Hervieu, D.Groult, M.Michel and B.Raveau, Physica C 159, 201-209 (1989).

[78] J.R.Min, J.K.Liang, X.L.Chen, C.Wang, C.Dong, G.H.Rao, Physica C 230 389(1994).

[79] X.X.Tang, D.E.Moris and A.P.B.Sinha, Physical Rev.B43, 7936(1991).

[80] A.Ono and Y.Uchida, Jpn.J.Appl.Phys., 29, L586 (1990).

[81] R.A.Hughes, Y.Lu, T.Timusk, J.S.Preston, Appl.Phys.Lett., 58, 762 (1991).

[82] R.A.Hughes, Y.Lu, T.Timusk, J.S.Preston, Appl.Phys.Lett., 59, 2597 (1991).

[83] S.H.H.Naqvi and I.W.Boyd, Physica C 213, 161-166 (1993).

[84] T. P. Beales, C. Dineen, W. G. Freeman, S. R. Hall, M. R. Harrison, D.M.Jacobson and S.J.Zammattio, Supercond. Sci. Technol. 5, 47(1992).

[85] R.S.Lui, D.Groult, A.Maignan, S.F.Hu, D.A.Jefferson, B.Raveau,C.Michel, M.Hervieu and P.P.Edwards, Physica C 159, 35 (1992).

[86] S. Koriyama, T.Maeda, K.Sakuyama, H.Yamauchi, and S.Tanaka, Physical Rev. B, 45, 7424 (1992).

Chapter 4

Various deposition techniques and PLD

Since 1986, there have been many extensive studies on the growth of cuprate superconducting thin layers using existing deposition methods or modified techniques to meet the conditional requirements related to multi-elemental complexities of the high temperature superconductors (HTSC). Stoichiometrical uniformity, oxygen content, orientation and epitaxy, absence of impurity phases, defects, voids, stresses and cracks, small superconducting transitional width (ΔT), high critical current density (J_C) and commercially feasible processing are considered the most important requirements for the superconducting thin layers using any thin layer processing technique.

Most HTSCs are multicationic materials having the nature to form more than one phase. Therefore, it is difficult to deposit a large area, single phase and uniform thin layer. Stoichiometric or non-stoichiometric single targets and multitargets of different constituents have been used to provide the required stoichiometry in the films. The oxygen content is also crucial in some materials such as Y-Ba-Cu-O and Pb-Sr-Y-Ca-Cu-O where small deviations from the optimum value can induce a noticeable change in superconducting properties. To meet the above mentioned requirements for good quality films, during the synthesis, adatoms should be provided sufficient energy to move by heating the substrate to an appropriate temperature in order to enable them to occupy the appropriate positions to form single crystals. Sometimes, the required structure and oxidation are not obtained in-situ and so, the films must be post annealed in an appropriate ambient to make them superconducting (ex-situ). The roughness, defects, stresses, droplets and outgrowths present in the films are dependent on the deposition parameters, physicochemical property of the substrate as well as the deposition technique used.

There are two main categories of thin layer growth, one is chemical vapour deposition (CVD) and the other is physical vapour deposition (PVD). In this chapter, the salient features of various deposition processes are described before proceeding towards pulsed-laser deposition (PLD) as a main concern of this chapter.

4.1 Chemical vapour deposition (CVD)

In chemical vapour deposition, high vapour pressure species containing the desired metal ions are vaporised and transported to the substrate where they dissociate and react to form the necessary stoichiometry. Usually, high deposition temperatures are required to decompose the transported species which then react into the desired stoichiometric compound. Most CVD processes involve a deposition reactor in which a mixture of gases is introduced from sources located externally, where they are decomposed and interact on the heated substrate surface to form thin layers. Deposition is often performed at low pressures (~1mbar) to improve film thickness uniformity and increase the deposition rate. The chemical reaction rate in CVD may be enhanced by the application of light, x-rays, heat, rf-fields, glow discharge, electron bombardment, or by taking advantage of any catalytic nature of the substrate surface [1, 2].

Metal-organic chemical vapour deposition (MO-CVD) is a technique used for large area coating without requiring the use of high vacuum systems. Precursors of the required metals are evaporated into a constant steam of an oxygen containing carrier gas (in the case of superconductors) that passes over the substrates in the susceptor in a separate chamber [3]. Suitable precursors need to have high vapour pressures and the composition of the films is controlled by adjusting the rate of evaporation of the precursors which can be solids or liquids. Hydrocarbon- or fluorocarbon-based chelates are sufficiently volatile to be used as precursors. In early work, researchers used these chelates for the growth of both $YBa_2Cu_3O_{7-\delta}$ and Bi-Sr-Ca-Cu-O thin films [4, 5, 6]. Several authors [7, 8] have described in detail the growth of $YBa_2Cu_3O_{7-\delta}$ layers from β-diketone chelate precursors on (100) single-crystal $SrTiO_3$ substrates and polycrystalline yttrium-stabilised ZrO_2

substrates at around 900°C, using oxygen/ argon mixtures or N_2O as the carrier gas. The films were highly oriented on $SrTiO_3$ had a $T_{c,\ zero}$ of 94K and critical current density $10^6 A/cm^2$ at 77K in zero magnetic field, decreasing to $10^5 A/cm^2$ in 5.5T.

4.2 Physical vapour deposition (PVD)

In physical vapour deposition, material is removed either by evaporation using electron beam or resistive heating, or sputtering and transported to the substrate where adsorption, nucleation and growth take place. Usually, this is achieved by carrying out the deposition in such a vacuum where the mean free path of the ambient gas molecules is greater than the dimensions of the deposition chamber and the source-to-substrate distance to avoid collosions with evaporants [1]. Vapourisation of solids can be created either by thermal processes that include electron beam heating, or by physically knocking out the atoms or molecules, from the surface by using energetic heavy particles. The process of deposition in the former case is referred to as vacuum evaporation and in the latter case as sputtering. If the process is carried out in certain reactive ambient in a controlled manner, the process is termed as reactive evaporation/ reactive sputtering.

4.2.1 Evaporation methods

In this technique vaporisation of the material occurs in high vacuum by heating to sufficient high temperatures and then condensation of the vapours is achieved on a substrate. Heating of the materials can be performed directly or indirectly by a variety of methods. The simplest evaporation techniques use resistive or electron-beam heating. In resistive evaporation, the material is evaporated by loading in a boat, made of refractory material such as W, Mo, Ta, or Nd, with or without a ceramic coating, and heating to the vaporisation temperature. Crucibles of insulating materials such as quartz, alumina, berrylia, and zirconia can be heated indirectly by supporting them in a metal cradle. In the case of alloys and compounds, vaporisation generally occurs by decomposition because of differences in the vapour pressures of the various constituents or because of thermal instability.

However, if the constituent elements of the material are equally volatile *congruent evaporation* occurs [1, 2]. The rate of condensation of the vapours depends not only on the evaporation rate but also on the relative position of the substrate, its temperature and its composition. For superconducting cuprates, a reactive oxygen ambient at some predetermined pressure may be needed to enable the vapour to react with oxygen for homogeneous nucleation and growth on the substrate. The composition of the film differs from that of the source if the evaporation is not congruent. The deposition rate, oxygen partial pressure and substrate temperature control the properties of the layer. Evaporation can also be performed using an electron beam, where a thermionic source supplies the electrons that are accelerated by an electric field and allowed to strike the surface of the target. To eliminate the impurities from the filament of electron source, a magnetic field is applied to bend the electron beam path and thus screening the impurities.

Several groups [9, 10, 11] have synthesised $YBa_2Cu_3O_{7-\delta}$ and Bi-2223 phase layers by resistively heated evaporation or electron beam heating sources on MgO(100) substrates. They have demonstrated $T_{c,\ zero}$ values of 80K and 107K for $YBa_2Cu_3O_{7-\delta}$ and $Bi_2Sr_2Ca_2Cu_2O_{10+\delta}$ systems respectively. More recently, Berberich et al. [12] used the reactive co-evaporation process for homogeneous composition over an area of 3inch diameter by applying a substrate rotation technique. They obtained an average deposition rate 0.2nm/s, $T_{c,zero}$ of 86K and critical current density $2x10^6 A/cm^2$.

4.2.2 Molecular beam epitaxy (MBE)

Molecular Beam Epitaxy (MBE) involves fine control of evaporation and deposition in an ultrahigh-vacuum system (~10^{10}torr) equipped with structural and chemical characterisational facilities. MBE permits the in-situ layer-by-layer growth, resulting in crystalline structures of the highest quality, which is suitable for HTSC cuprates due to their layered structure. Usually this technique is used to grow semiconducting material in ultra high vacuum. Since, HTSC oxides need oxygen to make them superconducting, attempts have also been made to over come this incompatibility with high vacuum to oxidise cuprate materials. Several groups have used an external diffusion of oxygen close to the substrate where the vacuum

pressure close to the substrate is significantly increased while the ultra high vacuum is maintained in the rest of the chamber due to differential pumping [13, 14, 15].

The $Pb_2Sr_2(Re_{1-x}Ca_x)Cu_3O_{8+\delta}$ superconductor that has the potential for growth under rather low oxygen ambients as inferred from the synthesis conditions of bulk or films deposited by sputtering or ablation (PLD) [16, 17, 18]. More recently, a first report on the growth of the Pb-2213 (Re=Dy, Eu) films using MBE has appeared [19]. Pb, Sr, Dy (Eu), Ca and Cu metals were evaporated separately from the effusion cells onto a heated $SrTiO_3(001)$ substrate in the temperature range of 750°C-800°C. For the monolayer deposition, the shutters were opened for durations of between 30 and 60sec. Activated oxygen, excited by rf (13.56MHz) or microwave (2.45GHz) sources, was continuously supplied through a nozzle placed near the substrate to maintain an oxygen-pressure around $2.7x10^{-5}$mbar. After deposition, the films were cooled to 300°C within 14 minutes under the same oxygen pressure as used for deposition [19]. During the growth, it was found that the vapour pressures of PbO and Pb were higher than 10^{-2}mbar at the growth temperature, and the sticking probability of Pb in the films was low, depending on the substrate temperature and shuttering sequence. Thus, the incident fluxes on the substrate from the Pb source correspond to 0.5-1.2 monolayers per second. In the films, Pb was about 20-50% deficient in terms of the stoichiometry but the reported crystal structures of the films were identical to that of the Pb-2213 phase [16, 20]. The films grown were c-axis oriented with a c-lattice parameter of 15.8Å. It was considered that the Pb was compensated by an excess amount of Sr [21]. The highest $T_{c,onset}$ of the films having chemical composition $Pb_{1.03}Sr_{2.5}Ca_{0.57}Dy_{0.45}Cu_{3.04}O_{8+\delta}$ was reported as 55K and $T_c(0)$~28K achieved only when cooling from 600°C to room temperature was performed in ultra high vacuum. If the oxygen was supplied until the substrate temperature fell to 300°C, the superconductivity disappeared.

The growth mechanism of these films has also been reported by using in-situ reflection high-energy electron diffraction (RHEED). The oscillations of RHEED intensity during coevaporation [22, 23] indicated the nucleation of two dimensional islands and their growth into a flat terrace. Each metal, in the order of

Sr/Cu/(Dy,Ca)/Cu/Sr/Pb/Cu/Pb was supplied to the substrate, where a drastic change in the RHEED pattern was seen at the first layer of lead. A diffuse scattering pattern without any spot, or ring was observed 2 to 3 seconds later when the shutter used for lead was opened indicating a disordered surface. The others suggested that the disordered layer was thick enough (several monolayers) that the lattice periodicity of the underlying layer could not be seen. The appearance of the RHEED pattern with no sign of surface diffraction rods was not only restricted to the deposition of the first PbO layer: it also occasionally appeared at the deposition of the second Pb-layer in the second cycle. The absence of diffraction features were considered not to be due to a quenched amorphous state but rather due to a liquid like-state, since it occured at temperatures near the melting point of PbO (T_m=870°C). However, a RHEED pattern without any sign of surface diffraction rods during the growth of Bi-Sr-Ca-Cu-O, Bi-2212 phase was not reported. The difference was suggested to be due to the different properties of Pb and Bi oxides. For example, the Pb or PbO molecules may have a higher mobility on the surface, whereas the sticking coefficient of Bi is twenty times higher than that of Pb at the same temperature. The latent heat of fusion of PbO is 20-40% less than that of Bi_2O_3 [24]. Therefore, a liquid layer may form more easily during lead oxide deposition.

4.2.3 Sputtering methods.

Sputtering based removal of material from a surface of target uses the effects of collisions of energetic, reactive or non reactive ions with the target atoms. If the energy of the bombarding ions is much greater than the binding energy, the atoms will be removed and the ejection process is known as sputtering. In sputtering processes the collisions between electrons and charged or neutral species within the plasma dominate the properties of the glow discharge. Elastic, inelastic collisions and several chemical reactions generally occur in the plasma and enhance deposition or etching processes. The most common processes occur in glow discharge are ionisation, excitation, dissociation, dissociative ionisation, electron attachment and excited atom-neutral collisions. Usually, sputtering is classified into four categories: dc, rf, magnetron and reactive [1].

RF and dc sputtering systems are basically similar. The target (cathode) in each process is negatively biased and the substrate (anode) may be ground, positively or negatively biased. After the system is evacuated, a mixture of $Ar:O_2$ gas or pure Ar is introduced into the system and varies the pressure from 20 to 100mtorr to serve as a medium in which the discharge is initiated and sustained. A relatively cheap and simple means of producing ions for sputtering is provided by the well-known phenomenon of glow discharge, which occurs when a DC electric field of 1-5kV is applied between two electrodes, with a current density 1-10mA/cm^2, in a gas at low pressure. Usually the cathode (target) and the anodes are separated by about 5cm. After a visible glow is maintained between the electrodes, a current flows and a film condenses on the substrate. The deposition is the result of collisions of positive ions in the discharge with the cathode(target) which cause ejection of neutral atoms and ions from the target surface through momentum transfer. These atoms and ions pass through the discharge region to condense on the substrate. The characteristics of the sputtering process as a deposition technique can be summarised as follows [1, 2]:

The sputtering yields, in general, are neutral and defined as the number of ejected species per incident ion. These increase with the energy and mass of the bombarding ions. The variation with energy shows linear behaviour in a small region above a threshold value determined by the sublimation energy of the target material. For higher energies, the yield approaches saturation, which occurs at higher energies for heavier bombarding particles. However, very high energetic bombarding ions have higher penetration depths and hence loss increases below the surface and a decrease in yield. The yield increases as inverse of the cos θ value of incident ions, where θ is the angle between normal on target surface and incident ions beam. However, at large incidence angles, the effect decreases the yield drastically and varies by a maximum factor of 5 to 6 with the atomic number of the target with ions of a particular energy and mass. The yield is only sensitive to the target temperature when it is very high where it shows a sharp increase due to accompanying thermal evaporation. Sputter-deposition rates are invariably one to two orders of magnitude lower compared to thermal evaporation rates under normal conditions. In a DC sputter-deposition system, the target or cathode has to be electrically conductive, and hence dc sputtering is not suitable for the insulating materials. However, these materials can be sputtered by rf sputtering for two reasons. Firstly, electrons

oscillating in the glow region may acquire enough energy to cause ionisation collisions and sustain the discharge. Secondly, rf voltages can be coupled through any kind of impedance that means the electrode needs not to be a conductor. In rf sputtering gas ionisation is enhanced with the help of a suitable rf field of several megahertz, applied directly to the anode through a capacitor or via a high-frequency coil placed inside or out side the discharge region. The high frequency alternating potential is also used to neutralise the surface charges periodically with plasma electrons which have a higher mobility than the positive ions.

Perrin et al. [25] deposited $YBa_2Cu_3O_{7-\delta}$ films by DC sputtering at room temperature using superconducting targets and investigated the film composition at different positions of deposited layers as a function of applied voltage and pressure during deposition, and concluded that it is very difficult to obtain stoichiometrically uniform deposition using this technique. Hong et al. [26] deposited Tl-Ba-Ca-Cu-O thin layers from a single oxide target. Their ex-situ annealed films (from 800°C to 880°C) showed c-axis orientation of Tl-2223 phase with an onset of the superconducting transition temperature at 125K and a $T_c(0)$ value of 110K.

Magnetron sputtering is the most commercially used technique to deposit material on a variety of substrates due to its high deposition rates (e.g. 1μm/min. for Al [1]). In this technique a magnetic field of strength 'B' is applied to superimpose on the electric field 'E' between the target and substrate. The electrons in the magnetic and electric fields experience the Lorentz force in addition to an accelerating electric field. In the magnetron system, the electrons ideally do not reach the anode but are trapped near the target enabling more collisions with the sputtering gas, and leading to increase in positive ion production which in turn increases the deposition rates. This enhanced ionisation efficiency and the deposition rates are achieved by applying a magnetic field parallel to the target and perpendicular to the electric field.

The growth of lead-based superconducting films has been demonstrated by Adachi et al.[17], using rf magnetron sputtering. They used non-stoichiometric targets with a metal cation ratio of Pb/Sr/Ln/Ca/Cu=5/2/(1-1.5)/0.4//(2.7-3.3), pure argon

or 3% oxygen in argon as the sputtering gas, and deposited on (100) MgO single crystal substrates. The gas pressure during deposition was kept at $0.5x10^{-2}$mbar. The rf (13.56MHz) input power used was 100 Watt, and resulted in growth rates of 12nm/min. The deposited films were cooled down over 20 minutes in argon or nitrogen. The films grown in the temperature range from 500 to 600°C were reported as c-axis oriented Pb-2213 phase, with a superconducting transition temperature of 60K and critical current density of 10^4A/cm^2 at 50K.

4.3.1 Pulsed-laser deposition technique (PLD)

The removal of material from an irradiated target for the synthesis of thin layers of different materials has been in use for more than twenty five years. In 1965, Smith and Turner demonstrated the first laser-ablation-deposition of binary alloys on various substrates using a ruby laser [27]. Later, in 1986, just after the discovery of HTSC material above the boiling point of nitrogen, a large number of groups started synthesis of thin layers, using the old but undeveloped technique of laser-ablation-deposition. Presently, this technique has demonstrated the feasibility of controlled deposition with modification of the superconducting properties related to texturing and epitaxy of HTSC [28]. The pulsed nature of the laser has simple and good control over the layer by layer deposition and is comparable with MBE. However, this technique itself has been facing some problems with long, continuous and compositional uniformity in deposition.

Almost all the available pulse-durations or even continuous wave (CW) lasers have been used to synthesise thin superconducting layers. Usually, synthesis of thin layers using long pulses is avoided because of their deep thermal evaporating nature to stop segregation and incongruent evaporation in the case of multi-cationic materials. Whereas, if the short pulses are used, the evaporated material matches the composition of target surface and termed as congruent evaporation. Therefore, the term pulsed-laser-ablation (PLA) is used to describe the material removal phenomenon when short-pulsed lasers (pulse duration $\tau \leq$ 50ns) are used. Usually, the focused laser pulses are directed on to the target in an evacuated chamber to provide large mean free path for the ablated species. The targets are normally

rotated in order to reduce the exposure of any one area of the pellet to minimise the chances of the crater formation and progressive non-stoichiometric ablation. In some cases the laser beam is rastered to utilise a larger-surface area of the polished target and to cover a larger area by moving the forward directed plume relative to the substrate. The vaporised material from the surface of the target is commonly known as the plume. It can consist of submicron or even several micro-metre sized particles, electrons, atomic, molecular and ionised species, and has common characteristics of the plasma (such as plasma frequency, density, etc.) depend upon experimental conditions such as laser fluence, wave length, pulse duration, physicochemical properties of target material, pulse-shape of the laser and the quantity of the gas present in the chamber [29, 30, 31]. The plasma acts as a source of material for deposition on a substrate in the form of thin or thick layers that can also be controllably changed by deposition temperature, physicochemical properties and geometrical placement of substrate in the chamber.

The pulsed-laser deposition technique (PLD) is becoming more popular day by day for the synthesis of multicationic materials because of its good processing ability due to pulsed nature and simplicities to ablate multicationic material to form multi-layer devices. PLD, in comparison with other deposition techniques such as thermal evaporation, chemical vapour deposition (CVD), sputtering and MBE, has particular advantages and few disadvantages as summarised below [32, 33, 34].

4.3.2 Advantages

i)-One of the most significant features of PLD is the easy transfer of target stoichiometry to the substrate unlike sputtering and evaporation.

ii)-Simple to control deposition rates from <1Å/sec. to $>10^6$Å/sec. [32] and generation of species with high kinetic energy that depend on the experimental parameters such as, at nanosecond pulse duration and fluence of 10^8-10^9 W/cm^2, a typical energy spectrum of the ions is in the range of 20-1000eV with a mean energy of about 350 eV [29].

iii)-The experimental set-up can be changed easily and multiple sources can be ablated simultaneously by splitting and focusing the laser beams onto separate

sources or exposing individual targets to the laser beam separately. The fabrication of multilayers and designing new materials is fairly approachable.

iv)-Target holders can not be contaminated due to confined evaporating volume on the target and pulsed-heating for short duration that eliminates any impurity addition during material processing. Material consumption is also lower due to precise and localised heating that depends on the laser-beam parameters compared with thermal evaporation and quite attractive for the fabrication of thin layers of cost effective materials such as platinum, gold etc.

v) Laser ablating sources radiate less heat than conventional sources, such as are used in thermal evaporation, due to the small size of the evaporating volume and short pulse duration.

4.3.3 Disadvantages

i)-In conventional mode of pulsed-laser deposition, the uniformly deposited area is very small, or in another case, the large area deposition requires appropriate scanning of laser beam over the large area target or the substrate rotation that can allow an area as large as two or three inches [35, 36].

ii)-Showering of microscopic particles from the target could deteriorate the film quality and morphology specially in high power lasers. Therefore, power density of lasers should be decreased to minimise density of particulates on the deposited surface. Usually, the size of the particulates is 0.1 to 15μm or more and consists of solidified melt droplets that can be thrown out of their normal trajectories due to centrifugal force or using a velocity filter to stop slowly moving massive particles but allows the fast atomic and molecular evaporants through it. There is another approach to minimise the particulates by using highly homogeneous single phase and dense targets. Sankur et al. have demonstrated elimination of particulates by ablating molten target of Ge that has low vapour pressure but this method can not be used for multicationic materials due to large difference in melting temperatures of constituent element [37]. Usually, after removal of the few top layers from the polished target, the surface becomes rough with the formation of craters, microcracks, pits, and loosely attached particles. Therefore, using high density targets and polishing them after every few thousand laser shots could minimise the density of droplets in the deposited layers.

iii) Optical components can be degraded due to coating with ablated material during PLD processing. In particular, coating of the laser viewport can affect seriously the laser fluence in the case of UV laser pulses.

4.4.1 The ablation process

There are number of reports that have been published regarding the mechanism involved in the laser ablation process through models and fair approximations [32, 38-40], although a definite and real explanation of the ablation mechanism is still not available in literature. In this section a simple description of this process is included for better understanding.

The ablation process is described as a three-stage process: (I) pulsed-laser-target interaction (absorption, thermal conduction and surface melting), (ii) laser-interaction with the ablated vapour leading to the formation of high-temperature
expanding plasma, and (iii) anisotropic three dimensional adiabatic expansion of the laser-generated plasma giving rise to the forward-directed nature of the plume. These steps are repeated thousands of time in a typical deposition run [39]. *Figure 4.1* shows various stages involved during laser-target interaction.

The material removal from a solid-surface requires sufficient energy to overcome the cohesive energy of target material. It depends on the parameters of laser radiation and physicochemical properties of target. Any laser with sufficient energy output can be used to initiate evaporation in the target material. To avoid the radiation scattering and losses, the optical absorption must therefore be sufficiently strong so that the energy of the incident photons can be transferred to the atoms through electronic excitation, bond breaking and collisions.

By electron-phonon interaction, the absorbed energy is transferred in part to the motion of the atoms or ions making up the lattice and bond. Typical transfer times between hot electrons and the lattice are of the order of picosecond for most of the materials. In semiconductors and some insulators the photon energy must exceed the band gap in order to have significant absorption, where the basic process is the creation of an electron-hole pair, corresponding to a transition of an electron from the valence to the conduction band.

The density of electrons and holes may have a considerable kinetic energy to share with the lattice vibrations and leads again to heating of the semiconducting target on a time scale of picoseconds. The energy absorbed within the irradiated zone does not diffuse from the surface region, and is mostly used to excite the particles in a small volume, resulting in the collapse of the solid structure on a local scale by the breaking of interatomic or molecular bonds. Therefore, localised radiation heating leads to melting and ablation of the surface layers as a result of transition from a tightly bound solid to densely packed energetic particles. These expelled particles are very energetic, usually moving in the range of 0.02 to 5km/s, around the threshold of laser-ablation energy.

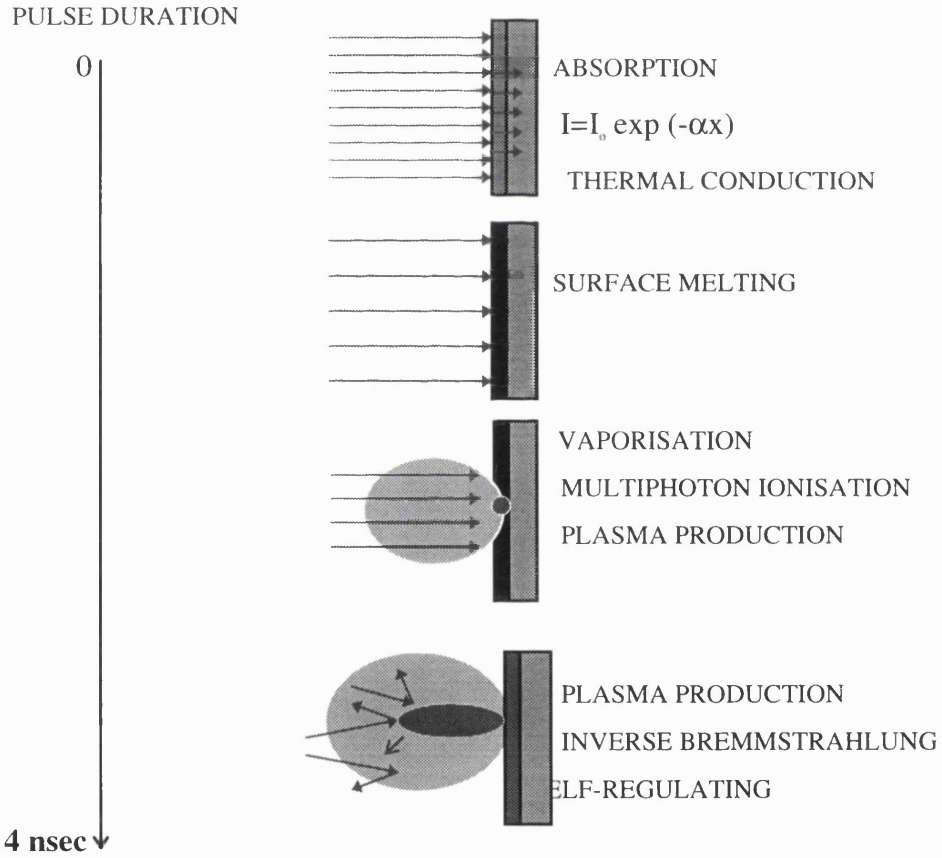

Figure 4.1. *Number of steps involved during PLA process (after S. R. Foltyn et al. [40]).*

For the synthesis of thin superconducting layers, high power pulsed Nd:YAG lasers or excimer lasers are commonly used. These deliver a flux of high energy photons which, upon interaction with the target material, causes a sudden rise in the surface temperature (melting points of $YBa_2Cu_3O_{7-\delta}$, $Pb_2Sr_2Y_{0.5}Ca_{0.5}Cu_3O_8$ and

$Bi_2Sr_2Ca_2Cu_2O_{10}$ are ≈1300°C ≈1050°C and 1140°C respectively). The thickness of the heated layer at time, t, after onset of laser radiation is on the order of $(2Dt)^{1/2}$, where D is the thermal diffusivity and indicates how much the heat is spread out during the pulse interaction. For evaporation to take place, the thermal energy density must exceed the heat of sublimation, U, in a time period, t, less than the pulse duration, τ. The temperature rise, ΔT, depends on the absorption coefficient, α, the thermal conductivity, K, the mass density, ρ, the reflectivity, R, the specific heat, C_V, laser intensity, I, and the pulsed duration, τ. Assuming that the optical and thermodynamic constants are temperature independent and the laser spot is homogeneous, the ΔT and the heating rate can be estimated approximately for two limiting cases, one where $(2D)^{1/2} >> \alpha^{-1}$ and the other $(2D\tau)^{1/2} << \alpha^{-1}$. In the case of $(2D\tau)^{1/2} >> \alpha^{-1}$, the energy absorbed during the laser pulse interaction time, τ, is $(1-R)I\tau$ which is used to heat a thickness $(D\tau)^{1/2}$, with D equal to $K/C_v\rho$. The approximate temperature [41, 39] rise is given as

$$\Delta T=[(1-R)I\tau\ ]/C_V\rho(2D\tau)^{1/2} \qquad (4.1)$$

In the case of $(2D\tau)^{1/2} << \alpha^{-1}$, where the thermal diffusion length is smaller than the optical absorption depth, α^{-1}, the temperature rise is dependent on the initial position of photons in the material during diffusion than the prior heat diffusion. The radiation absorption generates an exponential temperature profile along the depth, z. In this case, the maximum temperature is proportional to the pulse duration [32, 41].

$$\Delta T(z)=[(1-R)f\tau\alpha e^{-\alpha z\tau}]/C_V\rho \qquad (4.2)$$

In both limiting cases of temperature rise, the temperature dependence of the physical constants and the latent heat of any phase transformation have not been taken into account [41]. Since the absorption coefficient, α, changes with wave length, the above equations 4.1 and 4.2 are also influenced by the use of photonic flux of different wave lengths.

4.4.2 Ablation threshold

There must be a minimum amount of energy to overcome the cohesive energy of the solid constituent elements for removal in the form of vapour and known as *ablation threshold.* Since the HTSC cuprates have a black surface and a high carrier

concentration ($\approx 10^{21}/cm^3$) at room temperature [39], they provide a low reflectivity to laser radiation ($R \approx 0.1$) [40, 42]. Different wave lengths, even infrared (IR) and ultravoilet (UV) can satisfy the initial requirements for ablation. Practically, ablation requires the fluence that is equal to ablation threshold, plus conduction losses by the surrounding material and the absorption losses in the plasma, and depends on the pulse duration and laser wave length. By assuming that all the radiation energy is transferred to the target atoms and converted into heat energy, melting fluence, Φ_m, and evaporating fluence, Φ_e are given by [41],

$$\Phi_m = \rho_s [C_s(T_m - T_r) + L_m] / (1-R_s)\alpha_s \qquad (4.3)$$

$$\Phi_e = \rho_m [C_m(T_e - T_m) + L_e] / (1-R_m)\alpha_m \qquad (4.4)$$

where ρ_s is the mass density in solid form, C_s is the temperature-averaged specific heat, and α_s is the temperature-averaged absorption coefficient. T_m, T_r and T_e are the melting temperature, room temperature and the temperature of evaporants respectively. L_m and L_e are the latent heat of melting and evaporating material. Symbols used in the equation 4.4 have the same meaning but they refer to the melt-to-evaporant phase transition.

4.4.3 The ablation rate

When the laser energy is above the ablation threshold at the target surface, an intense heating leads to melting and vaporisation within the distance L_{th} of target material. The amount of material evaporated per pulse can be estimated from the energy equation. The energy deposited by the laser beam is equal to the energy needed to vaporise the surface layers plus the conduction losses by the target material and the absorption losses by the plasma. The process involved in this case can be written as

$$(1-R)[E-(\text{conduction losses} + \text{plasma losses})] = \delta x [\rho C \Delta T + \Delta H] \qquad (4.5)$$

where, R, E, C, ΔT, ΔH, ρ, δx are corresponding to the reflectivity, incident laser energy, heat capacitance, rise in temperature, volume latent heat of the target material, mass density and thickness of the target material evaporated per pulse, respectively. If the latent heat of vaporisation are much higher than its specific heat ($\Delta H >> \rho C \Delta T$), the above equation can be approximated by considering the threshold energy, E_{th}, required for evaporation and presented as

$$\delta x = (1-R)(E-E_{th})/\Delta H \qquad (4.6)$$

The above equation is used only when the diffusion length is much larger than the absorption depth $[(2D\tau)^{1/2} >> \alpha - 1]$, and suitable for metallic and HTSC cuprates which possess high absorption coefficients due to high carrier concentration at room temperature. This equation shows a linear relationship between evaporated thickness of target material and laser energy. At higher fluences (>3J/cm^2), the linear relationship is disturbed due to plasma losses and variations in reflectivity. If the thermal diffusivity does not play a major role it gives rise to a logarithmic dependence of δx with energy, E. This regime is generally valid for polymers or solids with low carrier concentrations [39, 41, 43].

To determine the dependence of the evaporated thickness with laser fluence, a bulk sintered $Pb_2Sr_2Y_{0.5}Ca_{0.5}Cu_3O_8$ target was irradiated with (532nm, 4ns, 10Hz) Nd:YAG laser pulses at different fluences. The variation in energy or fluence was achieved by placing neutral filters in the path of the laser beam whereas the spot size was kept constant. During ablation the chamber pressure was maintained at $4x10^{-3}$mbar. For every ablation-deposition process, the target surface was polished and cleaned by blowing nitrogen on the surface. The target before and after ablation was carefully weighed using electronic balance in the Department of Chemistry, at UCL, London. The ablated material was deposited on Si(111) substrate. The target-substrate distance was 3.5cm. The approximately uniform depositions were measured by Talystep.

Figures 4.2.a and 4.2.b show a linear increase in evaporated thickness of the surface layer in terms of ablated mass and the corresponding thickness of the deposited layers. However, a very small shift towards greater evaporation was observed with the increase in laser energy. Perhaps, it could be due to some higher uncertainties in lower laser energies used to ablate the target material.

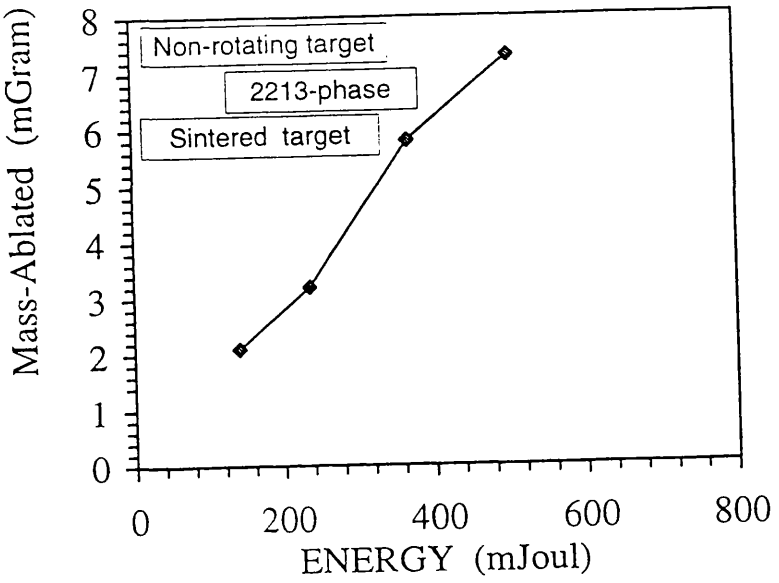

Figure 4.2. a) *Evaporated mass of Pb-2213 material versus laser energy (at 532nm, 4ns).*

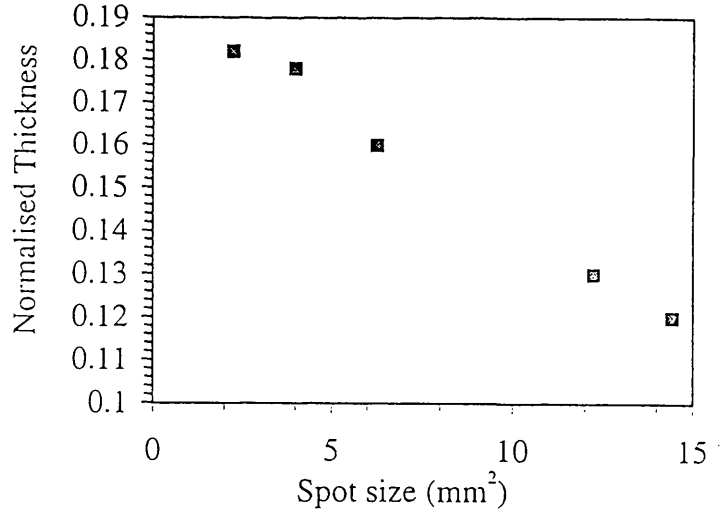

Figure 4.2. b) *Thickness of deposited Pb-2213 thin layers versus laser spot size.*

4.5 Plasma formation and expansion

The deposition of laser energy during the interaction with the target surface transforms into heat through hole/ electronic excitation that raises surface temperature and resulting outward emission of ions, electrons, cluster and neutrals. The time for producing the plasma may be considerably shorter than the duration of the laser pulse. Further laser-plasma interaction heats the plasma by inverse Bremsstrahlung to a temperature on the order of 10^4K or more [44].

The quantity of emitted species from the surface is non-linear with laser fluences. Increasing the laser energy above the threshold, the flux of emitted species or plume can be further heated by the absorption of laser energy and the fraction of ionised species increases with increasing fluence.

Several kinds of ionisation processes take place within the plume such as thermal, collisional and photoionisation. However, the penetration and absorption of the laser beam by the plasma depend on the electron-ion density, initial temperature, as well as the wave length of the radiation. If the plasma frequency is less than the laser frequency, the incident laser beam can penetrate the plasma otherwise the beam is reflected due to sheilding effect. The plasma frequency is directly proportional to the square root of the electronic concentration in the plasma. The absorption would occur by an inverse Bremsstrahlung effect, involving the absorption of a photon by a free electron. The value of electron density at which, the plasma frequency is known as the critical electron density and increases with decreasing wavelength. At UV wave lengths, the critical electron density is close to the concentration of electrons in a solid or liquid $\approx 10^{22} cm^{-3}$ [39] . For carbon dioxide lasers (10.6μm), the electronic concentration is smaller and the laser beam is highly absorbing [38].

An adiabatic expansion of the plasma takes place after the termination of the laser pulse when there is no additional input to the plasma from target material or laser energy. The initial dimensions of the plasma are much larger in the transverse direction than in the forward perpendicular direction. As the velocities are dictated by the pressure gradient, the expansion is anisotropic in the direction of the smallest dimension. The gas dynamic behaviour of the plasma shows the rate of change of expansion velocities is inversely proportional to the dimensions of the expanding gas and can be written as [39, 45]

$$X(t)d^2X/dt^2=Y(t)d^2Y/dt^2=Z(t)d^2Z/dt^2=(6kT_o/M)[X_oY_oZ_o/X(t)Y(t)Z(t)]^{\gamma-1} \quad (4.7)$$

where X_o, Y_o, and Z_o are the initial orthogonal edges of the plasma just after the termination of the pulse, T, M, k, and γ are the temperature, mass of the atomic species in the plasma, Boltzmann constant and the ratio of the specific heat at constant pressure and volume.

4.6 Effect of wave length

The quality of the deposited thin layers also depends on the wave length of the laser, ablating the target material and interacting with the plasma. At increasing wave lengths, the complex refractive index increases rapidly in metals and HTSC, such that the absorption coefficient of the target material is wave length dependent. As the wave length decreases, the possibility of droplet formation reduces [46]. For example, the Pb-2213 thin layer deposited using 266nm is not showing any droplet (figure 4.4-a), whereas, deposited thin layer using 532nm has several large and small droplets (figure 4.4-b). Plasma heating and droplet fragmentation can also be achieved by the absorption of the laser radiation in the plume.

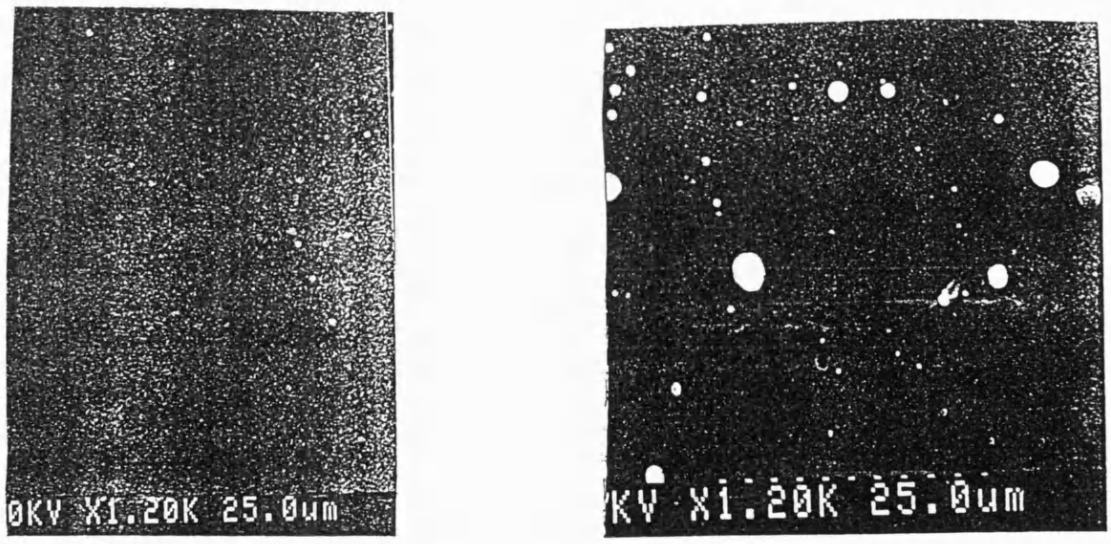

(a) (b)

Figure 4.4. SEM micrograph of the Pb-2213 phase film deposited using a) 266nm b) 532nm laser wave lengths.

The shorter wave lengths are more suitable for absorption, bond breaking and heating that creates further ionic and atomic species and fewer droplets of smaller sizes. A report for YBaCuO ablation indicates that the energy threshold for ablation

increases with decreasing wave length [47] from 1064nm to 248nm. The estimated energy thresholds are 70mJ/cm^2 for 248nm and 26mJ/cm^2 at 1064nm [41].

4.6.2 Surface segregation and deposition

The unique advantage of PLD among the other techniques based on evaporation is its correct stoichiometric transfer from multi-cationic target to the substrate, in spite of the surface modification of target that has been reported by several authors [30, 40, 44, 48, 49, 50]. Since the laser-target interaction can be categorised according to fluences: (i) The surface ablation region, where laser energy is absorbed and material in this region is ablated from the surface under high laser fluence $> 10^8$ W/cm^2 [29]; (ii) The evaporation region, below the ablation region occurs at lower energy densities, where the components are preferentially evaporated according to the vapour pressure of each individual component [30]; (iii) The heated region, where the temperature is below the sublimation temperature of any constituent in the target.

A little segregation is possible even with a use of single thermal pulse of a few hundred nanoseconds. In PLD the cycle is repeated thousands of times. In case of $YBa_2Cu_3O_7$ target, Cu and Ba are removed by evaporation during successive pulses, leaving behind a yttrium-enriched surface. Lynds et al. [48] used single, short, Nd:YAG (1064nm) laser pulses with fluences that range from 0.1 to 0.7J/cm^2. An ablated crater floor appeared to contain vitrified material and the average stoichiometry was deficient in Cu. Foltyn et al. [40] demonstrated a modification and segregation on the target surface using 2000 XeCl laser pulses in the range of 2-8 J/cm^2 fluence. The diameter of cones created were found about 10μm with Y-enriched surface. They also reported a decrease in growth rate but did not find any compositional variation in the deposited layers [40]. After 1000 shots/site, the cone tips were analysed and showed a Y:Cu ratio of 10:1.

Riet et al. [49] deposited magnetic material ($Fe_{72.3}Si_{14.5}Ru_{7.3}Ga_{5.8}$) using different fluences with an excimer laser (28ns, 308nm) and found congruent transfer only at 3.2J/cm^2, whereas near the threshold value (1.9J/cm^2) the film

contained excess gallium due to its preferential evaporation from the target surface. At higher laser fluences ($6J/cm^2$) the films were deficient in gallium, perhaps due to preferential sputtering of gallium atoms from the films.

Singh et al. [44] pointed out that compositional variations can occur in films of complex materials due to off-stoichiometric evaporation from the target or different sticking coefficients of the incident species on the substrate and different expansion velocities of the respective species in the plume.

These results suggest that both laser ablation and preferential evaporation occur during a long period of laser-target interaction. Kwo H. Young [50] deposited $YBa_2Cu_3O_7$ film and reported that, initially, preferential evaporation dominated near the edge of the irradiated area, and later, it appeared throughout the trench for the long periods of irradiation (30,000shots). During deposition, the deposition rate fell down but the stoichiometry of the film remained roughly unchanged, considered as a result of preferential sputtering effect from the deposited layers.

4.6.3 Cone-formation

There is no comprehensive model to describe laser-cone-formation due to complex interactions occurring during target irradiation. However, surface modification and cone formation are also a characteristic of sputtering. It is related with impurities which develop cones during sputtering. Unlike laser cones, sputtering cones can alter the angular distribution of sputtering flux. In sputtering, cones are the transient features that can shrink and disappear with continuing ion bombardment. The case in laser ablation is different where the cone formation is a stable and common feature. Here it is an accepted fact that impurities are resistant to vaporisation, and responsible for cone-formation. It is also observed that conical morphologies develop during ablation either in air or vacuum. Ablation in air produces much greater quantities of cones than ablation in vacuum. It could be the reason of segregation of target in air leaving more impurities as oxides on the surface that plays a role in cone formation during ablation for next coming pulses. However, impurity shielding is not the only explanation for laser cone formation. It is also observed by Kelly and Rothenberg [51] in pure aluminium and it was

suggested to result from outward thermal expansion and capillary waves that are always present on laser-melted surfaces.

During initial laser-target interaction, the material breaks up into atoms, ions, and molecules that boil off the surface as vapour, but leaving a minute amount of non crystalline or modified oxide molecules due to fast cooling. These modified molecules or amorphous phases behave differently for further incident pulses because of different melting points and heats of vapourisation. For example, $YBa_2Cu_3O_7$ crystals decompose into Y, Ba, Cu and some oxides during first laser pulse interaction. Because of the fast evaporation, rapid cooling solidifies remaining species without evaporation and can create different oxides such as BaO, CuO and Y_2O_3. These oxides or elements can work as impurities for further pulses on the $YBa_2Cu_3O_7$ surface, due to large differences in melting temperatures (T_m for Y=1500°C, Ba=770°C, Cu= 1083°C, Y_2O_3 =2410°C, BaO=1923°C, and CuO=1362°C) and responsible for cone formation.

4.7.1 Basic processes on the substrate surface

In this section the basic processes involved during thin solid layer formation and crystal orientations are described. A detailed description can be seen in a number of books on this subject of which the [1, 2, 52, 53] and [54] are good examples. Nucleation and growth of thin films are a process that depends on many factors such as density, energy, ionisation degree and type of the condensing particles, temperature and lattice parameters of substrate, degree of cleanliness and related chemical properties of substrate material. The growth of the thin layer from vapour phase involve the arrival of the appropriate atomic or molecular species on to the substrate surface, surface diffusion of the adsorbed species, nucleation of species, coalescence of individual nuclei to form interconnected islands and finally filling the network vacancies, before continuous thin layers can be formed.

Figure 4.5 describes the model processes involved in the initial stage of growth on the surface of substrate. In the initial stages of thin layer formation, vaporised species arrive at the substrate and are adsorbed with a surface concentration n(t) (the atoms/cm^2). The adatoms diffuse on the surface of substrate as

$$\langle x^2 \rangle = 2D.t \qquad (4.8)$$

Where $\langle x^2 \rangle$ is the average value of the square of diffusion distances in a certain direction after diffusion time t. D is the diffusion constant given by [53],

$$D = D_0 \exp(-E_d/K_b T_s) \qquad (4.9)$$

Where E_d is the activation energy for diffusion, K_b the Boltzmann constant, T_s the substrate temperature, and $D_0 = a_0 . V_d$ with V_d being the velocity of adatoms and a_0 the distance of one jump.

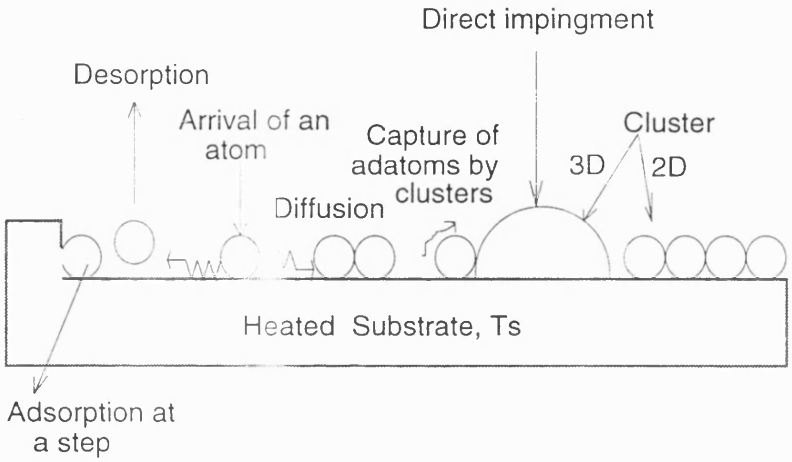

Figure 4.5. *Basic processes on the surface of substrate [53].*

After an average stay time τ_A, some of the adatoms desorbs into the vacuum at a desorption rate given by [53],

$$R_{des} = n/\tau_A \qquad (4.10)$$

The ratio of (adsorbed rate)/(arrival rate) is known as the "sticking coefficient" that is used frequently in the description of film growth. If R is the arrival rate, the differential sticking coefficient $\beta(t)$ is given by,

$$\beta(t) = [R - R_{des}(t)]/R = [1 - n(t)]/R.\tau_A \qquad (4.11)$$

The integral sticking coefficient, $\alpha(t)$, is the average value of $\beta(t)$ in time t,

$$\alpha(t) = 1/t \int \beta(t') dt' \qquad (4.12)$$

Under special conditions (three dimensional growths at high substrate temperature, T_s, if the arrival rate is constant, an adsorption-desorption equilibrium exists for a short period of time whereby [53],

$$n = \text{constant}, \quad dn/dt = R - n/\tau_A = 0$$

$$\text{or} \quad n = R.\tau_A \qquad (4.13)$$

4.7.2. The modes of growth

There are three basic modes of growth that depends on the interactions between the atoms of the substrate and the atoms of deposit. These three conventional modes are shown in *figure 4.6* and also described below [53].

(I)Frank van der Merwe growth (LG): This is a two-dimensional (2-D) mode of growth where the adhesive interaction energy between the adatoms and the substrate is greater than the cohesive interaction energy between the adatoms. A consecutive next layer can grow if the layer before is completed.

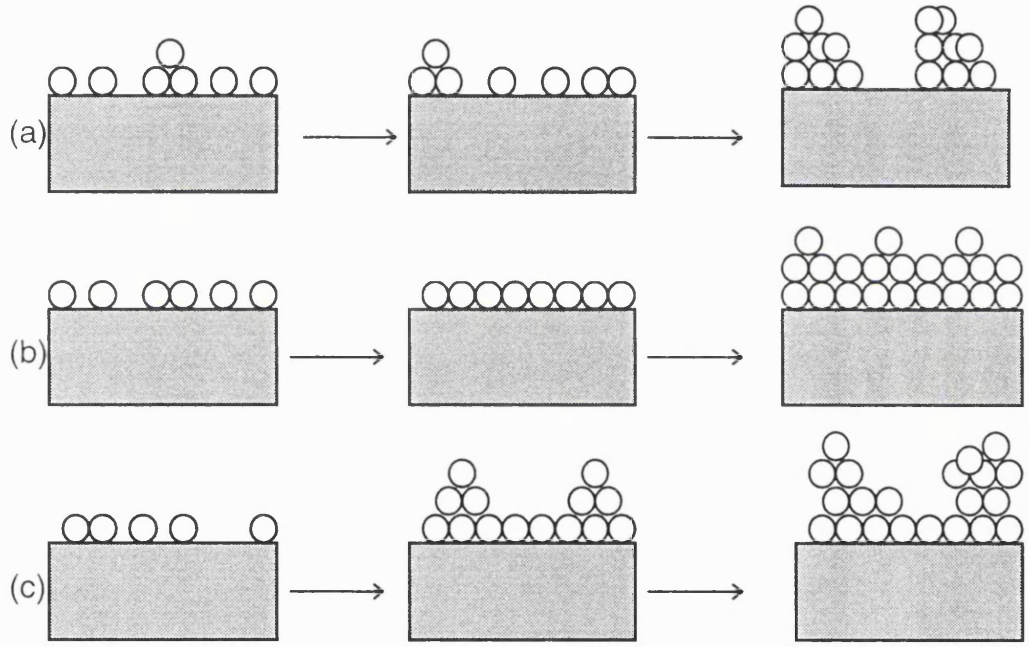

Figure 4.6. *Basic growth processes (a) island, (b) layer-by-layer and (c) Stranski-Krastanov type [1].*

(II) Volmer-Weber Growth (VW): This is a three-dimensional (3-D) mode of growth which takes place from the beginning of condensation, if the interaction energy between atoms of the deposit (cohesion) is larger than that between the atoms of the deposit and the atoms of the substrate (adhesion). It is also known as island growth (IG).

(III)Stranski-Krastanov Growth (SK): In certain circumstances, such as an increase in stress due to mismatch of lattice spacing with increased film growth, one or many monolayers are initially formed, following by subsequent growth of 3D islands on the top of them. Atoms in the vapour form are assumed to impinge on

the substrate surface, creating layer or island depending on the relations between the surface tension of the substrate, the surface tension of the deposit and the interfacial tension between the substrate and the deposit. The free-energy change accompanying the formation of an aggregate of mean dimension, r, is given by equation,

$$\Delta G = a_3 r^3 \Delta G_v + a_1 r^2 \gamma_{vf} + a_2 r^2 \gamma_{fs} - a_2 r^2 \gamma_{sv}. \qquad (4.14)$$

The chemical free-energy change per unit volume, ΔG_v, drives the condensation reaction. There exists several interfacial tensions, γ, and these are identified by the subscript's f, s and v representing films, substrate and vapour respectively (figure 4.7).

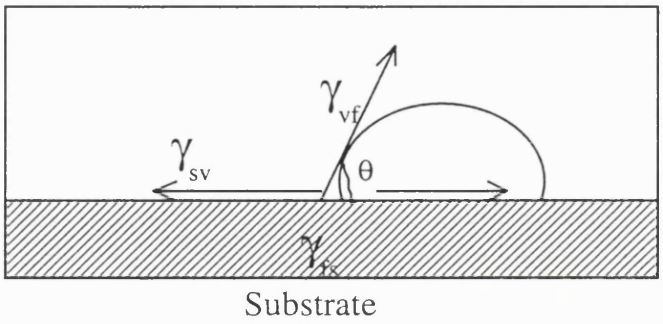

Figure 4.7. *Showing the different interfacial tensions.*

Condensation of the mechanical equilibrium between the interfacial tensions leads to following equation

$$\gamma_{sv} = \gamma_{fs} + \gamma_{vf} \cos\theta. \qquad (4.15)$$

Where θ, the contact angle, depends only on the surface properties of the materials. Three modes of growth can be distinguished through the above equation. For VW island growth, $\theta>0$, and therefore,

$$\gamma_{sv} < \gamma_{fs} + \gamma_{vf}. \qquad (4.16)$$

For Frank van der Merwe layer growth the deposit 'wets' the substrate and $\theta= 0$. Therefore, for example in ideal homoepitaxy

$$\gamma_{sv} = \gamma_{fs} + \gamma_{vf}. \qquad (4.17)$$

because the interface between film and substrate essentially vanishes, $\gamma_{fs}=0$. Lastly, for Stranski-Krastanov growth,

$$\gamma_{sv} > \gamma_{fs} + \gamma_{vf}. \qquad (4.18)$$

The growth mode is also dependent upon the supersaturation, ζ, which is defined as the ratio of the vapour pressure of the arriving atoms and the vapour pressure of the adatoms. Transitions from one growth mode to another are also possible. For example, by increasing the vapour pressure of the arriving atoms with respect to the

adatoms (increasing ζ) a transition from VW growth to LG growth is possible. In contrast, by increasing the substrate temperature, it is possible to promote VW growth as opposed to LG growth. Under suitable conditions the film growth occurs as a single crystal with respect to underlying crystal lattice of a single crystal substrate.

4.8.1 Crystallinity and orientation of thin films

Thin layers can grow in amorphous, polycrystalline textured or single crystalline form, depending on the nature of the substrate, substrate temperature, deposition rate and material. Generally, processes that raise the mobility of the adatoms on the substrate surface, cause an increase of grain size of the films. This may arise for instance from an increase in substrate temperature. In contrast, decreasing the substrate temperature also decreases the grain size [53]. The mobility of the adatoms can also be reduced by defects or impurities on the surface. During the growth of thin layers metastable phases and special structures are often formed which do not occur in the bulk [1].

The oriented layer growth can be described by the theory of Frank van der Merwe [54]. This theory assumes a sinus-shaped surface potential with the period of the lattice parameter of the substrate (a_0). The deposit is described by a spring model with a natural period 'a.' The springs are constrained to move longitudinally in the periodic field of the substrate. The result of their calculations is that with lower misfit [$(a_0-a)/a$ is small] a thin deposit layer fits to the substrate by strain (pseudomorphic growth). With increasing thickness the strain energy rises. Then surpassing a thickness threshold, it is energetically more favourable to decrease the strain energy by the successive introduction of misfit dislocations. For a thick layer the misfit is compensated by misfit dislocations and strain. Then the deposit has nearly its natural lattice parameter. In the two dimensional theories the dislocations are arranged in a plane lattice. The results of the theory have been confirmed qualitatively in many experiments with metallic double layers (Pd/Au; Ag/Au,..) [53]. If the misfit between substrate and deposit is large, the distances between the misfit dislocations observed are much larger than predicted by LG theory. Then 2D growth can be better described by the theory of the coincidence

lattice [55]. A coincidence lattice is formed when a large misfit film and substrate lattice relax near the interface. The calculations show that the coincidence lattice produces a strong minimum in the energy of the system. It will be assumed that the misfit of the coincidence lattice[$(ma_0\text{-}na)/na$; m, n integers] will be compensated by strain and misfit dislocations. In-situ observations have also shown that recrystallisation of clusters during coalescence plays a large role for epitaxy [56]. It is also found by several researchers [57] that for every deposition rate R, a critical temperature T_e exists. Above T_e, epitaxial growth takes place. Between the deposition rate R and the epitaxial temperature T_e, the following relation has been reported [53].

$$R < A \,.\, Exp\,(-Q/K_b \,.T_e\,) \qquad (4.19)$$

where, A is a constant having the same dimension of unit as R and Q is the activation energy for surface diffusion. It expresses the idea that an atom needs some time to reach an epitaxial position, which depends on deposition rate and substrate temperature. In most cases of epitaxial growth a good fit between the deposit and substrate does not play a decisive role. Whereas a large misfit can be compensated by misfit dislocations. A good example of this kind is the epitaxial growth of the fcc metals on rocksalt substrates. Summarising it must be concluded that epitaxy is a very complex phenomenon.

4.9 Summary

Various deposition techniques have been described which were used to deposit and grow cuprate superconducting layers by various researchers during last few years. The pulsed-laser deposition technique has been highlighted, and the ablation mechanism, modification of target surface and its effects on the stoichiometry and roughness of thin layers explored. Lastly, there is a brief discussion of the initial processes and different modes of growth during the thin layer formation.

References

[1] M. Ohring, "The Material Science of Thin Films," Academic Press, NewYork, (1992).

[2] J.L.Vossen and W.Kern (eds.), "Thin Film Processes", Academic Press, New York, (1978).

[3] K.Watanabe, H.Yamane, H.Kurosawa, T.Hirai, N.Koboyashi, H.Iwasaki, K.Note and Y.Muto, Appl. Phys. Lett. 54, 575 (1989).

[4] K.Shinohara, F.Munakata, and M.Yamanaka, Jpn. J. Appl. Phys., 27, L1683 (1988).

[5] H.Yamane, H.Msumoto, T.Hirai, H.Iwasaki, K.Watanabe, N.Kobayashi, Y.Muto, and H.Kurosawa, Appl. Phys. Lett. 53, 1548 (1988).

[6] M.Nemoto and M.Yamanaka, J. Mater. Res., 5, 1 (1990).

[7] F.Schmaderer and G.Wahl, J.de Phys., 50, 119 (1989).

[8] T.Tsuruoka, H.Takahashi, R.Kavasaki and H.Abe, Jpn.J.Appl.Phys. 28, L1800 (1989).

[9] J.Azoulay and D.Goldschmidt, Appl. Phys. Lett., 54, 2467 (1989).

[10] T.Satoh, T.Yoshitake, Y.Kubo and H.Igarashi, Appl. Phys. Lett. 53, 1213, (1988).

[11] T.Yoshitake, T.Satoh, Y.Kubo and H.Igarashi, Jpn. J.Appl.Phys. 27, L1262 (1988).

[12] P.Berberich, B.Utz, W.Prusseit and H.Kinder, Physica C, 497 (1994).

[13] M.Kanai, T.Kawai and S.Kawai, Appl. Phys. Lett. 58, 771 (1991).

[14] M.E.Klausmeier-Brown, G.F.Virshup, I.Bozovic, J.N.Eckstein and K.S.Ralls, Appl.Phys.Lett.60, 2806 (1992).

[15] M.Kanai, T.Kawai and S.Kawai, Appl.Phys.Lett.,58, 771 (1991).

[16] R.J.Cava, B.Batlogg, J.J.Krajewski, L.W.Rupp, L.F.Schneemeyer, T.Siegrist, R.B.von Dover, P.Marsh, W.F.Peck Jn., P.K.Gallagher, S.H.Glarum, J.H.Marsh, W.F.Farrow, J.V.Waszczak, R.Hull and P.Trevor, Nature, 336, 211 (1988).

[17] H.Adachi, S.Adachi, Y.Ichikawa, K.Setsune and K.Wasa, Jpn.J.Appl.Phys. 30, L39 (1991).

[18] S.H.H.Naqvi, M.Vickers, S.Tarling, P.Barnes and I.W.Boyd,"Preparation and Growth of PbSrYCaCuO Thin Films Superconductor", eds. B.Braren, J.J.Dubowski, D.P.Norton (MRS, Pittsburgh), pp. 287-292(November, (1992).

[19] S.Ikegawa, Y.Motoi and T.Miura, Physica C, 229, 280 (1994).

[20] H.W.Zandbergen, K.Kadowaki, M.J.V.Menken, A.A.Menovsky,

G.van Tendeloo and S.Amelinckx, Physica C, 158, 155 (1989).

[21] A.Tokiwa, T.Oku, M.Nagoshi, M.Kikuchi, K.Hiraga and Y.Shono, Physica C, 161, 459(1989).

[22] T.Terashima, Y.Bando, K.Lijima, K.Yamamoto, K.Hirata, K.Hayashi, K.Kamigaki and H.Terauchi, Phys.Rev.Lett. 65, 2684 (1990).

[23] S.Sakai, Y.Kasai and P.Bodin, Jpn. J. Appl. Phys.31, L399 (1992).

[24] Gmelin Handbook of Inorganic Chemistry, System no.47, p.77 (Springer, Berlin, 1969).

[25] A.Perrin, Z.Z.Li, O.Pena,J.Padiou, and M.Sergent, Rev.Phys. Appl. 23, 257 (1988).

[26] M.Hong, S.H.Liou, D.D.Bacon, G.S.Grader, J.Kwo, A.R.Kortan and B.A.Davidson, Appl.Phys.Lett. 53, 2102 (1988).

[27] H.M.Smith and A.F.Turner, Appl. Opt., 4, 147 (1965).

[28] J.G.Bednorz and K.A.Mullar, Z.Phys.B, 64, 189 (1986).

[29] S.Metev, in: Laser Processing and Diagnostics, Vol. 2, Edts. D.Bauerle, K.L.Kompa, and L.Laude, Proc. E-MRS, p143 (1986).

[30] D.H.A.Blank, R.P.J.Ijsselsteijn, P.G.Out, H.J.H.Kuiper, J.Flokstra and H.Rogalla, Mat.Sci.Eng. B, 13, 67 (1992).

[31] D.L.Lin, X.Li, Z.D.Lui, T.F.George, J.Appl.Phys. 72, 4227 (1992).

[32] J.T.Cheung and H.Sankur, CRC Critical Review in Solid State and Materials Science, 15, 63-108 (1988).

[33] L.Lynds, B.A.Woody, J.Electron Spect. and Rel. Phenom. 29, 147, (1983).

[34] G.Goch, J.Appl.Phys.39, 5804 (1968).

[35] J.A.Greer and J.B.Hook, SPIE proceeding 79, 1377 (1990).

[36] R.E.Muenchausen, R.C.Dye, X.D.Wu, L.Luo, and D.W.Cooke, Appl.Phys. Lett., 59,1374 (1991).

[37] H.Sanker, W.J.Bunning, J.DeNatale, J.F.Flintoff, Appl.Phys.Lett., 65, 2475 (1989).

[38] A.Richter, Thin Solid Films, 188, 275-292 (1990).

[39] R.K.Singh, O.W.Holland and J.Narayan, J.Appl.Phys. 68, 223(1990).

[40] S.R.Foltyn, R.E.Muenchausen, R.C.Estter, E.Peterson, W.B.Hutchenson, K.C.Ott, N.S.Nogar, and K.M.Hubbard, in Laser

Ablation for Material Synthesis, eds. D.C.Payne and J.C.Bravman (Mater. Res.Soc.Symp.Proc. 191, Pittsburgh, PA, 205 (1990).

[41] F.Beech and I.W.Boyd, in Photochemical Processing of Electronic Materials, edited by I.W.Boyd and R.B.Jackman, Academic Press, New York, 387 (1991).

[42] A.Inam, X.D.Wu, T.Venkatesan, S.B.Ogale, C.C.Chang, and D.Dijjkanp, Appl.Phys.Lett. 51, 1112 (1987).

[43] R.A.Neifield, S.Gunapala, C.Liang, S.A.Shaheen, M.Croft, J.Price, D.Simons, and W.T.Hill, Appl.Phys.Lett. 53, 703 (1988).

[44] J.F.Ready, "Effect of High Power Radiation", Academic Press, New York (1971).

[45] R.K.Singh and J.Narayan, Phys. Rev.B, 41, 8843 (1990).

[46] D.Bhattacharya, R.Singh and P.Holloway, J.Appl.Phys. 70, 5433 (1991).

[47] W.Kautek, Thin Solid Film, 191, 317 (1990).

[48] L.Lynds, B.R.Weinberger, D.M.Potrepka, G.G.Peterson and M.P.Lindsay, Physica C 159, 61 (1989).

[49] E.van de Riet, J.C.S.Kool and J.Dieleman, J.Appl.Phys. 73, 8290 (1993).

[50] K.H.Young, Physica C 211,1-12 (1993).

[51] R.Kelly and J.E.Rothenberg, Nul.Instrum.Meth.,3718, 755 (1985).

[52] J.Y.Tsao, "Materials Fundamentals of Molecular Beam Epitaxy", Academic Press, Boston, (1993).

[53] K.Reichelt, Vacuum, 38, 1083 (1988).

[54] H.J.van der Merwe, Advances in Epitaxy and Endotaxy (edited by H.G.Schneider and V.Ruth), p129. VEB Deutscher Verlag fur Grundstoffindustrie, Leipzig (1971).

[55] J. W. Matthews, IBM Report RC 4266, No 19084 (1973).

[56] R.Kern, G.de Lay and J.J.Metois, in current topics in Material Science, 3, North Holland, Amsterdam (1979).

[57] J.W.Matthews, in Epitaxial Growth, Edited by J.W.Matthew, p559, Academic Press, NewYork (1975).

Chapter 5

Experimental and characterisation techniques

In this chapter a detailed experimental procedure for deposition of thin layers using PLD is described. A description of the characterisation techniques used to analyse bulk or thin layers are presented.

5.1 Experimental set-up

An experimental set-up for PLD of thin films designed and used is illustrated in figure 5.1. A deposition cell, different ports, vacuum gauges, rotary pump, diffusion pump and optical components were used in the construction of PLD system. Nearly all the experiments were performed using Q-switched Nd:YAG laser (Quantel, model YG 571C-10) with 4ns duration (FWHM), 532nm wave length and an energy of 1Joule that could be reduced by the help of neutral density filters. The repetition rate could be set to 10Hz, 5Hz, 2Hz or single pulse (controlled manually). Normally, the laser beam was directed to a vacuum chamber via a series of mirrors and a lens (f=15cm) at an angle of 30° with the normal to the surface of a slowly rotating target (5 Rev./min). The laser energy at the target was measured using a Molectron, J50 joule meter. Targets, 13mm in diameter, were synthesised using ceramic technique for ablation-deposition purpose. The distance between the target and substrate could be varied by moving the target back and forth.

Usually, prior to deposition the chamber was flooded with oxygen, evacuated to a pressure of $1x10^{-3}$mbar by only a rotary pump but some time it could be further pumped down to $1x10^{-5}$mbar by a diffusion pump. To obtain partial pressure of any gas during deposition, a needle-valve was used near the substrate. Superconducting thin Pb-Sr-(Y,Ca)-Cu-O layers were grown on single crystal, MgO (001) or Si(111) substrates. The choice of the substrate was made on the ground of i) chemical stability above 700°C ii) availability on economical basis iii) or minimal lattice mismatch.

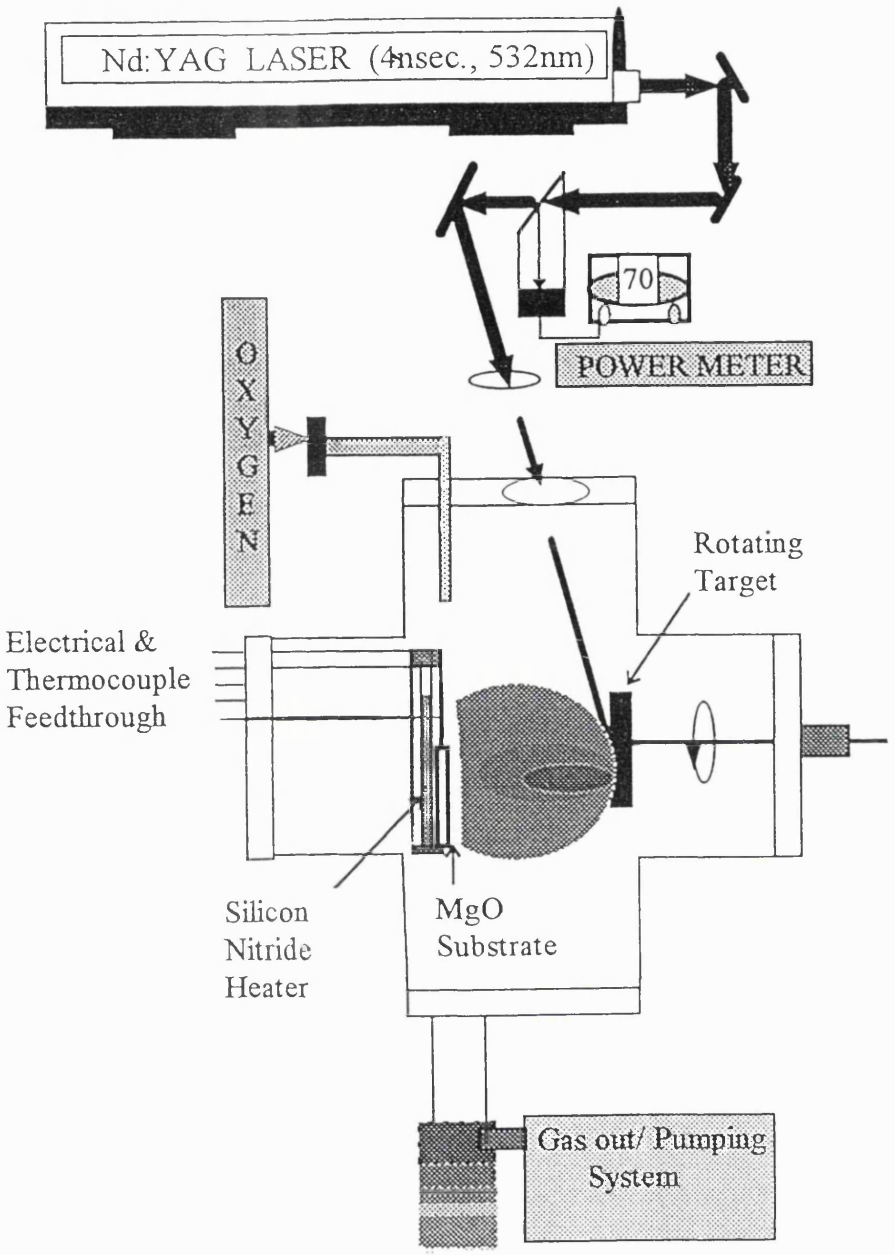

Figure 5.1. Schematic diagram of the experimental set-up for PLD of Pb-Sr-(YCa)-CuO thin films.

Initially, a home made substrate heater was used for in-situ deposition. It was prepared using a 3mm thick plate made of high density alumina ceramic and was delicately machined with 1.0mm deep grooves on one surface. The heating wire (FeCrAlY) was inserted in the grooves and covered with cement (mixture of water, sodium silicate or silica glass as a binder and fine alumina powder). FeCrAlY has the property that once fired its surface oxidises without affecting the inner core of the wire. This heater can reach up to 800°C in oxygen ambient. A Chromel-alumel thermocouple wire was spot welded at one end and connected to the nearest position of the substrate. Therefore, the growth temperatures of the films are referred to in this thesis, are of the heater and not exactly of the substrate. After several cycles of heating, the home made heater was degrading, realised by an

increase in its electrical resistance. Later, a commercial silicon-nitride substrate heater (R=56Ω), with longer life the home-made one, and which could be heated up to 950°C at 100V even under 0.5mbar oxygen pressure, were used by connecting directly to step-down variac.

5.2 The multi-target holder

A multi-target holder was designed and manufactured out of stainless steel at UCL, Electronic and Electrical Engineering workshop to deposit in-situ multilayers of different materials. It can accommodate up to five different targets and could be adjusted one by one manually in front of laser beam without breaking vacuum. A shield was placed in front of the multi-target holder so that it can protect the other targets from contamination during the ablation of the one rotating target. A schematic diagram of the multi-target holder is shown in figure 5.2.

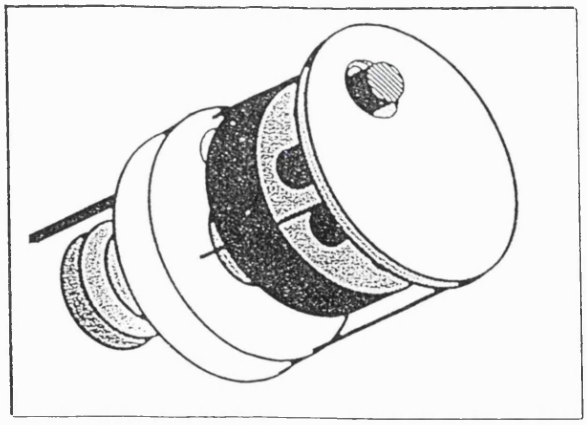

Figure 5.2. *Schematic diagram of the multi-target holder.*

5.3 The processing furnace

The bulk material processing or ex-situ annealing of the deposited thin layers was carried out in a quartz tube furnace controlled by a programmer to run different required annealing procedures. After home made winding and using insulation paste of alumina cement, the furnace was calibrated for temperature with in the quartz tube of 6 cm in diameter and 100 cm in length. The temperature of the samples was monitored by a Chromel-alumel thermocouple wire placed near the samples. A uniform temperature was found only with in the length of 4cm at the centre of the tube. All the heat

treatments were performed in the range of uniform temperature by keeping the samples at the mid of the furnace on platinum foil.

5.4.1 DC resistivity measurements

All the electrical and magnetic characterisations were performed using an APD cryostat in Imperial College, at Physics department. The DC electrical characterisation records an electrical resistance versus temperature for a sample. This is commonly performed by attaching four leads at the periphery of the sample and cooling down to the temperature where the resistance of the sample becomes zero. The Van der Pauw technique [1] facilitates the comparison of different samples of different shapes by using the four point contact configurations into geometry independent resistivity measurements. The method is valid for a flat sample, homogeneous and isotropic, uniform in thickness of any arbitrary shape if the contacts are sufficiently small, located at the circumference of the sample as shown in figure 5.3. Between two points, a dc current, I, flows that must be below the critical current, I_C of the sample. The other two leads measure the voltage across the sample. The reversal of the current direction serves to eliminate any dc offset voltages, for example, thermo-electric effects in the leads and the contacts due to temperature inhomogeneities and connections could result in errors in the order of few micro volts. To minimise this error, it is necessary to measure voltage response, ΔV of the film with or without current flowing through it.

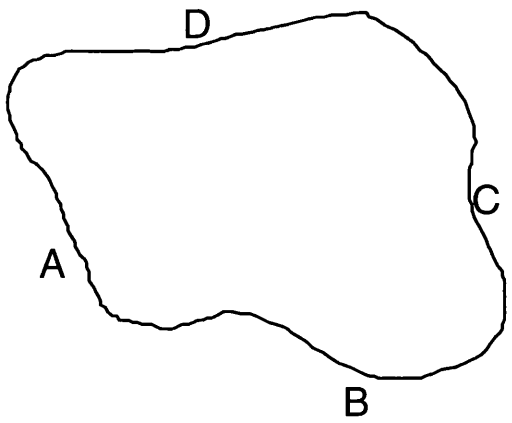

Figure 5.3. *A sample of arbitrary shape with four points contacts on its periphery.*

Hence, a dc current is applied through the sample in forward (+) and reverse (-) direction; the corresponding voltages V_+ and V_- are measured and the sample resistance is then obtained as

$$R = (V_+ - V_-)/ 2I. \qquad (5.1)$$

For the determination of the zero resistance, a voltage criterion is selected, which depends on the noise level in the set-up, but is typically 1μV/cm (i.e. per cm of distance between the voltage leads). If the measured value falls short of this limit, then a zero voltage drop and no electrical resistance, R is registered in computer programme, Lotus 123 spread sheet.

5.4.2 Contact problem

Connecting the leads onto the thin film samples by using silver paste causes deterioration of these contacts upon cooling, during several thermal cycles and disconnection usually occurs while cooling below 80K. The technique of annealing the contacts prepared by silver past at low temperature (400°C) in air or oxygen is not applicable as in the case of Y-Ba-Cu-O or Bi-Sr-Ca-Cu-O films due to serious oxidation problem with Pb-2213 phase. Annealing of contacts made by silver paint in nitrogen deteriorated the superconducting properties and usually the contacts became insulating. Evaporating indium pads onto the film for connection purpose is time consuming and lengthy process. Another trick was used to prepare connections. The film at the corners was slightly removed and then silver paint was applied on the substrate and joined with film. The connecting wires were attached to the part of the silver on the substrate instead of the films.

5.5.1 Diamagnetic measurements

The experimental set-up for the diamagnetic transition (Meissner effect) was also used at Imperial College, London. It is a modified apparatus of a design by Xeninkos and Lemberger [1]. The sample is laid on top of a flat spiral coil that forms part of a resonant LC circuit, operating at about 1MHz. During diamagnetic transition, a superconducting sample induces changes in the inductance of the coil, that shift the dc voltage versus frequency curve. Due to diamagnetic transition of superconducting sample, a sudden change is induced in the inductance of the coil.

These variations, typically several percentages, are detected by the system. The magnetic flux lines, Φ, emanating perpendicularly to the coil are equal to the product of inductance, L, and current, I, flowing through the coil:

$$\Phi = LI \qquad (5.2)$$

When the magnetic lines of induction are excluded from the interior of the superconducting sample on the top of the coil, they are deformed, as depicted in figure 5.4. As a result of this deformation, Φ decreases lightly which in turn leads to a slight change in the inductance L.

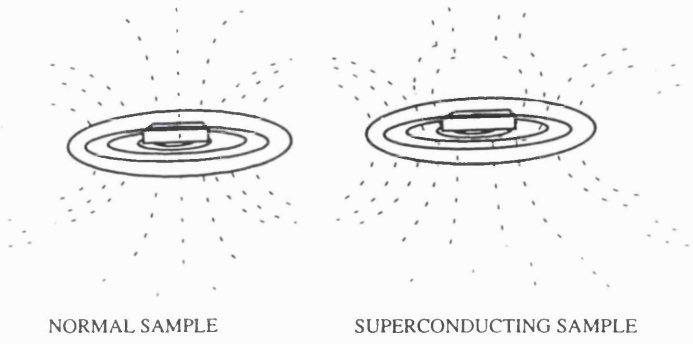

Figure 5.4. *Shows the effect of diamagnetism of a superconducting sample on top of the spiral coil.*

Figure 5.5 represents a block diagram of the apparatus. The resonant circuit is formed by the capacitor C_{LC} and inductor L, a flat coil with 15 turns of no. 36 copper wire forming a circular spiral. It has inner and outer diameters of 0.5 and 6mm. Its inductance (including the leads connecting it to the rest of the circuit) is approximately 4.6 μH (+3%) while the capacitance of C_{LC} is around 4.73 nF (+3%). The coil is glued onto the tufnol tip of a dipstick probe which fits into the sample well of the APD Cryogenics HC-2 refrigeration system. The remaining components of the circuit, including C_{LC}, are kept at room temperature in a shielded metal box. The LC circuit is connected via a 2.2pF coupling capacitor to an rf sinusoidal signal generator, an RS 17A, which supplies 500mV. The voltage that appears across the resonant circuit has a reactive component that is in-phase with the generator voltage as well as a resistive out of phase component. To measure only the in-phase component that depends on the coil inductance, the voltage across the resonant circuit is amplified with a PSSRMC8824 rf amplifier. Subsequently, it is multiplied by the generator signal $V_g\text{Cos}(\omega t)$, using an

MC1595L balanced mixer. The dc voltage resulting from this electronic multiplication is amplified ten times by a 741 operational amplifier. The undesired out of phase voltage appears as an rf signal at the output of the mixer and is filtered out in the final stage of the circuit, using two 1μF capacitors in parallel.

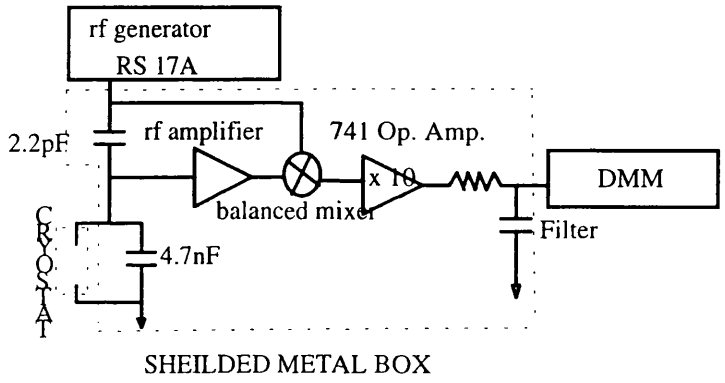

Figure 5.5. Showing a block diagram of the inductive apparatus.

The value for the resonant frequency depends naturally on the superconducting property of the material and effective size of the sample that screening the coil magnetic field.

5.6.1 Thickness measurements

A step was made on the deposited film by masking a portion of the substrate during deposition. Normally, a Talystep is used to measure the thickness of superconducting thin film. A Talystep consists of a stylus that has a small tip and a light load to limit penetration of the surface. The instrument measures the vertical movement of the stylus travelling across the sample surface. The vertical displacement is converted to a signal that is then amplified and recorded on a strip chart. A wide variety of vertical amplifications are available, thus film thicknesses from about 20Å to 10μm can be measured. However, for very thin films it was found that masking technique did not give satisfactory results. On removing the mask, the step produced was not always well defined.

5.6.2 Colour comparisons

The variation of colour with film thickness has long been known. This technique is a fast and reliable method of estimating film thickness. A detailed colour chart was used in this thesis for colour comparison similar to Pliskin and Conrad [2]. The films deposited at room temperature on Si (001) substrates were used for thickness estimation using colour comparison and also checked by Talystep.

5.6.3 Ellipsometry

Ellipsometry provides a fast reliable method for measuring both thickness and refractive index [3]. Ellipsometry is based on evaluating the change in the state of polarisation for light reflected from a substrate. The state of polarisation is determined by the relative amplitude of the parallel component, ρ_p, and perpendicular component, ρ_s, of radiation and the phase difference between the components. On reflection from a surface, the ratio ρ_p/ρ_s, and the phase difference undergoes changes which are dependent on the optical constants of the substrate n_3 and k_3, the angle of incidence θ, and n_2k_2 of the film and film thickness d. If the optical constants of the substrate are known, and $k_2=0$, the film is non absorbing at incident wavelength, then the only unknowns d and n_3 can be determined.

In a typical ellipsometer, a He-Ne laser light is linearly polarised and then elliptically polarised by a compensator. After reflection from the sample, the light is transmitted through a second polariser that analyses the polarisation. Finally, the light intensity is detected by a photomultiplier. The angle of incidence and reflection can be varied but are generally set at 45° from the substrate plane. The user places the sample on the ellipsometer, levels the sample table, and aligns the optics in order to maximise the signal intensity. The computer then rotates the polariser and analyser until extinction is obtained. From the readings obtained, the phase difference and amplitude ratio are determined, the refractive index and thickness values are obtained. When the film thickness is $t \cong n\lambda/2$, the lines of the constant refractive index merge and the refractive indices cannot be determined.

The films deposited on Si at room temperature were characterised by ellipsometer to measure the thickness at different positions of different colour and compared with the chart of colour comparision given in reference [2]. Those films were sufficient to get an estimate of the deposition rates at the room temperature and an idea about thickness non-uniformity of thin layers.

5.7 X-ray diffraction measurements

The x-rays are created by bombarding a soft metallic target (Cu, Mo or Co) with an energetic electron beam and a characteristic monochromatic radiation is used to determine crystalinity, orientations, inter-atomic distances and bond length for inorganic solids. To determine the orientations or structure of thin films and bulk materials, x-ray diffractometers are the most commonly used instrument where the diffracted radiation is detected by counter tubes which move through the angular range of reflections and recorded in a computer programme for data processing.

X-rays are diffracted by the atomic plane of any crystalline material. Considering two ions of adjacent planes are spaced by 'd', reflecting rays which interfere constructively, then the path difference between the two rays is equal to $2d \sin\theta$, where 'θ' is the angle of incidence. For the constructive interference, the path difference must be an integral number of wave length leading to the Bragg's law [4].

$$n\lambda = 2d \sin\theta \qquad (5.3)$$

where n is the order of corresponding reflection. Obviously, to investigate systematically x-ray reflections from crystalline material, some of the experimental parameters such as wave length, x-ray beam direction or sample orientation must be allowed to vary over a sufficiently large range. Obtaining a powder diffraction pattern requires the measurement of angular positions, as well as of intensities of reflections. The commonly used powder diffractometer consists of a primary beam slit system, sample holder, and electronic detectors such as proportional or scintillation counters and associated slits, mounted on the detector arm. The sample is rotated at a constant angular velocity about a line passing through the centre of the sample.

The relationship between the lattice spacing, d, Miller indices (hkl) and the lattice constants of an orthorhombic (a, b, c), and tetragonal crystal (a=b, c) are given by,

$$1/d^2 = h^2/a^2 + k^2/b^2 + l^2/c^2 \qquad (5.4)$$

and

$$1/d^2 = (h^2 + k^2)/ a^2 + l^2/c^2 \qquad (5.5)$$

respectively. For cubic crystal it is related as

$$1/d^2 = (h^2 + k^2 + l^2) / a^2 \qquad (5.6)$$

Most of the x-ray scans were provided by the Department of Crystallography, at Birkbeck College, using Siemens x-ray diffractometer and CuK_α radiation (λ=1.5418Å). The 'd' spacings were obtained for each scan using computer programme. The estimated line intensities could be compared with those either listed in the Powder Diffraction File or in the literature.

5.8 Scanning Electron Microscopy (SEM)

Scanning electron microscopy (SEM) is one of the major analytical tools used routinely in micro structural analysis. In this section SEM and electron-probe micro-analysis (EPMA) techniques are described which were used to study the surface morphology of the samples and the identification of constituent elements to measure their relative composition. The basic principle of these techniques consists in scanning a focussed-monochromated electron beam that is produced in an electron microscope column. Electrons are emitted from a conventional thermionic sources such as hairpin type filament made of tungsten (W) or LaB_6 or field emission electron source consisting of a pointed cathode, made of a single crystal tungsten tip polished to 1,000Å in radius of curvature, and the emission intensity of

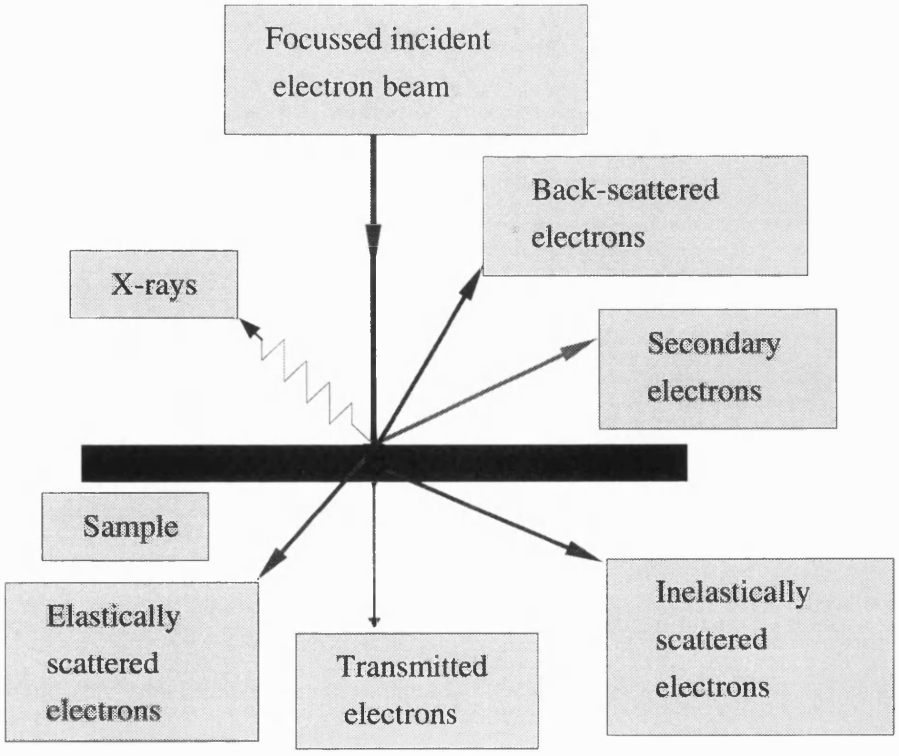

Figure 5.6. *The interaction of an electron beam and output from specimen.*

the order of $10^5 A/cm^2$ over the surface of the sample. The electrons are scattered by the atoms of the sample whereas the scattering factor increases with atomic number. The various forms of output emission shown in figure 5.6 provide the basis for different analysing techniques. The best SEM columns can achieve focusing on the sample surface into a spot of about 10Å. This spot size is the essential factor determining the spatial resolution of the SEM. Usually magnetic lenses are used since they are more effective for high electron energies than electrostatic lenses (**F=evxB**); aberration errors are smaller too. The x-y scan is usually performed by two magnetic coils arranged perpendicular to one another between the two magnetic lenses. The amplification of the SEM is produced simply by electronically varying the deflection angle of the scanning electron beam. A video tube is employed as optical display; its electron beam is scanned synchronously with primary probing beam of the microscope column, i.e., both beams are controlled by the same scanning electronics and the amplification of the SEM is adjusted by a scaling factor introduced essentially by a resistance divider circuit. The intensity of the electrons emitted from the sample determines the intensity of the TV tube beam. Different detectors sensitive to various energy ranges of the emitted electrons can be used. A solid surface irradiated by an electron beam of energy E_0, emits electrons of various origins. Besides elastically backscattered electrons of energy E_0, there is a regime of inelastically backscattered secondary electrons, where the spectral structure stems from energy losses due to plasmon excitation and interband transitions. These excitations are specific to every solid. A detector tuned to this energy range thus yields an image of the surface that is extremely sensitive to composition (BE detector). The major part of the emission of secondary electrons forms a strong and broad spectral band between 0 and 50eV, but extends as a weak tail up to E_0, called true secondary electrons. Their specific distribution and intensities are not very specific to a particular material. The detector SE is tuned to record low energy secondary electrons and thus yields a different image of the surface from that obtained by detector BE and less shadowing is observed due to the lack of forward scattering. In principle, SEM pictures are not stereoscopic, good insight into the geometry of an object or a surface can be achieved by using various detectors and different irradiant geometries. A work-function variation and other electronic factors give rise to contrast changes.

The x-rays are used to provide local-chemical analysis of the surface. An x-ray detector is typically placed perpendicular to the axis of the microscope at the level of the specimen. When this detector is used the specimen is tilted 30° or more. An important factor is to see the volume penetration by the incident electron beam, and the volume from which signals come for detection. The characteristic differences between the information depth and the volume probed by the different techniques is presented schematically in figure 5.8.

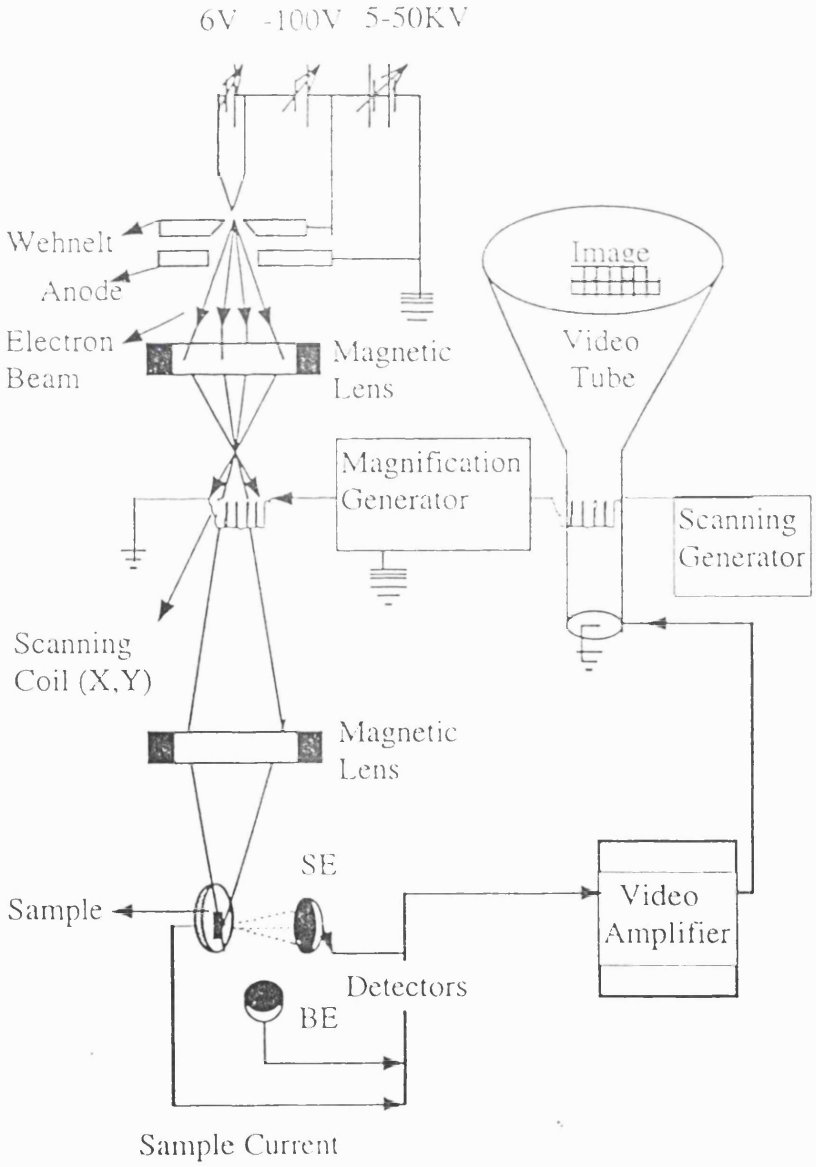

Figure 5.7. *Schematic set-up of a scanning electron microscope.*

The initial elastic and inelastic scattering are only through small angles and beam spreads slowly during the initial penetration that originates pear-shape. As electrons

are repeatedly scattered the beam broadens and electrons eventually lose all their kinetic energy. The result is a roughly spherical penetration volume some distance below the surface with a radius of a micron or more depending on the initial electron energy and the material. X-rays are generated throughout this volume, except for the thin shell near the extreme range of the electrons in which they no longer have sufficient energy to ionise atoms.

SEM equipped with an energy dispersive X-ray analysis facility gives an average chemical composition over a volume of a cubic micrometer or more. The selection of accelerating voltages(1-20keV) of the electron beam for quantitative analysis is governed by the ranges available on the microscope and the particular application for which the system is used. The lower the accelerating voltage, the shorter the penetration depth of the incident electron beam into the specimen and consequently the absorption of x-rays generated within the specimen is minimised. The EDX technique is widely used for the stoichiometric analysis of bulk material and has certain error (10%) for quantitative analysis of thin films, >1μm in thickness. Mostly, the compositional analysis of lead-based materials were performed using EDX (cobalt as a standard reference) or EPMA.

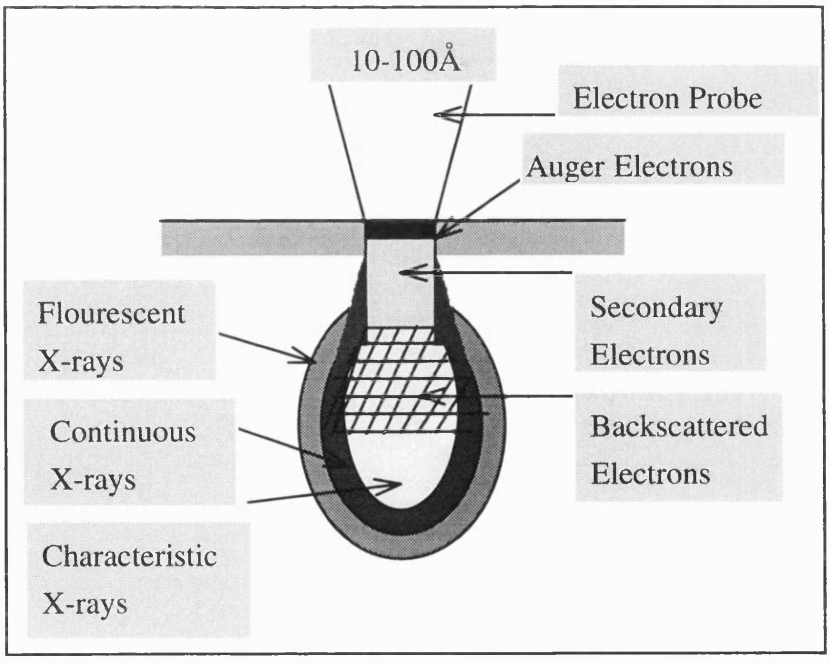

Figure 5.8. *Drawing representing different microprobe signals when electron beam penetrating into a solid surface.*

In an EDX spectrometer solid-state x-ray detectors are employed which record the whole spectrum simultaneously. The pulse heights produced in detector are stored according to x-ray energy. Usually, liquid-nitrogen cooled Si(Li) detectors are used to intercept x-rays emitted from sample interacted with energetic electron beam. The Si(Li) detector is a reversed-biased Si diode doped with lithium (Li) to create a wide depletion region. An incoming x-ray generates a photo-electron that eventually dissipates its energy by creating electron-hole pairs. The incident photon energy is linearly proportional to the number of pairs produced or to the amplitude of the voltage pulses they generate when separated. Si(Li) detectors typically have a resolution of about 150eV, so overlap of peaks occurs when they are not separated in energy by more than this amount. Overlaping always occurs in multicomponent samples when neighbouring elements of the periodic table are present.

5.9 Electron-probe micro-analysis (EPMA)

The electron microprobe (EPM) is an instrument specially designed to perform wavelength-dispersive (WDX) analysis. This technique functions by measuring the intensity of characteristic x-rays from a sample by a finely focused electron beam on it. Individual elements in the sample can be distinguished from the corresponding wavelength and their concentration can be estimated from the intensity of the particular wavelength and compared with those from standards, usually are taken as pure elements. This technique provides a much higher accuracy (3%) for quantitative analysis compare to EDX. The electron probe is effective tool and can be used to scan along a line or over a large surface area of about 200mm edge length, whereby the output is displayed on a screen to show the elemental distribution [3]. The disadvantage is the high cost of equipment, longer period of analysis and inadequate supply of standards. A JEOL-JXA (8600) machine, a bulk PbSrYCaCuO pellet and pure individual elements as standards were used for analysis of thin Pb-2213 phase films.

Although the EDX method is much faster than the WDX method, the resolving power obtainable is substantially inferior to WDX. In both techniques, certain corrections are applied such as relationship between intensity and composition, "ZAF correction", the

correction factors for the atomic number, Z, the absorption, A, and the fluorescence, F, produced by the x-ray lines or from background [5].

5.10 Summary

In summary, the deposition set-up and the synthesising systems have been described. Most of the characterisations which were used during the course of research, either for the thin films or bulk materials have been described. It includes the details about XRD, EDX, EPMA, thickness measuring techniques, diamagnetic, and Van der Pauw method for resistive transition temperature measurements.

References

[1] D.G. Xeninkos and T.R. Lemberger, Rev. Sci. Instr. 60, 831 (1989).

[2] W.A.Pliskin and E.E.Conrad, Nondestructive determination of thickness and refractive index of transparent films, IBM J.Res.Develop, 8, pp.43-51(1964).

[3] L.I.Maissel and R.Glang, "Handbook of thin film technology", Mc-Graw Hill (1970).

[4] J.B. Watchman, "Characterisation of Materials", Manning Publications Co., Boston, p299 (1993).

[5] S.J.B. Reed, "Electron Microprobe Analysis", Cambridge University Press, (1993).

Chapter 6

Various Compositions, Synthesis and Superconductivity

Usually, HTSC materials contain three or more cations and have a wide range of solid solubilities. The composition of these materials is crucial, because of the sensitivity of electrical properties to their stoichiometry. For example, the electrical properties of $Nd_{2-x}Ce_xCuO_{4-\delta}$ and $Pb_2Sr_2(Y_{0.5}Ca_{0.5})Cu_3O_{8+\delta}$ can be altered dramatically at low temperatures with minute changes in the values of x and δ [1, 2]. In this chapter, it is attempted to present experimentally obtained results during various bulk-preparation conditions, modifications in common solid-state reaction methods and related effect on the superconducting transition temperatures of various stoichiometric lead-based materials.

6.1.1 Synthesis of $Pb_2Sr_2(Ln_{1-x}Ca_x)Cu_3O_{8+\delta}$ (Pb-2213) material

Initially, stringent conditions were reported as being required for the synthesis of the lead-based Pb-2213 phase material [2]. Direct synthesis of the $Pb_2Sr_2(Ln,Ca)Cu_3O_{8+\delta}$ (Ln=Y or rare earth) phase by the reaction of the component metal oxides or carbonates in air or oxygen at temperatures below 900°C is not possible due to high stability of $SrPbO_3$-related perovskite oxides or possibly because of the compounds Ca_2PbO_4, Y_2SrO_4 and Sr_2PbO_4 being formed in preference at low temperatures. Furthermore, Pb in the Pb-2213 phase is in the +2 valence state while sandwich copper is in +1 state. The mixture of oxidised and reduced cations in the same crystallographic unit cell is the unique feature of the Pb-2213 phase material and creates much difficulty in synthesising the superconducting phase. It requires a low oxygen partial pressure at high temperature to keep the sandwich reduced while simultaneously oxidising the planar copper atoms to a CuO_2 state. Therefore, it was suggested that the synthesis has to be performed under mildly reducing conditions, typically in an atmosphere of N_2 containing 1-2% O_2 [2].

The most common method that is employed for the synthesis of lead cuprates is the ceramic-precursor technique which comprises two steps [2]. In order to create the $Pb_2Sr_2(Ln,Ca)Cu_3O_{8+\delta}$ (Ln=Y or rare earth) phase, a precursor is formed by mixing oxides and carbonates containing all the metal cations except PbO ($SrCO_3$, Ln_2O_3 or Y_2O_3, $CaCO_3$ and CuO in the appropriate ratios) and heating to around 950°C in air for 16 hours [2]. The precursor is then taken with an appropriate amount of PbO,

ground thoroughly, pressed in the form of pellet and heated at 865°C overnight in flowing stream of nitrogen containing 1% O_2. Generally, short reaction times and quenching the product from sintering temperatures in flowing gaseous or liquid nitrogen to keep them in reduced state give better-quality samples [2]. Typical resistivity curves for both polycrystalline and single-crystal samples of the optimal composition are shown in figure 6.6.1. The single crystals were grown from PbO and CuO-rich melts using a two-step precursor technique (adapted from ref.[2]).

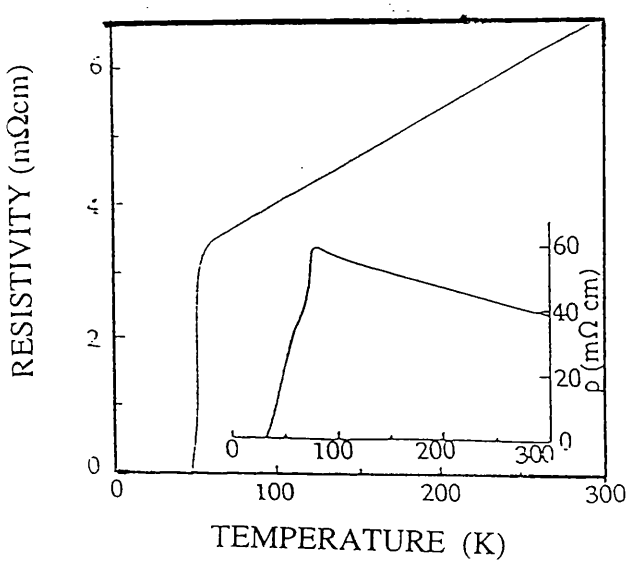

Figure 6.1.1. DC resistivity trace in the a-b plane as a function of temperature for a single crystal $Pb_2Sr_2(Dy_{0.5}Ca_{0.5})Cu_3O_8$ and polycrystalline sample (Inset) of $Pb_2Sr_2(Y_{0.5}Ca_{0.5})Cu_3O_8$.

Even though the method described above is commonly used for preparing Pb-2213 phase material, it is not easy to obtain samples exhibiting reproducible and good superconducting properties using such a two-steps precursor technique.

The lead-based materials synthesised according to the method described above generally show broad transitions in the Resistance-Temperature (R-T) plots with a negative temperature coefficient of resistance above T_c. Applying the same precursor technique several pellets were formed. The second step in the above method involves the introduction of the PbO, which was accomplished in this case by grinding the precursor and adding PbO powder to the mixture. This was then mixed and ground thoroughly for 30 minutes, pressed into a 13 mm die in the form of tablet using 10 ton pressure, and heated at 865°C for 7 hours in a mixture of 1% O_2 in N_2, flowing at the rate of 6cc/minute through the processing quartz tube furnace. After 7 hours, the pellet was cooled in the gas stream over10 minutes. It was observed at this stage that the pellet had expanded by approximately 1.2 mm across its diameter and had become very fragile. To ensure a homogeneous reaction between the PbO and the precursor,

the sample was further reground and after final pelletising step, was sintered at 865°C for total 18 hours, using the same gas flow conditions as described earlier.

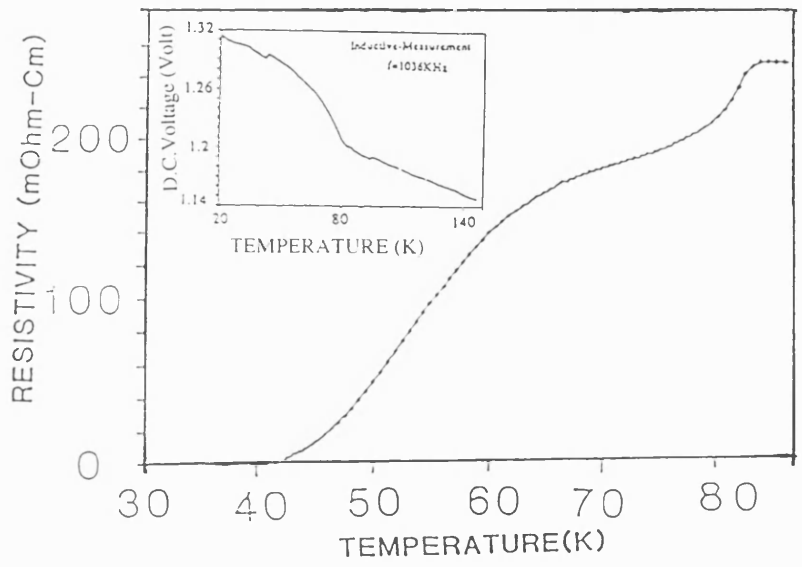

Figure 6.1.2. DC resistivity of a typical Pb-2213 bulk pellet prepared in 1% O_2 in N_2 using Cava's procedure. Inset shows diamagnetic behaviour of the same pellet.

Figure 6.1.2 shows the DC resistivity of a typical bulk pellet prepared in this manner. In common with Cava's results, the value of $T_{c,\ onset}$ is around 82K, while the transition remains wide with $T_{c,\ zero}$ of 43K. This wide range of transition temperatures is attributed to inhomogeneities in the metal and oxygen distribution rather than to exogenous phases at the grain boundaries [1]. It seems however that the unreacted metal or oxide formed in this two-step technique creates an amorphous filling between the crystallites which is more responsible for suppressing the transition temperature and increasing its width than is the role of oxygen in the CuO_δ sandwich layer [2]. It is found that the ultimate characteristics of the material are extremely sensitive to some of the preparation conditions. For example, when the sintering temperature was 855°C rather than 865°C under otherwise identical gas flow conditions, the transition temperature was found to be 82K rather than 70K, whereas $T_{c,\ zero}$ did not even reach 20K [3]. Annealing in air for 15 minutes even at 850°C made the pellet completely semiconducting [4].

Figure 6.1.3 shows XRD pattern obtained by the Department of Geology, UCL, using standard Philips PW 1050 diffractometer. The radiation used was from an iron filtered CoK_α source ($K_\alpha 1$:λ=1.78896Å, $K_\alpha 2$: λ=1.79285Å) and all the data points were collected at room temperature between 2Θ angles 0° to 60° in steps of 0.04°. The XRD patterns of both samples (SN1 and SN5A) were found to be single phase but the peak intensities were different, with the more intense peaks being related to

the oxidised pellet. The splitting of (020) and (200) peaks is greater in the superconducting sample compare than in the semiconducting (SN5A) sample, showing that the material is still orthorhombic and has partial oxidation after 15 minute annealing in air at *850°C*. Otherwise the peaks separation between 020 and 200 should disappears for tetragonal structure ($\delta < 1.2$) [5] wherethe lattice constant a=b.

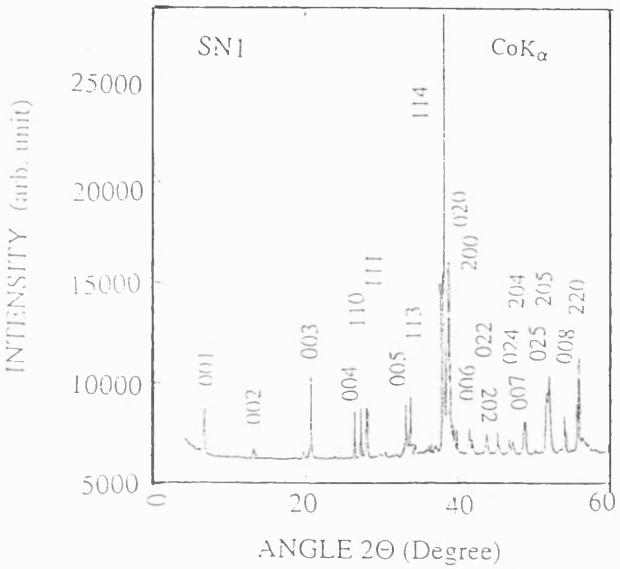

Figure 6.1.3. a) XRD pattern of the typical Pb-2213 bulk pellet prepared in 1% O_2 in N_2 after sintering for 18 hours

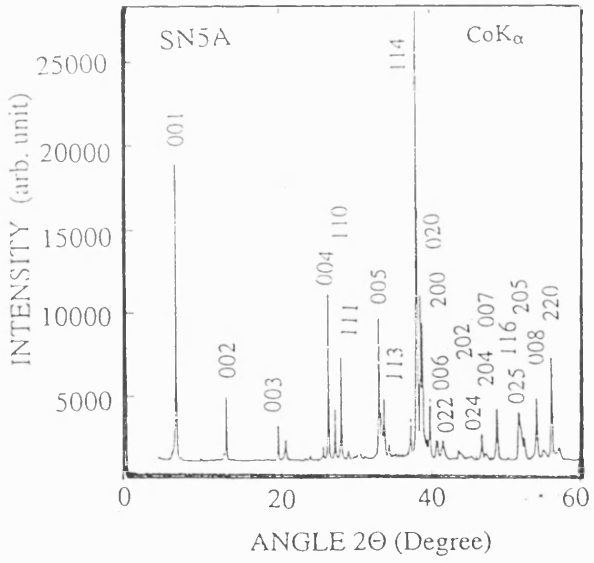

Figure 6.1.3. b) XRD pattern of the Pb-2213 bulk pellet prepared in 1% O_2 in N_2 after sintering for 18 hours then sintered in air for 15 minute at 850°C.

Another important factor is the loss of lead due to its volatile nature. This leads to micro inhomogeneities during high temperature processing. For example, the pellet sintered at 865°C for a total of 18 hours has shown non-stoichiometry of lead. The formula obtained by energy dispersive x-ray spectroscopy (EDX) is $Pb_{1.78}Sr_{2.19}(Y_{0.53}Ca_{0.52})Cu_3O_8$ whereas the starting composition before synthesis

was $Pb_2Sr_2(Y_{0.5}Ca_{0.5})Cu_3O_X$. It seems that the Pb deficiency is compensated by the substitution of excess Sr for Pb. Figure 6.1.4 presents an EDX spectrum for superconducting pellet that has minor lead loss.

Masuzawa et al. [6] altered the recognised preparation conditions by using a three-step processing method where a shorter heating period of 5 hours was used in the formation of the precursor $Sr_2(Y_{0.5}Ca_{0.5})Cu_3O_X$ matrix at 900°C. After pulverising, mixing with PbO, pressing in the form of pellet and sintering in $1\%O_2$ in N_2 at 925°C for 3-4 hours, the samples were then cooled to 750°C and held in the same flowing gas for 12 hrs, before being quenched in liquid nitrogen and post-annealed in flowing pure nitrogen at 400-500°C for a further 12 hours. This 36 hour processing period was used to achieve a good superconducting transition temperature, $T_{c,\ zero}$ of 75K together with a positive temperature coefficient of resistivity.

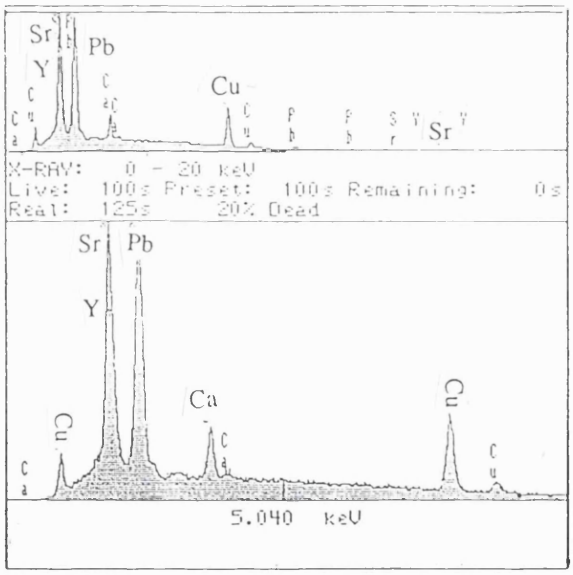

Figure 6.1.4. The EDX pattern of superconducting pellet.

The improved properties of nitrogen annealed samples were suggested to be due to the decrease in crystalline disorder and to the possible ordering of oxygen atoms in the PbO layers and calcium in Y layer under low temperature annealing in pure nitrogen. It was also pointed out that excess heat treatment (60 hrs) in 1% O_2 below 850°C could decompose the Pb-2213 phase to a $SrPbO_3$-based perovskite or to impurities such as Ca_2PbO_4 or Sr_2PbO_4 [6].

The XRD pattern and the plot of resistivity versus temperature for the samples prepared by Masuzawa et al. [6] are shown in figs. 6.1.5 and 6.1.6 respectively.

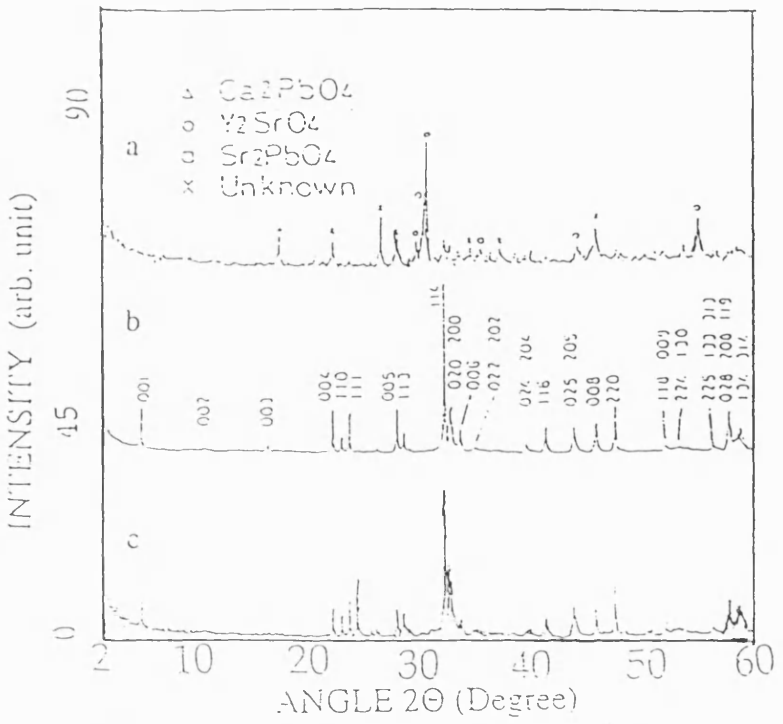

Figure 6.1.5. XRD pattern of polycrystalline pellets (a) a sample quenched from 900°C to room temperature after a first heat treatment for 2 h in 1% O_2 in N_2 b) a sample quenched in liquid nitrogen after a second heat treatment for 12 h at 750° C, c) a sample post-annealed in flowing nitrogen at 500°C for 12 h after first and second heat treatments.

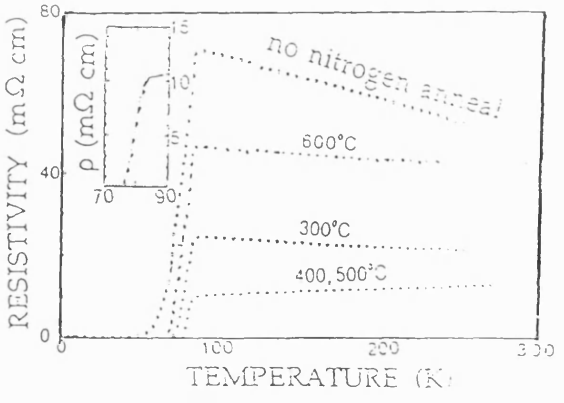

Figure 6.1.6. DC resistivity traces for the samples with and without post-annealing in N_2 for 12 hrs at various temperatures. Inset shows the trace for material post-annealed at 500°C for 12 h. (Adapted from ref. [6].)

To compensate for the lead loss and achieve the desired stoichiometry, a set of experiments was performed using the three-step procedure described above but with the lead content being varied while the ratio of the other cations kept constant. The results have been presented (in figs. 6.1.7-a, 6.1.7-b and 6.1.7-c) and tabulated in table 6.1.1.

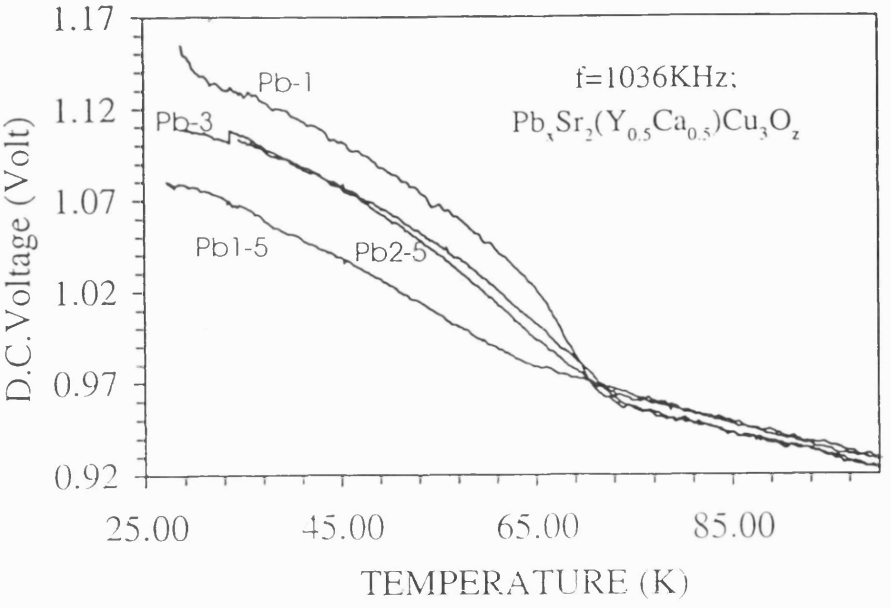

Figure 6.1.7-a). DC voltage versus temperature of inductive measurement shows diamagnetic behaviour of $Pb_xSr_2(Y_{0.5}Ca_{0.5})Cu_3O_x$ samples.

Figure 6.1.7-c shows the XRD pattern obtained for the samples x=2 and x=2.5, using CuK_α radiation at I.C.London, analysis performed by Dr. F. Saba. Comparing both XRD patterns, and from the resistive and diamagnetic characterisations, it appears that the excess amount of lead did not made a big difference in superconducting transition temperature or to impurity phase formation. It seems that a small amount of lead and Pb-2213 phase can form a composite material which exhibits only a slight deviation in superconducting properties. An analysis of critical current may provide information regarding the effect of lead along the grain boundaries.

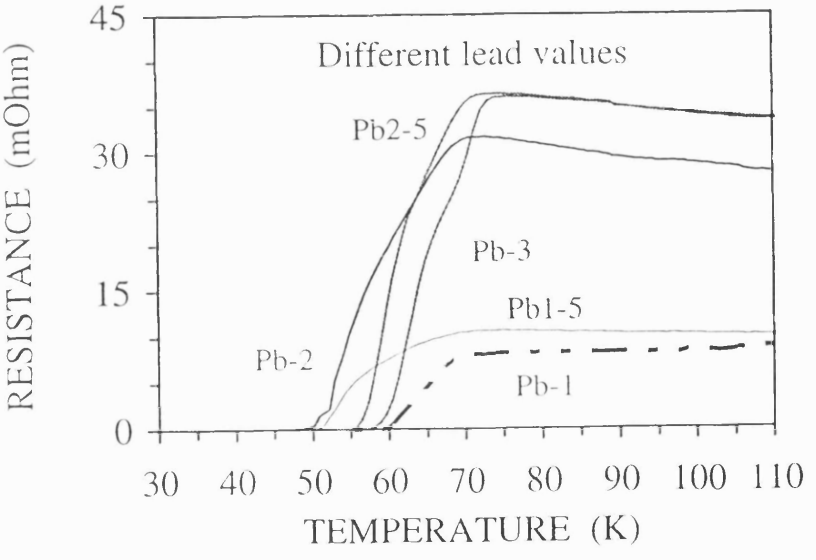

Figure 6.1.7-b). DC resistance versus temperature of $Pb_xSr_2(Y_{0.5}Ca_{0.5})Cu_3O_x$ after N_2 annealing (Masuzawa's technique).

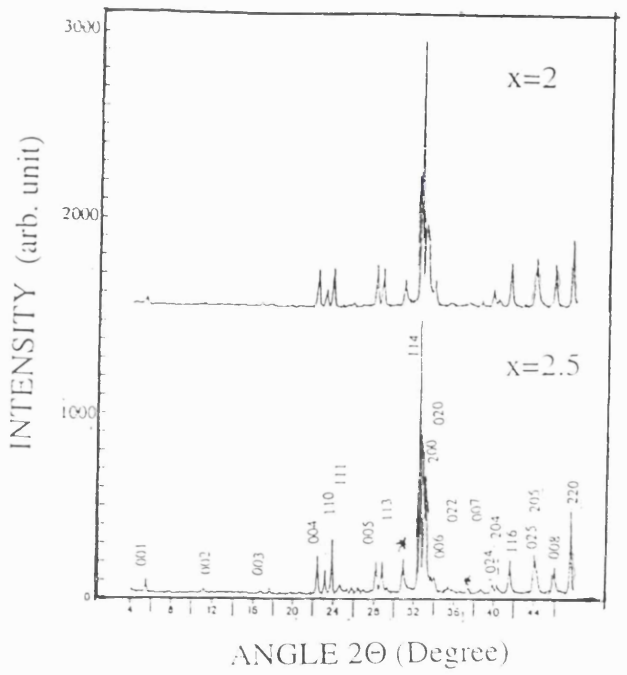

Figure 6.1.7-c). XRD pattern of $Pb_xSr_2(Y_{0.5}Ca_{0.5})Cu_3O_x$ samples (x=2, x=2.5), where asterisks are unidentified peaks.

Table 6.1.1 Starting stoichiometry and obtained stoichiometry (normalised with Cu) and related superconducting transition temperatures of $Pb_xSr_2(Y_{0.5}Ca_{0.5})Cu_3O_y$ samples.

Starting stoichiometry	Obtained stoichiometry	$T_{c,onset}$	$T_{c,zero}$
$Pb_3Sr_2(Y_{0.5}Ca_{0.5})Cu_3O_8$	$Pb_{2.52}Sr_2(Y_{0.5}Ca_{0.5})Cu_3O_8$	70K	58K
$Pb_{2.4}Sr_2(Y_{0.5}Ca_{0.5})Cu_3O_8$	$Pb_2Sr_2(Y_{0.5}Ca_{0.5}Cu_3O_8$	68K	56K
$Pb_2Sr_2(Y_{0.5}Ca_{0.5})Cu_3O_8$	$Pb_{1.68}Sr_2(Y_{0.5}Ca_{0.5})Cu_3O_8$	65K	49K
$Pb_{1.5}Sr_2(Y_{0.5}Ca_{0.5})Cu_3O_8$	$Pb_{1.35}Sr_2(Y_{0.5}Ca_{0.5})Cu_3O_8$	70K	51K
$PbSr_2(Y_{0.5}Ca_{0.5})Cu_3O_8$	$Pb_{0.89}Sr_2(Y_{0.5}Ca_{0.5})Cu_3O_8$	70K	60K

6.1.2 Modification in synthesis

Several experiments were performed to reproduce the results described by Masuzawa et al. [6] but those were all unsuccessful. Perhaps one of the main problems is the control of oxygen stoichiometry using $1\%O_2$ in N_2, as oxygen content during synthesis whereas the purity of gas depends on supplier. The another one is the

serious loss of lead during processing above the melting point of PbO (>875°C) for 2-4 hours. To stop the lead loss, a direct one-step synthesis of $Pb_2Sr_2(Y_{0.5}Ca_{0.5})Cu_3O_{8+\delta}$ from metal oxides (PbO_2/PbO, SrO_2, CaO_2/Y_2O_3 and CuO) in sealed gold tubes by simply reacting around 950°C for 12-48 hours has already been achieved by using ceramic technique [7]. The onset transition temperature was reported at 70 K and $T_{c,\ zero}$ of 55 K (10^{-8} ohm) [7].

Use of carbonates such as $CaCO_3$ and $SrCO_3$ requires relatively higher energy input to evolve out CO_2 other than impurity formation, whereas PbO has lower melting point (<875°C) causing a large deficiency of lead above 900°C due to evaporation during reaction. A two-step precursor technique can evolve out CO_2 after reacting above 950°C a mixture of all the carbonates and oxides (other than PbO) for longer period with intermediate grindings but can induce some loss of precursor and inhomogeneity in second step. Some oxides need a water and CO_2 free environment during their weighing and mixing. Storage of some oxides is also difficult. To overcome this problem, the polycrystalline samples of Pb-2213 were synthesised without using a precursor, with two-step technique in different mode. In the first step, all the oxides and carbonates of the starting stoichiometric ratio ($Pb_{2.4}Sr_2(Y_{1-x}Ca_x)Cu_3O_8$ x=0.4, 0.45, 0.5) including PbO were mixed in ethanol for 15 minutes to obtain right stoichiometric $Pb_2Sr_2(Y_{1-x}Ca_x)Cu_3O_8$ proportions. A few drops of diluted nitric acid (HNO_3, 1:10 by volume in distilled water) were added into the mixture and stirred. After few minutes, the material was dried at 50°C and the dried mixture was ground and pressed in the form of tablets. These tablets were placed inside the tube furnace in platinum container, under flowing pure nitrogen. Temperature of the sample was raised to 300°C within 10 minutes. After few minutes stay, the temperature was gradually increased to 750°C, left for 1 hour in flowing nitrogen, and then quenched to room temperature. In this manner any carbon present in the material was flushed out.

The resulting pellets were ground and pressed in the form of tablets of 1.0 mm thickness and 13 mm diameter. The smaller thickness (>1.5mm) of pellet was chosen to overcome the difficulty of oxygenation or reduction of the interior of the bulk at high temperature. It is observed when pellets are thick enough (>2mm), an upper thick layer due to partial melting envelopes the material. The inner part of the pellet remains similar to unreacted greenish coloured material (figure 6.1.8). The pellets were placed into the furnace and temperature was raised to 925°C at the rate of 10°C /min in flowing nitrogen, then flow was stopped, pellets were left for 4 hours in the closed-end tube furnace, then cooled down to 875°C and sintered for 2 hours in air, further cooled to 700°C to soak the sufficient oxygen from air and quenched to room

temperature. At this stage the pellets were checked by a multimeter and found to be highly resistive (resistance~100 kOhm across the pellet).

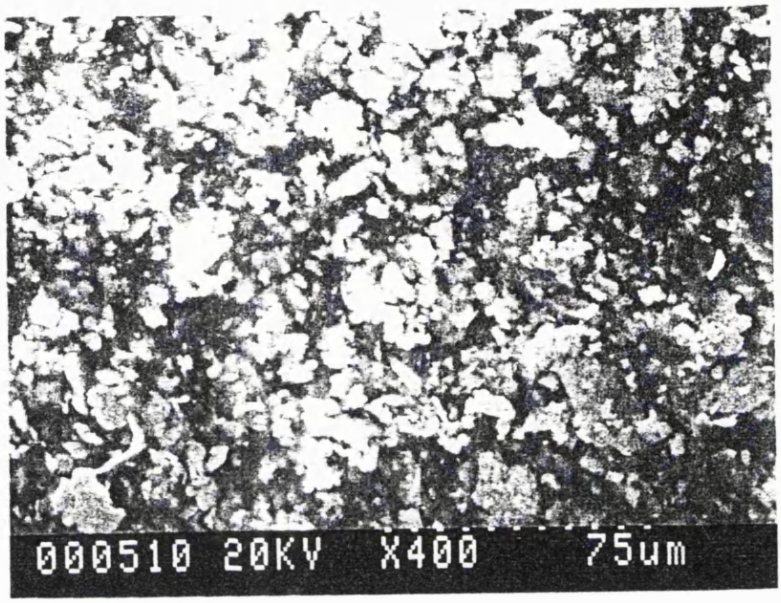

Figure 6.1.8. *An SEM picture of fractured surface of thick pellet after reacting at 925°C for 4 hours.*

In a second step, pellets were again crushed, ground, pressed in the form of tablets and placed into a platinum container inside the furnace. The temperature was raised to 875°C for 8-10 hrs with the ends of the furnace then closed and the flow of pure nitrogen at a rate of 6cc/min was started. The pellet annealed in flowing nitrogen for 2-3 hrs at 870°C, and was then checked by a simple resistancemeter. The resistance for x=0.45 was lower than other pellets containing different calcium contents (x=0.4, 0.45, 0.5). The resistive transition and diamagnetic behaviour of these pellets are shown in figures 6.1.9. and 6.1.10. respectively.

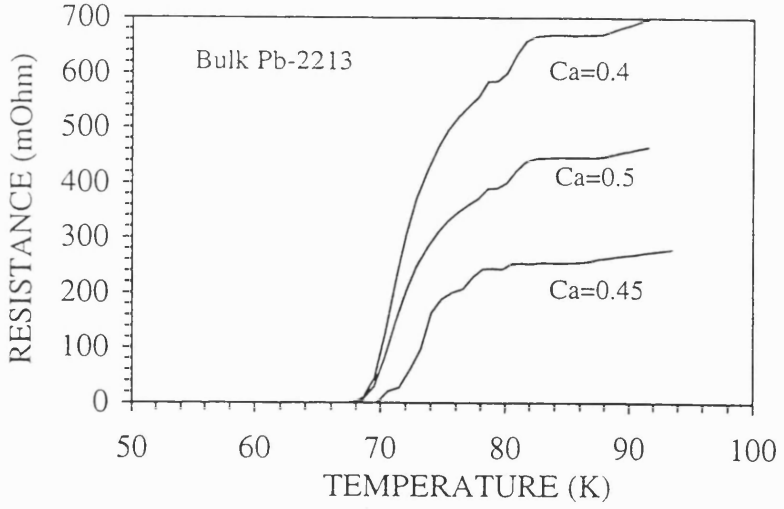

Figure 6.1.9. *Superconducting transition temperatures of $Pb_2Sr_2(Y_{1-x}Ca_x)Cu_3O_8$ samples synthesised with modification in ceramic method.*

Among these results, the sample containing Ca=0.45 value shows better onset resistance and the resistive transition temperature ($T_{c.\,zero}$=70K and $T_{c.\,onset}$=78K) compared with the samples contain Ca=0.4 or 0.5 values. However, the diamagnetic onset superconducting transition temperature for the sample Ca=0.4 is clearly different from the resistive one. This difference seems due to formation of small number of Cooper pairs during transitional state that is not much effective to exclude the magnetic field. The results also demonstrate that the charge transfer to the CuO_2 layers from charge reservoir block through the substitution of Y^{3+} by Ca^{2+} ions and oxygen adjustment is important factor for superconductivity in Pb-2213 phase.

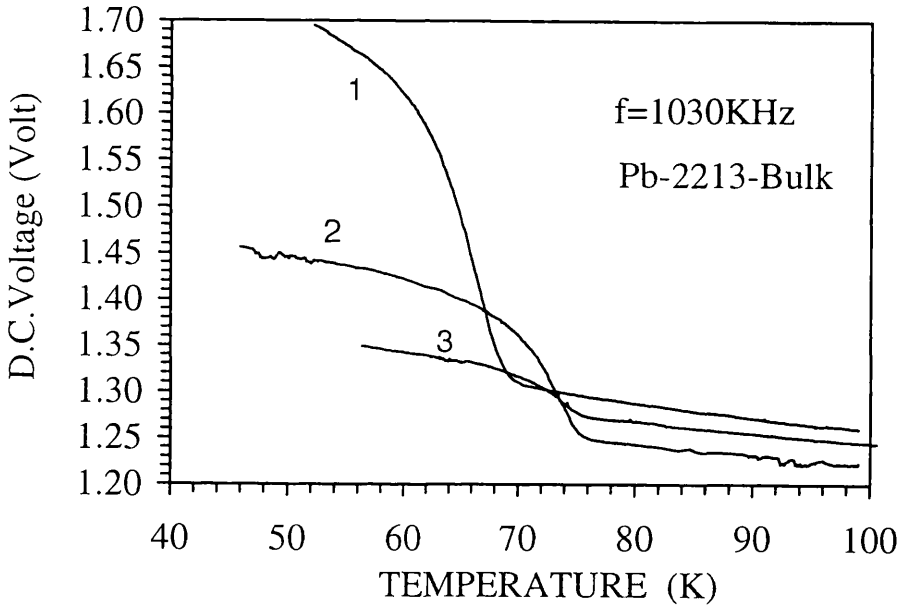

Fig. 6.1.10. *DC voltage versus temperature shows Meissner effect of* $Pb_2Sr_2(Y_{1-x}Ca_x)Cu_3O_8$ *samples (numbers 1, 2, 3 stand for x=0.4, 0.45, and 0.5 respectively).*

The obtained results through modification in synthesis are better than the other suggested methods. The applied method is easily approachable and independent of percentage of oxygen in nitrogen.

6.1.3 $Pb_2Sr_2(Y_{0.55}Ca_{0.45})Cu_4O_Z$ composition

The same technique was adopted to prepare a Pb2214 composition as described in section 6.1.2. Two pellets were synthesised and sintered at 800°C in nitrogen for 2 hr and 1hr (called SY2214A and SY2214B respectively) and characterised using XRD, CuK_α radiation (at Birkbeck College, Crystallography Department) (figure 6.1.11 and table 6.1.2) and resistivity measurements (figure 6.1.12) (at Imperial College, Department of Physics, London). Sample subjected to reducing conditions for longer periods show better

superconducting transition temperatures with a $T_{c,\ zero}$ of 62K. Sample SY2214B exhibits just such a transition temperature, but around 55K it shows positive curvature. This curvature has not been seen in sample SY2214A and can be interpreted in terms of oxygen distribution in the sample.

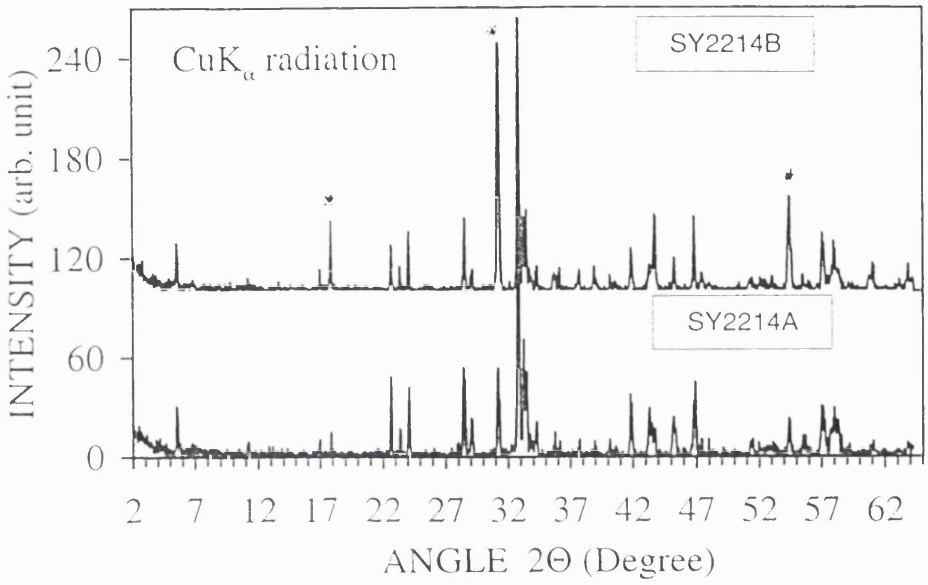

Figure 6.1.11. XRD pattern of SY2214A and SY2214B samples where asterisks are $Sr_3Pb_{2.03}Cu_{0.73}O_{7.7}$ *peaks.*

The XRD also shows minor differences in peak intensities for the sample SY2214A compared with sample SY2214B this might be a result of different oxidation states. Observed values of d-spacings and relative percentage of intensities are slightly higher than in the Pb-2213 phase material. Possible impurity of $Sr_3Pb_{2.03}Cu_{0.73}O_{7.7}$ material (d=5.05Å, 2.91Å, 2.06Å, 1.91Å, and 1.68Å) may be present but the proper interpretation to clarify of the XRD patterns must await a further study.

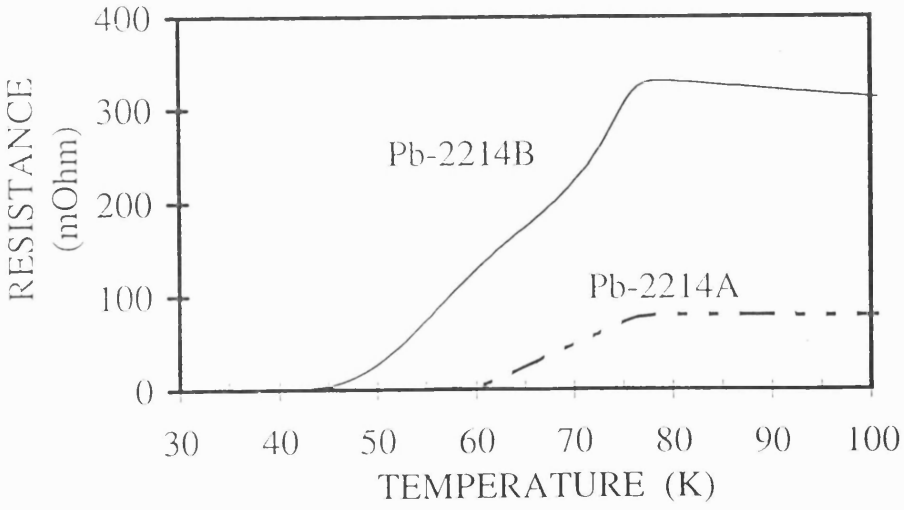

Figure 6.1.12. *DC resistance versus temperature of SY2214A and SY2214B samples.*

Table 6.1.2. Characteristic XRD pattern for sample SY2214B (Pb-2214) composition.

d(Å)	I/I(%)	d(Å)	I/I(%)	d (Å)	I/I(%)
15.9416	11.5	2.7449	100.0	2.0463	4.3
5.2658	3.5	2.7147	7.8	2.0345	4.6
4.9978	5.0	2.7084	26.7	1.9737	9.7
3.9475	20.7	2.6901	21.2	1.9679	5.0
3.8220	5.9	2.6287	8.8	1.9109	12.4
3.7129	18.0	2.4964	3.2	1.9071	16.1
3.1614	23.0	2.3927	3.6	1.8870	3.1
3.1534	16.9	2.2553	3.5	1.7530	3.1
3.0899	8.8	2.1687	16.1	1.6637	9.1
2.8842	22.6	2.1643	10.6	1.6311	4.2
2.8733	13.1	2.0546	10.1	1.5934	11.5
				1.5703	8.4
				1.5633	8.8

6.1.4 $Pb_3Sr_3(Y_{0.55}Ca_{0.45})Cu_4O_z$ composition

A single crystal of the superconducting, Pb-2213 phase was grown from PbO- and CuO-rich melts of composition $Pb_{3.5}Sr_3(Dy_{0.5}Ca_{0.5})Cu_4O_x$ by Cava et al.[2] using the two-step precursor technique. The midpoint of the superconducting transition was reported as 51.5K and $T_{c,\ zero}$ of 46K. Above the $T_{c,\ onset}$ the temperature coefficient of resistivity was also fairly linear as shown in figure 6.1.1. Furthermore, to observe the effects of excessive cationic ratio on normal state and superconducting transition temperature, a set of experiments was performed. Samples of bulk $Pb_3Sr_3(Y_{0.55}Ca_{0.45})Cu_4O_z$ and $Pb_3Sr_3YCu_4O_z$ compositions were synthesised by using the same procedure as described above in section 6.1.2. The XRD, EDX and resistive characterisations were performed and the results shown in figures 6.1.13, 14, 15 respectively and tabulated in tables 6.1.3 and 6.14. The samples without calcium remained highly resistive after annealing in N_2. In figure 6.1.13, the unannealed sample shows semiconducting behaviour with onset transition in two-steps, one at 70K and another near 40K but could not reach to zero resistance down to 25K. Slight negative temperature coefficient of resistance could be seen in both cases, samples being annealed in flowing nitrogen for half an hour or 70 minutes. The linear behaviour, minimum onset resistance and maximum $T_{c,\ zero}$ are obtained for samples annealed only at 870°C for 45minute in nitrogen. This

reduction shows that oxygen stoichiometry is an important factor, affecting normal and superconducting properties. However, the transitional width is large and small positive curvature around 70K remains in each case. This can be clearly attributed to small inhomogeneity at the grain boundaries. The calcium content plays an important and necessary role in lead-based materials. The composition without calcium, $Pb_3Sr_3YCu_4O_z$ remained highly resistive as was found by simply checking the resistance across the diameter of pellet by AVO meter (Ampere, Volt, Ohm meter).

Figure 6.1.15 shows the XRD pattern and table 6.1.4 includes corresponding relative intensities. It is observed that the d-spacings and the related intensities match the published data of the compound here described regarding the Pb-2213 phase. Any impurity phase in this composition was not detected. It appears that both the Pb-2213 and Pb3314 compositions have same XRD pattern.

Table 6.1.3. *Obtained-stoichiometry and superconducting transition temperatures of* $Pb_3Sr_3(Y_{0.55}Ca_{0.45})Cu_4O_y$ *samples annealed for different period in nitrogen at 870°C.*

Annealed inN for the period→	1/2 hrs.		45 minute		70 minute		without flowing N_2	
Obtained stoichiometry ↓	$T_{c.}$ on	$T_{c.}$ z.	$T_{c.}$ on	$T_{c.}$ z	$T_{c.}$ on	$T_{c.}$ z	$T_{c.}$ on.	$T_{c.}$ z.
$Pb_{2.54}Sr_3(Y_{.55}Ca_{.45})Cu_{4.5}O_z$	79K	59K	79K	62K	79K	40K	72K	-
$Pb_{2.54}Sr_3YCu_{4.5}O_z$	ısulating		insulating	-	400KΩ	-	insulating	-

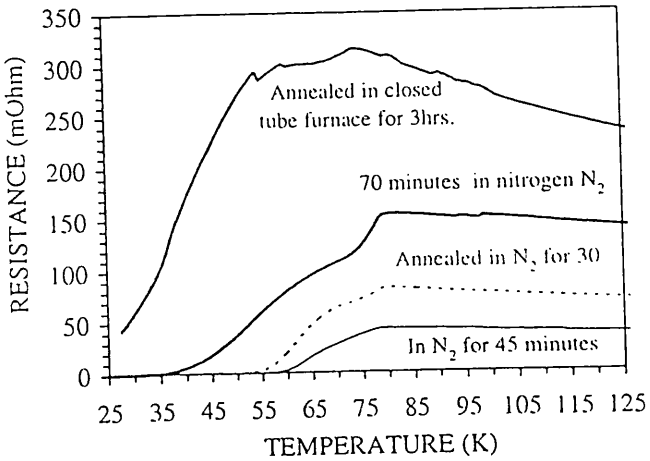

Figure 6.1.13. *DC resistance versus temperature of* $Pb_3Sr_3(Y_{0.55}Ca_{0.45})Cu_4O_z$ *samples synthesised without precursor method.*

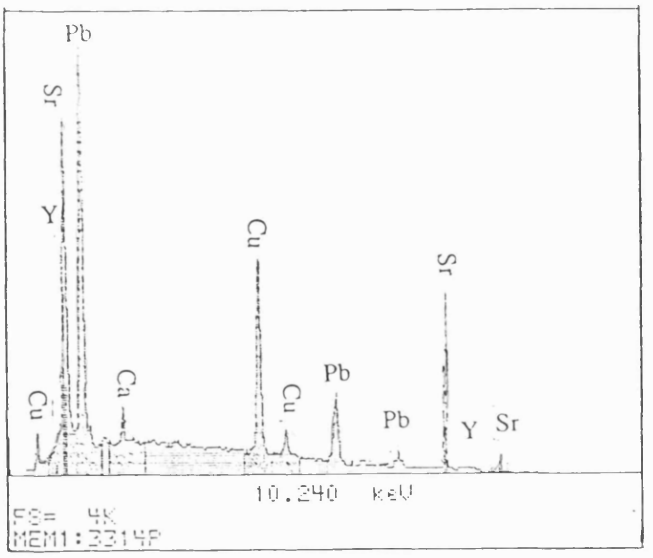

Figure 6.1.14. EDX pattern of sample $Pb_3Sr_3(Y_{0.55}Ca_{0.45})Cu_4O_z$.

Table 6.1.4. Characteristic XRD shows d-spacings and corresponding relative intensities for Pb-3314 (Ca=0) composition.

d (Å)	I/I (%)	d (Å)	I/I (%)	d (Å)	I/I(%)
15.8220	29.4	2.7166	35.0	1.5976	15.4
7.8643	9.9	2.6968	32.3	1.5950	27.6
5.2516	8.5	2.6266	14.7	1.5764	21.0
3.9426	28.4	2.2514	6.3	1.5740	22.8
3.8350	6.2	2.1737	17.5	1.5667	7.3
3.7227	21.2	2.1657	11.9	1.5452	5.6
3.1528	37.1	2.0582	21.0	1.3748	4.5
3.0910	9.8	1.9717	18.5	1.3583	5.2
2.7490	100.0	1.9143	26.6		

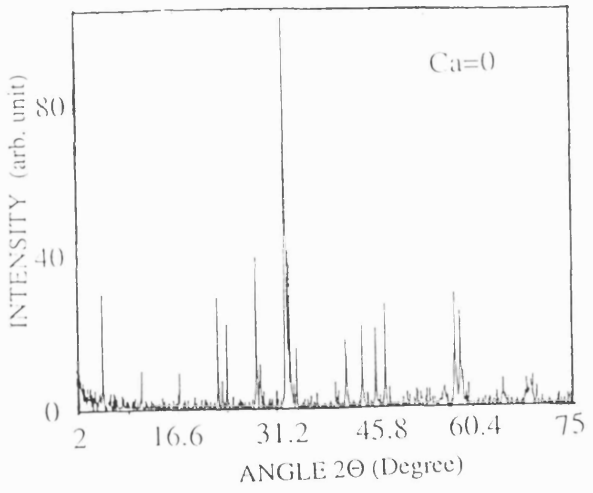

Fig. 6.1.15. XRD pattern of $Pb_3Sr_3YCu_4O_z$ sample (Ca=0)

6.2.1 $(Pb_{0.75}Cu_{0.25})Sr_2(Y_{0.5}Ca_{0.5})Cu_2O_{7-\delta}$ (Pb-1212 phase)

High-pressure ceramic synthesis has been employed to prepare lead based Pb-1212 material [8, 9]. In order to prepare $(Pb_{0.5}Cu_{0.5})Sr_2(Y_{0.5}Ca_{0.5})Cu_2O_{7-\delta}$, sintering is carried out at 940°C for 15 hours under an oxygen pressure of 10-150 bar followed by fast cooling to 100°C. The samples obtained from high-pressure oxygen treatment show higher transition temperatures in the range of 50-70K. Rouillon et al. [10] have reported the synthesis of Pb-1212 lead cuprates by the direct reaction of the component oxides in the evacuated silica ampoules. The method described in this thesis has the advantage of adjusting oxygen partial pressure required for the synthesis. Both Pb-2213 and Pb-1212 phases have been prepared using the nitrates of the metal ions as the starting materials [11]. Although this procedure yields Pb-2213 or Pb-1212 phases in a single step, the product obtained always has impurities such as CuO and Y_2O_3.

Here, it is shown that superconductivity can be readily achieved in polycrystalline samples by carefully manipulating oxygen stoichiometry during sintering without using either toxic materials such as cadmium oxide or thallium oxide to replace Cu in the $(Pb_{0.75}Cu_{0.25})$ layer or using any high-pressure oxygen annealing step.

6.2.2 Removal of CO_2 before processing HTSC materials

In conventional processes for fabricating cuprate superconductors, mixed carbonates and oxides are heated to 950°C for several hours with a few intermediate grindings stages, causing the salts to give off CO_2 during reaction. In this method complete removal of CO_2 is difficult and causes micro-inhomogeneity. The problematic metal oxides of salts cannot be used due to absorbing ability of water and CO_2 from ambient and hence are difficult to weigh or store them. The new technique removes the CO_2 before it is mixed with the other oxides. The stoichiometric amounts of ($CaCO_3$ and $SrCO_3$) carbonates are mixed in ethanol, dried and pressed in the form of tablets. These tablets are placed inside a platinum crucible and heated in a quartz furnace to only 1000°C for 15 minutes in flowing nitrogen, then cooled down to 950° C over a few minutes and left for half an hour before being quenched to room temperature in the same gas flow. The samples were immediately reground and mixed with 99.9% Y_2O_3 and CuO powders in the appropriate stoichiometric ratio to form a $Sr_2(Y_{0.5}Ca_{0.5})Cu_{2.25}O_x$ precursor. The mixture was again fired (at 950°C for 2h) and cooled down to room temperature at a rate of 7°C /min.

6.2.3 $(Pb_{0.75}Cu_{0.25})Sr_2(Y_{1-x}Ca_x)Cu_2O_{7-\delta}$ (0.4<=x<=0.8) synthesis.

In a second step, the fired precursor $Sr_2(Y_{0.5}Ca_{0.5})Cu_{2.25}O_x$ material was mixed with PbO to form the composition of $(Pb_{0.75}Cu_{0.25})Sr_2(Y_{1-x}Ca_x)Cu_2O_{7-\delta}$ ($0.4 \leq x \leq 0.8$). The resulting mixture was pressed into pellets (13 mm in diameter and 2 mm in thickness) under a pressure of 1.2 tons/cm^2. Each pellet was inserted into a furnace at 500°C (inside a platinum crucible) and raised to 1000°C at a rate of 20°C /min for 1 hour, cooled to 800°C over a few minutes and subsequently quenched in air. In the third step, the partially melted material was reground and pelletised in the manner described earlier, placed in the furnace at 500°C and raised to 900°C at a rate of 20°C /min, sintered in air for two hours, then cooled down to 820°C and sintered in nitrogen for 2 hour and quenched to room temperature. All the pellets were completely fabricated within a 9 hour period. This is by far the shortest period yet used to synthesis Pb-1212 phase.

6.2.4 Characterisation

DC electrical resistivity measurements were performed using the Van der Pauw technique with an applied current of 1.0 mA. The electrical contacts to the samples were made by fixing o.1 mm silver wires with a conductive silver paint. The temperature was recorded using silicon diodes calibrated against the Rh/Fe thermometer.

Magnetisation data were obtained using an inductive characterisation apparatus which was a modified version of an AC susceptibility apparatus designed elsewhere [12]. The sample was laid on top of a flat spiral coil, which had 15 turns of copper wire and inner and outer diameters 0.5 and 6 mm, respectively, and formed a part of resonant LC circuit. During diamagnetic transition, the superconducting sample induces sudden changes in the inductance of the flat spiral coil which shifts the DC voltage. The DC voltage drop recorded depends crucially on the effective superconducting area screening the coil's magnetic field and provides the best results when operated in the region around 1030kHz.

6.2.5 Results and discussion

Figure 6.2.1 shows the XRD patterns of various pellets with different Ca contents (x=0.5, 0.6, 0.7) in the Pb-1212 phase. All the diffraction lines were indexed for a tetragonal unit cell with lattice constant values of a=3.815Å and c=11.8Å. Some peaks due to impurity phases were also observed similar to those reported by Kosuge et al. [13] who found as much as 20% of the material to consist of secondary phases

when a calcium content of 0.35 was used. However, Maignan et al. [14] reported that samples with 0.2<x<0.5 values which were heated in an evacuated quartz tubes at 880 °C for 48 hours and then quenched to room temperature formed only the pure phase. After annealing in oxygen pressures ranging from 5 to 80 bar at temperatures from 200 to 600°C for 10 to 65 hours the samples became superconducting but were not characterised by the XRD to see the effects after the high-pressure oxygen annealing [14]. In this work, by increasing the value of the calcium from 0.5 to 0.7, the c-axis lattice constant was found to decrease from 11.9184Å to 11.860Å in agreement with the work of Adachi et al. [15].

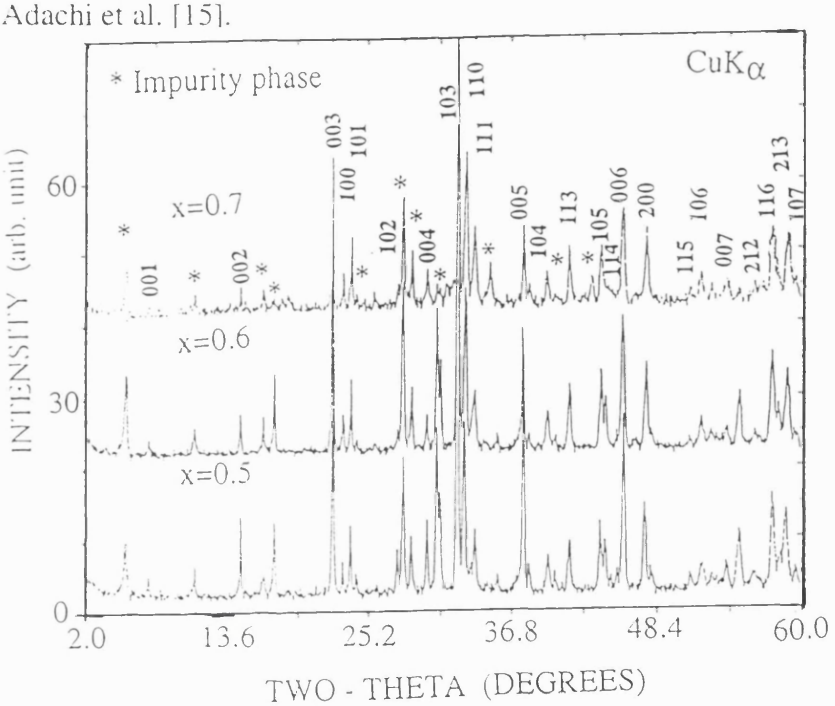

Figure 6.2.1. XRD pattern of polycrystalline pellets containing calcium x=0.5, 0.6, 0.7; (*) indicate unidentified peaks.

The resistance versus temperature traces of samples with a calcium content of x=0.7 is shown in figure 6.2.2. The samples were annealed in nitrogen at 850°C for (a) 6 hrs and (b) for 12 hrs while sample (c) was annealed in air at the same temperature for 4 hrs in the third processing step as described earlier. From this set of experiments it is observed that neither the longer annealing period in a reducing atmosphere nor the annealing in air for shorter durations can produce a better superconducting material.

A specific feature to be noted here is that the samples reduced and quenched in nitrogen from a high temperature also had smaller values of the normal state resistance. Clearly, any excess oxygen not only decreases the T_c but can even convert the material into a non-superconducting form. Further reducing the annealing period to 2 hrs in nitrogen at 850°C resulted in the same $T_{c,\,onset}$ but improved $T_{c,zero}$ from 33 K to 55 K as shown in fig.6.2.3. Reducing the annealing period even more, however, did not lead to further improvements in $T_{c,\,zero}$.

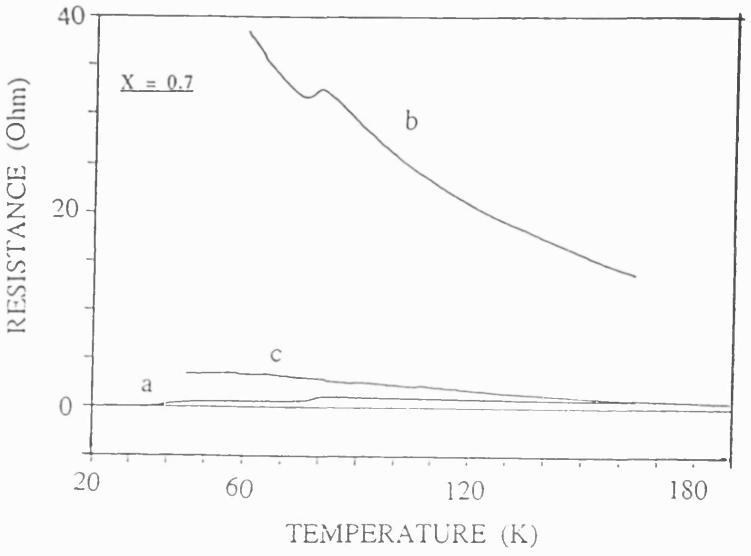

Figure 6.2.2. DC resistance versus temperature for samples annealed in th third processing step at 850°C for (a) 6 h in nitrogen (b) 12 h in nitrogen (c) 4 h in air.

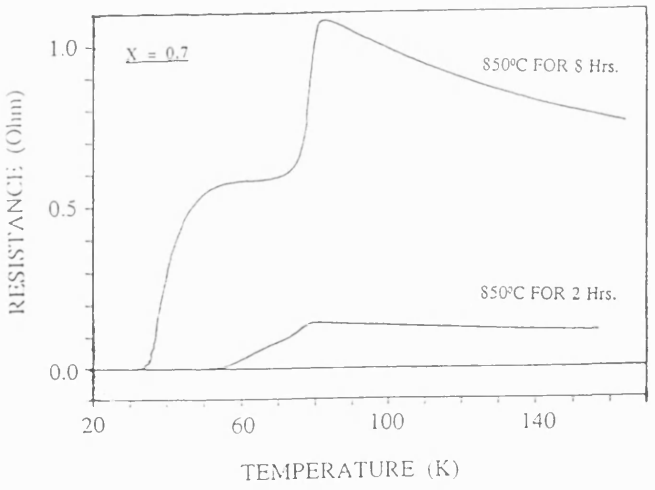

Figure 6.2.3. DC resistance versus temperature of the samples with calcium content x=0.7 annealed in nitrogen in a third processing step at 850°C for 2h and 8h.

Figure 6.2.4 shows the effect of oxygen reduction for samples with the same calcium content (x=0.7), the reduction being performed at different temperatures for a two hour period. Both $T_{c,\,onset}$ and $T_{c,\,zero}$ clearly change with annealing temperature with the optimum characteristics being obtained at 820°C. At higher temperatures, the oxygen loss is excessive, while at lower temperatures the oxygen content is greater and thus longer periods are required for reduction. The presence of oxygen correlates with the charge carrier density which is important in controlling the superconducting

transition temperature. It therefore, seems that the key factor required to achieve superconductivity in Pb-1212 cuprate is not necessarily the high-pressure oxygen annealing but the precise adjustment of the oxygen content. Previous attempts to prepare this phase at high temperatures in an evacuated quartz tube after 48 h heat treatment [14] resulted in oxygen deficiency which was only compensated by using high-pressure-insertion (50 bar) of oxygen near 500°C to achieve the maximum $T_{c,\ onset}$. Tang et al. [9] also demonstrated the effect of high-pressure oxygen annealing at high temperature (940°C) but reported that excess oxygen taken up during subsequent annealing at lower temperatures destroyed the superconductivity.

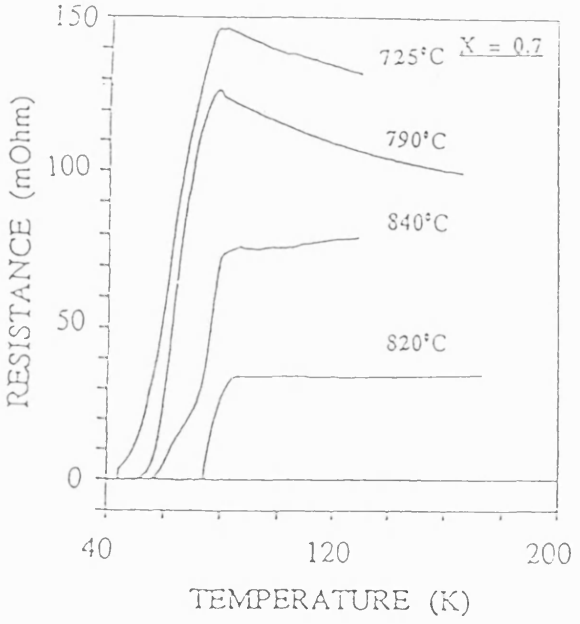

Fig.6.2.4. DC resistances versus temperatures of the samples annealed in nitrogen for 2 h containing calcium with x=0.7 in the Pb-1212 phase.

Figure 6.2.5 shows the temperature dependence of the resistance of the samples with different calcium contents ranging from 0.4 to 0.7 after annealing in nitrogen for two hours at 820°C. The x=0.4 sample exhibits semiconducting behaviour in its normal state with $T_{c,\ onset}$ at 79 K and $T_{c,\ zero}$ near 48 K. $T_{c,\ onset}$ values for calcium values of x=0.5 and x=0.6 are similar but $T_{c,\ zero}$ improves to 58 K and 63 K, respectively, but the best $T_{c,\ onset}$ and $T_{c,\ zero}$ values, for Ca=0.7, are found near 82 K and 76 K.

Figure 6.2.6 shows the diamagnetic characterisation of samples for calcium values x=0.4 to 0.8 using inductive rf measurements. Near the onset transition, the diamagnetic behaviour is very weak in each case and it is thought that the paired charge carrier density may be small enough at this stage for magnetic flux exclusion. As the temperature approaches to $T_{c,\ zero}$, a prominent sharp transitional increase in DC voltage can generally be observed. For x=0.4, the transition starts at 79 K but is not sharp and only rises gradually as is usually the case for situations where the

transition width ΔT is quite large and the temperature coefficient of the resistivity is negative. The superconducting transition is still apparent even at x=0.8.

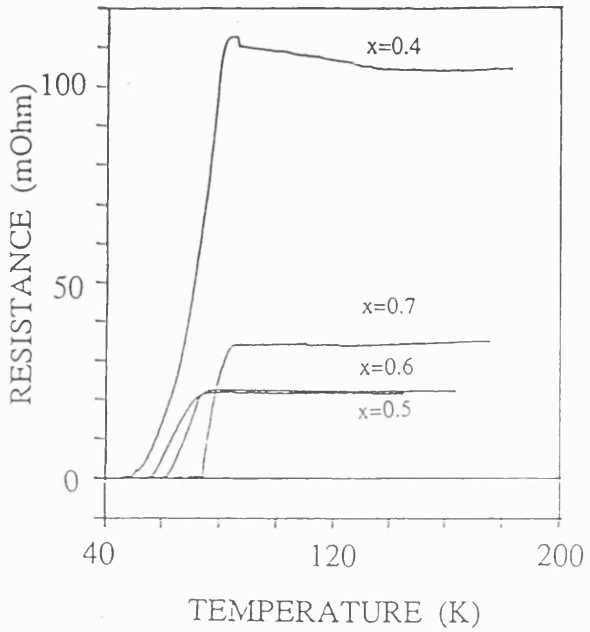

Figure 6.2.5. DC resistance versus temperature for the $(Pb_{0.75}Cu_{0.25})Sr_2(Y_{1-x}Ca_x)Cu_2O_{7-\delta}$ samples with calcium content x=0.4, 0.5, 0.6 and 0.7.

However, the measured $T_{c,\ onset}$ near 58 K and at 35 K shows that the hole carrier density decreases as the calcium content approaches the x=0.8 value.

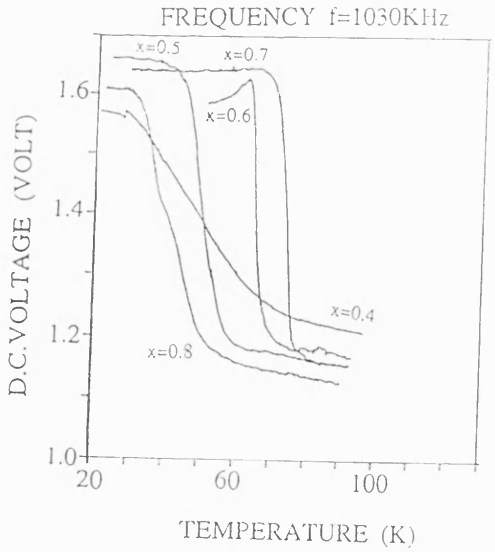

Figure 6.2.6. DC voltage versus temperature in rf-inductive measurements showing the diamagnetic behaviour of the samples containing calcium values from x=0.4 to x=0.8.

These results show that in the $(Pb_{0.75}Cu_{0.25})Sr_2(Y_{1-x}Ca_x)Cu_2O_{7-\delta}$ system, the Y^{3+} layer can easily accommodate the larger Ca^{2+} ion: this leads to an increased charge carrier density in the parent material. The adjustment of the carrier density can also be controlled by varying the oxygen content for a constant calcium content. The work conducted as a part of this thesis has achieved the largest $T_{c,\ onset}$ of 82 K and

$T_{c,\ zero}$ of 76 K yet reported by optimising both the Y/Ca ratio and the oxygen content. The latter plays an important role in determining the hole concentration and subsequent superconducting characteristics in the Pb-1212 phase. These results suggest that oxygen annealing at pressures as high as 10-150 bar for long periods (10 to 65 h) at 500 or more is not a required condition for the enhancement of the superconducting transition temperature through the insertion of oxygen to increase the hole carrier concentration. This conclusion is in agreement with coulometric titration for the oxygen analysis for samples with x=0.3 which showed that the value for $(Pb_{0.65}Cu_{0.35})Sr_2(Y_{0.7}Ca_{0.3})Cu_2O_z$ decreases from z=7.1 (for slowly cooled non-superconducting samples) to 6.99 (quenched superconducting sample) [16,17].

Table 6.2.1. *Starting stoichiometry and after fabrication obtained stoichiometry with the related superconducting transition temperatures.*

Actual stoichiometry	Starting stoichiometry	%Ca/Y content	$T_{c.\ onset}$	$T_{c.\ zero}$
$(Pb_{0.75}Cu_{0.25})Sr_2$ $(Y_{0.6}Ca_{0.4})Cu_2O_7$	$(Pb_{0.85}Cu_{0.25})Sr_2$ $(Y_{0.6}Ca_{0.4})Cu_2O_7$	Ca=6.67 Y=10	79 K	47K
$(Pb_{0.75}Cu_{0.25})Sr_2$ $(Y_{0.5}Ca_{0.5})Cu_2O_7$	$(Pb_{0.85}Cu_{0.25})Sr_2$ $(Y_{0.5}Ca_{0.5})Cu_2O_7$	Ca=8.34 Y=8.34	79 K	58 K
$(Pb_{0.75}Cu_{0.25})Sr_2$ $(Y_{0.4}Ca_{0.6})Cu_2O_7$	$(Pb_{0.85}Cu_{0.25})Sr_2$ $(Y_{0.4}Ca_{0.6})Cu_2O_7$	Ca=10 Y=6.67	79 K	63 K
$(Pb_{0.75}Cu_{0.25})Sr_2$ $(Y_{0.3}Ca_{0.7})Cu_2O_7$	$(Pb_{0.85}Cu_{0.25})Sr_2$ $(Y_{0.3}Ca_{0.7})Cu_2O_7$	Ca=11.7 Y=5.0	82 K	75 K
$(Pb_{0.75}Cu_{0.25})Sr_2$ $(Y_{0.2}Ca_{0.8})Cu_2O_7$	$(Pb_{0.85}Cu_{0.25})Sr_2$ $(Y_{0.2}Ca_{0.8})Cu_2O_7$	Ca=13.4 Y=3.34	58 K	47 K

Maeda et al. also reported, using a titration technique, that the oxygen content values were z=7.1 for samples slowly cooled from high temperature, and 7.0 for quenched samples, regardless of the calcium content [18]. Moreover, superconductivity appears in samples with x>0.3 when they are quenched [19] and these results show that the excess oxygen content in slowly cooled samples can suppress the superconducting properties. Neutron diffraction analysis has shown that the excess oxygen (0.1) is located at the irregular sites (chain sites)of the Pb-1212 structure [20]. The random potential introduced by these extra oxygen atoms will affect the electronic state of the CuO_2 plane and result in localisation of holes [13]. Thus, removal of the oxygen atoms should lead to an increase in the hole carrier concentration and improvements in the superconducting transitional temperature instead of high-pressure oxygen anneal and excess oxygen. More recently, a report on $(Pb_{0.6}Cu_{0.4})Sr_2(Y_{0.5}Ca_{0.5})Cu_2O_y$, Pb-1212 phase has appeared by Jian-zhou et al. [21]. They found a two-step resistive transition, with the $T_{c,\ onset}$~110K, and $T_{c,zero}$ of 43K whereas the diamagnetic effect was not observed at 110K in slow

cooled samples after firing at 1000°C for 4hrs in air. The samples post-annealed in N_2 at 800°C for12 hrs exhibited semiconducting behaviour after $T_{c,\ onset}$~110K. They concluded that within the composition (Pb,Sr)-1212, there are two phases, low-T_c and high-T_c.

6.2.6 (Pb, Bi)-1212 composition

In the Pb-1212 phase, one further attempt was made to check the effects of Bi concentration on resistance versus temperature characteristics. The higher valent Bi was tried to substitute Pb in PbO-sheets. Two samples of $(Pb_{0.6}Bi_{0.4})Sr_2(Y_{0.3}Ca_{0.7})Cu_2O_7$ and $(Pb_{0.75}Bi_{0.25})Sr_2(Y_{0.3}Ca_{0.7})Cu_2O_7$, compositions with different Bi-contents were synthesised following the technique described in sections 6.2.2 and 6.2.3. In a third step, the samples with Bi-content =0.25, were annealed at 820°C for two hours, and two plus half an hour in N_2. The sample annealed for the longer period had a larger resistance in the normal state but a better $T_{c,\ zero}$ of 34K than the other one that had 32K. The $(Pb_{0.75}Bi_{0.25})Sr_2(Y_{0.3}Ca_{0.7})Cu_2O_7$ composition had constant normal state resistance up to onset transition whereas all three samples had $T_{c,\ onset}$~85 K but $(Pb_{0.6}Bi_{0.4})Sr_2(Y_{0.3}Ca_{0.7})Cu_2O_7$ exhibits semiconducting behaviour in normal state. After the onset transition, all three samples show broad transition width and positive curvature for resistances but curvature is more prominent in the sample of higher Bi-content. Bi content can be a cause of inhomogeneous distribution of oxygen in the samples but it seems that main reason for its presence is unreacted metal in between the grain boundaries.

The broad transitional width and positive curvatures in resistances after onset transition in (Pb, Bi)-1212 phase can be described in terms of the insufficient annealing period and higher sticking coefficient of Bi than the other cations [22]. From a survey of the literature concerning the synthesis of BSCCO-phases compared to PSYCCO-phases or other cuprates, It is clear that BSCCO- phases take longer to synthesise. The main reason seems to be that Bi is more 'sticky' and takes a longer time to diffuse during solid-state reactions and needs several grindings and pressings during processing of any BSCCO-phase. It is also experienced during processing of (Pb, Bi)-1212 phase, the sample with higher Bi-content was harder to crush and more difficult than the (Pb, Cu)-1212 phase with any calcium content. These points suggest that the (Pb, Bi)-1212 phase needs a longer synthesising period and several grindings to obtain good quality samples. Given that the same processing technique and annealing period have been applied to the two different cationic substitutions in the PbO-layers in Pb-1212 phase, the (Pb, Cu)-1212 and (Pb, Bi)-1212 phases it may be suggested that these phases show different attitudes towards the flow of current.

From the $T_{c,\ onset}$ it seems that $T_{c,\ zero}$ of (Pb, Bi)-1212 would be better than that of the (Pb, Cu)-1212 phase of comparable composition and annealing period.

In summary, a systematic study of the effect of variation of the calcium level in the Pb-1212 phase from x=0.4 to 0.8 has been performed. At a level of x=0.7, a transition temperature of 82K (onset) and 76K (zero) was obtained, the highest so far achieved in (Pb,Cu)-1212 phase. Different CO_2 removal and shortest cuprate fabrication time by this technique have been reported and dispense with the need for a high-pressure oxygen anneal. Bi-cations substituted in the PbO-layer enhances the onset superconducting transition temperature (85K) but suppress the $T_{c,\ zero}$ of 34K, and this seems due to sticking and poor-diffusive ability compared with Pb. These compounds need further sufficient annealing period to achieve better properties.

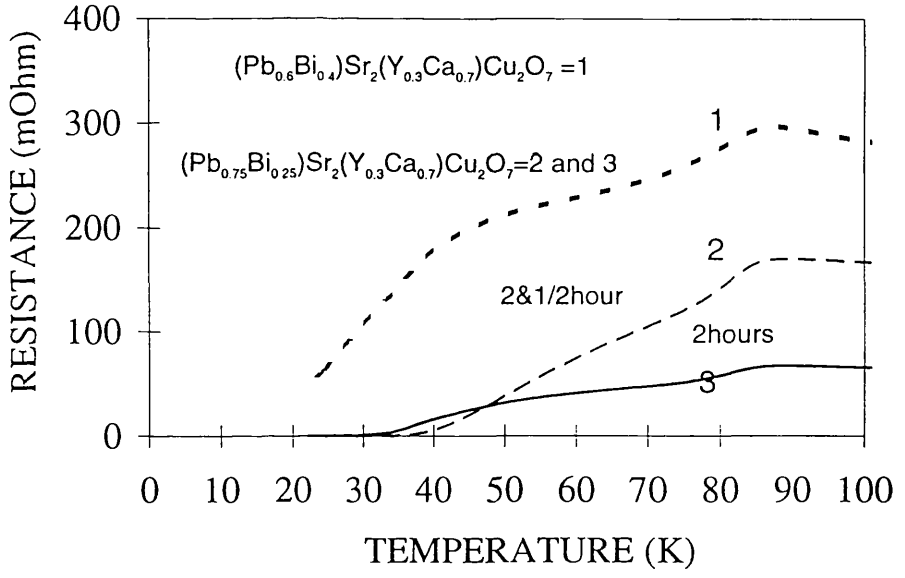

Figure 6.2.7. *DC resistance versus temperature for the* $(Pb_{0.6}Bi_{0.4})Sr_2(Y_{0.3}Ca_{0.7})Cu_2O_7$ *and* $(Pb_{0.75}Bi_{0.25})Sr_2(Y_{0.3}Ca_{0.7})Cu_2O_7$ *samples.*

6.3.1 Pb-1213 cuprate superconductor

Lead-based superconductors which contain the $-CuO_2-(Y,Ca)-CuO_2-$ block and $(MO)_n$ layers with n=2, where M is partly Pb and partly Cu are known as Pb-1213 or Pb-2212 phase. Initially, this seven-layer compound was reported by Tokiwa et al.[23] and Rouillon et al.[24]. These authors [23] found a wide range of oxygen contents which were determined by an iodide titration method to be 7.0, 8.2 and 8.4 among quenched, slow-cooled, and oxygen-annealed specimens, respectively. The range was as large as 1.4 per formula unit, but bulk superconductivity was not found

in any sample [23, 24]. Later, Tang and Morris [25] reported that superconductivity can be induced by precise adjustment of the composition, the synthesis procedure, and the oxygen content in this phase. Their optimum composition $Pb_{0.8}SrBa_{1.2}Y_{0.7}Ca_{0.3}Cu_3O_{8.35}$ had an onset superconducting transition temperature of 76K measured by the Meissner diamagnetic effect but resistive transition was not reported. They synthesised the optimum composition (using three step precursor methods) in 0.1%O_2 in nitrogen at 850°C for 15 hours. In the third step, samples were annealed at 450°C in O_2 at a pressure of 100 bars. They concluded that the $[(Pb, Cu)O_x]_n$ layers act as a charge reservoir, and the charge distribution between the $[(Pb, Cu)O_x]_n$ layers and the CuO_2 sheets is complementary; i.e., one increases when the other decreases at a given oxygen content [25].

6.3.2 Pb-1213 phase structure

Tokiwa et al.[23] proposed the structure shown in figure 6.3.1, based on high-resolution electron microscopy of $PbSrBaYCu_3O_7$ (reduced) and $PbSrBaYCu_3O_{8+x}$ (oxidised). In the reduced condition, Cu(1) is in linear co-ordination whereas in the oxidised state it has pyramidal co-ordination. This structure is similar to Tl-2212 ($Tl_2Ba_2CaCu_2O_8$), but with one PbO layer and one CuO_x layer replacing the two TlO layers. In the oxygen-deficient $PbSrBaYCu_3O_7$ compound, the Cu in the $[(Pb, Cu)O_x]_2$ block has linear co-ordination with two nearest oxygen atoms, but in oxidised Pb-1213, the $[(Pb, Cu)O_x]_2$ block contains an oxygen-deficient PbO rock-salt layer and a CuO_2 sheet with Cu in sixfold or fivefold co-ordination. This structure is similar to Cava's Pb-2213 structure but with one PbO layer deleted. The structure has a space group I4/mmm, tetragonal cell with a=3.852(1)Å and c=27.84(1)Å for slowly cooled samples, a=3.857(1)Å and c=27.84(1)Å for oxygen annealed samples and a=3.847Å and c=27.48Å for quenched specimens.

The Rietveld refinement result on Tokiwa's model obtained by Tang and Morris [25] was reasonable but has shown some differences over 110 and 200 peaks, even though they favoured the Tokiwa's model on the grounds of transmission-electron microscopy (TEM) images obtained by Tokiwa et el. and the similarity of oxygen take-up behaviour with Pb-2213 phase. We tried to check the effect of using strontium (Sr) instead of barium (Ba) in the above composition, which is variously referred to as the Pb-1213 or the Pb-2212 phase.

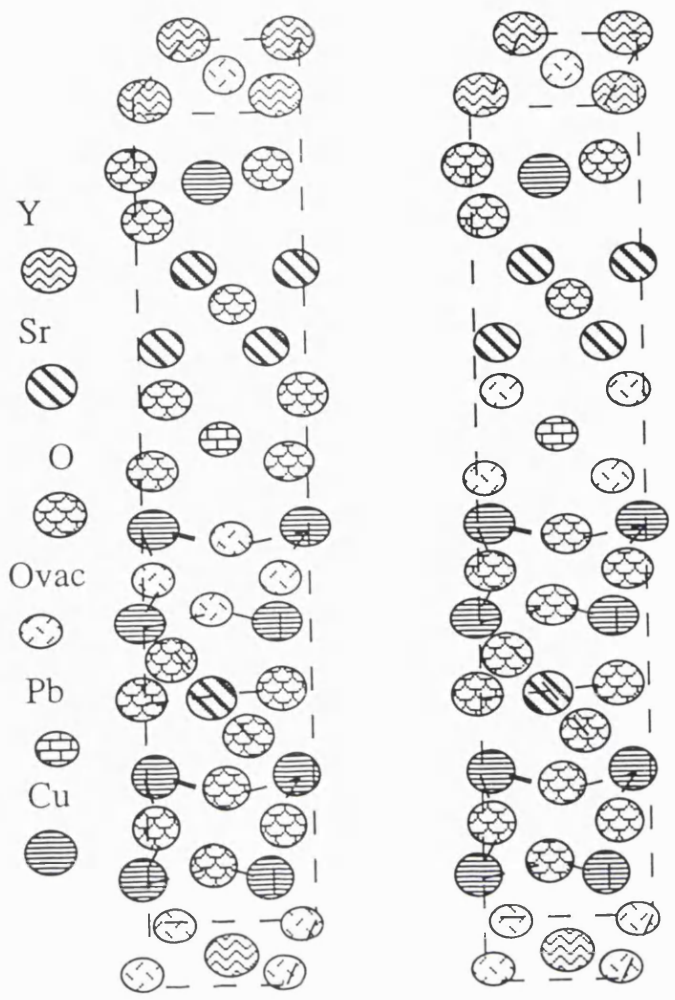

Figure 6.3.1. Structure of Pb-1213 material in a) oxidised b) reduced state [23].

6.3.3 Synthesis of $PbSr_2(Y_{1-x}Ca_x)Cu_3O_8$ and results

Polycrystalline samples of Pb-1213 composition were synthesised without using a precursor technique. All the oxides and carbonates of the starting stoichiometric ratio [$Pb_{1.2}Sr_2(Y_{1-x}Ca_x)Cu_3$, where x=0.35, 0.55, 0.65] including PbO (in excess to compensate the losses at high temperature heat-treatment) were mixed in ethanol for 15 minutes. A few drops of dilute nitric acid (1/10 in distilled water) were added to the mixture, then stirred, dried, remixed and pressed into tablets. These tablets were placed into platinum container, then placed inside a furnace with flowing nitrogen to stop the formation of impurity phases at low temperature. The temperature was raised to 400°C within 10 minutes. After a few minutes at 400°C, the temperature was gradually increased to 750°C, left for 1 hour in flowing nitrogen and then quenched to room temperature.Using these method, all the carbon present in the material was flushed out. The pellets were ground and pressed into the form of tablets of 1.0 mm thickness and 13 mm diameter. Again, the pellets were placed inside the furnace and the temperature was raised to 850°C at a rate of 10°C /min in flowing nitrogen for two

hours, then temperature raised to 880°C, flow was stopped, pellets were left for 2 hrs, the temperature was further raised to 1000°C for 1hr, cooled down at the rate of 6° C/min to 880°C was held for 8-9 hrs, further cooled down to 850°C for 10 hrs and then quenched to room temperature.

In next step, pellets were crushed, ground and pressed in the form of tablets 1.0 mm thick. These tablets were sintered in air at 870°C for 3 hrs, then cooled down to 800°C and nitrogen flow at the rate of 6cc/min started. The resistances across the diameter of 13 mm were checked by AVO meter during annealing after certain periods and tabulated in table 6.3.1. This method saved the time and effort of optimising the annealing period in nitrogen to achieve the maximum superconducting transition temperature. Fabricated samples were characterised to determine the obtained stoichiometry (EDX results normalised as Cu=3), resistive transition temperature (figure 6.3.3) and the results tabulated in the table 6.3.2. The results again suggest that the electrical properties and superconducting transition temperature are sensitive to oxidation state and calcium content helps the charge transfer to CuO_2 sheet. The maximum obtained transition temperature for zero resistance is 60K for Ca=0.55 value.

Table 6.3.1. *Resistances of $PbSr_2(Y_{1-x}Ca_x)Cu_3O_8$ samples before and after annealing in nitrogen ambient at 800°C* for different periods.

Composition of pellets	Resistance (air)	Resistance after15mint	Resistance after 30minute.
$PbSr_2(Y_{0.65}Ca_{0.35})Cu_3O_8$	300KΩ	320Ω	45Ω
$PbSr_2(Y_{0.45}Ca_{0.55}Cu_3O_8$	180KΩ	128Ω	15Ω
$PbSr_2(Y_{0.35}Ca_{0.65})Cu_3O_8$	238KΩ	150Ω	30Ω

Table 6.3.2. *Superconducting transition temperature of $PbSr_2(Y_{1-x}Ca_x)Cu_3O_z$ (Pb-1213) where x=0.35, 0.55, 0.65.).*

Starting stoichiometry	Obtained stoichiometry	$T_{c.onset}$	$T_{c.zero}$
$Pb_{1.2}Sr_2(Y_{0.65}Ca_{0.35})Cu_3O_z$	$PbSr_{1.9}(Y_{0.67}Ca_{0.34})Cu_3O_z$	55K	22K
$Pb_{1.2}Sr_2(Y_{0.45}Ca_{0.55})Cu_3O_z$	$PbSr_2(Y_{0.45}Ca_{0.55})Cu_3O_z$	69K	60K
$Pb_{1.2}Sr_2(Y_{0.35}Ca_{0.65})Cu_3O_z$	$PbSr_2(Y_{0.34}Ca_{0.65})Cu_3O_z$	55K	45K

Figure 6.3.2 shows the XRD pattern for the Ca=0.35 and 0.65 samples. The relative intensities have been normalised using(200) peak. The full width at half maximum (FWHM) and intensities increase with calcium values, indicating that a minor structural change is related to the calcium content and oxidation state, where bigger

Ca^{+2} ions replacing Y^{+3} ions and oxidation can induce modulation in the (Y,Ca) plane.

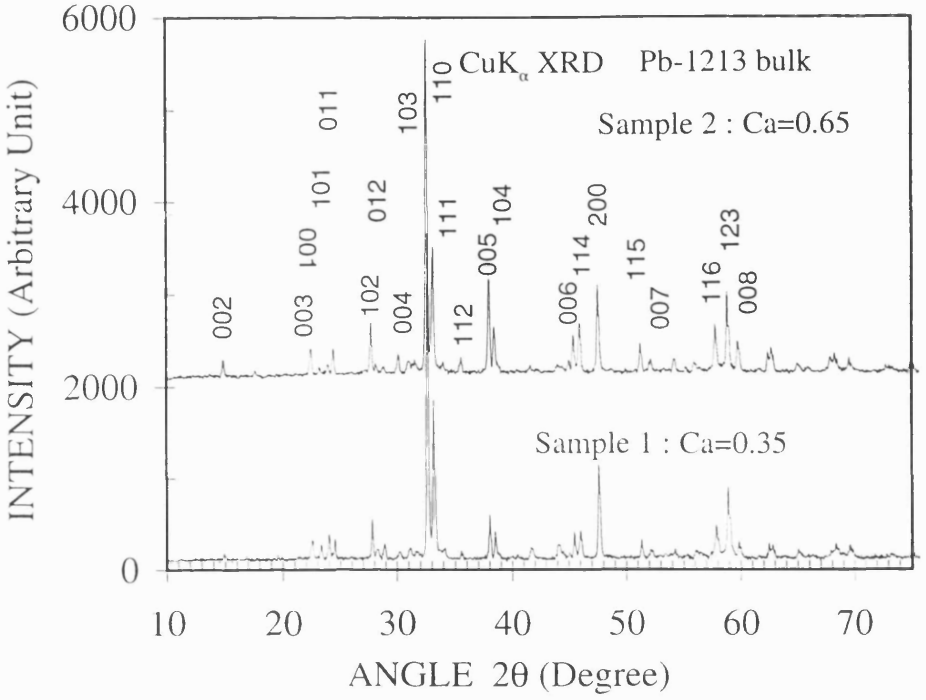

Figure 6.3.2. XRD pattern of $PbSr_2(Y_{1-x}Ca_x)Cu_3O_y$ samples (x= 0.35 and 0.65)

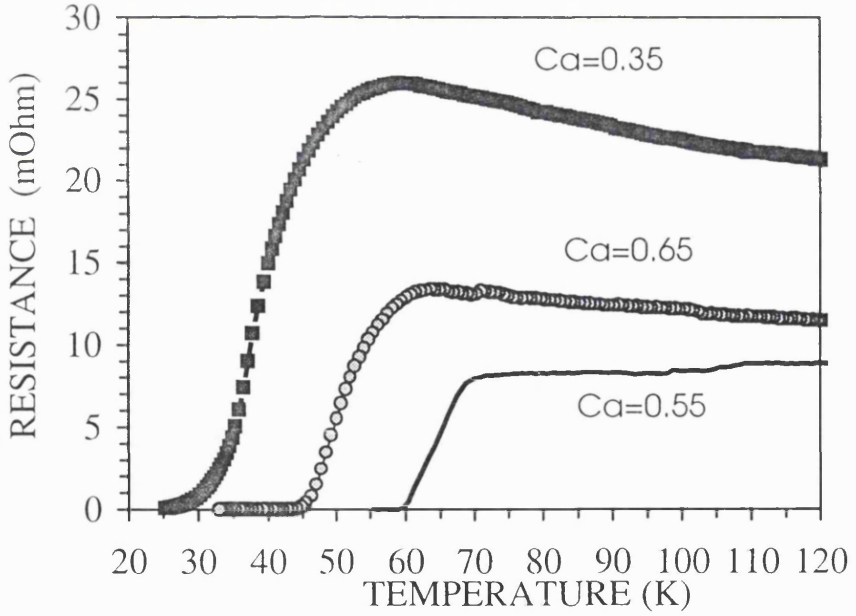

Figure 6.3.3. DC resistance versus temperature of $PbSr_2(Y_{1-x}Ca_x)Cu_3O_y$ samples (x= 0.35, 0.55, 0.65).

6.4.1 Synthesis of $PbSr_3(Y_{0.55}Ca_{0.45})Cu_3O_8$ (Pb-1313)

From the results obtained for the compositions of the Pb-1213 phase, it was considered that it would be interesting to know the effects of further increase in strontium content on the dc superconducting transition temperature and other

properties. A few samples were synthesised using the non-precursor solid state reaction method as described in section 6.1.2 (modification in ceramic method) and starting stoichiometry $Pb_{1.2}Sr_3(Y_{0.55}Ca_{0.45})Cu_3O_8$ to compensate for the lead losses. EDX results gave the true stoichiometry (table 6.4.1). Samples were also characterised by XRD (figure 6.4.1) and the Van der Pauw method was used to check the resistive transition by using 2.0mA dc currents (figure 6.4.2). This composition provided a small transition width only of $\Delta T \sim 4K$ after N_2-annealing for an hour at 800°C. However, a small positive curvature from 125K to 75K and then a minute negative temperature coefficient of resistance can be seen before onset transition. Sample A, annealed for half an hour in nitrogen exhibited a large negative temperature coefficient of resistance. From 60K a broad foot before onset transition temperature is present, and zero resistance has not been achieved down to 20K.

Table 6.4.1 *Superconducting transition temperatures of* $PbSr_3(Y_{0.55}Ca_{0.45})Cu_3O_y$ *samples annealed for different period in nitrogen at 800°C.*

Annealed in N_2 for the period ⟶	1/2 hr.		1 hr.		Without N_2 Annealing
Obtained stoichiometry	$T_{c.\,on}$	$T_{c.\,z.}$	$T_{c.\,on}$	$T_{c.\,z}$	Resistance
$PbSr_3(Y_{.55}Ca_{.45})Cu_3O_z$	38K	-	34 K	30 K	600Ω

Table 6.4.2. *Characteristic XRD d-spacings and relative intensities for Pb-1313 composition (sample A).*

d(Å)	I/I(%)	d(Å)	I/I(%)	d(Å)	I/I(%)
15.6884	14.2	2.7365	8.6	1.9107	42.6
5.9373	20.1	2.7047	45.6	1.8964	5.9
5.0262	64.7	2.6915	15.4	1.6952	13.5
3.9582	48.5	2.6412	8.3	1.6711	35.3
3.2178	11.8	2.5830	17.2	1.6435	12.0
3.1658	13.7	2.5121	4.9	1.5979	12.3
2.9671	41.2	2.3744	98.5	1.5694	30.9
2.9000	97.1	2.1721	7.4	1.5507	17.3
2.8876	56.9	2.0450	41.2	1.5042	10.3
2.8119	12.6	1.9981	11.2	1.4839	13.2
2.7513	100.0	1.9790	49.3		

The XRD pattern shows a mixture of Pb-2213 compared with d-spacings and relative intensities of published work, and impurity phases, however, the relative intensities are highly deviating. From the resistive transition temperature, it seems that the

material is different and needs XRD refinement and transmission electron microscopic analysis to determine structure.

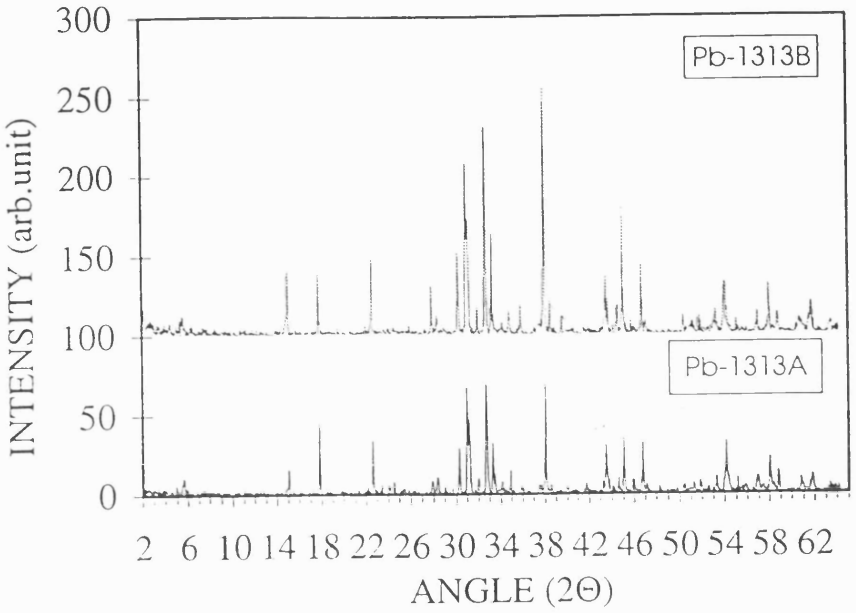

Figure 6.4.1. XRD pattern of polycrystalline $PbSr_3(Y_{0.55}Ca_{0.45})Cu_3O_y$ pellets characterised after annealing in N_2 for a period of (a) half an hour (b) one hour at 800°C.

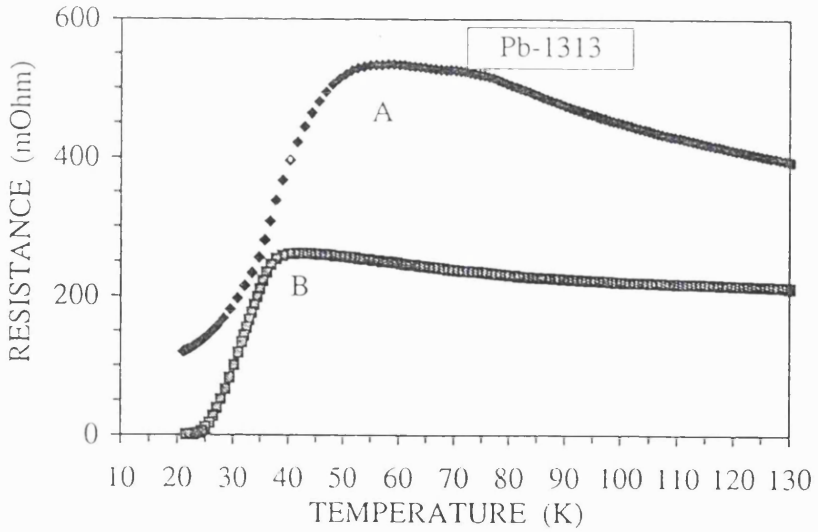

Figure 6.4.2. DC resistance versus temperature of $PbSr_3(Y_{0.55}Ca_{0.45})Cu_3O_y$ samples synthesised without precursor technique.

6.5.1 $Pb_3Sr_3(Y_{1-x}Ca_x)_{n-1}Cu_{n+1}O_{2n+4+x}$ (Pb-3324) composition

It is again demonstrated for the first time that superconducting transition can be readily achieved in polycrystalline samples of Pb-3324 compositions by manipulating oxygen stoichiometry. In fact, several lead-based compounds with layered-structures suitable for superconductivity are known, but it has been considered a very difficult

task to induce superconductivity in these materials. One can expect any possible increase in superconducting transition temperature with an increase in the number of CuO_2 layers, similar to other materials, such as $Tl_2Ba_2Ca_{n-1}Cu_nO_{2n+4}$- or $Bi_2Sr_2Ca_{n-1}Cu_nO_{2n+4}$-systems where n=1,2,3 and 4.

Synthesis using excess cationic ratios has been used to grow single crystals of Pb-2213 phase. These crystals were synthesised using two or three-steps precursor and non-stoichiometric melts with an excess of PbO, CuO, SrO and NaCl co-fluxes [2, 26, 27, 28]. Cava et al.[2] and Marezio et al.[26] used melts of excess PbO, CuO and two-step's precursor method but transition temperature was around 50K. Xue et al. used three-step precursor method, and the molar ratios of SYCCO:PbO:NaCl for starting compositions were 2:9:60. A long duration high-temperature processing then annealing around 600°C /15hrs in N_2 was required for the crystals to produce a sharp transition to zero resistance at 80K[3]. Whereas, Lukina et al.[28] used excess fluxes of PbO, SrO, CuO, high temperature range from 1030-800°C over a period of more than 50 hrs heat treatment. The cubic shaped single crystals extracted from melts of dimensions 0.6x0.6x0.5 mm possessed a $T_{c,\ onset}$ of 80K and $T_{c,\ zero}$ around 75K.

This attempt is also belonging to induce higher transition temperature in lead-based material through either variations in cationic ratios or keeping constant ratio of Pb, Sr, Cu and changing Y:Ca ratio. Following five different compositions were synthesised and first three compositions were checked by resistive transition or rf-inductive measurement (Meissner effect) and XRD.

1)$Pb_3Sr_3(Y_{0.5}Ca_{0.5})_2Cu_4O_z$ 2) $Pb_3Sr_3(Y_{0.65}Ca_{0.35})_2Cu_4O_z$

3) $Pb_3Sr_3(Y_{0.35}Ca_{0.65})_2Cu_4O_z$ 4) $Pb_3Sr_3Y_2Cu_4O_z$ 5) $Pb_3Sr_3Ca_2Cu_4O_z$

6.5.2 Synthesis of $Pb_3Sr_3(Y_{1-x}Ca_x)_{n-1}Cu_{n+1}O_{2n+6+x}$

Stoichiometric amounts of high purity powders were mixed to synthesise bulk superconductors [$Pb_3Sr_3(Y_{0.5}Ca_{0.5})_2Cu_4O_z$, $Pb_3Sr_3(Y_{0.65}Ca_{0.35})_2Cu_4O_z$, and $Pb_3Sr_3(Y_{0.35}Ca_{0.65})_2Cu_4Oz$].

The first step was the same as described in section 6.1.2. In the second step, the temperature of reformed pellets was raised to 880°C at the rate of 6°C /min for half an hour, cooled down to 875°C for 15 hours in air then cooled down to room temperature at the rate of 10°C /min. The air annealed pellets were cut into pieces of equal dimensions and placed into a furnace at 300°C and the temperature was raised to 800°C. Later the nitrogen flow was started to reduce the samples. The

resistances of each sample which were checked by a resistance meter. When approximately minimum resistance across the sample was obtained, other characterisation method were used.

6.5.3 Results and discussion

Figure 6.5.1 and table 6.5.1 show the resistances of samples with a $Pb_3Sr_3(Y_{0.35}Ca_{0.65})_2Cu_4O_z$ composition, annealed in a pure nitrogen for different periods at constant temperature (800°C). The constant calcium content in the composition shows the effect of oxygen reduction and its sensitivity towards dc electrical current of 2.0mA. The resistance of the sample annealed only 40 minutes shows higher value and semiconducting behaviour with minute negative slope. However, zero resistance was not achieved down to 25K but the $T_{c,\ onset}$ was around 74K. When the annealing period increases by 10 minutes the negative slope disappears but resistance remains constant up to $T_{c,\ onset}$ 72K and zero resistance is at 54K. Further increase in annealing period by 10 minutes, the resistance comes down but $T_{c,\ onset}$ is 71K. A positive curvature around 55K is present that can be due to oxygen inhomogeniety in the sample and $T_{c,\ zero}$ of 42K. Figure 6.5.2 and table 6.5.2 show the temperature dependence of the resistance of the $Pb_3Sr_3(Y_{1-x}Ca_x)_{n-1}Cu_{n+1}O_z$ samples with nominal values of calcium from x=0.35 to 0.65, after annealing in N_2 for 50 minutes at 800°C. The x=0.35 and 0.5 samples exhibit nearly constant resistances and minimum for x=0.5 in their normal state with $T_{c,\ onset}$ of 80K and $T_{c,\ zero}$ of 59K and 74K respectively. Increasing the calcium content to x=0.65 value, normal state resistance increases and a small semiconducting slope appears, showing that the charge carrier density is smaller than for the samples with x=0.5 and 0.35 values. The $T_{c,\ onset}$ is also shifted to 72K and $T_{c,\ zero}$ of 54.5K.

Table 6.5.1: *Superconducting transition temperatures of* $Pb_3Sr_3(Y_{0.35}Ca_{0.65})_2Cu_4O_z$ *samples annealed for different period in nitrogen at 800°C*

Annealed in N_2 for the period ⟶	40 min.		50 min.		60 min.	
Obtained stoichiometry	$T_{c.\ ons.}$	$T_{c.\ zer}$	$T_{c.\ ons}$	$T_{c.zer}$	$T_{c.\ ons.}$	$T_{c.\ zer.}$
$Pb_{2.5}Sr_3(Y_{.35}Ca_{.65})_2Cu_3O_z$	74 K	-	72K	54K	71 K	42K

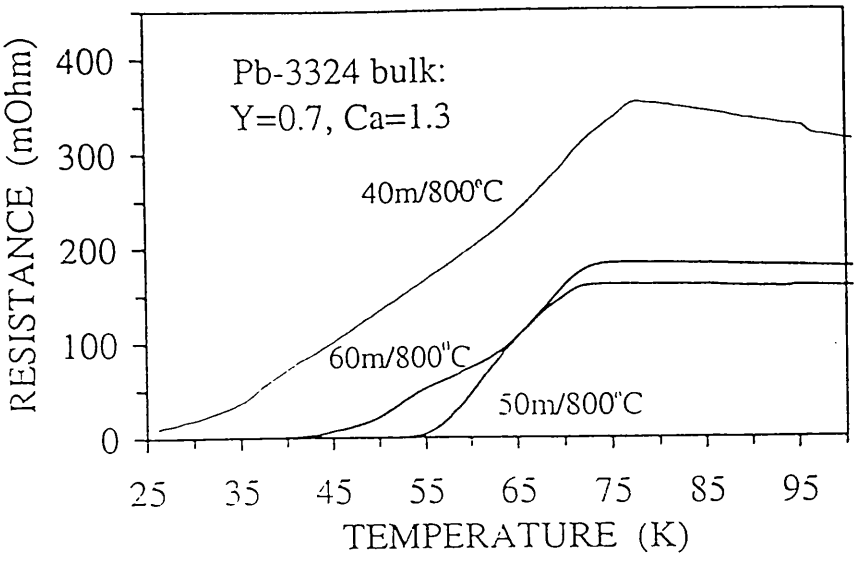

Figure 6.5.1. *DC resistance versus temperature of $Pb_3Sr_3(Y_{0.35}Ca_{0.65})_2Cu_4O_z$ samples synthesised without precursor technique and annealed for different periods.*

Table 6.5.2. *Superconducting transition temperatures of $Pb_3Sr_3(Y_{1-x}Ca_x)_2Cu_4O_z$ samples (x=0.35, 0.5 and 0.65) annealed for 50 minutes in nitrogen at 800°C.*

Calcium content ⟶	x =0.35		x =0.5		x =0.65	
Obtained stoichiometry	T_c. ons.	T_c. zer	T_c. ons.	T_c. zer.	T_c.ons.	T_c.zer.
$Pb_{2.5}Sr_3(Y_{1-x}Ca_x)_2Cu_{3.1}O_z$	80K	59K	80K	74K	72K	54.5K

Figure 6.5.3 exhibits the diamagnetic behaviour of two different compositions, $Pb_3Sr_3(Y_{0.5}Ca_{0.5})_2Cu_4O_z$ and $Pb_3Sr_3(Y_{0.35}Ca_{0.65})_2Cu_4O_z$. The samples were characterised by rf-inductive measurement at f=1040.0kHz, where dc voltage comes down at the transition temperature. The transition for sample x=0.5 starts around 80K but remains weak till the temperature reaches to 75K where a sharp fall is present. This shows that the diamagnetic volume fraction is quite large at 75K and confirms the zero resistance transition temperature. The sample with calcium content, x=0.65, shows a very small variation from 70K down to 55K and broadness remains to 46K. This is the case for most of the samples in each composition when the resistive transition is broader and semiconducting behaviour is present in normal state. This can be interpreted in terms of small number of Cooper pairs density that also relates the volume fraction of diamagnetism of superconducting sample.

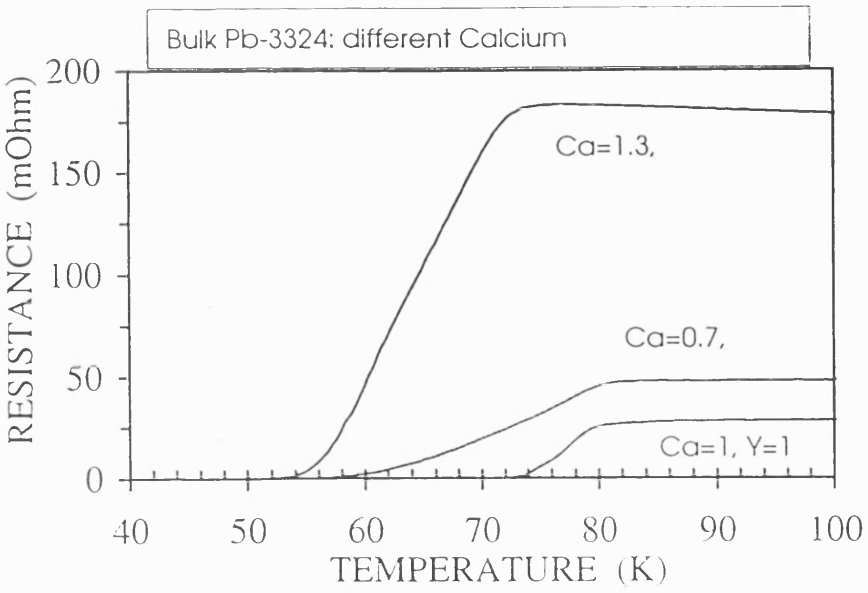

Figure 6.5.2. DC resistance versus temperature of $Pb_3Sr_3(Y_{1-x}Ca_x)_2Cu_4O_z$ (x=0.35, 0.5 and 0.65) samples annealed for 50 minute in N_2.

The compositions without Ca or Y remained highly resistive and were not characterised to show any transition at low temperature. These results again suggest that the variations in Y:Ca ratio can easily lead to an increased charge carrier density and the superconducting transition temperature, but higher transition temperature ($T_{c,\ zero}$ >80K) is difficult in lead-based material. These results further demonstrate a different mode of achieving high superconducting transition temperature that depends on air or pure nitrogen annealing.

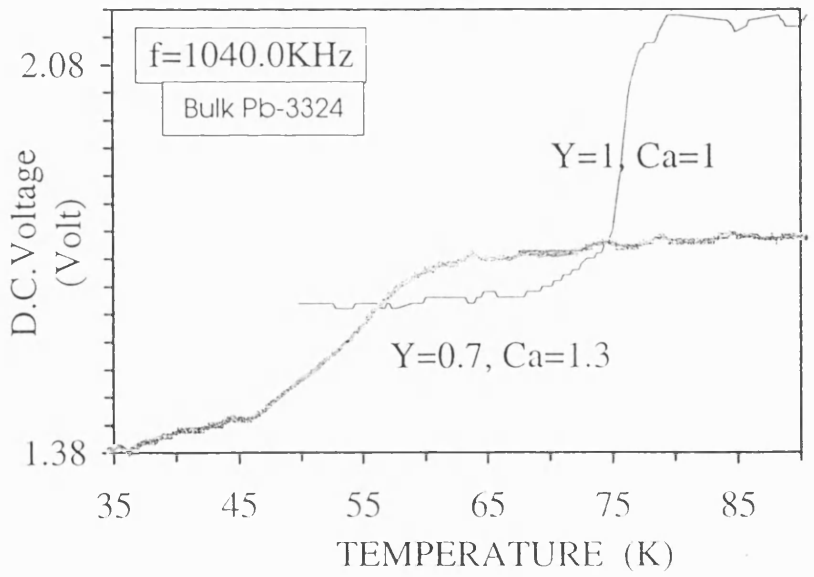

***Figure 6.5.3.** DC voltage versus temperature in rf-inductive measurements showing the diamagnetic behaviour of the samples containing calcium values (x=0.5 & 0.65).*

Table 6.5.3. Characteristic XRD d-spacings and relative intensities for $Pb_3Sr_3(Y_{0.35}Ca_{0.65})_2Cu_4O_z$ *composition (sample A).*

d(Å)	I/I(%)	d(Å)	I/I(%)	d(Å)	I/I(%)
5.0083	25.7	2.4924	6.4	1.6593	36.9
3.9545	2.0	2.3878	7.2	1.5928	3.3
3.8235	1.1	2.3263	5.0	1.5729	3.0
3.7248	3.6	2.2258	2.2	1.5468	1.8
3.6029	0.7	2.1642	2.1	1.4962	11.2
3.5092	1.5	2.0578	3.0	1.4385	6.4
3.2671	1.2	2.0311	29.2	1.4170	1.2
3.1581	3.5	1.9692	2.2	1.3803	2.3
3.0901	2.5	1.9126	4.6	1.2853	8.4
2.8757	100	1.8826	6.2	1.2819	7.2
2.7458	18.3	1.8656	3.1	1.2051	5.5
2.6927	6.2	1.7520	5.4	1.1733	3.9
2.5284	5.5	1.7261	2.0		

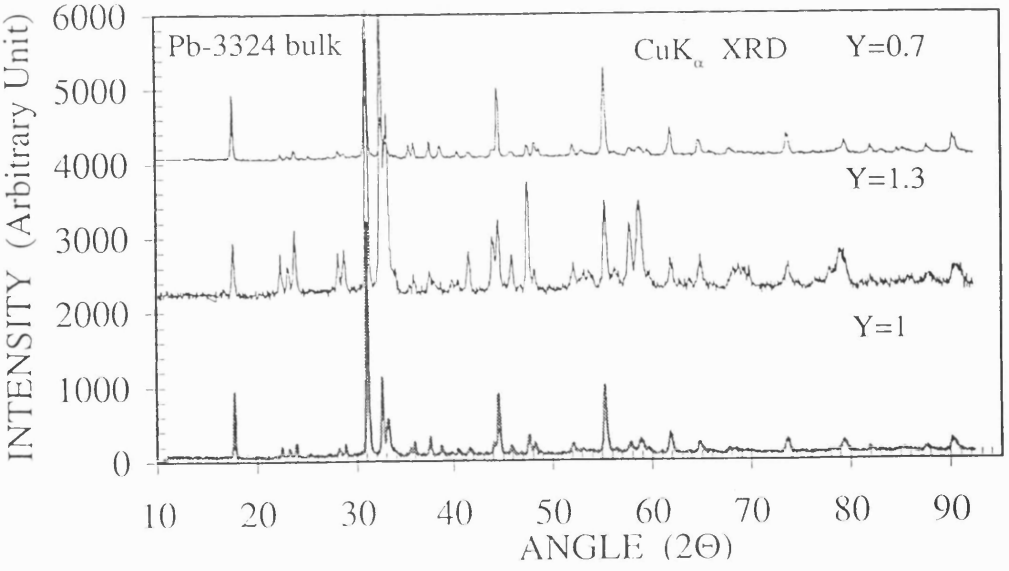

Figure **6.5.4.** *XRD pattern of* $Pb_3Sr_3(Y_{1-x}Ca_x)_2Cu_4O_z$ *(Y=0.7, 1 and 1.3) material.*

Figure 6.5.4 and table 6.5.3 show the XRD pattern of the data obtained in Imperial College, at Materials Department, by Dr.G.C.Tyrrell, using (CuK_α:λ=1.54060 radiation, step size 2Θ=0.04 and time per step=1sec) diffractometer type: PW1710, 45KV and 40mA generator current. In figure 6.5.4, all the intensity peaks have been

normalised with the peak intensity at Θ=17.695° (d=5.0083, I/I(%)=25.7) and showing variations in FWHM with the change in Y concentration in the samples, suggesting different oxidation levels. When comparing XRD of these compositions with Pb-2213 phase material, most of the I/I(%) values and peak positions are not matching with one another, required again a detailed XRD analysis.

In summary, a variation effect of the calcium level and period for reduction of oxygen in P-3324 composition have been studied systematically. At a level of x=0.5 and 50 minutes time scale for reduction in nitrogen at 800°C provide the optimum superconducting transition temperature of 80K. However, the structure of this composition has to be determined by any expert in Crystallography. The processing technique used to synthesise does not believes in the percentage of oxygen in nitrogen and provides some new results regarding lead-based materials.

6.6 Summary

A detailed study has been made to produce improvement in superconducting properties through various compositions and nitrogen annealing. It is observed that lead-based materials take up excess oxygen from air even at high temperature (>870°C) and can be converted into superconducting material through precise oxygen adjustment. A modification and minimum time scale for the synthesis of lead-based material was reported during processing.

Initially, the ceramic precursor technique was used for the synthesis of Pb-2213 phase that believes in two-step precursor technique, and can evolve out CO_2 after reacting above 950°C a mixture of all the carbonates and oxides except PbO for a period of 5-16hours with intermediate grindings. This method can induce some loss of precursor and inhomogeneity in second step. The second main problem was to control oxygen stoichiometry in lead cuprates using 1% O_2 in N_2 for oxidation during synthesis. A modification in method was developed to fabricate material without precursor to evolve out CO_2 that saves several hours of fabrication time, and the obtained results through modification in synthesis are better than the other published reports. The Pb-3314 composition was fabricated and characterised using EDX and XRD methods. It is observed that both Pb-2213 and Pb-3314 compositions have the same XRD pattern and nearly the same $T_{c,\ onset}$ and $T_{c,\ zero}$ values

but the reducing period of this composition in nitrogen atmosphere was found smaller compared with Pb-2213 phase.

A different approach was developed to remove CO_2 from a mixture of carbonates to fabricate Pb-1212 phase material. A shortest fabrication period was demonstrated with better superconducting transition temperature without high pressure oxygen anneal. In summary, a systematic study of the effect of variation of the calcium level, x, in the Pb-1212 phase from x=0.4 to 0.8 was performed. At a level of x=0.7, a transition temperature of 82K (onset) and 76K (zero) was obtained, the highest so far achieved in (Pb, Cu)-1212 phase. Bi-cations were substituted in the PbO-layer enhances the onset superconducting transition temperature (85K), but suppresses the $T_{c,\ zero}$ to 34K, and this seems due to sticking and poor-diffusive ability compared with lead.

A minimum time scale for the synthesis of lead-based material was reported during processing of various compositions. Polycrystalline samples of Pb-1213 compositions were synthesised without using a precursor technique. The obtained results again suggest that the electrical properties and superconducting transition temperature are sensitive to oxidation state and calcium content helps the charge transfer to CuO_2 sheets. The maximum obtained transition temperature for zero resistance is 60K for Ca=0.55 value. The full width at half maximum (FWHM) and intensities increase with calcium content and oxidation state, where bigger Ca^{+2} ions replacing Y^{+3} ions and oxidation can induce modulation in the (Y, Ca) plane.

It was interesting to know the effect of excess strontium in lead cuprates and their superconducting properties. The composition $PbSr_3(Y_{0.55}Ca_{0.45})Cu_3O_8$, (Pb-1313) was synthesised that exhibited a small transition width (ΔT~4K) after N_2-annealing for an hour at 800°C provided $T_{c,\ onset}$ of 34K and $T_{c,zero}$ 30K. The XRD pattern of Pb-1313 compared with Pb-2213 phase shows a deviation from relative intensities of published XRD data for Pb-2213 phase and small variations in d-spacings suggest that the material is different and needs XRD refinement and electron microscopic analysis.

A composition $Pb_3Sr_3(Y_{1-x}Ca_x)Cu_{n+1}O_{2n+4+x}$ was readily achieved in polycrystalline bulk form as a result of an attempt to induce higher superconducting transition temperature in lead-based material through either variations in cationic ratios or keeping constant ratio of Pb, Sr, Cu and changing Y:Ca ratio. The XRD of Pb-3324 phase material was compared with Pb-2213 phase material. It is found that most of the $Ix100/I_0$ values and peak positions are not matching with one another, required again a detailed XRD refinement analysis. A variation in calcium level for reduction of oxygen in Pb-3324 composition has been studied systematically. For the x=0.5 value of calcium content, a maximum

superconducting transition temperature of 80K was achieved just only for 50 minutes annealing period for reduction in nitrogen at 800°C.

References

[1] H.Takagi, S.Uchida and Y.Tokura, Phys. Rev. Lett. 62, 1197 (1989).

[2] R.J.Cava, B.Batlogg, J.J.Krajewski, L.W.Rupp, L.F.Schneemeyer, T.Siegrist, R.B.van Dover, P.Marsh, W.F.Peck, Jr, P.K.Gallagher, S.H.Glarum, J.H.Marshall, R.C.Farrow, J.V.Waszczak, R.Hull and P.Trevor, Nature 336, 211 (1988).

[3] S.H.H.Naqvi, F.Beech, I.W.Boyd, Elect. Lett., 27, 430 (1991).

[4] P.Goodman, D.G.Jensen and T.J.White, Physica C 158, 173 (1989).

[5] Y.Koike, H.Sunagawa, T.Noji, M.Masuzawa, N.Kobayashi, M.Namiki, K.Hirokawa and Y.Saito, Physica C 171, 331 (1990).

[6] M.Masuzawa, T.Noji, Y.Koike and Y.Saito, Jpn. J. Appl. Phys., 28, (1989).

[7] M.A.Subramanian, J.Gopalakrishnan, C.C.Torardi, P.L.Gai, E.D.Boyes, T.R.Askew, R.B.Flippen, W.E.Farneth, and A.W.Sleight, Physica C 159, 124 (1989).

[8] T.Maeda, K.Sakuyama, S.Koriyama, H.Yamauchi and S.Tanaka, Phys.Rev. B43, 7866 (1991).

[9] X.X.Tang, D.E.Morris and A.B.P.Sinha, Phys.Rev. B 43, 7936 (1991).

[10] T.Rouillon, J.Provost, M.Hervieu, D.Groult, C.Michel and B.Raveau, Physica C 159, 201 (1989).

[11] R.Mahesh, R.Nagarajan and C.N.R.Rao, J.Sol.State Chemis., 96, 5(1992).

[12] D.G.Xeninkos and T.R.Lemberger, Rev.Sci. Instr. 60, 831 (1989).

[13] M.Kasuge, T.Maeda, K.Sakuyama, T.Miyatake, N.Koshizuka, H.Yamauchi, C.Murayama and N.Mori, Phys. Rev. B45, 10713 (1992).

[14] A.Maignan, T.Rouillon, D.Groult, J.Provost, M.Hervieu, C.Michel, B.Raveau, R.S.Liu and P.P.Edwards, Physica C 177, 461 (1991).

[15] S.Adachi, H.Adachi, K.Setsume and K.Wasa, Jpn. J.Appl.Phys. 30, L1099 (1991).

[16] K.Kurusu, H.Takami, and K.Shintomi, Analyst 114, 1341 (1989).

[17] M.Kosuge and K.Kurusu, Jpn.J.Appl.Phys. 28, L810 (1989).

[18] T.Maeda, K.Sakuyama, H.Yamauchi and S.Tanaka, unpublished.

[19] A.Ono and Y.Uchida, Jpn.J.Appl.Phys. 29, L586 (1990).

[20] T.Maeda, K.Sakuyama, F.Izumi, H.Yamauchi, H.Asano and S.Tanaka, Physica C 175, 393 (1991).

[21] Jian-zhou, Wen, Sun-qi Feng, Qing-rong Feng, Hang Yu, Xin Zhu, Bing-jun Quan, Solid State Comm., 91, 93-95 (1994).

[22] Gmelin, Handbook of Inorganic Chemistry, System no 47(Springer, Berlin), p. (1969)

[23] A.Tokiwa, T.Oku, M.Nagoshi, M.Kikuchi, K.Hiraga and Y.Syono, Physica C161, 459 (1989).

[24] T.Rouillon, R.Retoux, D.Groult, C.Michel, M.Hervieu, J.Provost, B.Raveau, J.Solid State Chem., 78, 322 (1989).

[25] X.X.Tang and D.E.Morris, Phys. Rev. B, 44, 4553 (1991).

[26] M.Marezio, P.Bordet, J.J.Capponi, R.J.Cava, C.Chaillout, J.Chenavas, A.W.Hewat, E.A.Hewat, J.L.Hodeau, P.Strobel, Physica C 162-164, 281 (1989).

[27] J.X.Xue, M.Reedyk, Y.P.Lin, C.V.Stager and J.E.Greedan, Physica C, 166, 29 (1990).

[28] M.M.Lukina, V.N.Milov and V.V.Moshchalkov, Sov.Phys.-Supercond., 3, 2767(1990).

Chapter 7

Synthesis of lead cuprates using PLD technique

The synthesis of lead-based cuprates in the form of bulk or single crystals with optimised and reproducible superconducting properties has several steps during processing [1, 2, 3]. The difficulty in the chemistry of preparation of the lead cuprates has already been discussed in the chapters three and six.

The pulsed laser ablation-deposition (PLD) has demonstrated the ability of synthesis of several multicomponent materials stoichiometrically in the form of thin layers. Few groups have already tried to grow $Pb_2Sr_2(Y_{0.5}Ca_{0.5})Cu_3O_{8+\delta}$ phase thin layers by using PLD technique [4]. Their experiments were not successful in demonstrating in-situ growth of Pb-2213 phase films at 650°C, but they found the T_c variations from 10K to a maximum 86K in $(Pb_{0.75}Cu_{0.25})Sr_2(Y_{1-y}Ca_y)Cu_2O_7$ phase by systematic substitution of Ca for Y. The grown films did not show a single phase out of 15 thin layers characterised by XRD. A recent report on the growth of $Pb_{1.03}Sr_{2.5}(Dy_{0.45}Ca_{0.57})Cu_3O_8$ films, keeping the deposition temperature between 750-800°C by using MBE method has been published in which Pb, Sr, Dy(Eu), Ca and Cu metals were evaporated separately from the effusion cells onto $SrTiO_3$ (001) substrate in $2.7x10^{-5}$mbar oxygen pressure. Authors found the non-stoichiometric lead content and an excess amount of Sr for their growth conditions. The onset transition temperature was reported as 55K and $T_c(0)$ of 28K [5]. H. Adachi et al. [6] demonstrated in-situ growth on MgO(100) substrates by rf-magnetron sputtering using non-stoichiometric pellets containing metal cation ratios of Pb:Sr:Ln:Ca:Cu=5:2:1-1.5:0.4:2.7-3.3, where Ln is Y or Yb. The deposition temperature was reported to be 550 °C in a pure argon ambient and the films were found to be highly c-axis oriented, Pb-2213 phase with a c-axis lattice constant of 15.75Å. They considered that the oxygen from the targets was sufficient to synthesise this phase. The $Pb_2Sr_2(Y_{0.5}Ca_{0.5})Cu_3O_8$ films possessed a $T_{c,\ onset}$ of 60K and $T_{c,\ zero}$ of 48K. They reported that even the use of 3% O_2 in argon during the growth produced non-superconducting 214-like (La_2CuO_4) structured films with c=12.88Å.

For *ex-situ* synthesis of the Pb-2213-phase thin layers, deposition was performed on MgO (100) single crystal substrates at low temperature (300-500°C) in flowing oxygen ambient ($4x10^{-3}$mbar), using frequency doubled Nd:YAG laser pulses (532nm, 4ns). A set of ex-situ and in-situ growth conditions have been determined via a series of efforts of controlling lead and oxygen stoichiometry to achieve good quality single phase, c-axis oriented $Pb_2Sr_2(Y_{0.5}Ca_{0.5})Cu_3O_{8+\delta}$ films.

7.1 Ex-situ growth

7.1.1 Bulk target preparation

In a first step, polycrystalline bulk samples were fabricated using a cation stoichiometric ratio of Pb:Sr:Y:Ca:Cu = 2-6:2:0.5:0.5:3 and a two-step solid state reaction. In this method the precursor is prepared by mixing an stoichiometric amount of carbonates and oxides in ethanol, other than lead oxide. The mixed powder was pressed in the form of a pellet, fired in air at 950°C for 4 hours in a dense alumina crucible and self cooled to room temperature. These pellets were ground and thoroughly mixed together with an appropriate amount of PbO powder in ethanol for an hour. The dried powders were pressed at a pressure of 1ton/cm^2, placed inside the furnace in a platinum crucible. Their temperatures were subsequently raised to 800°C in nitrogen ambient at the rate of 10° C/minute, kept for 10 hours and then cooled down to room temperature. Partial or complete melting was observed only when value of lead oxide increased more than 3 atoms in the stoichiometric ratio. Each pellet was crushed, ground, pressed and again heat treated separately, first in air at 600°C for one hour only to soak some oxygen then in nitrogen ambient for several hours at 750°C.

7.1.2 Deposition and ex-situ annealing

Initially, 4ns frequency-doubled (532nm) Nd:YAG laser pulses were used to ablate the superconducting target that was placed inside the vacuum chamber, separated by a 3.5cm perpendicular distance from a heated MgO substrate. The angle between the incident-laser beam and the normal was 30°. The target was smoothed prior to deposition using

an emery paper, followed by blowing the surface with nitrogen to remove residual particles. The substrates were cleaned in acetone, methanol and dried with nitrogen. The chamber was flooded with oxygen and evacuated to $1x10^{-4}$mbar. The substrates were heated to 900°C for half an hour in flowing oxygen and then cooled down to room temperature. Before deposition started, the oxygen was leaked in the chamber to maintain $4x10^{-3}$mbar oxygen pressure. The ablated material was collected by a single-crystal substrate of (100) MgO. The deposition temperature of the substrate was kept constant at 350°C, and after 10 minute exposure to pulses at a fluence of about $5J/cm^2$ at 10Hz rate, 1mm thick films were grown. Initially, these deposited layers were insulating at room temperature.

The deposition parameters were kept constant for several films which were annealed inside the furnace in flowing nitrogen ambient for different periods and different annealing temperatures. The grown layers show different superconducting transition temperatures. The obtained results are presented in figure 7.1 and 7.2 and tables 7.1 and 7.2.

It is observed that when the insulating films were annealed in flowing nitrogen at (675±15)°C for different annealing periods, the resistances at the onset transition temperature were gradually decreased and found lowest for the four hours annealing period but remained in ohms that is very high comparing to other HTSC cuprates, such as Y-Ba-Cu-O and Bi-Sr-Ca-Cu-O systems.

Table 7.1: *Annealing periods and obtained transition temperatures for the ex-situ grown films in nitrogen ambient.*

$Pb_2Sr_2(Y_{0.5}Ca_{0.5})Cu_3O_x$ layers annealed at 675°C in nitrogen for the period of	$T_{c,onset}$ K	$T_{c,zero}$ K
6 hour (6N)	68	39
5 hour (5N)	77	62.5
4 hour (4N)	77	63
2-3 hour (2N, 3N)	65	38

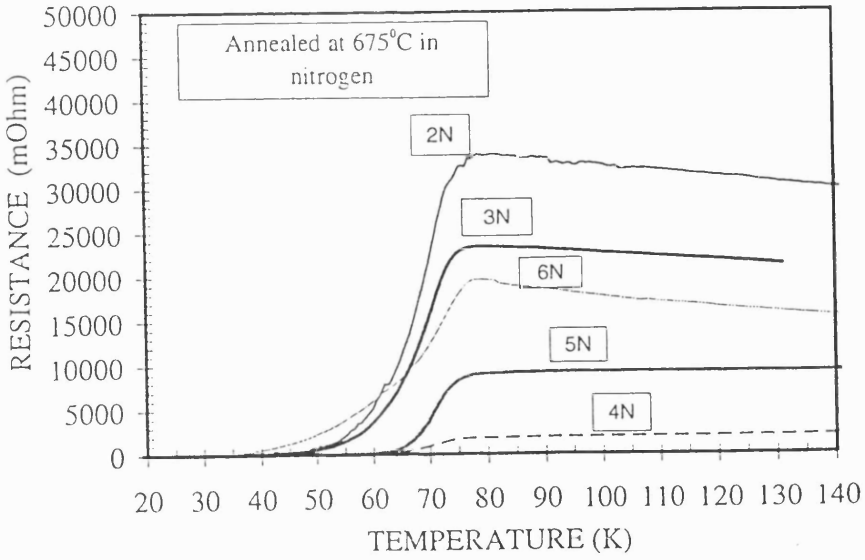

Figure 7.1. *Resistance versus temperature of the* $Pb_2Sr_2(Y_{0.5}Ca_{0.5})Cu_3O_x$ *layers grown at 675°C in nitrogen for different periods.*

The best obtained DC resistance versus transition temperature of the film annealed for 4 hours can be seen from figure 7.1. The gradual enhancement in $T_{c,\ zero}$ with the period of annealing up to 4 hrs can be interpreted in terms of lesser disordering of the grains, oxygen ordering, required reduction or minimum defects at the grain boundaries.

Table 7.2 and figure 7.2 show the effect of the annealing temperature for a fixed annealing period of four hours. The films annealed in nitrogen at (675±10)°C is shown to be optimum. The decrease in $T_{c,\ zero}$ is prominent when the annealing temperature was reduced by 25°C above or below of 675°C. The films annealed at 625°C has shown an onset transition temperature at 50K and could not achieve zero resistance. It indicates that the suitable annealing temperature for crystallinity and reduction for the fixed period of 4 hour is 675°C. The XRD characterisation show that the films with optimum superconducting transition temperature has mainly c-axis orientations.

Table7.2. *Various annealing temperatures and obtained transition temperatures for the ex-situ grown layers.*

$Pb_2Sr_2(Y_{0.5}Ca_{0.5})Cu_3O_x$ layers annealed in nitrogen for the period of 4 hour at various temperature	$T_{c.onset}$ K	$T_{c.zero}$ K
725°C	76	25
675°C	77	63
650°C	65	40
625°C	42	-

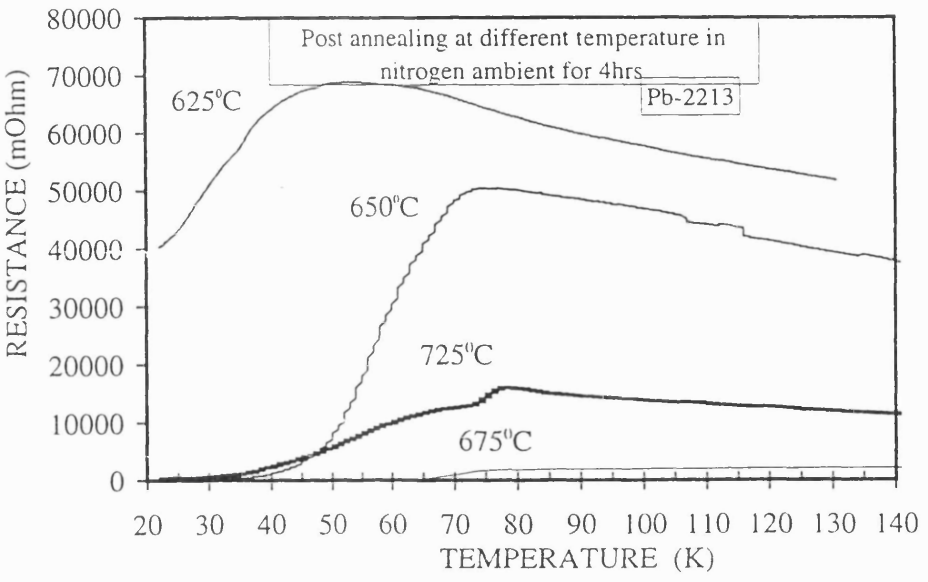

Figure 7.2. *Resistance versus temperature of the* $Pb_2Sr_2(Y_{0.5}Ca_{0.5})Cu_3O_x$ layers annealed at different temperature in nitrogen for 4 hours.

XRD scan indicates that the films annealed for two hours are mostly c-axis oriented and perpendicular to substrate plane. The (*00l*) peaks yield a lattice constant of 15.77Å. When the films annealed for four hours at the same temperature, other orientation (i.e., 110, 200, 220) appears. The (*00l*) peaks greatly diminished for longer annealing periods due to further reduction of oxygen from Pb-2213 phase films.

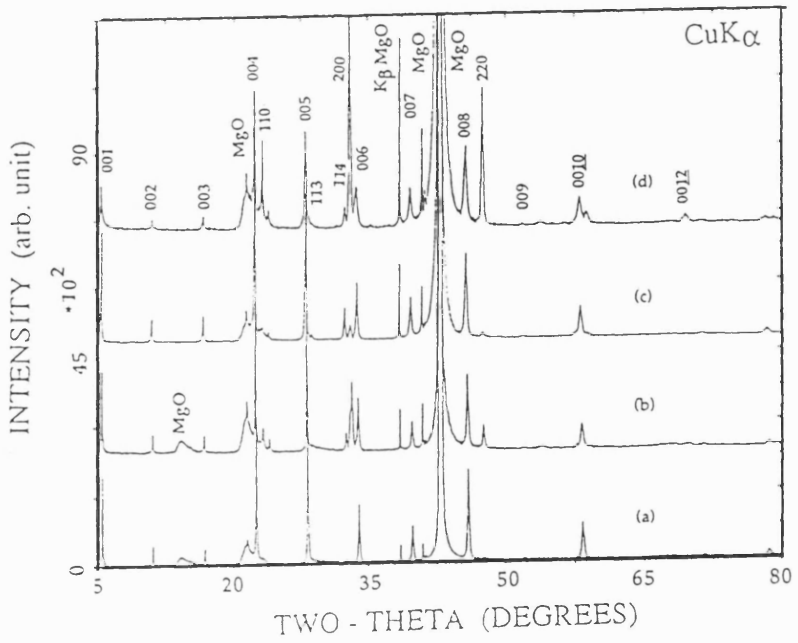

Figure 7.3. *XRD pattern of the* $Pb_2Sr_2(Y_{0.5}Ca_{0.5})Cu_3O_x$ layers annealed in nitrogen at 675°C for (a) 2hrs (b) 4hrs (c)5hrs (d) 6hrs.

7.2 Effect of laser fluence

Another set of experiment was performed using 1 to 7J/cm^2 fluences and a $Pb_{2.5}Sr_2(Y_{0.5}Ca_{0.5})Cu_3O_{8+\delta}$ melt textured target. Several films were deposited by varying fluences with the help of neutral density filters. All the depositions were carried out by operating a laser at 532nm and 10Hz. The laser beam was focused on the target to a spot size of 0.085cm^2. The target-substrate distances used in these experiments were 3cm and 6cm as possible limitations for the deposition system. All the films were deposited on MgO (001) single crystal substrates held at 350°C. After deposition completed, all the films were annealed in nitrogen at 725°C to observe the effects of higher temperature ex-situ annealing on composition. The compositional analysis of annealed films was performed by Dr.F.Saba at Imperial College, using EDX that induces error as high as 10% in compositional analysis. Therefore, the analysis is relative and performed under the same conditions. The values are presented in figures 7.4 and 7.5 for the depositions at 3cm and 6cm respectively. These values are the average of the measurements performed at five different points, one at the centre and the others on the four corners of 7x7mm^2 samples. The ideal values have been taken by normalising the total atomic percentage of cations to 100, resulting in the ratios: Pb 25%, Sr 25%, Y 6.25 %, Ca 6.25%, and Cu 37.5% in the case of optimised composition of Pb-2213 phase. During EDX the differentiation between elements with close atomic numbers such as Sr and Y are difficult and need a lower accelerating voltage (1~4keV) to separate the overlapped peaks.

For the set of deposition performed at 3cm away from the target, the EDX results relative to ideal values of Cu and Ca shows a large deviation for smaller fluences (<3J/cm^2), whereas, Pb and Sr values is larger than ideal values. Above 4J/cm^2 fluences, all the cations (Cu, Pb, Sr, Ca) approach the ideal values but the Y remains around the ideal value for all fluences. The values of Y and Sr could be obtained only by separating the overlapped peaks, using low accelerating voltage for electron beam during analysis. Therefore, an error of measurements can be induced due to differences in x-ray scattering produced for the two different accelerating voltages. Also, the values of Y and Sr are related to each other in terms of ratio present in the Pb-2213 phase. The value of Y is

only 0.5 whereas Sr is 2 out of 8 atoms, that can also induce experimental error during separation of peaks. It can be observed from the values of Y that is low enough but the Sr value is higher for the same fluence (3.5J/cm^2). From the figure 7.5 that is for the deposition performed at 6cm, nearly the situation is same, only the Sr is slightly lower and Y is higher than the ideal values. The situation for Pb and Cu is approximately the same in both cases, where the Pb decrease and Cu increase with fluence. It could be interpreted in terms of lower and higher melting points, heat of vaporisation and segregation of target material with higher laser fluences. The films were also characterised for resistive transitions after compositional analysis and results are tabulated in table 7.3 and presented in figure 7.6. The onset superconducting transition temperature is nearly the same (70K) but $T_{c,\ zero}$ is different and maximum for higher fluences, where the copper is at ideal value, lead is deficient and Ca is slightly higher. The thinner films show higher onset resistances and zero resistance was achieved at higher temperature than at the medium range fluences, where the Pb is higher and could be compensating to deficient Cu.

During EDX analysis it was observed that the films deposited at higher fluences have larger number of droplets and their sizes are bigger. At the same laser fluences, the quality of the films is better for larger target to substrate distances.

Table 7.3. *Characteristics of films deposited at 3cm and annealed for 2hrs/725°C before EDX analysis.*

Code	Laser fluence	Deposition rate/pulse	$T_{c,\ zero}$
E80	6.68 J/cm^2	9.5 Å	62K
E50	3.54 J/cm^2	4.5 Å	54K
E25	1.965 J/cm^2	2.1 Å	54K
E10	1.3 J/cm^2	0.6 Å	56K

The deposition rate was also influenced with the laser energy. For example, when the films were deposited below 2J/cm^2 fluence, the deposition rate is slightly smaller could be due to smaller plume size with respect to substrate position whereas the laser energy approaches to the threshold energy (figure 7.7).

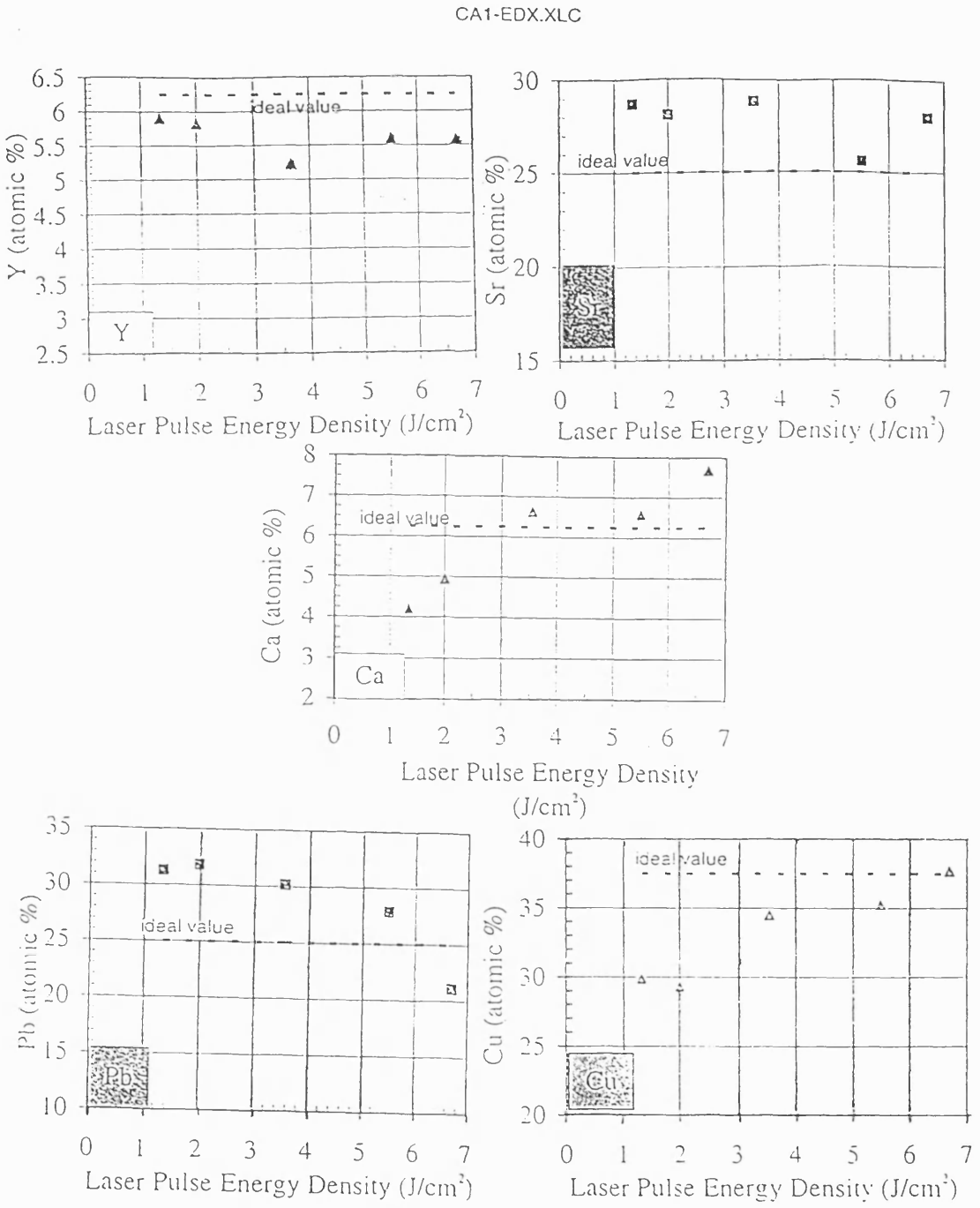

Figure 7.4. *Atomic percentage of Pb, Sr, Y, Ca, and Cu in films deposited in $4x10^{-3}$ mbar flowing oxygen at different fluence (d=3cm).*

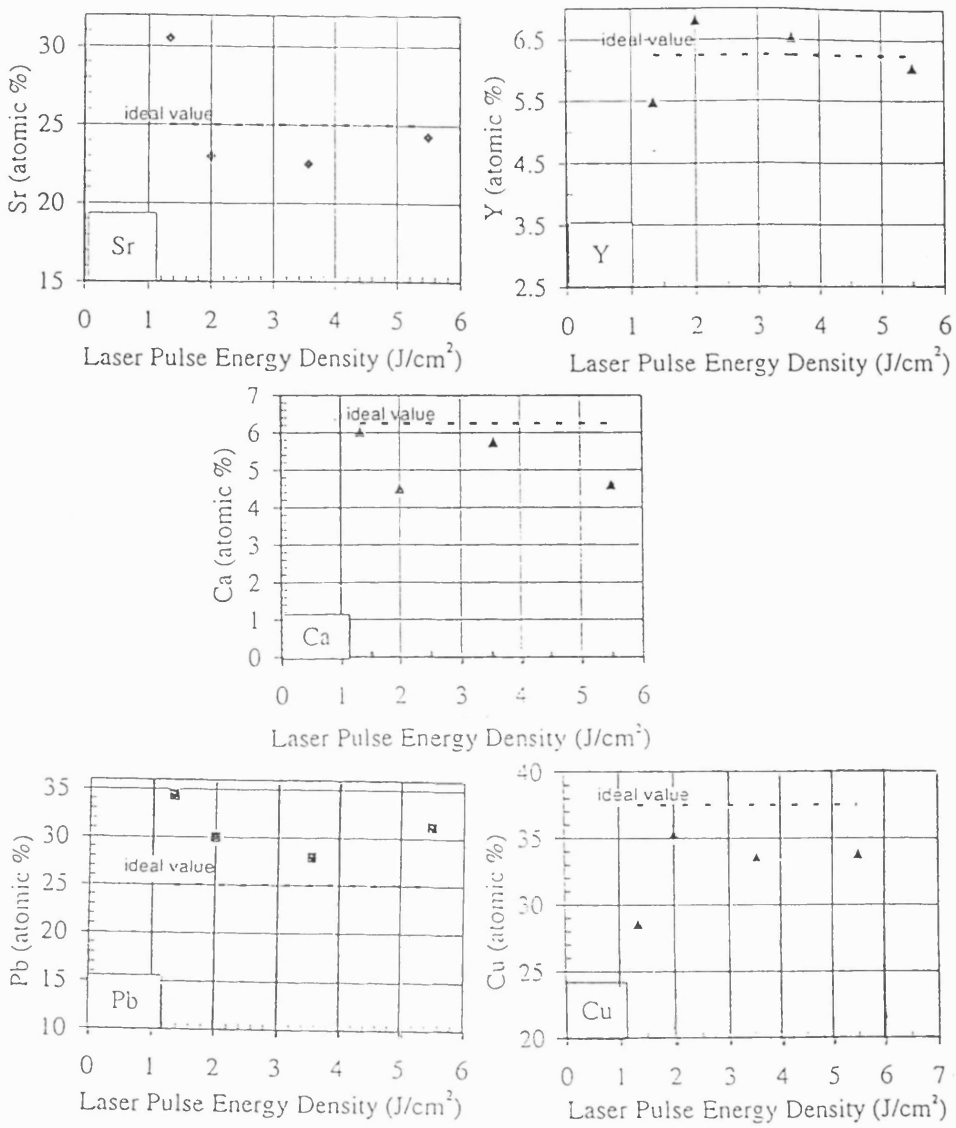

Figure 7.5. *Atomic percentage of Pb, Sr, Y, Ca, and Cu in films deposited in $4x10^{-3}$ mbar flowing oxygen at different fluences (d=6cm).*

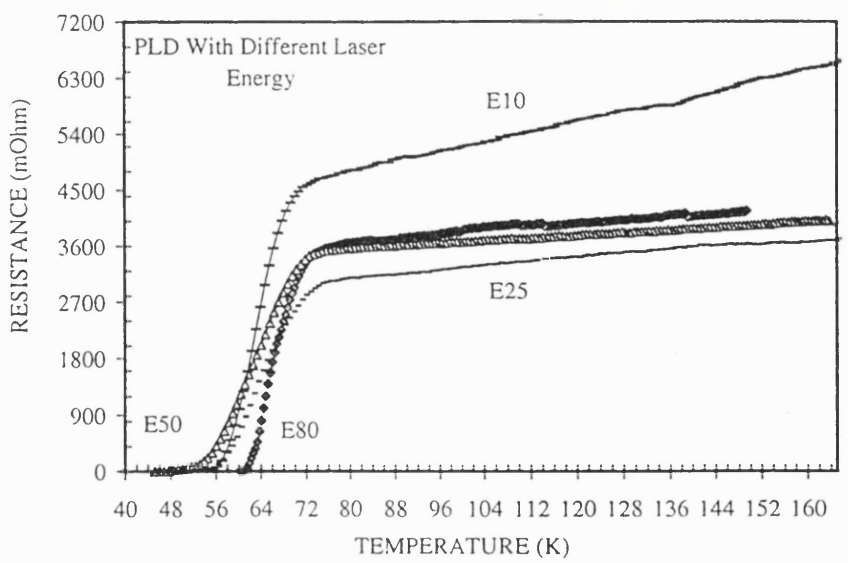

Figure 7.6. *Resistance versus temperature of the Pb-2213 phase films deposited at various laser fluences.*

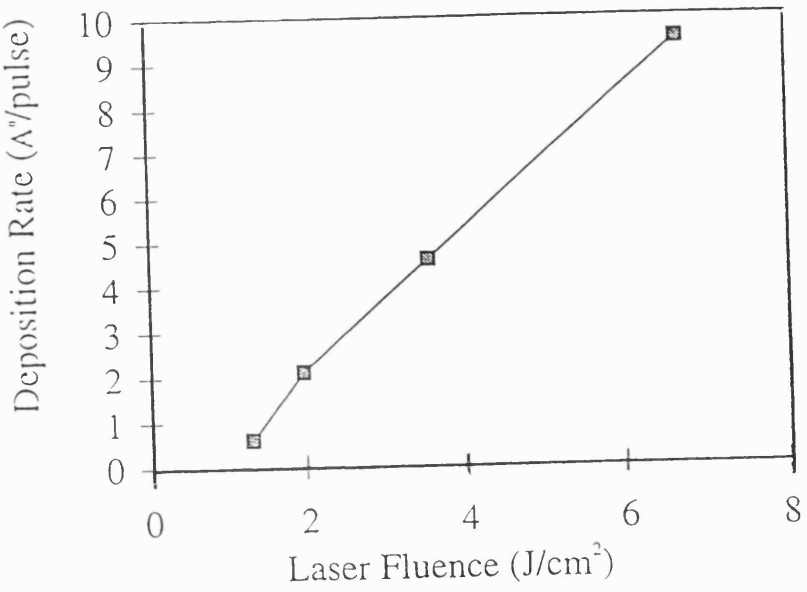

Figure 7.7. *Laser fluence versus deposition rate at the target-substrate distance, d=6cm.*

7.3 Different lead content and transition temperature

A set of deposition was performed to observe the effect of various amounts of lead on the superconducting transition temperatures (figure 7.8 and table 7.4). PLD technique has been applied to ablate pellets of different lead contents and collected on MgO (001) substrates by placing them in front of the plume, around 350°C in $4x10^{-3}$mbar pressure maintained due to flowing oxygen. A fluence of $5J/cm^2$ was typically used, and 10 minute exposure times at 10Hz, led to deposition of around 1-1.2μm in thickness at 3.5cm.

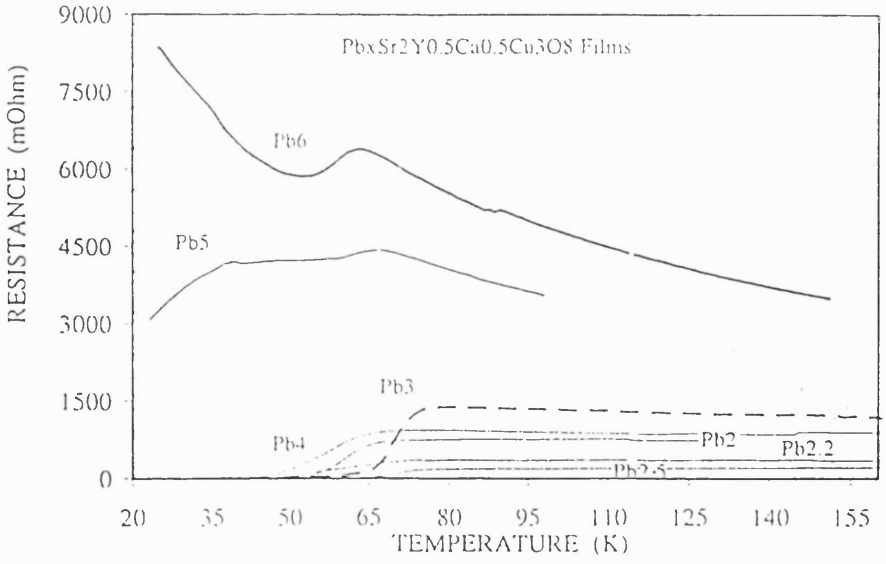

Figure 7.8. *Resistance versus temperature of the films deposited using* $Pb_xSr_2(Y_{0.5}Ca_{0.5})Cu_3O_z$ *pellets* (x=6 to 2).

It is obvious from the results that the lead content is playing an important role on superconducting properties. When the stoichiometric lead value is 6, the onset transitional fluctuation in resistance is found at 65K but after 55K, again the semiconducting behaviour can be observed.

Table 7.4. *Superconducting transition temperature of the films grown using PLD technique and pellets of different lead content.*

$Pb_xSr_2(Y_{0.5}Ca_{0.5})Cu_3O_z$ where 'x'	$T_{c.onset}$ K	$T_{c.zero}$ K
6	60	-
5	65	-
4	67	45
3	77	56
2.5	78	64
2.2	70	50
2	69	53

The semiconducting behaviour before 67K and two step transitions were found for the value of Pb=5. After second step of 35K transition, the resistance gradually decreases from 4.5Ω to 3.0Ω down to 25K. Clearly the superconducting transition temperatures gradually increase from 45K to 64K for Pb=4 to Pb=2.5 values, and then come down for Pb=2 to 2.2 values. This effect can be interpreted in terms of scattering of Cooper pairs from higher lead content that could be in between the grain boundaries as amorphous or impurity phases. The maximum onset transition temperature and temperature for zero resistance have been achieved for the film grown using $Pb_{2.5}Sr_2(Y_{0.5}Ca_{0.5})Cu_3O_z$ target composition.

7.4 Unreacted pellet and thin film synthesis.

One experiment was performed to observe the effect of lead loss and quality of the film if the pellet is just made of mixed powder of oxides and carbonates for $Pb_3Sr_2(Y_{0.5}Ca_{0.5})Cu_3$ composition without any reaction. In the first step, carbonates and oxides were mixed in methanol then few drops of diluted nitric acid were added, mixed and dried at 100°C in nitrogen, ground and pressed at 1.5ton/cm^2. The films were deposited by using laser fluences of 0.5J/cm^2 at 10Hz for 3 minutes, at the distance of 3.5cm from the target onto the MgO-substrate temperature of 300°C. Higher fluences were sufficient to shatter the target or producing dust-like powder. Apparently, the sound-waves and thermal shocks are sufficient to fracture the loosely bound material or

can evolve out the loosely bound big particles of several micrometers in size if the pellets were not sufficiently pressed. The deposited films were quite thick and even weighable (0.0065mgram). The composition of films was $Pb_2Sr_{1.3}(YCa)_{1.1}Cu_3$ analysed by EDX after annealing in air at 700°C for 1hour for reaction, then annealed at 700°C for 4hrs in nitrogen. The loss of lead and non-stoichiometry seems to be due to large differences in melting points and heat of sublimations of different metals and their oxides. The films annealed for several hours in nitrogen were characterised by using SEM (figure 7.9) and the Van der Pauw technique (figure 7.10).

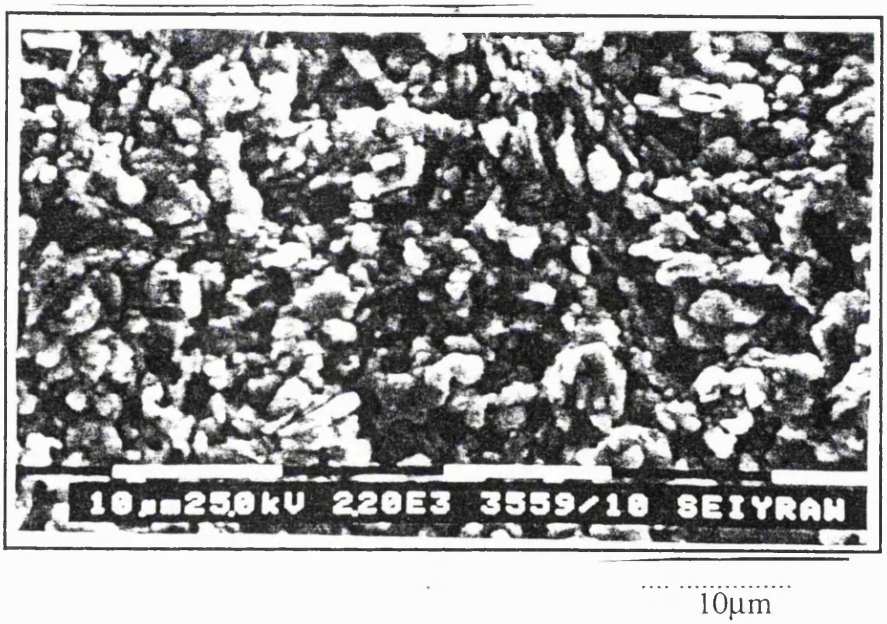

Figure 7.9. SEM micrograph of the $Pb_2Sr_{1.3}(YCa)_{1.1}Cu_3$ film.

SEM micrograph has shown a collection of partially melted big particles as a result of 4 1/2 hour heat treatment. XRD characterisation was performed using CuK_α radiation (figure 7.11) and showed the Pb-2213 phase material with minute impurities. From XRD pattern and (*00l*) peak it is found that the c-axis lattice constant is 15.6412Å. The smaller c-axis lattice constant, c, value compared with the bulk values of c=15.781Å could be due to non-stoichiometric value of Sr. The film annealed for 3 hours at 700°C in nitrogen has provided onset superconducting transition temperature of 73K and T_c, zero of 58K.

From this experiment, it is concluded that the Pb-2213 phase films can be grown after ex-situ annealing and using unreacted, pressed-powder target, but the morphology becomes very rough due to evaporation and collection of micron size particles.

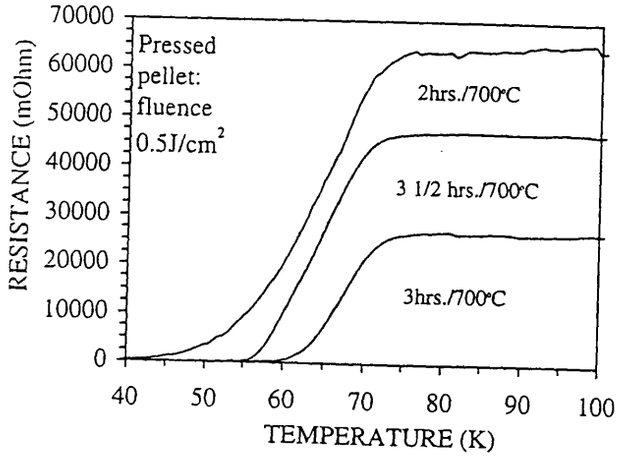

Figure 7.10. *Resistance versus temperature of the* $Pb_2Sr_{1.3}(YCa)_{1.1}Cu_3$ *film grown ex-situ and deposited using unreacted pellet.*

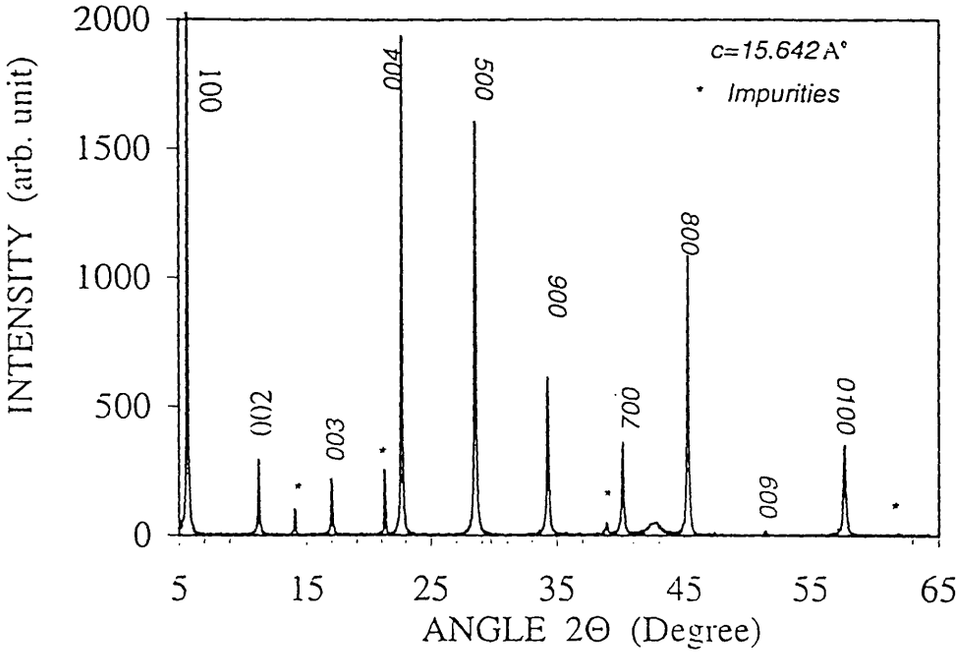

Figure 7.11. *XRD of the* $Pb_2Sr_{1.3}(YCa)_{1.1}Cu_3$ *films grown ex-situ and deposited using unreacted pellet.*

7.5.1 In-situ growth

A basic experimental set-up has already been described in chapter five and used to grow in-situ $Pb_2Sr_2(Y_{0.5}Ca_{0.5})Cu_3O_z$ phase films. The lead loss was observed at higher substrate temperatures when it was carried out using even non-stoichiometric, melt-textured $Pb_3Sr_2(Y_{0.5}Ca_{0.5})Cu_3O_z$ targets. An excess amount of lead in the target was used to compensate the lead loss. The deposited layers were coated with carbon to make them conductive and analysed for stoichiometric transfer using SEM (S570-Hitachi) that has heated tungsten filament as an electron source and the samples can easily be moved in three dimensions, equipped with an EDX analysing facility at Archaeology Department, UCL. The deposition temperature and obtained stoichiometry are given in table 7.5.

Table 7.5. *Variations in composition of deposited layers at different substrate temperatures.*

Target stoichiometry (Before ablation)	After interaction of 3000 pulses with target	Deposition temperature (°C)	f thin layers
$Pb_3Sr_2(Y_{0.5}Ca_{0.5})Cu_3O_z$,	$Pb_{1.06}Sr_{2.5}(Y_{0.5}Ca_{0.5})Cu_3O_z$,	250	$Pb_{3.1}Sr_{2.0}(Y_{0.5}Ca_{0.51})Cu_3O_z$,
		450	$Pb_{2.8}Sr_{1.9}(Y_{0.5}Ca_{0.53})Cu_3O_z$,
		500	$Pb_{1.73}Sr_{1.9}(Y_{0.42}Ca_{0.5})Cu_{2.9}O_z$,
		550	$Pb_{0.783}Sr_{2.05}(Y_{0.5}Ca_{0.493})Cu_3O_z$
		650	$Pb_{0.24}Sr_{1.9}(Y_{0.5}Ca_{0.47})Cu_{2.87}O_z$
		760	$Pb_{0.05}Sr_2(Y_{0.5}Ca_{0.532})Cu_{2.9}O_z$,

The lead loss becomes prominent around 450°C and is serious at 650°C where the composition of layer was achieved as $Pb_{0.24}Sr_{1.9}(Y_{0.5}Ca_{0.49})Cu_3O_z$. Other authors have also reported the loss of lead and tried to grow films using non-stoichiometric targets [4, 6, 7]. However, our previous results of in-situ growth have shown superconducting layers, when superconducting stoichiometric targets were used to ablate, and characterised by XRD with lattice constant 15.756Å, estimated from (005) peak. The technique behind it was to raise the substrate temperature from 300°C to onward at

the rate of 50°C/minute during 10 minutes of deposition time and 10Hz at the repetition rate of laser pulses, whereas the chamber pressure was $4x10^{-3}$mbar due to flowing oxygen near the substrate, can transform the lead ions into PbO that has higher melting point (>875°C). The deposited layers were left for 30 minutes without flowing oxygen to keep them in reduced condition and then heater was shut off. The deposition temperature of MgO (100) substrate varied from 575-800°C. The layers grown around 800°C were nonconducting while those grown around 650°C were mostly c-axis oriented with $T_{c,\ onset}$ being close to 70K and around 24K(figure 7.12)[8]. The films grown at other temperatures did not show zero resistance. If the deposition temperature was 750° C, the $T_{c,\ onset}$ was around 70K and zero resistance was not achieved even at 17K, towards the limit of our measurement capability. However, when this film was annealed in nitrogen at 400°C for 4 hours, the zero resistance was found to be at 20K, even though the $T_{c,\ onset}$ remained the same at 70K [8]. This behaviour shows that the oxygen take-up is in excess and reduction at low temperature is slow but can enhance superconducting properties.

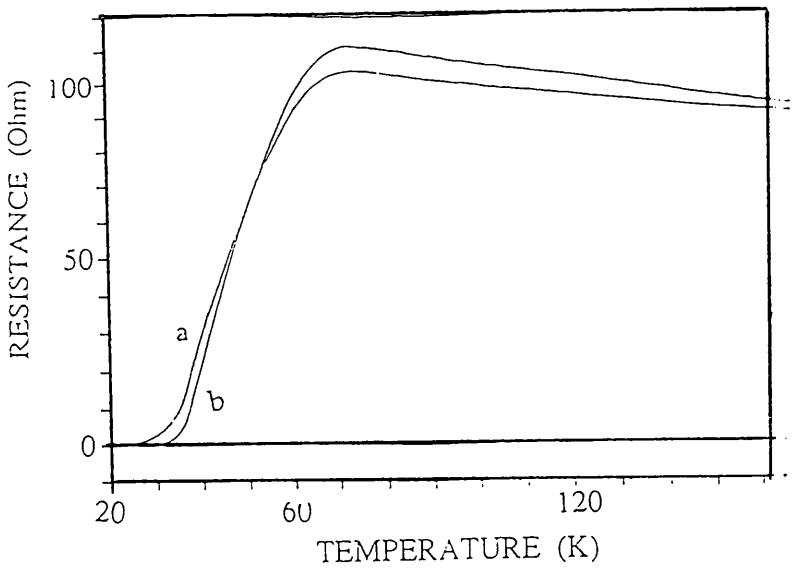

Figure 7.12. *Resistance versus temperature of a Pb-2213 phasefilm (a) grown in-situ at 650°C (b) the same film subsequently annealed in nitrogen at 400°C for 4 hours.*

Figure 7.13 is showing the XRD patterns obtained for the films grown in-situ at (650± 25)°C in flowing oxygen, has mainly c-axis orientations. The XRD patterns obtained for the films grown at (600±25)°C and (525±25)°C in oxygen ambient and rapid change of

temperature from 300°C to higher temperatures (525-600)°C during the course of ablation-deposition are showing polycrystalline, non-superconducting or amorphous thin layers (figure 7.14).

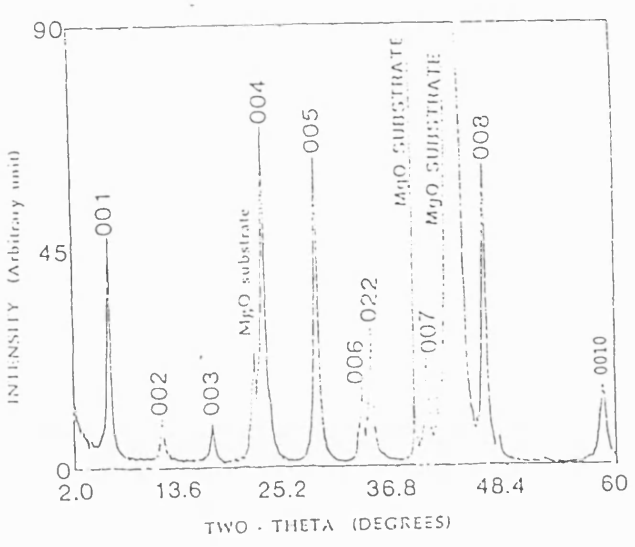

Figure 7.13. *XRD pattern of a mainly c-axis oriented Pb-2213 phase film grown in-situ at 650°C in oxygen ambient.*

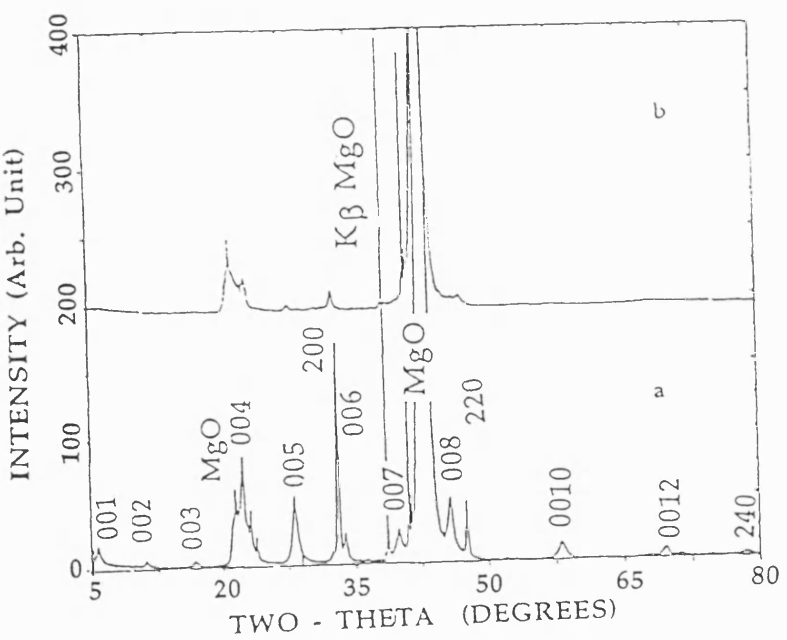

Figure 7.14. *XRD pattern of Pb-2213 phase film grown in-situ at (a) 600°C; (b) 525°C in oxygen ambient.*

7.5.2 In-situ annealing in N_2 ambient

The enhancement of the superconducting transition temperature during the in-situ growth of Pb-2213 phase thin layers was the main target to achieve. Unfortunately, the required higher temperature for oriented crystalline films causes the non-stoichiometry and can create Pb-1212 material with impurity phases if the highly lead-rich targets were used during ablation-deposition at 600-650°C [4, 7] in sufficient amount of oxygen. On the other hand, the oxygen is difficult to manipulate to keep Pb-2213 phase material in superconducting state. One alternate method was used to check any possible improvement in superconducting properties. All the deposition parameters were same as described in preceeding section 7.6.1, except the suitable deposition temperature (450°C) for better stoichiometric transfer. After completion of deposition, the substrate temperatures were raised from 450°C to 750°C at the rate of 10°C/min in flowing oxygen ($3x10^{-3}$mbar). Later, the pure nitrogen was leaked into the chamber to bring the pressure to around 0.01mbar and maintained during 25 to 45 minutes. XRD characterisation was performed for the films kept at 550°C, 650°C, and 750°C for only 35 minutes in 0.01mbar nitrogen. The film annealed at 550°C for 35 minutes exhibits a few low intensity peaks with a mixed state of 214-like (La_2CuO_4) material. The film annealed at 650°C has also shown the mixed phase material with better intensity peaks of Pb-2213 phase but remained highly resistive. The layer annealed at 750°C shows c-axis orientation and perfect crystallinity (figure 7.15).

Table 7.6: Superconducting transition temperature of the layers grown after post-annealing in N_2 at 750°C within the chamber.

Code of film	Annealing Period	$T_{c,onset}$ K	$T_{c,zeo}$ K
25M	25 minutes	75	42
35M	35 minutes	75	62
45M	45 minutes	75	50

Figure 8.16 is showing the microstructure of the film annealed in nitrogen ambient for the period of (a) 25minutes (b) 35 minutes (c) 45 minutes at 750°C in nitrogen ambient. Initially, few partially melted droplets were found after 25minutes annealing and later, the film annealed for 45minutes a complete disintegration can be seen.

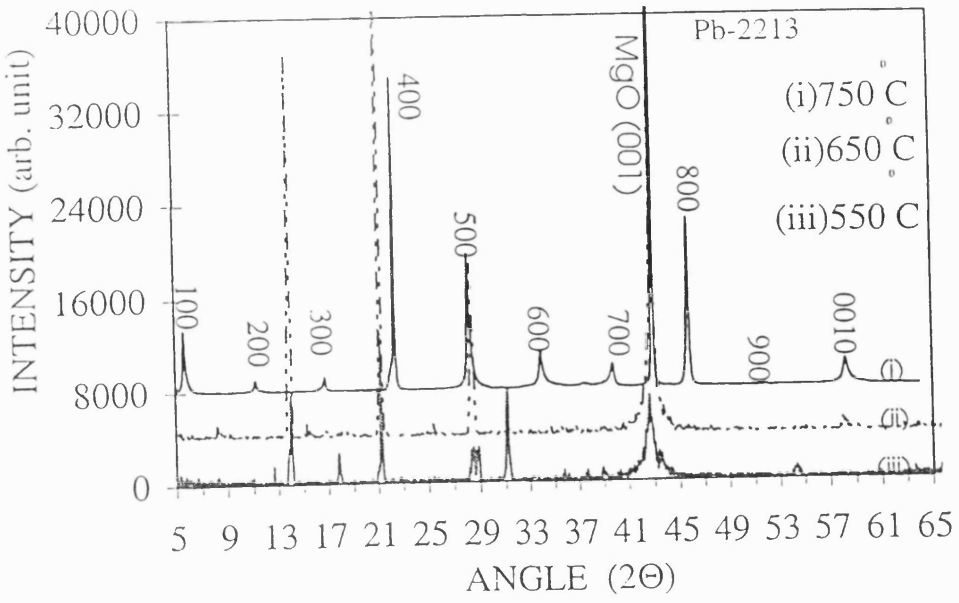

Figure 7.15. *XRD pattern of Pb-2213 film on MgO substrate grown in-situ after post annealing in N_2 ambient.*

The resistive transition temperatures obtained by this technique are shown in figure 7.17, and presented in table 7.6. The film annealed for 35 minute has better superconducting transition temperature than 45 or 25 minute annealing periods. All the films exhibited $T_{c,\ onset}$ of 75K but $T_{c,\ zero}$ remained low. A long tail of resistance has also been observed after a certain resistive drop. Even, the film that has shown high quality texturing and $T_{c,\ zero}$ of 62K has small resistive curvature around 65K, which could be an effect of inhomogeneous oxygen distribution during high temperature N_2 annealing, or amorphous filling between grains. This is similar to the effect that has been reported by Xue et al. [3] for the Pb-2213 phase single crystals.

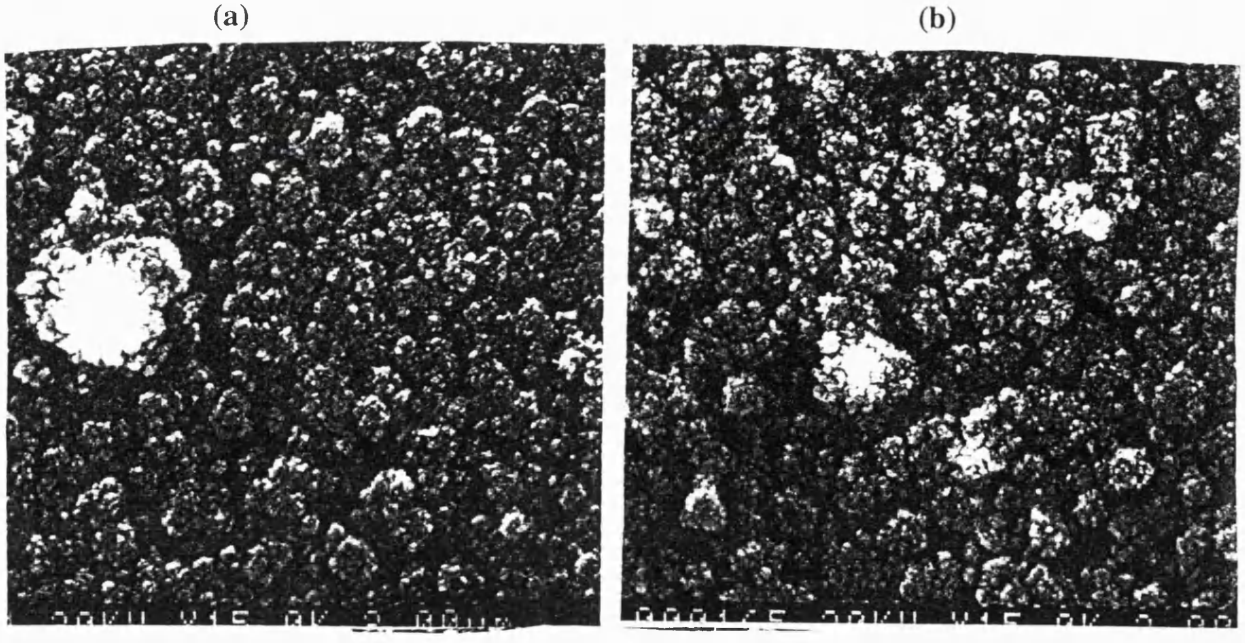

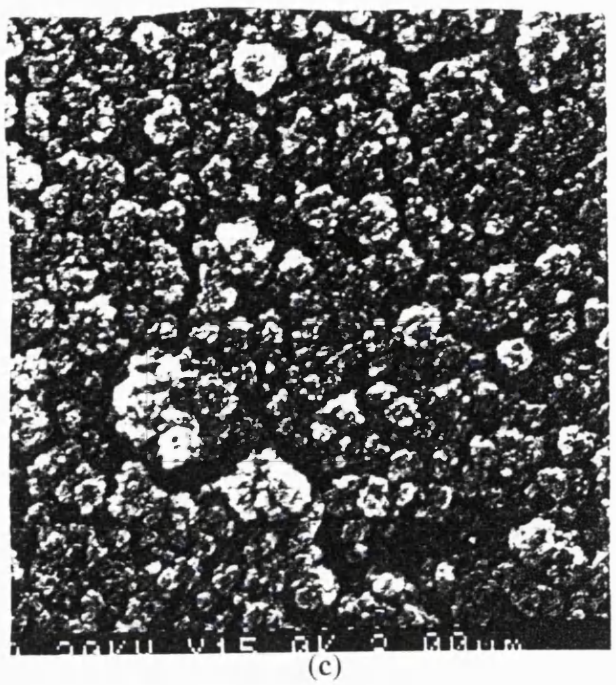

Figure 7.16. SEM micrograph of the films annealed at 750°C for a) 25minute b)35minute and c) 45minute.

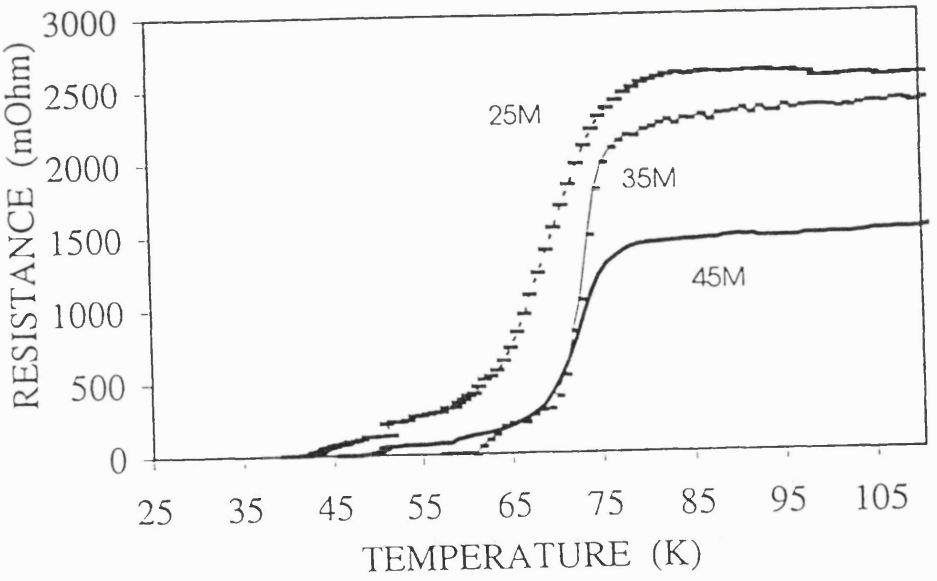

Figure 7.17. *Resistance versus temperature of a Pb-2213 phase film grown inside the chamber after post annealing in N_2 ambient.*

7.5.3 Deposition of Pb-2213 film in argon ambient

Thin layers of Pb-2213 phase were grown in-situ on MgO(100) substrates by rf-magnetron sputtering using non-stoichiometric pellets containing metal cation ratios of Pb:Sr:Y:Ca:Cu=5:2:1-1.5:0.4:2.7-3.3. The growth temperature was reported to be 550°C in a pure argon atmosphere and the films were highly c-axis oriented. It was also

reported that the use of 3% oxygen in argon during the growth produced non-superconducting 214-like phase (La_2CuO_4) with c=12.88Å [6].

A set of experiment was also performed to check whether the growth of thin $Pb_2Sr_2(Y_{0.5}Ca_{0.5})Cu_3O_8$ layers is possible in argon atmosphere or not when using PLD synthesis technique and was also a check of oxygen loss during ablation. The set-up of experiment was same as described in previous section except $4x10^{-3}$mbar flowing argon atmosphere was used in the chamber during deposition to provide an inert ambient. After deposition at various temperatures, all the layers were found to be insulating. The deposition temperature was varied and XRD characterisation was performed to know either crystallinity is possible or not in inert ambient. From the figure 7.19, it can be seen that the layers remain amorphous if either the temperature is low or high (>650°C). This indicates that oxygen feeding is also essential to grow Pb-2213 layers during PLD processing to control anion congruency.

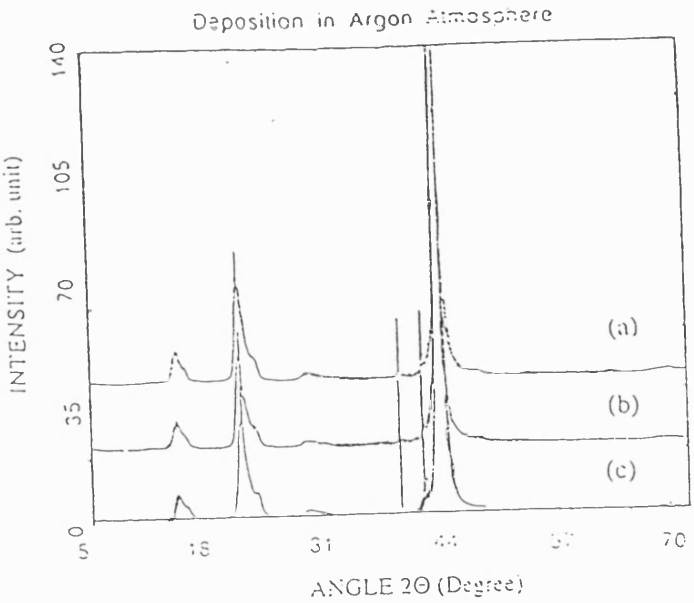

Figure 7.18. *XRD pattern of Pb-2213 amorphous films on MgO substrate deposited in-situ at (a)550°C(b)650°C (c) 750°C in argon ambient.*

Later, one of the films deposited at 550°C in argon ambient was annealed in air at 750°C for different periods and minimum room temperature resistance was found only for 10 minute annealing and presented in table 7.7. The film was characterised using Van der Pauw technique. Figure 7.19 shows the resistance versus temperature profile. It is not clear that the film either exhibits mixed state of semiconducting and possible superconducting phases or something else. It required a complete analysis and is left for future work.

Table 7.7. Resistance versus post annealing period.

Annealing temperature	Annealing Period	Resistance at room temperature
750°C	2 minute	10MΩ
750°C	4 minute	0.4MΩ
750°C	8minute	4900Ω
750°C	10minute	325Ω
750°C	12 minutes	789Ω

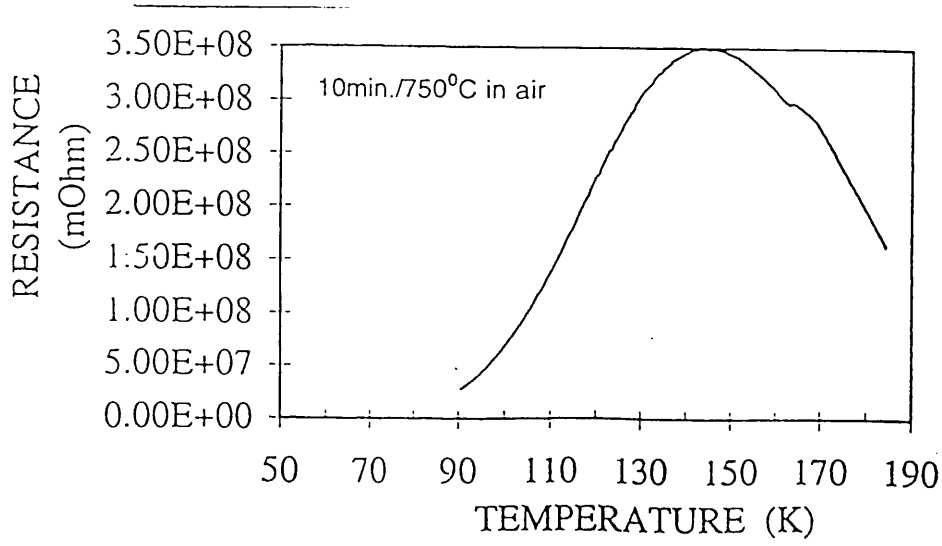

Figure 7.19. *Resistance versus temperature of a film annealed in air.*

7.6 Ultra thin layer

It is highly desirable to grow high quality ultra thin layers to form multilayered superconducting devices. Several authors have reported the superconductivity in a few unit-cell thick layers or even in a single unit cell of $YBa_2Cu_3O_7$ material, grown by using buffer and cap layers of $PrBa_2Cu_3O_7$ on MgO (001) or $SrTiO_3$ (001) substrates. However, their results regarding superconducting properties are not consistent [9, 10, 11, 12]. The growth of a ultrathin layer is the difficult task due to several reasons such as slight lattice mismatching, unevenness on atomic scale level and chemical nature of the substrate can cause distorted lattices, imperfection and discontinuity. The $PrBa_2Cu_3O_7$ material (lattice mismatch≈1.5%) is highly resistive and semiconducting even in its fully oxidised state and gifted by nature for buffer layer to grow a continuous and a flat surface

of $YBa_2Cu_3O_7$ material on the atomic scale. To observe the effects on transition temperature of $Pb_2Sr_2(Y_{0.5}Ca_{0.5})Cu_3O_8$ material as an ultrathin layer, a good quality buffer layer is required that was not available in literature till the experiments were performed. However, the $Pb_2Sr_2(Y_{0.5}Ca_{0.5})Cu_3O_8$ material itself can be used as insulating buffer layer for Bi-system or other superconductors, when it is in oxidised state.

To deposit ultra thin layers, MgO(001) single crystal substrates were chemically cleaned and placed in the vacuum chamber. Later, the chamber was flooded with oxygen and evacuated down to $1x10^{-3}$mbar using simple rotary pump. To clean perfectly, the substrates were heated to 900°C in flowing oxygen for half an hour then cooled down to room temperature. Nd:YAG (532nm, 4ns, $4J/cm^2$) laser pulses were used to deposit on heated substrate at 450°C in a $4x10^{-3}$mbar pressure with flowing oxygen. The deposition parameters were kept constant and number of pulses (5, 10, 50, 150) was changed for several thin layers. After deposition was completed, the thin layers were taken out and annealed at 675°C in nitrogen ambient for 4 hour. XRD measurements using CuK_α source ($K_{\alpha1}$:λ=1.5406Å, $K_{\alpha2}$:λ=1.5444Å, K_β:λ=1.3922Å) were carried out at the Department of Crystallography, Birkbeck College, London. Figure 7.20 shows the XRD spectrum of the films grown using 10, 50, and 150 pulses and coded as S10, S50 and S150 respectively. These films show highly c-axis orientations. It can be seen that the full width at half maximum (FWHM) of the peaks is different for different thicknesses, depending upon the mean crystallite size. The broadening effect of the diffraction line profile can also be due to the combination of instrumental and physical factors. The well known Scherrer's equation can relate the size of a crystallite with FWHM in the form: $L=K\lambda/\beta\cos\Theta$, where L is the mean dimension of the crystallite, β the FWHM, λ the wave length of the radiation source ($K_{\alpha1}$:λ=1.54Å), Θ the peak position, and K a constant. From peak positions and FWHM it can be inferred that the reduction in FWHM with increasing thickness is mainly due to increase in crystallite size.

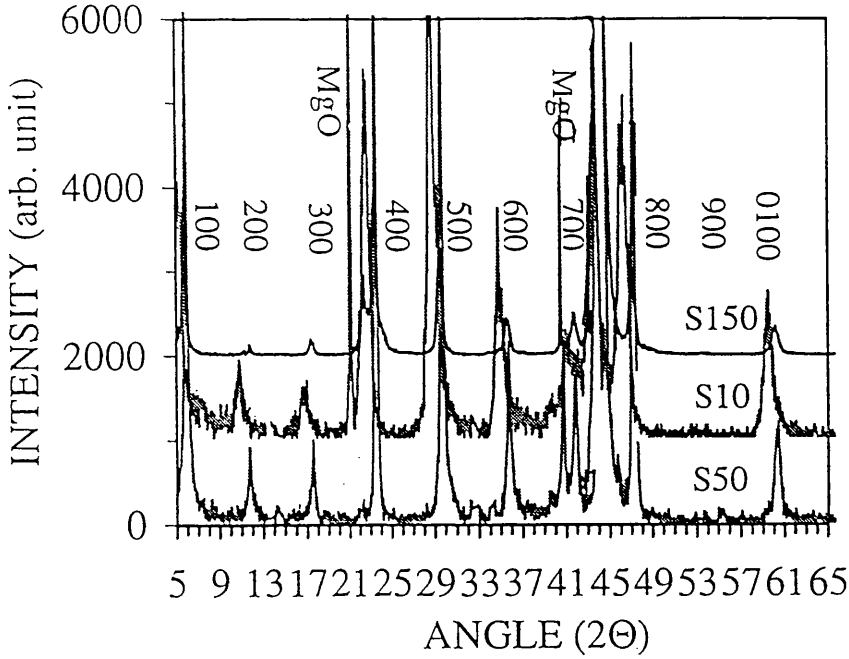

Figure 7.20. *XRD spectrum of the ultra thin layers.*

The deposition-rate was determined using 0.1μm thick film and Talystep, just after ex-situ annealing and then thicknesses of the films were estimated by the number of laser pulses used to deposit. Figure 7.21 shows the resistance versus temperature of the ultra thin-layers grown ex-situ using only 10, 50 and 150 pulses (thickness 8.5nm, 45nm, and 135nm). The film grown using 5 pulses did not superconduct and was highly resistive. The reason could be the ultra thin (~ two unit cells) layer on MgO(001) substrate that has itself only 1μm surface smoothness, can easily create disconnected terraced islands during deposition and ex-situ annealing, causing scattering effect in flowing current, and also the variation in oxygen at grain boundaries. It also includes the heating effects due to connection made for measurement using silver paint and silver wire. It was found that 10 pulses provided the best quality film with the highest transition temperatures. By increasing the number of pulses, the onset resistances, $T_c(0)$ as well as onset transition temperatures were decreased which could be because of intergrain boundaries effects and decreases in the number of short-lived pairing effect during transition. Figure 7.22 shows the resistance versus temperature response for different dc currents passing through the film deposited only by using 10 pulses.

The onset resistance was increased for higher currents (0.01mA, 0.1mA) when the same connections and condition were used during resistivity measurements, and shows thermal effects and scattering of electrons.

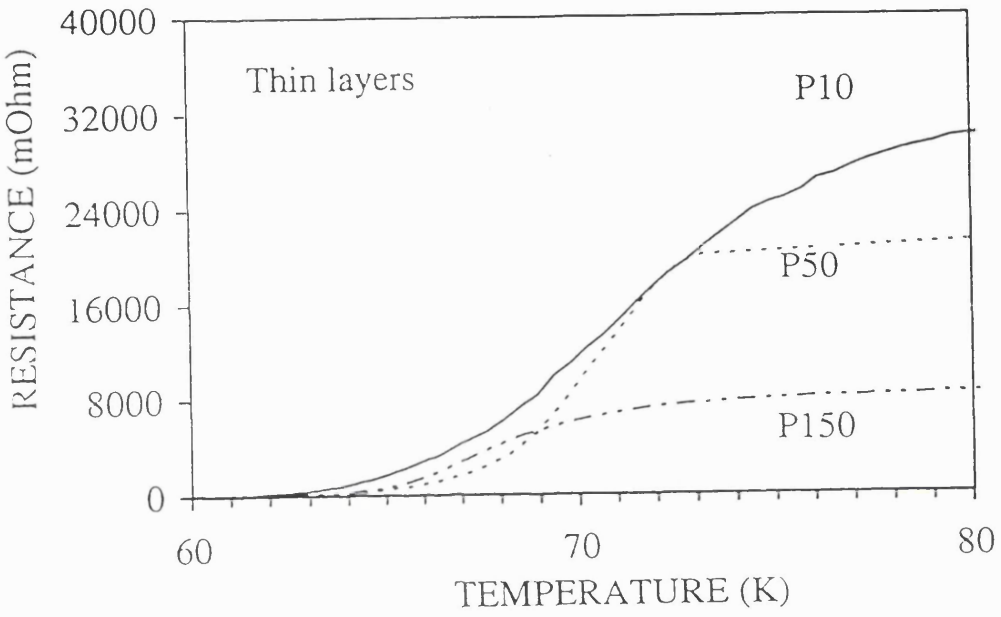

Figure 7.21. *Resistance versus temperature of the ultra thin layers i)P10=8.5nm, ii) P50=45nm and iii)P150=135nm.*

Further increase in currents, only provided the onset transition temperatures when the current reached to 0.5 or 1mA and after falling down to some resistance it remained as residual resistance. This shows that the film suffered some damages and strains after passing higher currents more than the transport critical current.

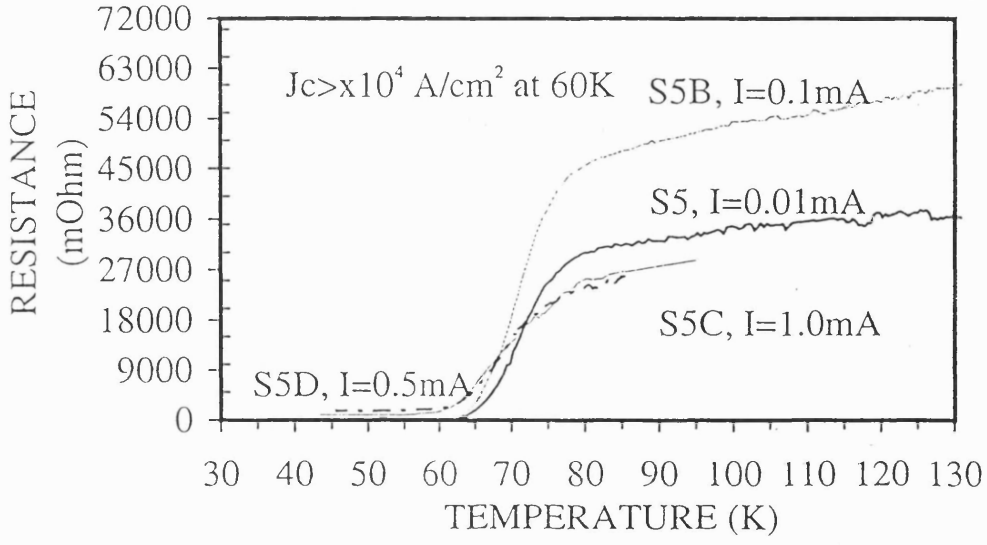

Figure 7.22. *Resistance versus temperature of the ultra thin layer (8.5nm) for various currents.*

The rounding of the traces near or above the onset transition temperatures could be attributed to their thermodynamical fluctuations which produce short-lived cooper pairs that lead an apparent increase in the conductivity as has been observed in Bi-Sr-Ca-Cu-O and Tl-Ba-Ca-Cu-O systems [13, 14, 15]. From these direct measurements, the transport critical current density, J_c, has been estimated as more than $2x10^4 A/cm^2$ for S10 thin layer.

7.7.1 Annealing temperature and microstructure

To observe the influence of annealing temperatures on morphology of Pb-Sr-(YCa)Cu-O film, several thin layers were deposited at 550°C under the same deposition conditions using Nd:YAG (532nm, 4ns) laser pulses and annealed at various temperatures (750°C, 775°C, 800°C, 825°C, and 850°C) for 20 minute in nitrogen ambient. A high resolution SEM (type HITACHI S800) equipped with a field emission gun (FEG), was used to analyse the microstructure of the thin layers.

The image in figure7.23-(a) presents the morphology of a as-deposited (unannealed) film and those in figures 7.23-b) to f) of the films annealed at various increasing temperatures. It is observed from the microstructure of the as deposited film that some small cubic crystals are present on the surface which subsequently grow when the annealing temperature is increased. At 775°C, the growth of small needle-like crystals can be observed (figure 7.23-c), together with cubic ones. Further increase in annealing temperature, results in increasing the density and dimensions of the needle-like crystals as well as increasing the dimensions and decreasing the density of the cubic crystals (fig. 7.23-d and fig.7.23-e). Annealing in nitrogen at 850°C shows a completely disappearance of needle-like crystals and the whole surface consists of only cubic crystals (fig.7.23-f). In thicker areas these cubic crystals overlap and produce a continuous film, while in the thinner areas the film is interrupted.

The number density of droplets on the surface of thin layers was found different. Their diameter and number density decrease with the gradually increasing annealing temperature. The reason seems to be due to recrystallisation of the material and

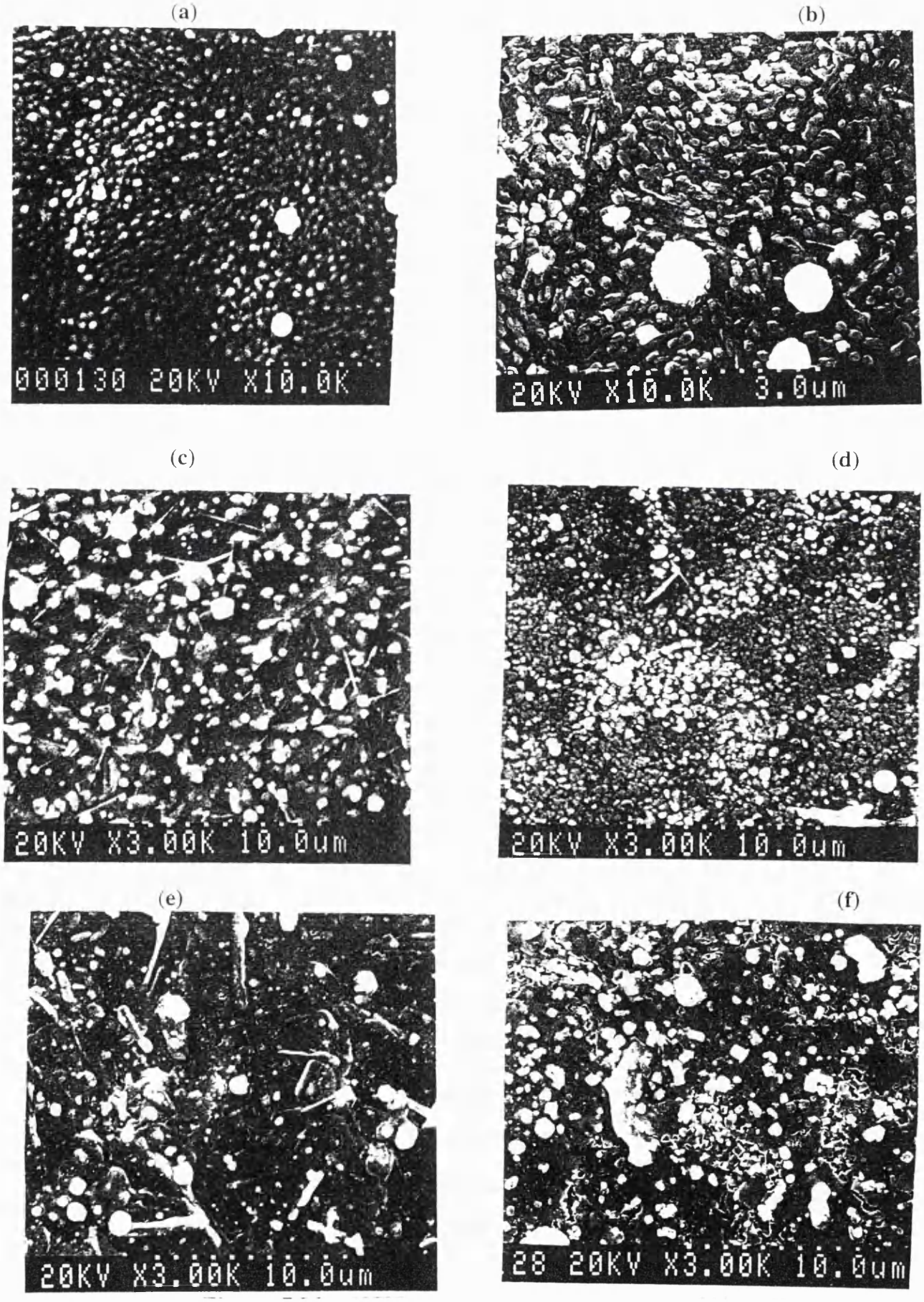

***Figures 7.23**-a)550°C b) 750°C c)775°C d)800°C e)825°C and f)850°C of the films annealed at various increasing temperatures.*

7.7.2 Effect of oxygen partial pressure

The films were deposited at room temperature so that the morphology could not affect the droplet density and smoothness. The images 7.24-a) to 7.24-f) show the morphology of the films deposited in different oxygen partial pressures under the same deposition parameters. It is observed from SEM micrographs that the number density and mean diameter of the droplets increase with the increase in oxygen partial pressure. However, the dependence is not a linear function. A maximum for the density and the mean diameter of the droplets was observed for the film deposited in 1.0mbar oxygen partial pressure. The image in figure 7.24-(g) presents the morphology of this film, at a lower magnification. Further increasing in oxygen partial pressure resulted in decreasing the number density and mean diameter of the droplets but also in a coarsening of the surface (an orange-skin-like morphology).

It is worth noticing that the morphology of the droplets was modified by the variation of oxygen partial pressure. At low pressure, their surface is smooth and the shape is almost perfectly spherical; whereas, increase in the oxygen partial pressure, produces the same orange-skin-like morphology and the shape is of an irregular sphere (see fig. 7.24-d). A similar effect of oxygen partial pressure on the smoothness of YBaCuO thin layers were also reported by Wu et al.[16]. Other researchers have also reported that the oxygen partial pressure determines the size of the plume thus determining the position of the substrate with respect to the tip of the plume at certain target-substrate distance [17] that can affect the droplet density of the layer.

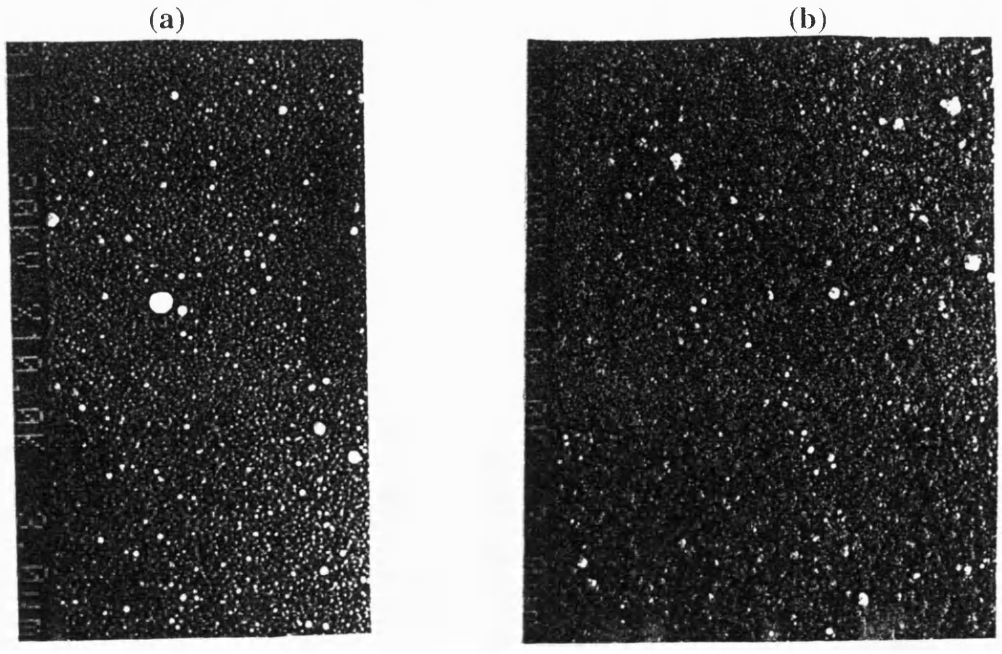

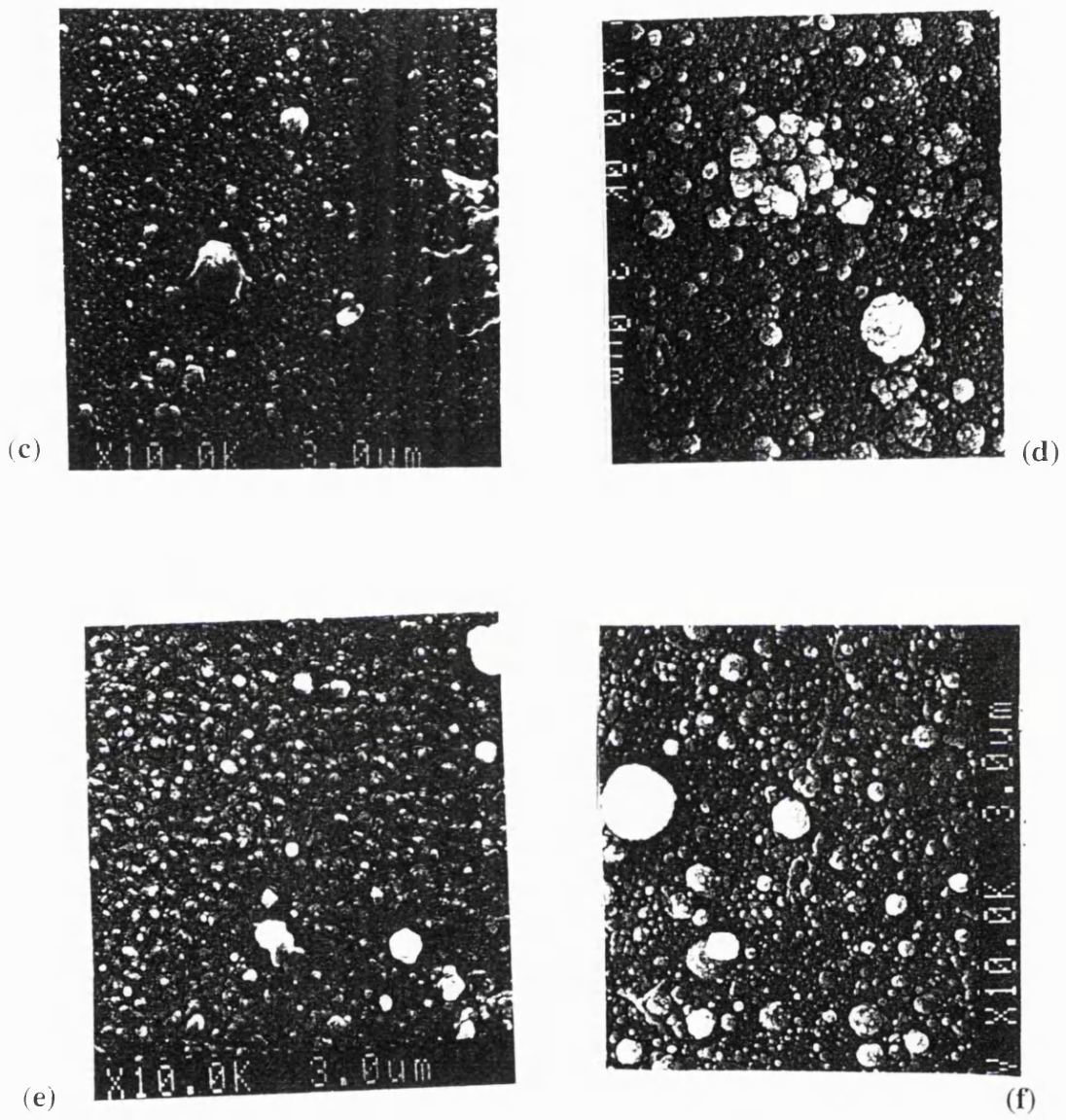

Figure 7.24 Showing the morphology of the films deposited in different oxygen partial pressures a)0.08mbar b)0.2mbar c)0.5mbar d)1.0mbar e)2.0mbar f)3.0mbar.

7.9 Multilayering growth of PSYCCO by Pb and SYCCO

For multilayering, non-superconducting $Sr_2(Y_{0.5}Ca_{0.5})Cu_3O_z$ targets (SYCCO) were prepared from $CaCO_3$, $SrCO_3$, Y_2O_3, and CuO. After grinding and mixing of the appropriate amount of carbonates and oxides, pellets of 13 mm in diameter were made at pressing force of 10 tons. The samples were heated for 10hrs in air at 900°C with intermediate grinding. The PbO powder was also pressed by the same force and die, and annealed for 10hrs at 100°C below the melting point of lead oxide. The deposition rates of both PbO and $Sr_2(Y_{0.5}Ca_{0.5})Cu_3O_z$, were calculated separately by initially growing thick films of each pellet. With this knowledge of the number of pulses required to

achieve a stoichiometric layer, a multilayered structure for $Pb_2Sr_2(Y_{0.5}Ca_{0.5})Cu_3O_z$ was prepared. The laser pulse parameters were used as described in earlier section. The deposition periods for each layer of PbO and $Sr_2(Y_{0.5}Ca_{0.5})Cu_3O_z$ were 2.5 minutes and 3.5 minutes respectively at the deposition temperature of 500°C in $4x10^{-3}$mbar oxygen pressure. Following deposition, these multilayered films were annealed in air at 864°C for three hours. At this stage, resistivity characterisation was performed to provide a mean for monitoring the effect of further annealing step. The onset transition temperature was around 83K with zero resistance at 22K. The films also exhibited a positive temperature coefficient of resistivity between room temperature to onset temperature.

The XRD pattern of the film annealed for 8 hours has shown Pb-1212 phase with some unknown impurity phases (figure 7.25). The DC resistivity of thin films grown by using the multilayering procedure and post-annealed in air at 864°C for 3, 5, and 8 hours is presented in figure 7.26. A positive temperature coefficient of resistivity before onset transition temperature can only be obtained after 5 hour annealing in air, although the temperature for zero resistance can be improved for 8 hour exhibited at 22K.

Further annealing in air did not improve the superconducting properties. It was also interesting to find out the effect of nitrogen annealing at low temperature so that any reduction or oxygen ordering could improve the superconducting transition temperature. When 5hrs air annealed film was reannealed in nitrogen at 400°C for 4-5 hrs, the superconducting transition was found in two steps whereas the zero resistance could not achieved down to 20K (figure 7.26b).

The SEM micrograph showed mainly plate-like morphology, cracks and other oriented crystals, which could be due to high temperature annealing that was performed to react the PbO with SYCCO material to form the PSYCCO layers(figure 7.27).

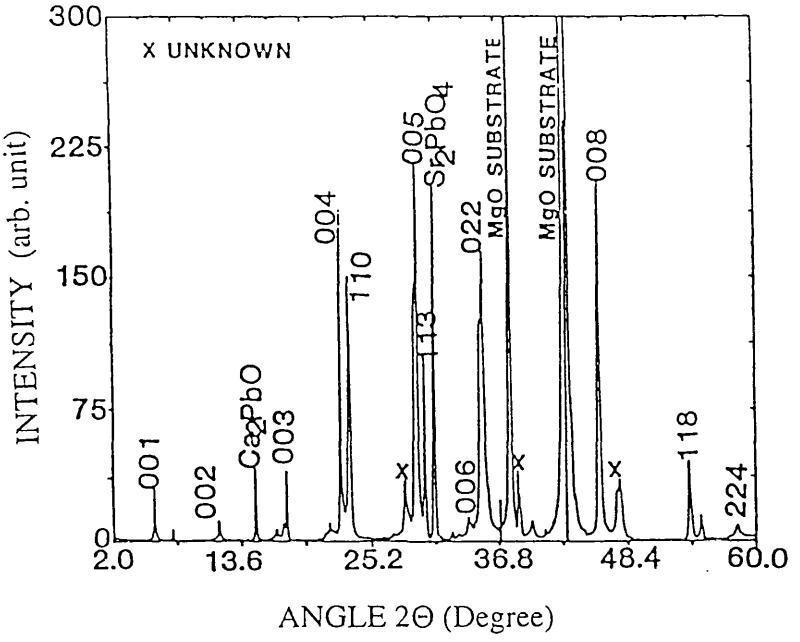

Figure 7.25. XRD pattern of the film annealed for 8 hours at 864°C after multilayering of PbO and $Sr_2(Y_{0.5}Ca_{0.5})Cu_3O_z$ shown mainly Pb-1212 phase.

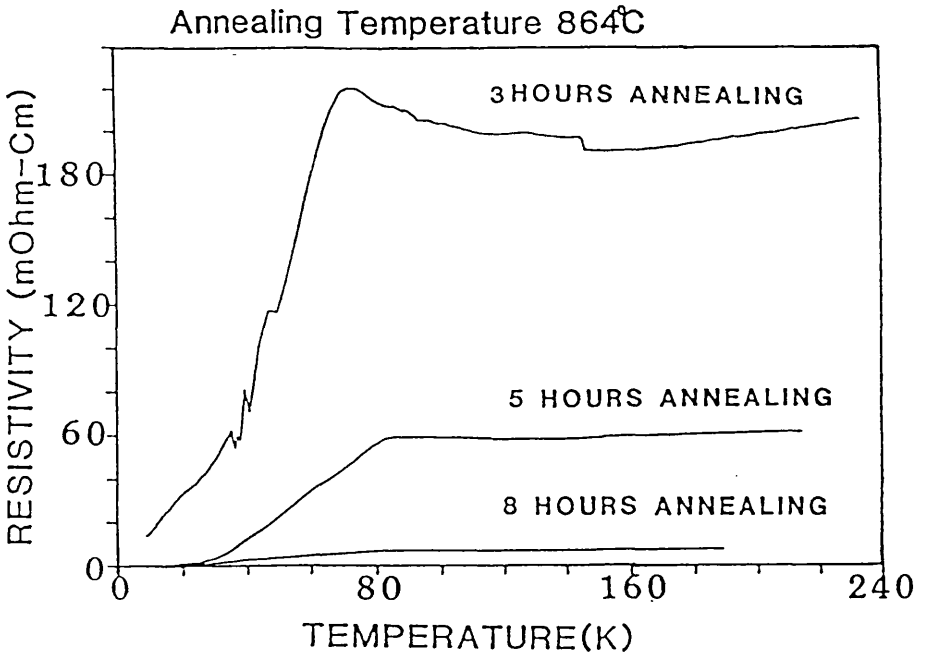

Figure 7.26. a) DC resistivity versus temperature of multilayered films.

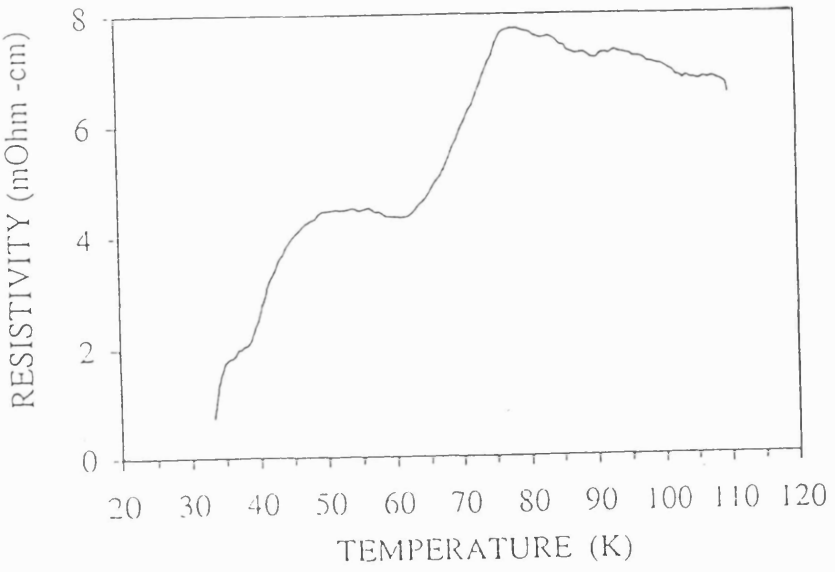

Figure 7.26. *b)* DC resistivity versus temperature of a multilayered film annealed in nitrogen ambient after air annealing.

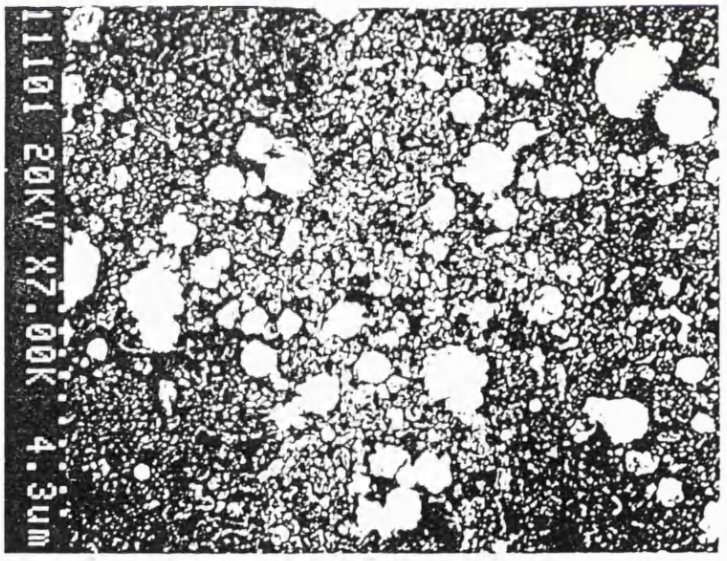

Figure 7.27. *SEM micrograph of the film annealed for 8 hrs at 864*°C.

A layer of SYCCO was also deposited on MgO (001) and annealed for 8 hrs in air at 864 °C and characterised to know the electrical property without lead. Figure 7.28 shows the DC resistance of 0.2μm $Sr_2(Y_{0.5}Ca_{0.5})Cu_3O_z$ thin layer. The resistance increases gradually to 75K, then it becomes constant till 40K where it shoots-up to the order of 10^6ohms. This behaviour could be explained in terms of charge carrier density (holes) in this material. Initially, the charge carrier density is low enough that let the layer to behave as semiconducting material, but as the temperature goes down to 75K it achieves

a nearly constant value to 40K where a decrease in carrier density is not high enough with the decrease in temperature. Perhaps the material has the point where it can be converted into superconductor if certain amounts of holes are induced through some doping. It is the onset transition point of Pb-2213 phase where the material becomes superconductor when lead is added. At 40K the charge carriers are blocked and the layer transforms into nearly insulating phase.

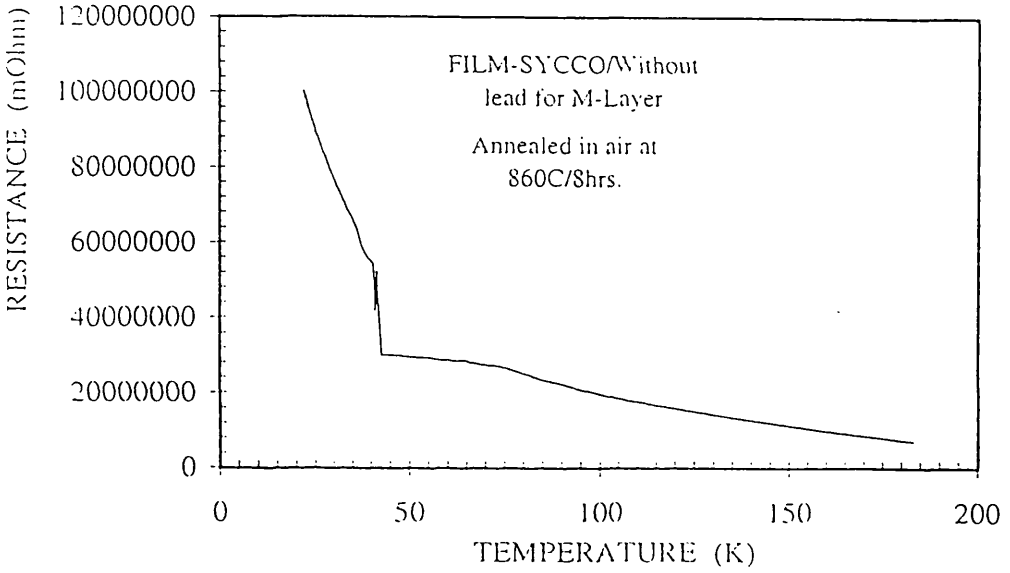

Figure 7.28. .Resistance versus temperature of the $Sr_2(Y_{0.5}Ca_{0.5})Cu_3O_z$ film grown after post annealing in air.

Multilayering from superconducting $Pb_2Sr_2(Y_{0.5}Ca_{0.5})Cu_3O_z$ and insulating PbO targets was also performed by using the same deposition parameters and layering scheme to observe the effect on resistive transition temperature. When the film was annealed in air for the range of 2 to 8 hours at 864°C, it did not show even semiconducting behaviour. The layers remained insulating unless it was annealed in N_2 ambient. A multilayered thin $Pb_2Sr_2(Y_{0.5}Ca_{0.5})Cu_3O_{8+\delta}$ film grown and annealed at 800°C for 15 minutes in nitrogen has shown 70K onset transition temperature and $T_{c,\ zero}$ of 35K. It demonstrates that the Pb-2213 phase film cannot superconduct when heat treatment is performed in air due to oxidation of the PbO-Cu-PbO block that stops the required charge transfer to CuO_2 layers, necessary for Pb-2213 phase cuprate superconductor. After nitrogen annealing, due to reduction the material becomes superconducting (figure 7.29).

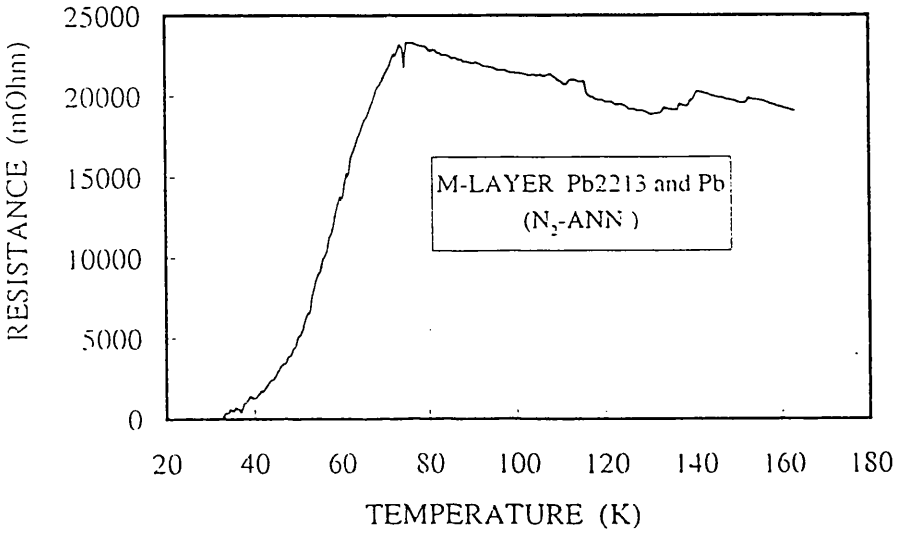

Figure 7.29. Resistance versus temperature of a multi-layered $Pb_2Sr_2(Y_{0.5}Ca_{0.5})Cu_3O_z$ film grown after annealing in air and nitrogen.

7.9 Multilayering growth of Bi-Sr-Ca-Cu-O/Pb-Sr-(YCa)-Cu-O/MgO system

The $Bi_2Sr_2Ca_{n-1}Cu_nO_{4n+2+\delta}$ system has a number of superconducting phases which can be differentiated by the number of CuO_2 sheets in the crystal structure. The three main superconducting phases of this system are $Bi_2Sr_2Cu_1O_{6+\delta}$, $Bi_2Sr_2CaCu_2O_{8+\delta}$, and $Bi_2Sr_2Ca_2Cu_3O_{10+\delta}$ [18, 19, 20] usually known as Bi-2201, Bi-2212 and Bi-2223 respectively. These phases have superconducting transition temperatures of 20K, 80K and 110K for Bi-2201, Bi-2212 and Bi-2223 materials respectively. Since the Bi-2212 and Bi-2223 phases superconduct above the boiling point of nitrogen and interesting to grow multilayers for device purpose.

It is desirable for good quality multilayering to grow smooth surfaces for the similar chemical constituents for sharp interfaces between layers to minimise interdiffusion and chemical reactions between layers. A large lattice misfit is also considered as a disadvantage to grow multilayered structure that could cause dislocations. The orthorhombic unit cell of the $Pb_2Sr_2(Y_{0.6}Ca_{0.4})Cu_3O_{8+\delta}$ phase with [3] lattice parameters a=5.383(1)Å, b=5.423(1)Å, c=15.765 (2)Å. and the lattice parameters of Bi-2212 or Bi-2223 phases with a=5.401(2)Å, b=5.401(2)Å, c=30.83(2)Å [21] and a=5.4029Å, b=5.4154(2)Å, c=37.074(2)Å respectively have reasonable matching [22,

23]. The Bi-2223 phase is an interesting family member due to its highest superconducting transition temperature among the other phases but the growth of single phase thin layers are difficult due to intergrowth of lower T_c phases, loss of Bi at higher temperature and impurity formation such as $CaCuO_3$, whereas the Bi-2212 phase is more thermodynamically stable than the Bi-2223 phase and has not any narrow window of synthesising temperature. From x-ray microanalysis of the lead doped Bi-2212 and Bi-2223 phases, it is known that a sufficient amount of lead incorporates into the crystal structure, and can substitute Sr and Ca sites as well as Bi sites in both phases [24]. Therefore, the systems having nearly the same chemical constituents such as PbSr(YCa)CuO and BiSrCaCuO systems can not make much difference due to interdiffusion of volatile lead.

Usually, both phases of the Bi-system are synthesised for long durations at elevated temperatures (>850°C). Therefore, the survival of Pb-2213 layer for the case of ex-situ film growth conditions of Bi-phases for long duration annealing above 850°C is a basic requirement to form multilayering structures such as Bi-2212/Pb-2213/Bi-2212, where Pb-2213 phase can work as insulating or semiconducting layer, depending upon oxidation and reduction level for superconducting (S)/Insulating (I)/superconducting, (SIS) or S/semiconducting (sem.)/S layers. To check the possibility of whether normal growing conditions for both systems are workable or not, the following set of experiments was performed.

Initially, to form a multilayered structure, a $Pb_{2.5}Sr_2(Y_{0.6}Ca_{0.4})Cu_3O_{8+\delta}$ phase target was ablated for 2 minutes using Nd:YAG laser (532nm, 4ns, 10Hz) and the normal deposition and ex-situ annealing conditions were employed to grow Pb-2213 phase thin layers on MgO (001) single crystal substrate. To deposit thin layer of Bi-2212 phase film on Pb-2213/MgO(001) heated substrate at 350°C under an oxygen pressure of $3x10^{-3}$mbar, a synthesised target of $(Bi_{1.85}Sb_{0.15})Sr_2CaCu_2O_y$ was ablated for 10 minutes using the same laser parameters. The low deposition temperature was used only to minimise the loss of Bi during deposition. After ex-situ annealing of multilayered structure at 865°C in air for different period, normal electrical characterisation was performed to observe the superconducting transition temperature. Figure 7.30 is presenting the resistive behaviour of multilayered structure of

(BiSb)SrCaCuO/PbSr(YCa)CuO/MgO, annealed in air at 865°C for different periods. It could be observed that in each case onset resistive transition starts at 82K but after a little drop in the resistance, the resistances adopt a constant value up to 40K, when the films were annealed either for 200 minutes or 700 minutes. The zero resistance can only be obtained when the film was annealed for 500 minute. However, a slight curvature from 78K to 30K was found due to multiphase growth and fast oxidising ability of Sb and Pb that suppresses superconducting properties.

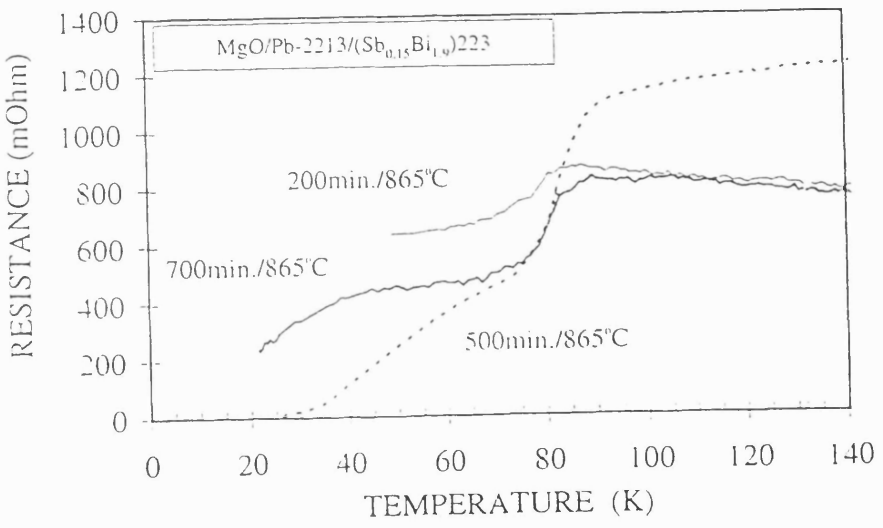

Figure 7.30. *Resistance versus temperature of a multi-layered* (BiSb)SrCaCuO/PbSr(YCa)CuO/MgO *film grown after annealing in air.*

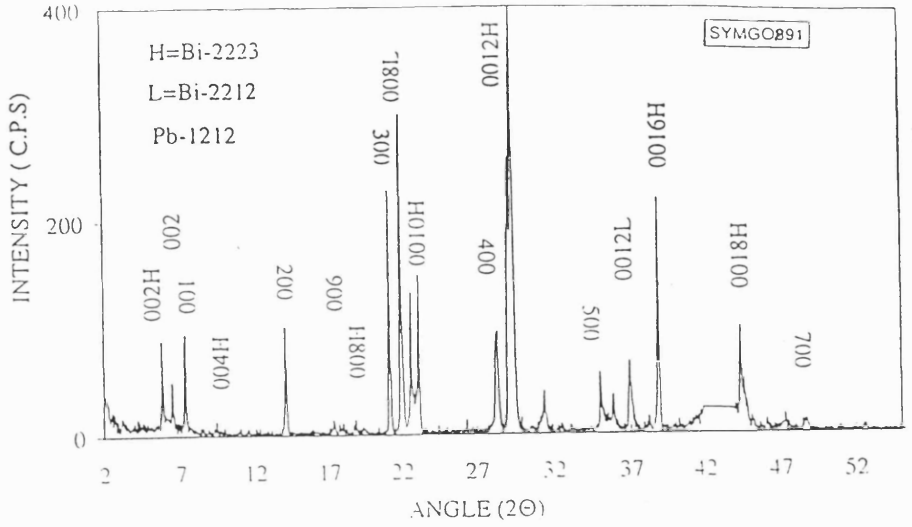

Figure 7.31. XRD pattern of a Bi-Sr-Ca-Cu-O/Pb-Sr-(YCa)-Cu-O/MgO multilayered film.

7.10 Deposition of Pb-2213 phase on Si(111) substrate

The quality of the films deposited by PLD, either in-situ or ex-situ, depends upon many parameters, i.e., the deposition geometry, environment, temperature, post-annealing conditions, as well as any substrate properties such as chemical stability, minimum mismatch of lattice constants and thermal expansion coefficient. Single-crystal substrates such as MgO, $SrTiO_3$ and $LaAlO_3$ generally enable superior quality films to be grown, but these are relatively expensive and difficult to fabricate in large areas, thereby possibly limiting their potential use in device applications. The formation of superconducting layers on relatively cheap and less restricted substrate size such as alumina or silicon is desirous. The effort of growing $YBa_2Cu_3O_{7-\delta}$ films on Si substrate with native oxide layer (SiO_2) using high-temperature annealing or low-temperature (600°C) in-situ processing resulted $T_{c,\ zero}$ of 45→50K, with film thickness of 0.5μm [25]. However, an intermediate buffer layer between the superconducting film and the substrate is generally necessary to avoid the problem of chemical interdiffusion during high temperature annealing processes.

A few Pb-2213 phase films were deposited directly on Si(111) substrate without removing native oxide while the substrate was separated by 3.5cm perpendicular distance from the target. A melt-textured $Pb_{2.5}Sr_2(Y_{0.5}Ca_{0.5})Cu_3O_{8+\delta}$ pellet was ablated using Nd:YAG (532nm, 4ns) laser fluence of 5J/cm^2 at 10Hz for 5 minutes. The substrate temperature was kept at 450°C. The temperature was slowly raised to 750°C then left for 20 minutes in flowing pure nitrogen, cooled down to 300°C at the rate of 6°C/minute then power was shut off. The EDX, XRD and resistivity measurement were performed. The EDX analysis has shown $Pb_{2.1}Sr_{1.9}(Y_{0.5}Ca_{0.45})Cu_3O_{8+\delta}$ stoichiometry of 0.5μm thin film that has an onset superconducting transition temperature of 75K and $T_{c,\ zero}$ of 40K (figure 7.32). This is the best result obtained for Pb-2213 phase thin layer on silicon substrate. The XRD characterisation has shown c-axis oriented Pb-2213 film (figure 7.33) with lattice constant c=15.65Å. It becomes more difficult to control the oxygen stoichiometry in PSCCO films when the Si substrates are used due to large difference in thermal expansion coefficient of both materials. The films cannot be quenched from higher temperature to keep in reduced condition and avoid possible stresses or cracks due to large differences in thermal coefficients of expansion of the substrate and films.

Therefore, it is not possible to quench from high temperature and keep the layers in reduced conditions.

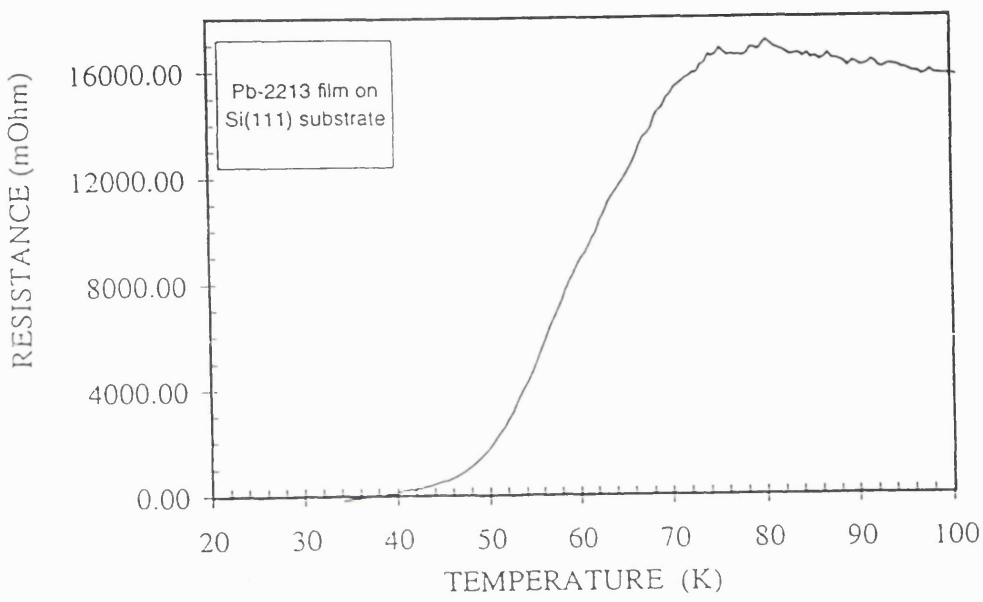

Figure 7.32. Resistance versus temperature of a film grown on Si(111).

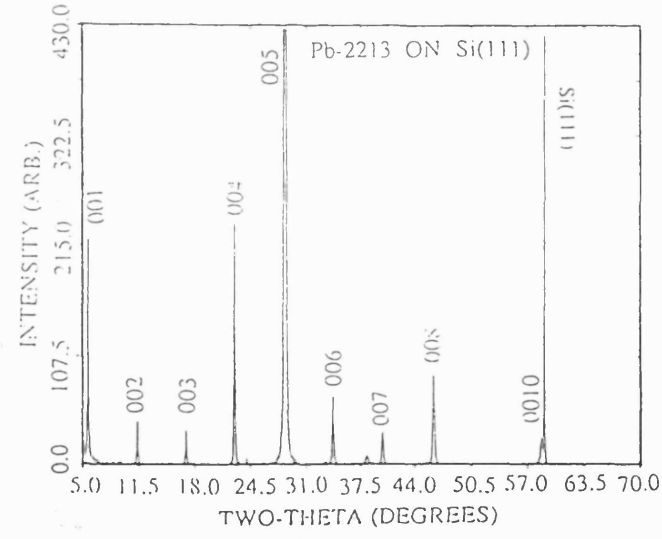

*Figure 7.33. XRD pattern of a 0.5*μm thin *layer on Si(111) substrate.*

7.11.1 Water effects on thin Pb-2213 layer

Most of the applications of HTSC materials require protection against environmental degradation both with respect to water vapours, CO_2, liquid water (produced by condensation on warm-up and cooling cycle from cryogenic conditions) and intense magnetic field or radiation damage. Increasing environmental stability can involve

improving the processing methods to eliminate pores, cracks and other macroscopic defects such as leachable impurity phases created during ceramic sintering. In case of films, protective coatings are required for the applications of most popular Y-Ba-Cu-O and (BiPb)-Sr-Ca-Cu-O materials due to sensitivity with the humid atmosphere. Specially, humidity can alter or degrade the superconducting properties of HTSC cuprates due to absorption, reaction with water or material-dissolving ability of the water. Several authors [26, 27] demonstrated that the water can affect the Y-Ba-Cu-O system when it is kept only for 16 hours and decomposes into CuO, $BaCuO_3$, and Y_2CuO_5 characterised by XRD pattern, and superconductivity disappears. Similar results have also been shown by Yasuhiro et al. [28] that the superconducting films of $Tl_2Ba_2CaCu_2O_8$ (T_c~100K) or $EuBa_2Cu_3O_7$ were degraded only within 18 hours when kept in 80% humid environment at 35°C. They shown that some parts of the film were dissolved and their colour appeared to be transparent brown rather than black, and some strain appeared on the surface of $EuBa_2Cu_3O_7$ films. The degradation is also possible due to reaction of Sr and Ca with water to form carbonates or hydroxide if it is present in between the grain or on the upper surface that is more close to water.

7.11.2 Experimental, results and discussion

Ex-situ annealed thin $Pb_2Sr_{1.9}(Y_{0.5}Ca_{0.45})Cu_3O_{8+\delta}$ layers were grown on MgO (001) substrate after partial annealing in nitrogen (for 2 hour) at 675°C and characterised by XRD then broken into two pieces, one was characterised for resistivity measurement and another was kept inside the deionised water at 30°C for 36 hrs. After taking out the sample from water, XRD was performed and then characterised for resistivity measurement. From XRD characterisation (fig.7.34), for the first time it is demonstrated that the thin $Pb_2Sr_{1.9}(Y_{0.5}Ca_{0.45})Cu_3O_{8+\delta}$ layers do not show any decomposition of material. However, a slight intensity difference has been observed that is due to different experimental set up used for XRD characterisation before and after keeping in water.
The dc resistivity versus temperature has shown a very small deterioration (figure 7.35). The onset transition temperature remained same but the onset resistance increased, whereas the zero resistance was achieved slightly (1K) at higher temperature.

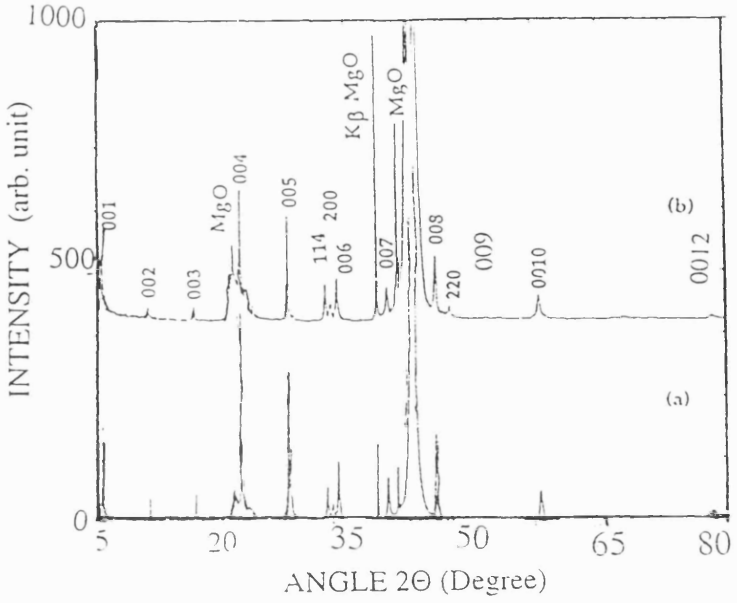

Figure7.34. *XRD pattern of the film a) before water effect (F2N)* b) after 36 hrs at 30 *°C in deionised water (F2NW).*

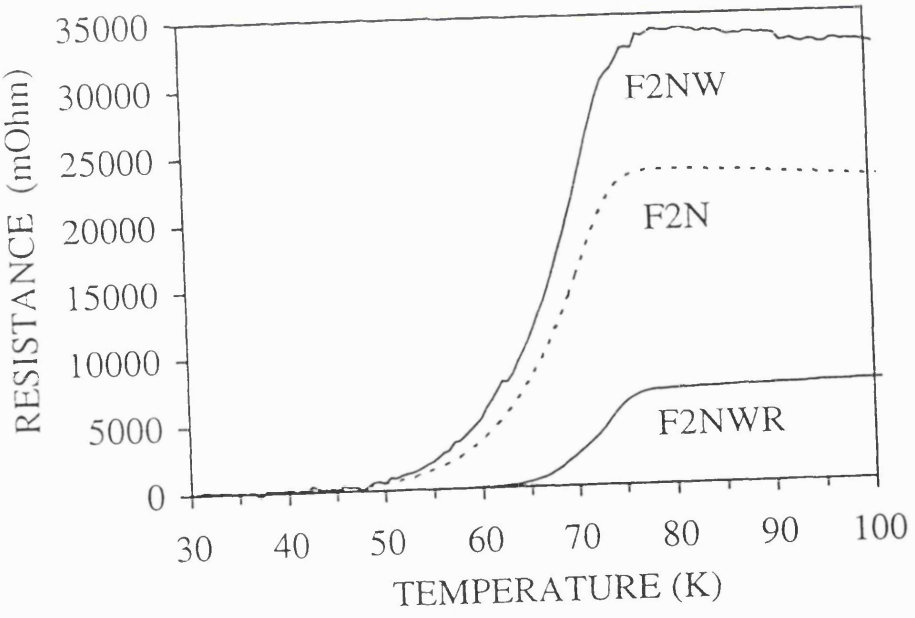

Figure 7. 35. *Resistance versus temperature of a film grown after i) 2 hrs/675 °C in N_2 (F2N)* ii) 36 hrs/30 *°C in deionised water (F2NW) iii) 2 hrs/675 °C in N_2 after water effect (F2NWR).*

These results suggest that the water is not as effective as in other superconducting materials. A change in resistance could be due to water absorption and simply creation of strain in the layers. After water effect when the layer was reannealed in flowing nitrogen for two hours at 675°C, the film showed better transition temperature due to

further better reduction and texturing. Figure 7.36-a) and b) is showing SEM micrographs of the film 'F2N' and 'F2NW' before and after water treatment

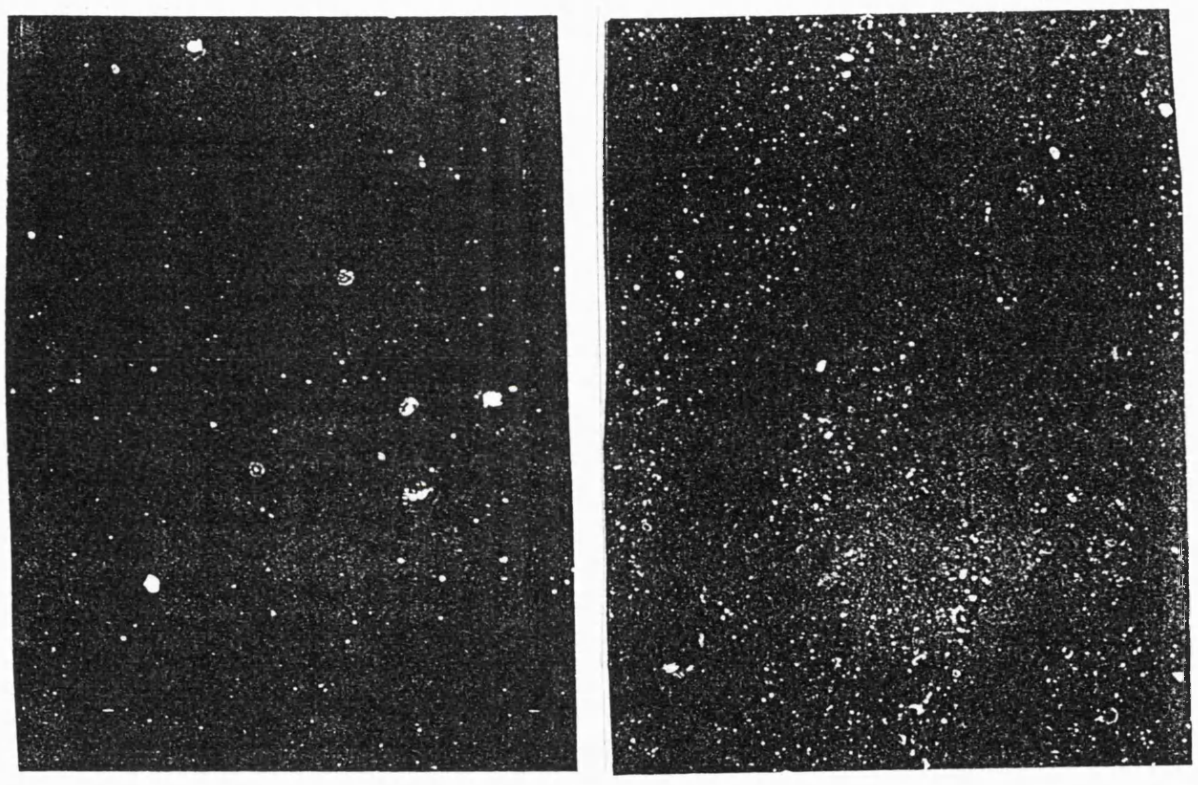

(a) (b)

Figure 7.36. SEM micrograph of the nearly pores free film a) before water effect (F2N) b) after water effect (F2NW).

Figure 7.37 shows resistance versus temperature of fully reduced film (5hrs/ 675°C, F5N) before water effect and after water effect (F5NW), and later reduced in nitrogen , but has large number of pores as showed in SEM pictures (figure 7.38). It is clear from the figure that onset resistance has increased but onset transition temperature remained same. In this experiment the zero resistance could not achieved down to 25K. After 2 hours annealing at 675°C in N_2 the onset resistance is brought down but the zero resistance could not be achieved, perhaps due to excessive reduction. To observe the environmental corrosion a fully annealed thin layer (S30) was left open to atmosphere for one year. The figure 7.39 is showing resistance versus temperature of film after one

year that also exhibited higher onset resistance, same onset transition temperature but zero resistance could not achieved, but a large tail of resistance was seen around $T_c(0)$. The reason could be the trapped water vapours inside the pores or reaction with elements present in the film.

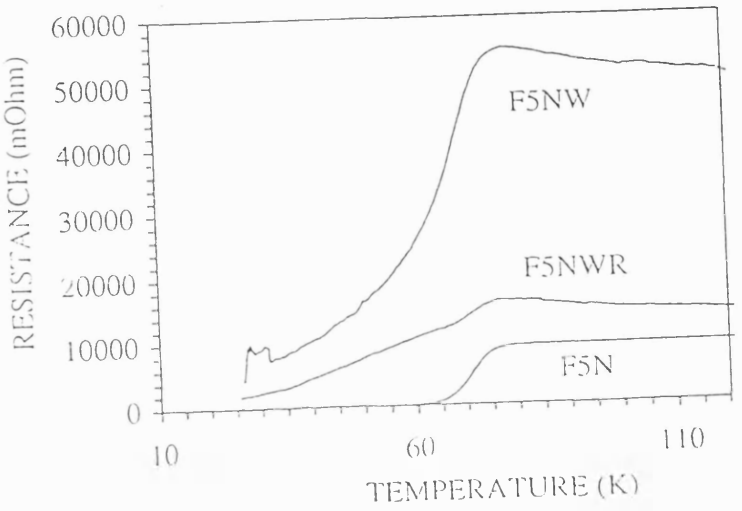

Figure 7.37. Resistance versus temperature of a porous film grown after i) 5 hrs at 675°C in N_2 (F5N) ii) 36 hrs at 30°C in deionised water (F5NW) iii) 2 hrs at 675°C in N_2 after water effect (F5NWR).

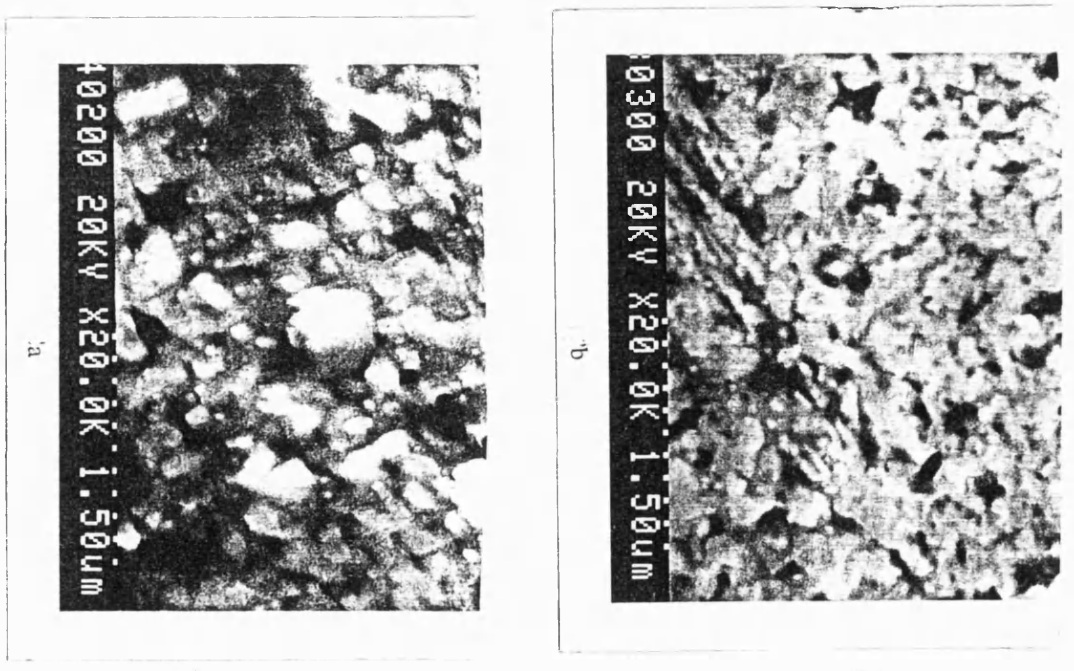

(a) **(b)**

Figure 7.38. *SEM micrographs of the porous films before water effect a) F5N after water effect b) F5NW*

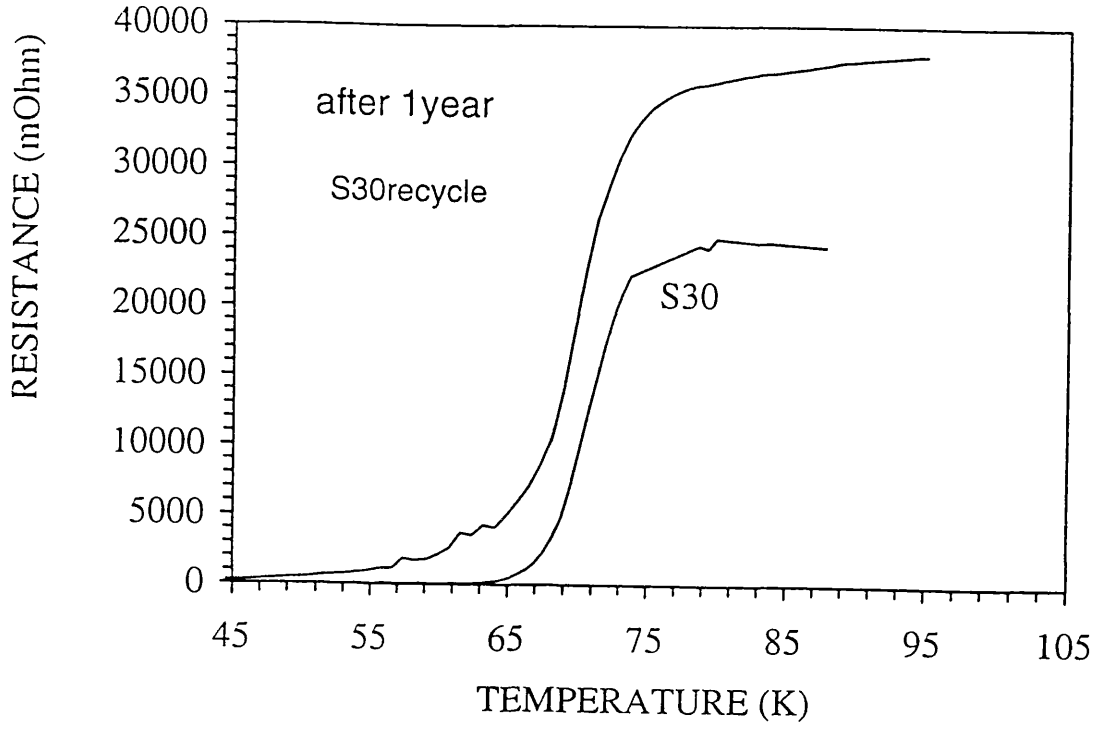

Figure 7.39. Resistance versus temperature of a porous film grown after i) 4 hrs at 675°C in N_2 (S30) ii) after one year in open atmosphere (S30 recycle).

7.12 Summary

The main objective of this research was to optimise growth conditions of Pb-2213 phase superconductor using PLD technique. In-situ and ex-situ annealing methods have been applied to obtain good quality lead-based superconducting thin layers. A set of experimental conditions has been demonstrated for the first time to the growth of Pb-2213 thin layers in nitrogen ambient. For ex-situ synthesis of the Pb-2213 phase thin layers, deposition was performed on MgO (100) single crystal substrate at low temperature (300-500°C) in flowing oxygen ambient ($4x10^{-3}$mbar) using Nd:YAG (532nm, 4ns, 10Hz, 5J/cm^2) laser. The best result obtained was for the film annealed for 4hours at 675°C in N_2-ambient and quenched to room temperature. The films annealed in nitrogen at (675 ±10)°C for a fixed annealing period of four hours have shown to be optimum ($T_{c,onset}$~77K, $T_{c,zero}$~63K). XRD scan indicates that the films annealed for two hours are mostly c-axis oriented and perpendicular to substrate plane. The (*00l*) peaks yield a lattice constant of 15.77Å.

In-situ growth of Pb-2213 phase material is a difficult task due to lead losses at high temperatures and controlling oxygen stoichiometry to keep CuO_{δ} layer in reduced condition. An unusual technique has been demonstrated to produce c-axis oriented superconducting Pb-2213 phase thin layer, by starting deposition at low temperature and rapidly increasing substrate temperature from 300°C to 650°C within 10 minute ablation period in low pressure oxygen ambient. Low temperature deposition in oxygen ambient and high temperature in-situ annealing in nitrogen ambient only for 35 minute can enhance the superconducting transition temperature from 65 to 75K. Deposition of lead based material in inert atmosphere using PLD technique is not possible as claimed by Adachi et al. [14] using rf-magnetron sputtering and non-stoichiometric target.

A set of deposition was performed to observe the effect of various amounts of lead on the superconducting transition temperature. The superconducting transition temperatures gradually increase from 45K to 64K for Pb=4 to Pb=2.5 values, and then come down for Pb=2 to 2.2 values for the films grown using non-stoichiometric $Pb_{2.5}Sr_2(Y_{0.5}Ca_{0.5})Cu_3O_z$ target.

A pellet of a mixture of $Pb_3Sr_2(Y_{0.5}Ca_{0.5})Cu_3O_z$ composition without reacting elemental components was ablated using a $0.5J/cm^2$ (at 10Hz for 3minutes). It is observed that the films were quite thick and even weighable (0.0065mgram). The composition of films was non-stoichiometric even deposited at low temperature (300°C). The obtained XRD pattern shows some impurity phases and (*00l*) orientation. It is found that c-axis lattice constant is smaller (15.6412Å) than usual value (15.821Å) and could be due to non-stoichiometric value of Sr. This experiment has demonstrated that the Pb-2213 phase film can be grown after ex-situ annealing and using unreacted, pressed-powder target, but the morphology becomes very rough due to evaporation and collection of micron size particles.

The effects on transition temperature of $Pb_2Sr_2(Y_{0.5}Ca_{0.5})Cu_3O_z$ material as an ultra thin layer grown on MgO (001) single crystal substrate has also been presented. The layer of 8.5nm thick just grown by using only 10 pulses, provided a best quality film with highest transition temperatures and reasonably high transport critical current ($J_c>10^4A/cm^2$ at 60K).

It is also demonstrated that the synthesis of Pb-1212 phase material by multilayering of non-superconducting materials (PbO and $Sr_2Y_{0.5}Ca_{0.5}Cu_3O_z$) and annealing at high temperature in air is also possible. Synthesis of Pb-2213 phase thin layer using multilayering of superconducting $Pb_2Sr_2Y_{0.5}Ca_{0.5}Cu_3O_z$ and PbO does not improve superconducting properties.

The low cost Si(111) substrate can also be used to grow Pb-2213 phase thin layer instead of MgO (001) substrate, but the same annealing period at certain temperature and slow cooling suppresses superconducting transition temperature. Whereas quenching of Si-substrate is not possible due to thermal shock as it is applicable in case of MgO substrate.

Multilayered structure of Bi-Sr-Ca-Cu-O/Pb-Sr-(YCa)-Cu-O/MgO intermixes with one another after a long period and high temperature annealing in air. It needs a different scheme to obtain good quality multilayers of superconducting BSCCO and insulating PSYCCO material.

The influence of annealing temperatures on the morphology of Pb-2213 phase films deposited at 550°C, under the same deposition conditions using Nd:YAG (532nm, 4ns) has been shown. The number density of droplets on the surface of thin layers was found different. The diameter and number densities of droplets decrease with the gradual increase in annealing temperature. The reason seems to be due to recrystallisation of the material and disintegration of the droplets during the annealing treatment. The morphology of the droplets can also be modified by the variation of oxygen partial pressure. At low pressure, their surface is smooth and shape is spherical whereas increasing the oxygen partial pressure, produces the same orange-skin-like morphology and shape is an irregular sphere.

Surface smoothness is also desirable for multilayering of different materials. To reduce the number density of droplets of during processing of lead cuprates, one possible mode can be adopted by depositing thin layer in low oxygen pressure, and using high temperature, short term annealing (>775°C for 20 to 30 minute) in nitrogen ambient to disintegrate most of the droplets.

It is demonstrated that the envoirnmental and water effects can degrade the superconducting properties but the PbSrYCaCuO material is not as serious as other HTSC materials. If the thin layer is not porous and kept inside the deionised water around 30°C, the Pb-2213 phase thin layer does not exhibit any change in its chemical or superconducting properties.

References

[1] R.J.Cava, B.Batlog, J.J.Krajewski, L.W.Rupp, L.F.Schneemeyer, T.Siegrist, R.B.vanDover, P.Marsh, W.F.Peck, Jr., P.K.Gallagher, S.H.Glarum, J.H.Marshall, R.C.Farrow, J.C.Waszczak, R.Hull, and P.Trevor, Nature, 336, 211 (1988).

[2] M.Masuzawa, T.Noji, Y.Koike and Y.Saito, Jpn.J.Appl.Phys., 28, L1524 (1989).

[3] J.S.Xue, M.Reedyk, Y.P.Lin, C.V.Stager and J.E.Greendan, Physica C, 166, 29 (1990).

[4] R.A.Hughes, Y.Lu, T.Timusk and J.S.Preston, Appl.Phys.Lett., 58, 762 (1991).

[5] S.Ikegawa, Y.Motoi and T.Miura, Physica C, 229, 280 (1994).

[6] H.Adachi, S.Adachi, Y.Ichikawa, K.Setsune and K.Wasa, Jpn. J. Appl. Phys., 30, L39 (1991).

[7] R.A.Hughes, Y.Lu, T.Timusk and J.S.Preston, Appl.Phys.Lett., 59, 2597 (1991).

[8] S.H.H.Naqvi, F.Beech and I.W.Boyd, Appl. Surf. Sci. 54, 166 (1992).

[9] D.H.Lowndes, D.P.Norton and J.D.Budai, Phys. Rev. Lett. 65, 1160 (1990).

[10] D.P.Norton, D.H.Lowndes, S.T.Pennycook, and J.P.Budai, Phys. Rev. Lett. 67, 1359 (1991).

[11] T.Terashima, K.Shimura, Y.Bando, Y.Matsuda, A.Fujiyama, and S.Komiyama, Phys. Rev. Lett. 67, 1362 (1991).

[12] I.N.Chan, D.C.Vier, O.Nakamura, J.Hasen, J.Guimpel, S.Schultz, and I.K.Schuller, Bull. Am. Phys. Soc. 37, 481 (1992).

[13] G.Weigang and K.Winzer, Z.Phys.B77, 11 (1989).

[14] P.W.Anderson and Z.Zou, Phys.Rev. Lett. 60, 132 (1988).

[15] V.P.N.Padmanaban and K.Shahi, Physica C 172, 427 (1990).

[16] K.H.Wu, J.Y.Juang, C.L.Lee, T.C.Lai, T.M.Uen, Y.S.Gou, S.L.Tu, S.L.Jang, and S.E.Hsu, Physica C, 195, 241 (1992).

[17] R.Pinto, S.P.Pai, C.P.D'Souza, L.C.Gupta, R.Vijayaraghavan, D.Kumar and M.Sharon, Physica C, 196, 264 (1992).

[18] C.Michel, M.Hervieu, M.M.Borel, A.Grandin, F.Deslandes, J.Provost, and B.Raveau, Z.Phys.B 68, 421 (1987).

[19] M.A.Subramanian, C.C.Torardi, J.C.Calabrese, J.Gopalkrishnan, K.J.Morrissey, T.R.Askew, R.B.Flippen, U.chowdhry, and A.W.Sleight, Science 239, 1015 (1988).

[20] H.Maeda, Y.Tanaka, M.Fukutomi, and T.Asano, Jpn. J. Phys. 27, L209 (1988).

[21] P.Bordet, J.J.Capponi, C.Chaillot, J.Chenavas, A.W.Hewat, J.L.Hodeau, M.Marezio, J.L.Tholence, D.Tranqui, Physica C, 143-55, 623 (1988)

[22] K.Kijima, H.Endo, J.Tsuchiya, A.Sumiyama, M.Mi Zuno, and Y.Ouri, Jpn.J.Appl.Phys. 28, L787 (1989).

[23] G.Miehi, T.Vogt, H.Fuess, and M.Wilhelm, Physica C 171, 339 (1990).

[24] O.Eibi, Physica C 168, 215 (1990).

[25] T.Venkatesan, E.W.Chase, X.D.Wu, A.Inam, C.C.Chang and F.K.Shokoohi, Appl. Phys. Lett. 53, 243 (1988).

[26] M.F.Yan and R.L.Barns, Appl. Phys. Lett. 51, 532 (1987).

[27] M.F.Yan, R.L.Barns, H.M.O'Bryan Jr., P.K.Gallagher, R.C.Sherwood, and S.Jin, Appl. Phys.Lett. 51, 532 (1987).

[28] Y.Nagai, N.Suzuki, M.Sato and T.Konaka, Jpn. J. Appl. Phys. 30, 2751 (1991).

Chapter 8

Smoothness and large area deposition

Pulsed laser deposition has been facing mainly two serious problems, one is thickness and compositional uniformity over a large area, and another is large particles (even greater than 1μm in size) commonly known as droplet, causing roughness on the surface of thin layer. This chapter addresses these two main problems, and attempts are to solve them using a simple mode of deposition. An unusual deposition geometry is presented.

8.1.1 Problem of droplet emission

The emission of microscopic particles from the target is a very common phenomenon in laser-induced ablation or evaporation. The presence of particles in deposition hinders the use of PLD in the electronic industry, because any multilayered quality device fabrication needs to control compositional uniformity and surface smoothness [1, 2]. The sizes of particles vary from submicron to several micrometers, and usually are found in spherical shapes. The droplet size can be enlarged by joining one another within the plasma or on the substrate. For example, a picture given below is presenting a possible attachment of two droplets (fig. 8.1) produced during PLD of lead-based material, using 4J/cm^2 fluence of 532nm laser pulses in 0.5mbar oxygen partial pressure. The deposited number densities of these solid particulates are considered as dependent on laser fluence, wave length, pulse duration and shape, material properties, target inhomogeneities, gas pressure that dilutes the ablating material and affects the size of the plume, and the target to substrate distance [3, 4]. Following are the commonly suggested reasons for droplet formation:

i) The rapid expansion of trapped gas bubbles beneath the surface during laser-induced heating (can be avoided by out gassing the target in vacuum prior to deposition).

ii) Due to superheating of a subsurface layer before the surface itself has reached the vapour phase.

iii) The roughness and texturing of target surface increases the density of droplets. The removal of top layers from the virgin polished target converts it into rough surface that has

pits, craters and loosely attached particles. Weakly attached particles disintegrate under the thermal shock induced by subsequent laser pulses and form micron-size particles. Polishing of the target surface and maximising the target density are the approaches considered for reducing particle emission.

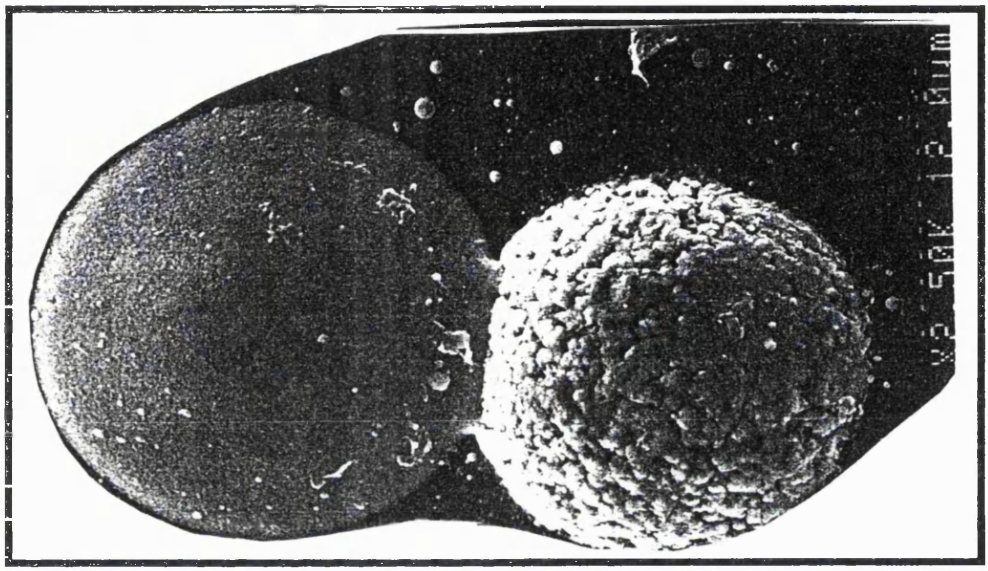

Figure 8.1. *The attachment of droplets during PLD using Nd:YAG(532nm,4ns,10Hz)laser and Pb-2213 material (wide=14μm, length=35μm).*

8.1.2 Superheating and micro-explosions

Singh et al. [5] simulated the thermal effects of pulsed laser-ablation in a silicon target by solving the heat flow equation 8.1, with boundary conditions arising due to the formation and movement of a solid-liquid and vapour-liquid interface. In their calculations, they assumed that (i) the evaporating surface is at boiling point (ii) the thermal loss from the front surface of the target is negligible due to nanosecond ablation (iii) only the planar evaporating surface is present with planar movement of the ablation front. The heat flow equation 8.1 [5, 6] and simulated results are given as:

$$\rho(T)C_p(T)\partial T(x,t)/\partial t=(\partial/\partial x)[K(T)\partial T(x,t)/\partial x]+[1-R(T)]I_0(t)\alpha(T)\exp\{-\alpha(T)x\} \quad (8.1)$$

Where, $\rho(T)$ = temperature dependent density

$C_p(T)$ = heat capacity per unit mass of the material

x = depth directed perpendicular to plane of target in time 't'

$R(T)$ = reflectivity coefficient of the target

$\alpha(T)$ = absorption coefficient of the target

K(T)= thermal conductivity of the target

$I_0(t)$= the time dependent laser intensity.

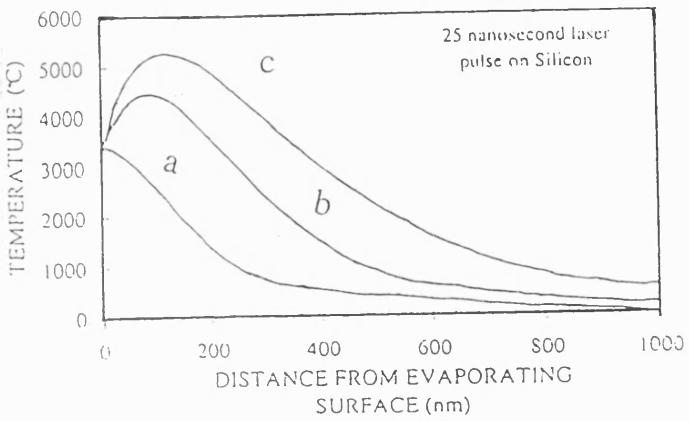

Figure 8.2. *Near surface temperature profiles for three different times: (a)1.44ns (b)5ns, and (c)25ns developed in a Si target with absorption coefficient $1x10^5$/cm during irradiation with 25ns excimer laser pulses with fluence of $10J/cm^2$ [5].*

Their results show that at higher fluences, the subsurface temperatures are greater than surface temperatures, and considered to be a result of cooling effect and latent heat of vaporisation of the surface particles as well as an increase in absorption with the penetration of laser radiation. This subsurface superheating may nucleate gaseous regions leading to micro explosions beneath the upper surface of target that give rise to volume expulsion or 'emission' of molten droplets. The emission of molten droplets depends on the internal superheating effects, cohesion between the grains and the time for the nucleation of the gaseous phases. The heating effects have also been found to be strongly dependent on fluence and become more severe above $3J/cm^2$ for $YBa_2Cu_3O_7$ target where violent evaporation and ejection of droplets were observed [7]. Therefore, in order to keep the superheating effects to a minimum, thereby minimising the emission of droplets, the pulse energy should not be much greater than the ablation threshold.

The absorption coefficient of a target irradiated by a laser is wave length dependent. As one proceeds towards the shorter wave length, the target has a higher absorption coefficient, $\alpha >> 1/L_{th}$, where L_{th} is the thermal diffusion length, $(2Dt)^{1/2}$, leading to a smaller degree of superheating that can help in reducing droplet formation [8]. The degree of superheating is defined as $(T-T_{evap})/T_{evap}$, where T_{evap} corresponds to the evaporation temperature of the target material. The factors that control the degree of superheating are latent heat of vaporisation and the thermal conductivity of target materials. When the latent heat of

vaporisation increases, the superheating inside the target (subsurfaces) also increases and the velocity of evaporated species decrease [8].

Singh et al. used a model to describe the process of pulsed-laser ablation but it does not describe the temperature profile with respect to time and depth in the target. Recently, D.L.Lin et al.[3] tried to calculate the temperature profile inside the $YBa_2Cu_3O_7$ target and its variation with the pulse shape and intensity. Their calculations depend on the heat flow equation where temperature T(x, t) is the function of time and position, x>X, where X is the depth from which material is removed by the laser pulse. The equation 8.2 was used is given below.

$$(\partial\theta/\partial\tau)-u(\partial\theta/\partial s)-(k/C)(t_o/l_o^2)(\partial^2\theta/\partial s^2)=\alpha Be^{-bl_os},$$
$$\text{and} \quad u=o, \quad \text{when} \quad \theta<1 \qquad (8.2)$$
$$\text{or} \quad u=kt_oT_V/L_VI_o^2(\partial\theta/\partial s)_{S=O}, \ \theta=1$$

Where, u stands for the speed of the moving interface, and it can not move until the surface reaches the vaporisation temperature, $\theta=T/T_V$, $\tau=t/t_o$, $s=(x-X)/I_o$, $L=\rho L_V$, $C=\rho Cp$, and $B=Ibt_o/CT_V$, where $t_o=30ns$, $I_o=3x10^{-4}cm$ and $T_V=3000K$ for YBaCuO (this is the boiling temperature, as supposed to the melting temperature of 1300K). By extrapolating from available experimental data they used thermal conductivity, $k=0.042+\lambda\Delta T$, $\Delta T=T-300K$ and $\lambda=1.2x10^{-5}W/K^2cm$, the temperature dependence of $Cp=1.82+2.6x10^{-8}\Delta T$ in J/gmK, and an absorption coefficient to produce $b=2.27x10^5(1-9x10^6\Delta T)$ in the unit of cm^{-1}.

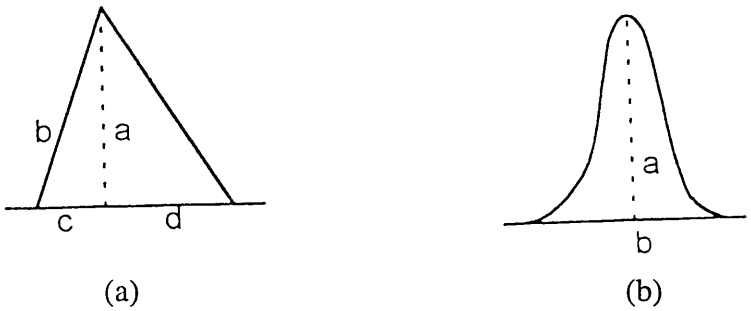

(a) (b)

Figure 8.3. a) Triangular pulse shape b) Gaussian pulse shape.

The temperature variation with the depth into the material was calculated for various intensities of incident laser pulses and shows that subsurface temperatures are higher than the surface temperature, leading to a reasonable explanation for droplet emission. The concluding

remarks favour the pulse shape that has quickly diminishing tail such as a narrow Gaussian pulse or triangular pulse shape to reduce droplet emission.

8.1.3 Shock wave theory

Several authors have reported [9, 10, 11] that the average velocity of ablated particles ranges from 0.02 to 60km/sec during plasma expansion depending on experimental conditions. This kind of fast adiabatic expansion generates shock fronts moving towards the target surface. A possible and more reliable mechanism for droplet emission can be considered as a result of compressional front generation and reflection from the surface of target. The species ablated off the target surface travel much faster than the speed of sound (331m/sec in air) and to preserve the conservation of momentum, the shock wave propagates into the molten region of the target and is reflected at the solid-liquid boundary, leading to the expulsion of loosely bound particles. The following reports support this mechanism.

Michael Thomson et al. [12] used a ruby laser (694nm, 500μs, 1J) to ablate brittle materials and found a second major proportion of big particles in the form of sharp-edged cleavage fragments, about of the same size as the spheres. Obviously this is the material that has not been subjected to melting temperatures and is produced by thermal or mechanical shock.

Fujimori et al. [13] deposited carbon films by using cw CO_2 laser and pressed pellets of graphite and diamond powder as a carbon source material. They reported that the films quality was strongly dependent on source material. Films deposited from graphite powders were graphitic, and films deposited from diamond powders showed some diamond like properties. This effect shows that droplets or crystallites were transported from target to films could be as a result of compressional emission of particles from the targets along with the ablated species.

Kuper et al. [14] reported that the droplets density is the function of atomic or molecular mass of the gas used in constant ambient pressure during ablation. The radius, R, of the droplets shows an approximate relationship with the inverse third root of the ambient pressure. Their results also suggest that for a given pressure, decreasing the atomic or molecular weight of ambient gas, can result in a less momentum transfer on the target surface from the shock front. This effect can be seen as a result of reduction in droplet size. Using a molten Ge target and

CO_2 laser, Cheung and Sankur demonstrated droplet free deposition [15]. Since the target is liquid, the loosely attached particles or cone are not formed during laser-target interaction and shock waves can not produce droplets. However, this technique is not applicable for multicationic superconducting material due to different high vapour pressures of constituent elements at the melting point.

8.1.4 Droplet elimination

Two different approaches have been used to eliminate droplets from deposition. One considers the optimisation of target and laser parameters so that droplet formation and splashing is minimised, and another is manipulation of the plume with respect to position of deposition. In the first case, lower number density of droplet can be achieved by using smaller wavelength, leading to a greater absorption coefficient, fluences just above the threshold, smaller gas pressure and higher thermal conductivity of target. Different groups have demonstrated lower droplet densities using polished and high density targets [16, 17, 18] and homogeneous beam profile [19].

Most of the work has been performed to eliminate droplets simply by manipulating the plume during deposition [20, 21, 22, 23]. A reduction in droplet-density and size has also been demonstrated by using a second synchronised UV laser at a distance of 1.25-2.75mm above the target to further heat the plasma and disintegrate the droplets before they reach to substrate, but it is not real solution even though it is expensive [24].

Holzapfel et al.[20] and Kennedy [21] deposited thin layers using an XeCl excimer laser (308nm, 10Hz) and an unconventional deposition technique in which one can place a substrate parallel to the initial plume direction (major-axis). This off-axis deposition technique uses an effect of scattering due to collisions among the ambient gas molecules and the ablated light particles such as atom, ions and molecules. While the heavy particles or droplets are constrained to travel along their initial direction. The deposition rate is reduced only a factor of 3 that can be compensated by increasing laser energy to densify plasma.

Gaponov et al. [22, 23] used gas dynamic and spatial separation by splitting the out put from a Nd:YAG laser to form two crossed fluxes for the deposition of $YBa_2Cu_3O_7$ films in 'shadow region' where the resultant plasma flux is directed. The important feature of this technique is

the creation of an artificially droplet free area by intersecting two ablated fluxes. The intersecting fluxes do not change the direction of motion of the droplets that have greater forward momentum, whereas smaller species are deflected or stopped.

An alternative mechanical approach to eliminate droplet is based on the fact that the heavier species are much slower than atomic or molecular species. For example, typical droplet velocities are in the range of 0.02-0.5km/s, that is at least an order of magnitude smaller than other species. Using this velocity difference among the species, a selective velocity filter has been used by many authors [25, 26, 27, 28] to prevent droplets from reaching the substrate. Two kinds of choppers are used, whereby an asynchronous chopper spins with an angular speed (20-30krpm) independent of laser firing and synchronous chopper spins with a particular phase relationship to the laser triggering. These methods complicate the simple PLD techniques and make them relatively more expensive than some other techniques.

8.2 Ablated-mass and laser-target interaction

Since the quality of the films synthesised using PLD process depends on the nature of the substrate, laser parameters, optical, thermal and mechanical properties of the target, the droplet emission can be minimised using high density targets compared with brittle and porous material. To observe the effects of laser-target (Nd:YAG laser, 532nm, 4ns, and lead-based material) interactions, the following experiments were performed.

8.2.1 Laser spot size and mass ablation

The ablated material can influence the dimensions and density of the plume that can change the deposition rate (fig.8.4) and in some cases the stoichiometry of the film. Some initial experiments were performed to observe the effects of different laser parameters on Pb-2213 material. Using Nd:YAG (532nm, 4ns, 10Hz) laser and maintaining vacuum of $4x10^{-3}$mbar inside the chamber during the ablation processes, all the experiments were carried out.

A simple experiment was performed to observe the effect on uniformity by keeping the deposition parameters constant and varying the target-substrate distances. The spot size of laser beam varies according to the distance between the target and the focal point of lens through which the laser pulses of constant energy were entering to the chamber. A laser beam entering into the chamber at an angle of 30° was used to ablate a melt-textured

$Pb_{2.5}Sr_2(Y_{0.5}Ca_{0.5})Cu_3O_{8+\delta}$ target placing at the focal point of lens through which the laser beam enters into the chamber, back and forth at different positions.

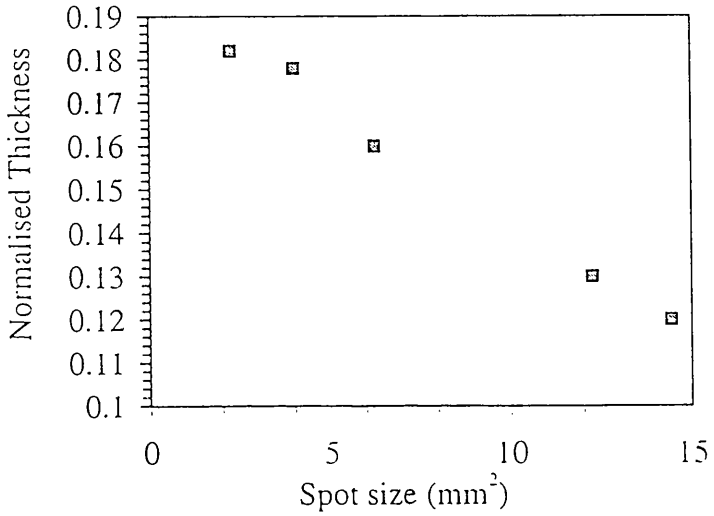

Figure 8.4. Thickness of the films versus spot size at constant laser energy.

The ablation of material at different positions provided the different values of ablated-mass found by weighing the pellet after each ablation, where the spot size was found different. Therefore, by oscillating the target with respect to mean position (focal length of lens), the laser beam was scanned on the target. It resulted the scanning of ablated plume on substrate due to the change in target-substrate distances that shifts the position of burn-spot on the target and the plume. It was found that the irradiated area on the target varies with the target position, and the laser fluence changes as the target moves back or forth from the focal point of the lens. The maximum mass ablation was found at the focal point of lens. It could be considered in terms of maximum use of the photons for ejection of material from the target surface at the focal point, and greater probability of reflection and conduction losses from other positions due to larger area of spot-size that reduces the ablation rate. Therefore, to compensate the smaller amount of mass ablation for larger spot-sizes, the target has to be ablated for longer durations. The time of ablation was iterated to equalize ablated-mass at different positions, and deposition was performed accordingly. Therefore, the target pushing and pulling from the mean position worked similar to a simple pendulum of focused laser pulses. Table-1, figure 8.5-a and 8.5-b show the ablated-mass at different positions due to variations in spot size. During ablation of Pb-2213 target material, normally the shape of the visible plume follows the candle-flame-shape in double portions, one is a denser part thought to be mainly consist of droplets, large and small ablated species, similar to big carbon particles in mid-portion of the candle-flame, and another is the large angle scattered portion, keeping mainly smaller and atomic species. It was observed simply by eye that the visible plume

dimensions increase with decreasing spot size. A situation also exists where the spot size decreases and the energy is tightened enough to drill a hole of small area (S~2.56mm^2) where the ablation becomes explosive. This situation could be due to high energy heating where the particles are dissociated, achieve greater momentum and also the repulsive nature of the same kind of ions within the smaller area of hole creates scattering and explosions, just after the action of few pulses. Figure 8.6 shows the film deposited in 4x10^{-3}mbar on Si(111) substrate at room temperature during the oscillation of the pellet, and photograph was obtained by a camera using filters. It is observed that the area of the central stoichiometric portion increases up to 2.5cm^2 whereas the deposited area is 4cm^2. Using higher vacuum, the central portion of the deposition could further be increased by avoiding the collisions from ambient gas. The rings of different colours show the non-uniformity, however, the film was stoichiometric up to 2.5cm in diameter with in the range of 10% accuracy of EDX characterisation limit. To investigate this further, a precise computer controlled target oscillation in front of laser pulses using large size of target can enhance the homogeneity and deposited area but this was not possible due to our experimental limitations.

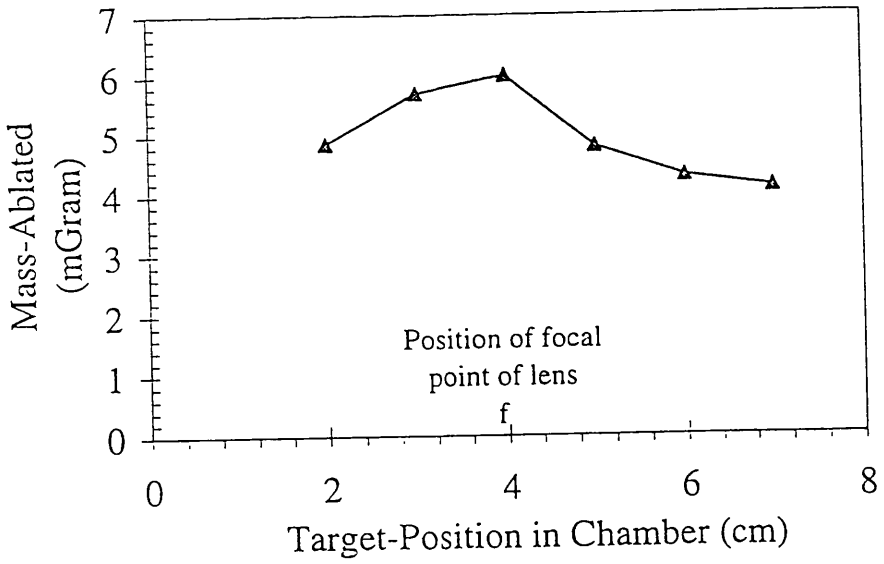

Figure 8.5-a. The mass-ablation at different positions(at the focal point of lens, forward and backward directions) in front of a 225mJ Nd:YAG laser pulse (532nm, 4ns, 10Hz).

The ablated spots (burn-spot) are found approximately circular, and the centre of the spot is deeper, and depth decreases towards the edge of burn-spot. Each burn spot was analysed using EDX characterisations. Lead loss and an increase in Sr, Ca and Cu were observed from large to small spot sizes.

Table 8.1. Spot size and ablated mass at different positions in front of laser pulses.

Target position	Area of spot (mm^2)	Mass ablated (mgram)
1	14.44	4.1
2	12.25	4.3
3	6.25	4.8
4	2.56	6
5	4	5.7

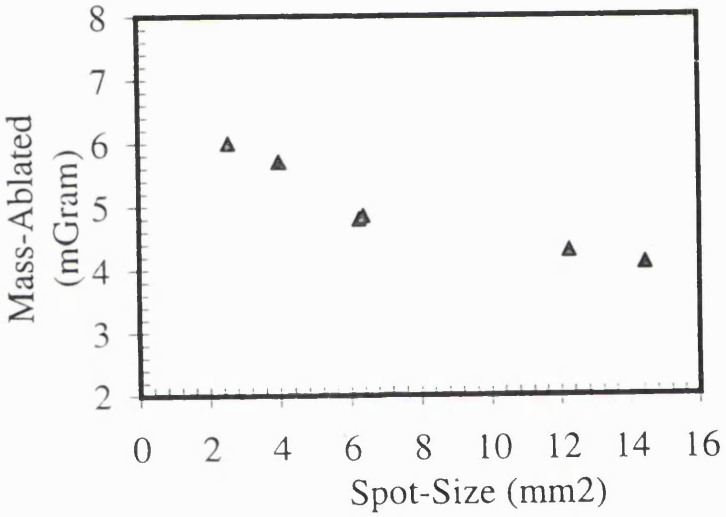

Figure 8.5-b. *The effect of the spot size of a 225mJ Nd:YAG laser pulse (532nm, 4ns, 10Hz) on the mass ablation of melt textured target.*

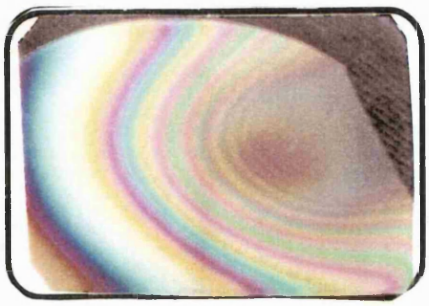

Figure 8.6. *Deposition made on Si(111) at room temperature using oscillated spot on Pb-2213 phase target.*

Figure 8.7 shows SEM micrographs of virgin target and ablated spots on the target. Initially, it was observed that the biggest laser spot in this experiment (fig.8.7b) removed smaller amount of mass, with smallest depth but has not any significant cone formation other than melting. The depth of the burn-spot and the length of cones gradually increased with the decrease in spot-size. For the second largest spot, cones started appearing significantly (fig.8.7.c). For the third spot size ($d=6.25mm^2$), the cones are clearly directed upward at

certain angle (fig.8.7.d). For the smallest burn-spot (e=2.56mm^2) of this experiment, the cones are much bigger, and some are welded with one another(fig. 8.7.f). By adjusting the target-substrate distance~6cm and keeping the laser energy constant, the spot size was varied to check the thicknesses of the central deposited portions on Si(111). It was observed that the thickness increases with the decreasing spot-sizes and then it saturates. It seems the saturation in thickness for higher fluences (smallest spot size) is due to explosive scattering of ablated material that stops futher increase in deposition rate (figure 8.4).

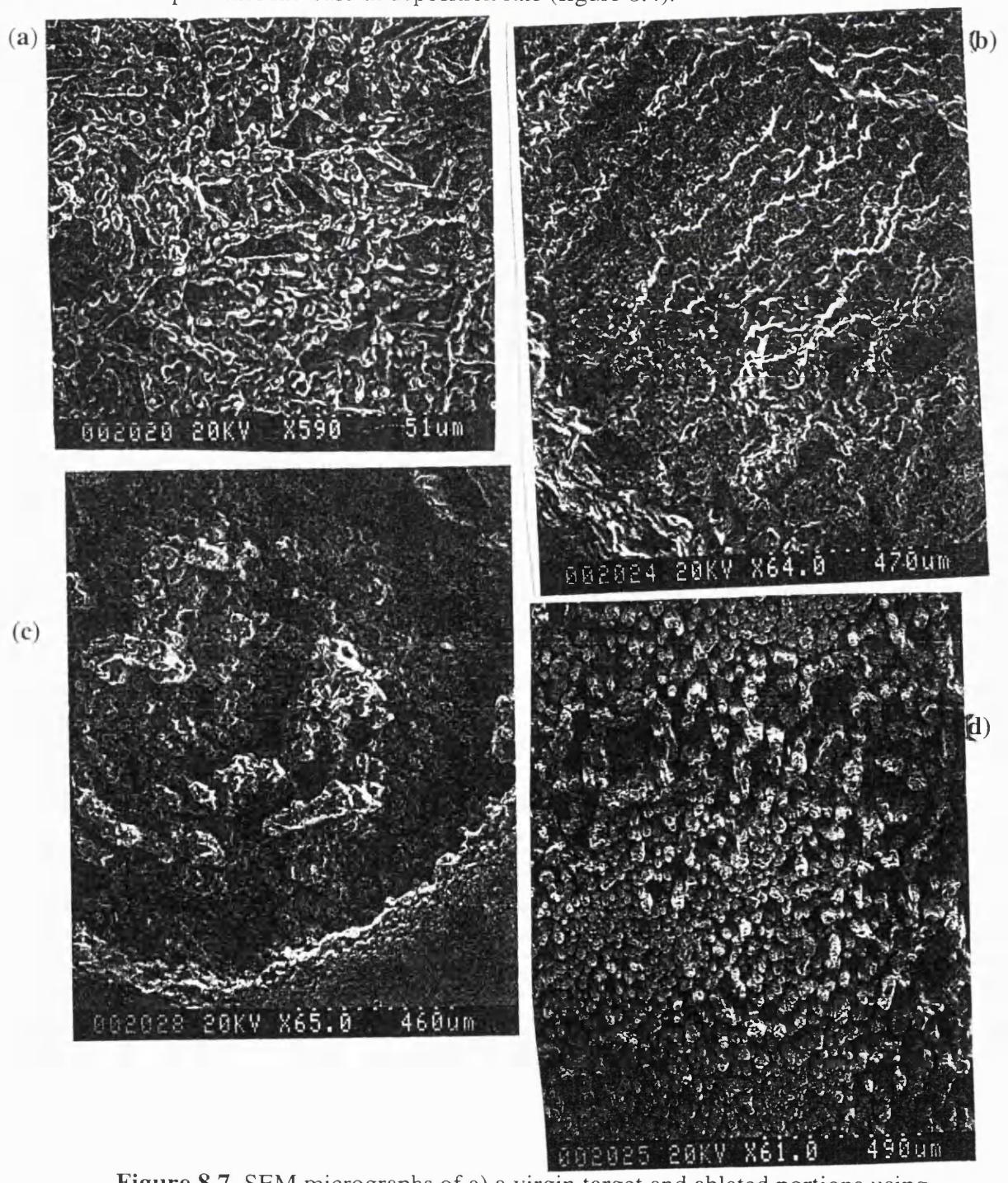

Figure 8.7. SEM micrographs of a) a virgin target and ablated portions using various laser spot-sizes b)14.44mm^2 c)12.25mm^2 d) 6.25mm^2.

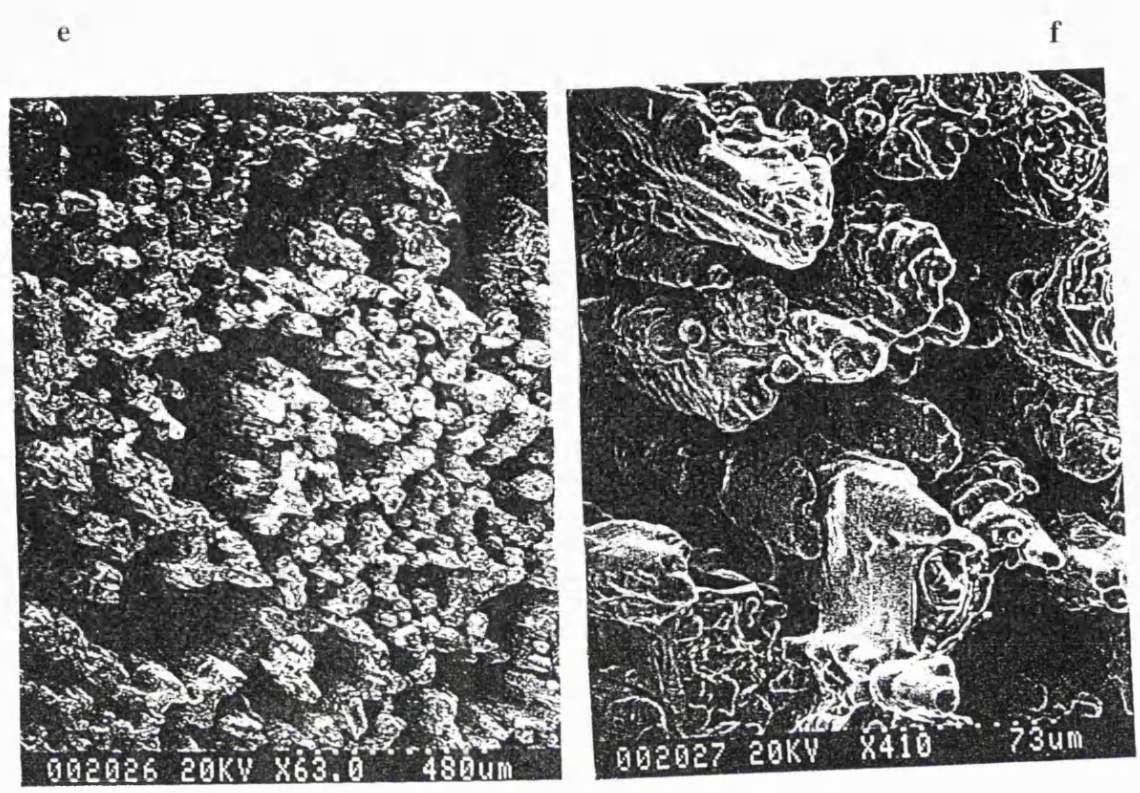

Figure 8.7. SEM micrographs of a) a virgin target and ablated portions using various laser spot-sizes e)2.56mm^2 f)2.56mm^2 with higher magnification.

The number density of droplets with the change in spot size was found using SEM micrographs. In each case, all the droplets are in spherical shape with three different sizes, having the diameters of ≥1μm, ~0.6μm and ~0.25μm as the large, medium and small sizes. For the big spot size (14.44mm^2), large droplets are few, but the number of medium and small droplets is significant compared with the droplet density obtained for other spot sizes. For the another spot size (12.22mm^2 and 6.25mm^2), the number of large size droplets is not increasing significantly, whereas number of medium and smaller droplets increase with the decrease in spot size. This experiment shows that for the constant laser energy, the bigger spot-size can reduce the number density of droplets, whereas the cone formation and their sizes are also related with the spot-sizes of fixed laser energy for the Pb-Sr-(YCa)-Cu-O material (figure 8.8.a, b,c).

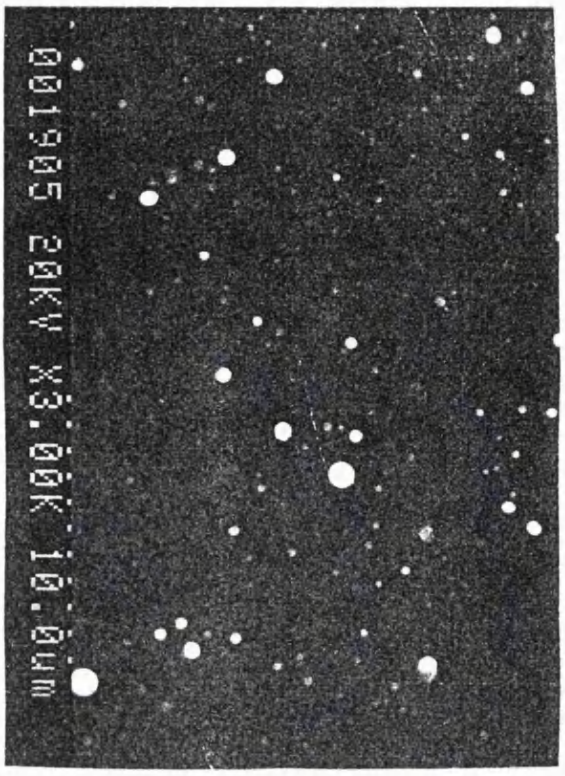

(a)

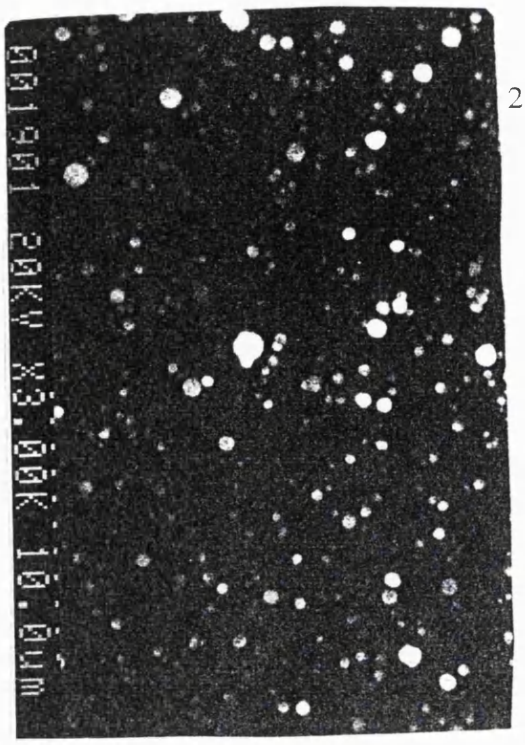

(b)

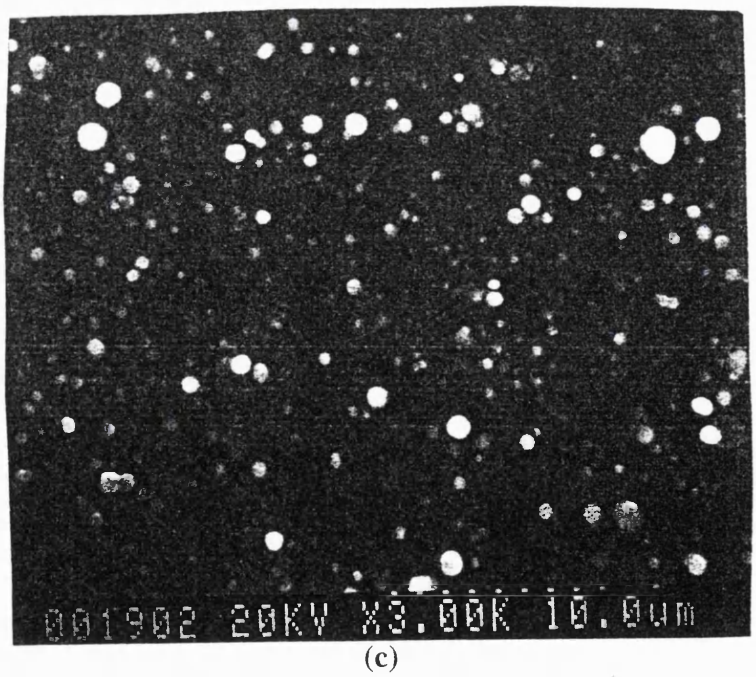

(c)

Figure 8.8. SEM micrograph of thin layer deposited using laser spot sizes of a)14.44mm^{2}b)12.25mm^2(c) 6.25mm^2.

8.2.2. Fixed fluence and ablation period

The mass-ablation experiments were also performed for fixed laser parameters using a 225mJ, Nd:YAG laser pulse (532nm, 4ns, 10Hz) forming a laser spot of 0.085mm^2 on a non-rotating and sintered-melt textured target of $Pb_{2.5}Sr_2(Y_{0.5}Ca_{0.5})Cu_3O_{8+\delta}$ material. The target

material was homogenised by several grindings and sintered before placing inside the chamber. The ablations were carried out for various durations at different places on target and are presented in figure 8.9. It is clear that the ablation follows linearity up to 1200 pulses and later a divergence could be seen by increasing ablation time using fixed laser energy pulses.

Each burn spot was analysed using EDX characterisation. From the analysis it was observed that long period laser-target interaction decreases the percentage of lead and increases the value of Sr, Cu and Ca. It seems that the reason behind it, is the segregation and some oxide formation during ablation reaching in a situation where the melting and heat of vaporisation of different oxides are playing an effective role. For example, after certain amount of oxide formation, the melting points of PbO, SrO and CaO (880°C, 2407°C and 2557°C) can provide preferential evaporation, and the amount of the ablated mass decreases during long period of laser-target interaction.

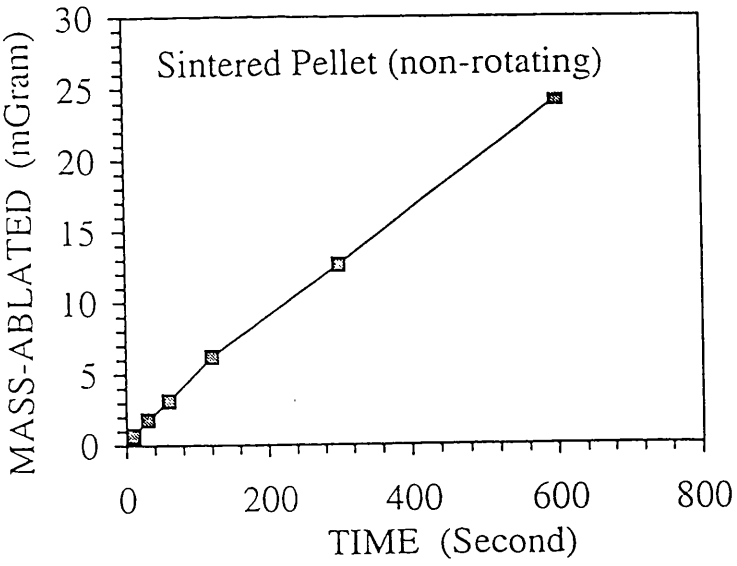

Figure 8.9. *Ablated mass versus laser-target interaction period.*

8.2.3 Unsintered pellet and mass ablation

Using solid-state reaction method, well reacted and sintered $Pb_{2.5}Sr_2(Y_{0.5}Ca_{0.5})Cu_3O_{8+\delta}$ bulk pellets were synthesised. Later, the pellets were crushed and ground for 1hour to make nearly the same size of crystallites. 1.5gram powders were pressed to form tablets at different pressing forces (7.54ton/cm^2 and 9.79ton/cm^2) with our laboratory limitations.

Figures 8.10-a and 8.10-b show the ablated mass versus laser energy for a fixed laser-spot, number of pulses (1200pulses) and stationary pressed-pellet formed at different pressures. For less denser pellet, the ablation increases exponentially with the increase in laser energy, whereas for denser pellet, the increase is approximately exponential but slightly smaller in amount. The ablated-mass has a slight shift towards higher values with the same laser energy when it is rotated during ablation. This shows that the fresh target surfaces are more ablative. Another reason is the possible segregation (that creates oxides of higher heat of sublimation) due to increase in number of pulses per unit area in case of non-rotating target.

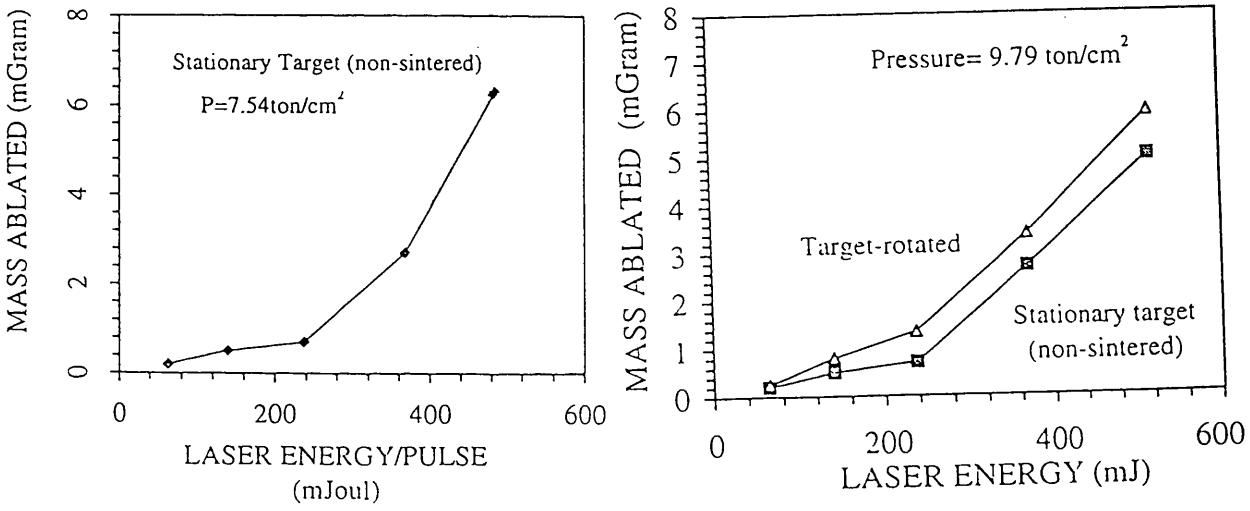

(a) **(b)**

Figure 8.10. *Laser energy versus ablated mass of unsintered pellets a) pressed at 7.54ton/cm^2 b) 9.79ton/cm^2.*

8.2.4. Pressing force and ablated-mass

Three different superconducting materials ($YBa_2Cu_3O_7$, $(BiSb)_2Sr_2Ca_2Cu_3O_{10+\delta}$ and $Pb_{2.5}Sr_2(Y_{0.5}Ca_{0.5})Cu_3O_{8+\delta}$) were synthesised using appropriate ceramic technique. The sintered pellets were crushed, ground to make nearly the same size and smaller particles, so that could be compacted well. Later, the fixed amount (1.5gram) of powders of each material was pressed into 1.32786cm^2 area forming tablets at different pressing forces. Prior, the ablation started, the vacuum chamber was evacuated to $4x10^{-3}$mbar pressure. The laser energy was taken just above the ablation threshold of targets (0.835J/cm^2). The number of

pulses used to ablate each pellet were same. From this set of experiment two different points are clear:

i) the ablated mass is dependent on the compactness or density of the materials, other than the laser parameters,

ii) different superconducting materials have different ablation rate and can form different plume dimensions and densities for the same laser parameters that provide a rough and comparative idea about absorption of laser energy and removal of material.

Figure 8.11 shows ablated masses versus pressing forces, used to form different pellets. The Bi-2223 material has lowest mass-ablation compared with Pb-2213 and YBaCuO materials. It was also observed from plume dimensions that PSYCCO has larger visible size than Bi-2223 or Y-Ba-Cu-O. It must effect the deposition rates and some time stoichiometries if the same deposition set-up is used for different materials. It is also observed that loosely compacted pellets are more ablative and ablation is small enough after certain pressing forces. It seems that micro holes are letting to enter the laser pulses inside, where the evaporants are pushing out the particles from upper layers which are loosely attached above the surface. Shock compressions can also take out the loosely attached particles from the surface.

It is demonstrated from experiments regarding the laser-target interaction that the sintered target and compacted pellets (target-density) can seriously affect the ablation rate, droplet density and size if the laser parameters are kept constant. Figure 8.12 shows SEM micrographs of the films grown using a) the sintered pellet, b) a pressed compact and the same deposition parameters. However, the droplets are few but their sizes are large compared to the deposition made from pressed pellet. It is clear from image (b) that the most of the particles in the range of 0.2 to 0.5μm were transfered from the pressed pellet, but the big droplets were not found as the case of sintered pellet (a).

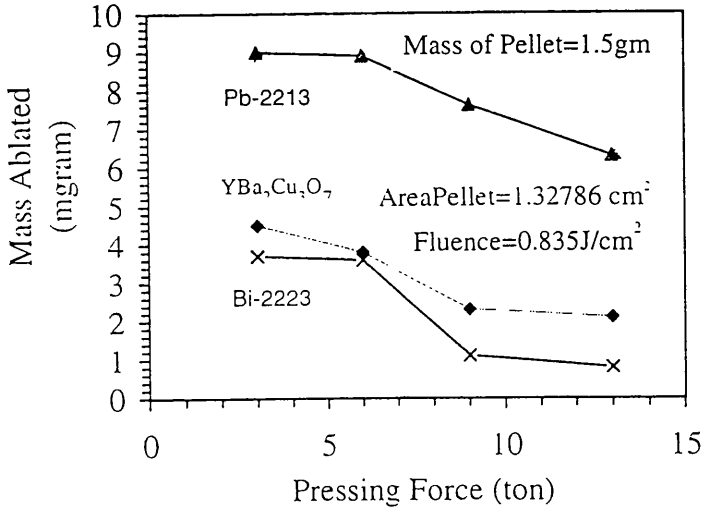

Figure 8.11. Mass ablated using1500 laser pulses versus compacting forces.

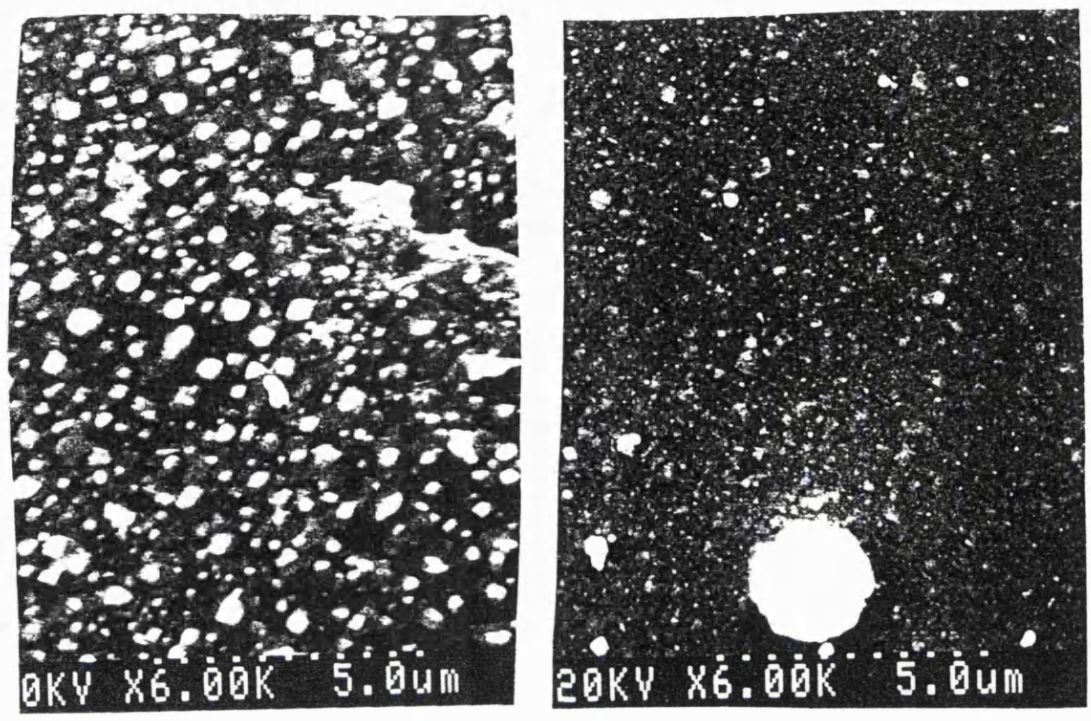

(a) (b)

Figure 8.12. SEM micrographs of films deposited from a) melt texture and b) pressed pellet.

8.3.1 Kinetic energy distribution of ionic species

It has been shown that the ablated mass or product of laser-target interaction is depending on laser fluence, target material and its characteristics. The constituents of the Pb-Sr-(YCa)-Cu-O plume, and the kinetic energy associated with them has not previously been studied. To find out the nature of ablated species and the kinetic energies of a plume of $Pb_2Sr_2(Y_{0.5}Ca_{0.5})Cu_3O_{8+\delta}$ material above the ablation threshold, experiments were performed with the assistance of Dr.G.C.Tyrrell. Usually, the plume consist of variety of species, where the emitted ions can be attributed to a result of different mechanism which are dependent upon the absorbed energy, thermal, photodissociation and collisional processes or ion-ion repulsion [29]. The ionic species of the ablated material from Pb-2213 target were detected and isolated using a modified cylindrical mirror analyser (CMA) and quadrupole mass spectrometer (QMS). The results obtained have been included in this section for better understanding. However, the energy and mass response could be changed with the laser fluences, plume dimensions or the changes in the correct position of the target and orifice, and needs a detailed study.

8.3.2 Apparatus, experimental and results

Laser ablation was performed in a chamber (designed by Mr.T.York) that was equipped with an atomic mass filtering and charge analysing facility (figure 8.13). The chamber can be pumped using a 200*l*/s turbomolecular pump with routinely obtained base pressure of 10^{-7}mbar. A frequency doubled Nd:YAG laser with a fluence of 1.5J/cm^2 (λ:532nm=2.33eV, 4ns, 10Hz, maximum energy of 470mJ/pulse) was focused on a melt textured $Pb_2Sr_2(Y_{0.5}Ca_{0.5})Cu_3O_{8+\delta}$ target, at an angle of incidence of 45°. The pellet was rotated at a constant speed of 0.5 rotation per minute to minimise target segregation problem. The target-orifice distance was kept 65mm during experiment. The ablated plume was sampled by means of an 450μm orifice at the entrance to a differentially pumped region. The orifice was earthed to ensure a field free region between the plasma and ion optics. The plasma ions could be retarded or accelerated by application of a potential to the orifice plate. The base pressure in the differentially pumped detection chamber was 10^{-7}mbar. The differentially pumped region has a quadrupole mass spectrometer (QMS; VG Quadrupoles SXP-600 Elite: range 0-600amu) with a modified cylindrical mirror analyser(CMA, range 0-500eV) with accompanying ion transfer optics and ionisation source to filter out a certain energy and mass. The quadrupole analyser consist of an ion source, a quadrupole mass filter and a detector. Ions are generated in the ion source or externally generated ions are allowed to enter into quadrupole mass filter that selects a particular mass to charge(m/e) value, and the selected ions are sensed by the detector (could be a Faraday cup or electron multiplier).

The quadrupole mass analyser actually consist of four cylindrical rods which are mounted in a square array, and driven with a specific combination of radio frequency (rf-voltage) and direct voltages (U-V Cosωt, -U+VCosωt). The resulting electric field allows ions of a given charge to mass ratio entering the quadrupole to follow a stable oscillatory trajectory between the rods and so reach the detector. All other ions entering the QMS are forced to follow unstable trajectories of increasing amplitude and so collide with the rods or housing and not reach the detector. The performance of the quadrupole is determined by the physical size of the rods and the frequency of the applied rf field. In order to achieve good resolution, the energy of the transmitted ions should be as low as possible. However, the transmission decreases with decreasing energy. The specific ion of (m/e) is

transmitted and others are rejected depending also on applied direct voltage, U. The CMA/QMS analyser could be operated in several modes to obtain information on both positive, negative and neutrals, but this experiment was focused only on the positive ions and neutrals present in the plasma. The QMS offers a high mass range detection and is free from magnetic fields.

The ions passing through the orifice are interacted by the ion transfer optics that collimate them and let to proceed in parallel towards the modified CMA. The ion transfer optics is an Einzel lens constructed from two outer electrodes set at earth potential with a negative potential applied to a central electrode. The collimated ions cross the ionisation source area with the non-active filament (off), otherwise it is used to ionise neutral species. Conventionally, a cylindrical mirror analyser for electron energy would be expected to accept particles from a point source and pass them through an angle of 42°, but this is not compatible with a QMS, which requires a broadly parallel beam of charged particles. The initial development of modified CMA/QMA has been reported by Shi et al.[30].

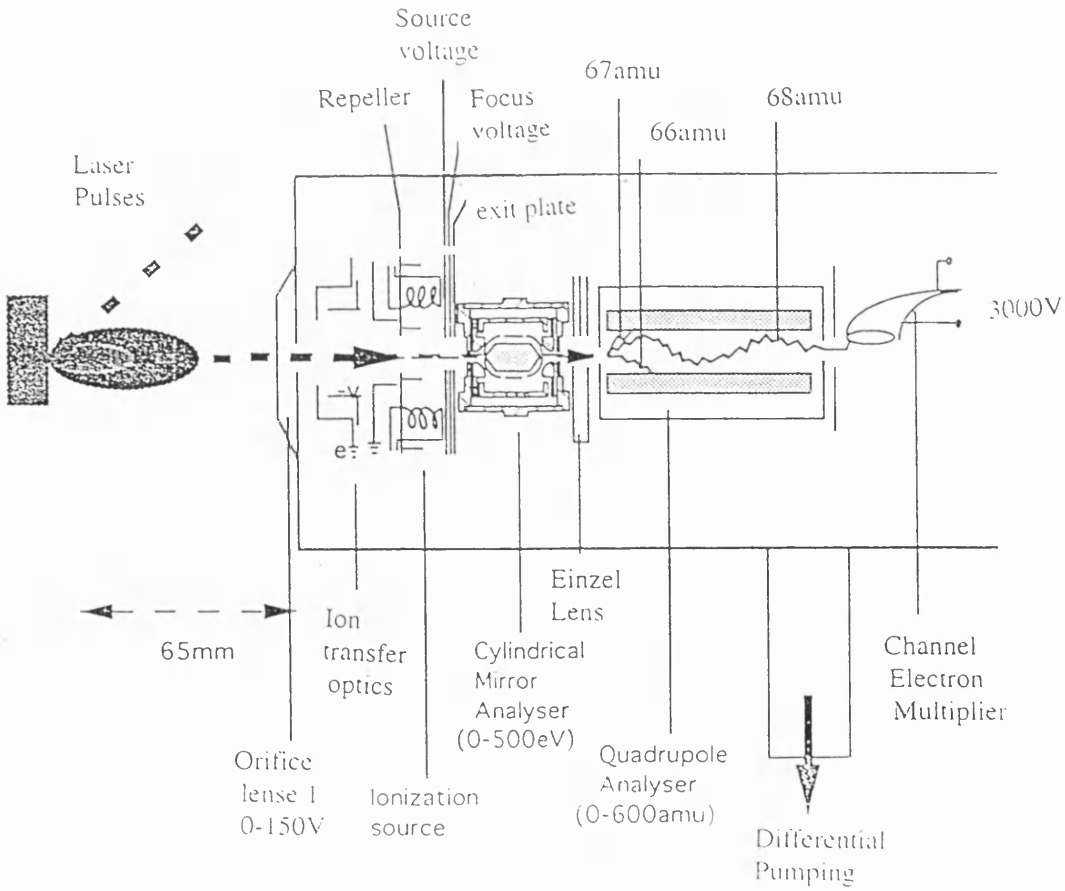

Figure 8.13. An energy and mass analysing system equipped with CMA/ QMA.

This problem was solved by providing virtual source/ image for the CMA using an inverted hemispherical type analyser/detector at the entrance and exit of the CMA. The modified design of CMA transforms the incoming ions energy (E_0) to E_{pass} value at the entrance by a retarding or accelerating voltage (V_{cma}) according to the following equations:

$$E_0 = E_{pass} + eV_{cma} \qquad (8.3)$$

with $V_{cma} < 0$ when $E_0 < E_{pass}$

$V_{cma} > 0$ when $E_0 > E_{pass}$

The energy analysed beam exits the CMA into another Einzel lens which modifies the ion energy to few eV in order to maximise the efficiency of the quadrupole mass filter. The ions are detected by by channeltron electron multiplier, mounted off axis where a potential of 3000V was applied. A final ion count is determined by the set rate in the pulse counting electronics. The collection time used in this work was 0.1second, whereas the ions transit time from the plume is several micro seconds. The timescale of each individual pulse counting event, however, was of the order of a few nanoseconds. Therefore, for a large number density of ions arriving within this period, quantitative data collection could be difficult due to saturation of the channel electron multiplier used for detection.

The manipulation of dense 'packets' of charged particles by applying potentials at any of the regions can not be straightforward if the charge density is large enough to screen the inner regions of the charged packets. The ion energy measured by the CMA was equal to the sum of V_{CMA} (the voltage on the CMA lens) and the pass energy which was set to 25eV for the experiments. Figure 8.14-a) and figure 8.14-b) show the number of maximum counts recorded at certain energy position for singly and doubly ionised ablated species from $Pb_2Sr_2(Y_{0.5}Ca_{0.5})Cu_3O_{8+\delta}$ target in a 10^{-3}mbar oxygen partial pressure. Each count period was over 0.1second with the ablation at 10Hz.

A broad band from low to high energies of ions was detected in the range of 20 to 160eV. There are two kinds of energy distributions, one for singly and another for doubly ionised atoms. The singly ionised atoms have broader energy spectrum ranges from 20eV to 160eV compared with doubly charged ions ranges from 40eV to 160eV. Figure 8.15.(a-c) shows the singly and doubly charged isotopes of Cu, Sr and Pb ions. The count intensities of each isotope approximately follow the natural percentage of abundance. It

is also observed that the count intensity of singly ionised isotopes is higher than the doubly charged isotopes.

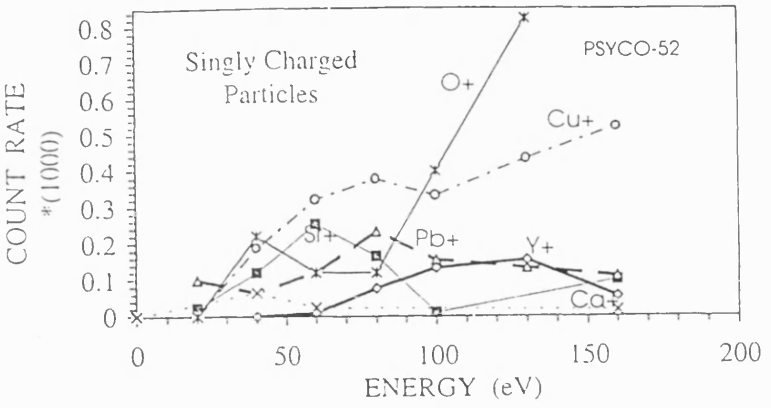

(a)

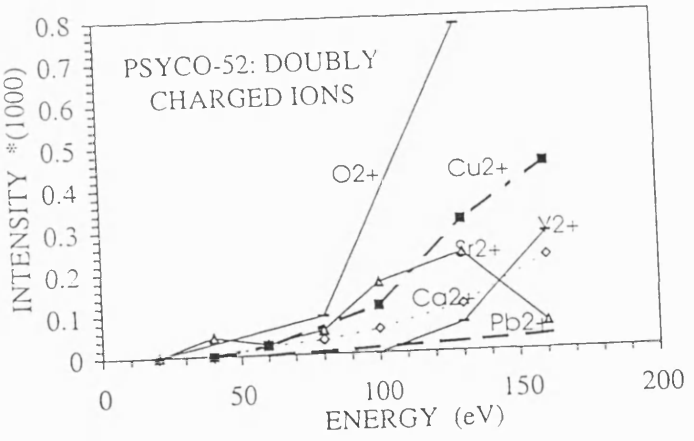

(b)

Figure 8.14. Energy spectra for ejected a) singly b) doubly charged ions from Pb-2213 target.

To find out the thermal neutrals among the ablated particles, the ionisation source voltage was used to ionise the neutral species using 5Volt and 150 volt through electron emission. Figure 8.16.a is presenting the relative intensities of molecular and atomic pulses of oxygen separated from other species when the source voltage was 150volt. The energy and intensity of neutrals depends on ionisation source voltages. For example, figures 8.16-b) and 8.16-c) show the energies and intensities of neutral Cu and atomic

oxygen (O^0) pulses at 5Volt and 150Volt. However, the ionisation or molecular dissociation ($e+O_2 \rightarrow 2O^0$) probability is very small to separate out neutrals from ionic species already present in the plume, even though the intensity is large enough giving an idea about the relative presence of neutral species in the plume.

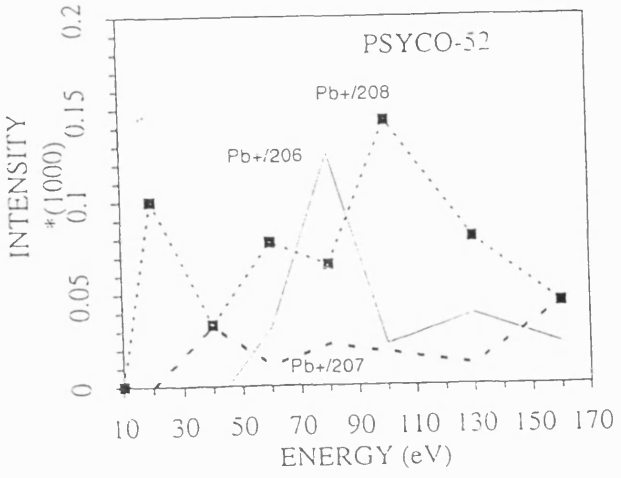

(c)

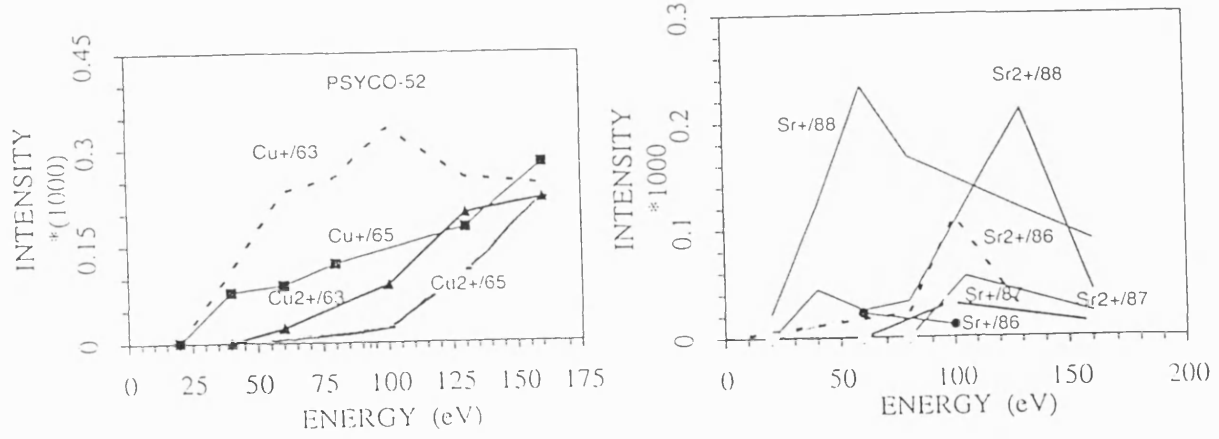

(a) (b)

Figure 8.15. Energy spectra for ejected singly and doubly charged a)Cu, b)Sr and c)Pb ions relating the abundance present in the Pb-2213 target.

The obtained results show that the atomic and molecular species of various isotopes, ions and neutrals and their energies can be determined easily using a combination of modified CMA and QMS filter. Neutrals, singly and doubly ionised species were detected, whereas the oxides of constituent elements of Pb-Sr-(YCa)-Cu-O material were not found in the plume.

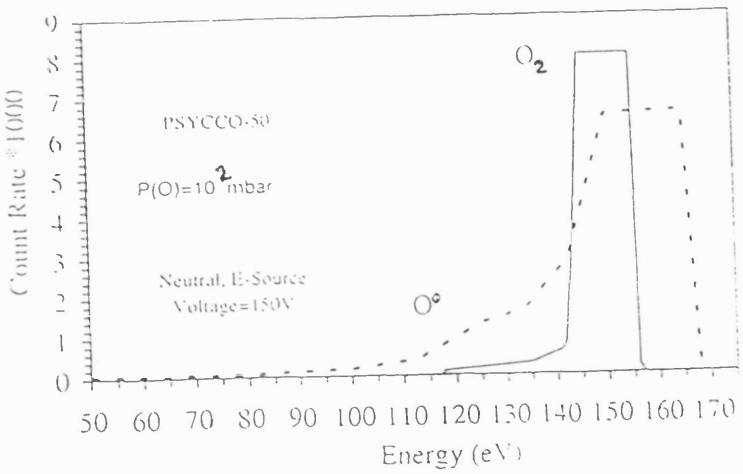

Figure 8.16.a) The relative intensities of molecular and atomic oxygen.

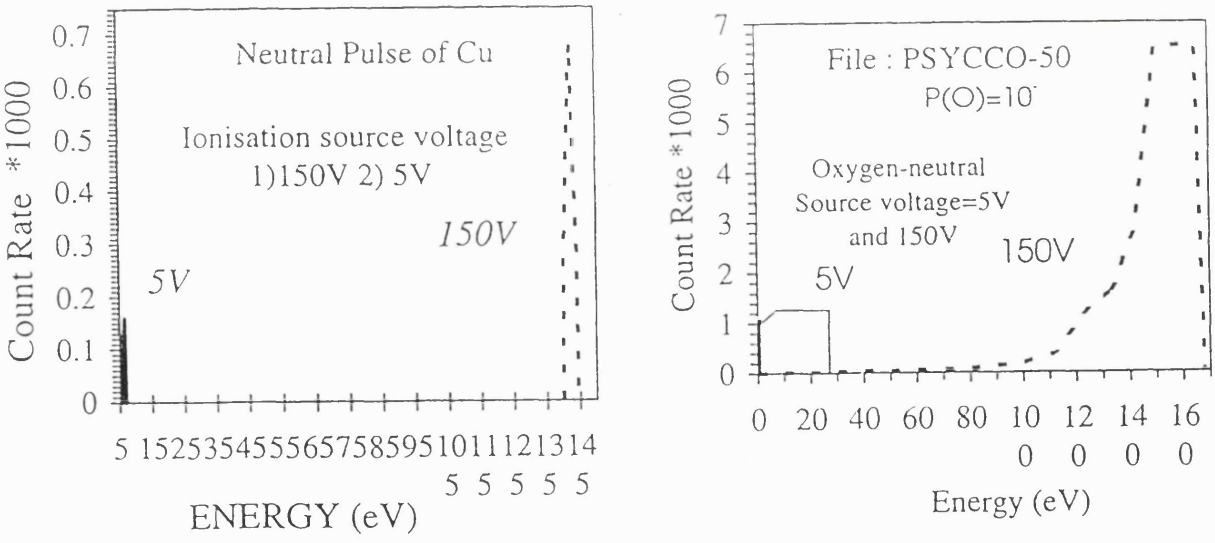

(b) **(c)**

Figure 8.16 The energies and intensities of neutral (b) Cu and (c)atomic oxygen (O^0) pulses at 5Volt and 15Volt.

8.4 Oxygen partial pressure and smoothness

Since the initial PLD work started, it was considered only as a reasonable process for synthesising various multicationic materials as compositionally uniform thin layers over a square centimetre area due to forward directional nature of the plume. Even though the deposited stoichiometric area is small, it is facing the problem of roughness due to

droplets. The droplets number density changes for a fixed target to substrate distance with respect to the oxygen partial pressure during the deposition. Reason behind it is the collision effects between the ablated species and the gas molecules that broadens the width and rarefies the density of the plume. The smaller ablated species can change their path due to collision with molecules present in ambient pressure but the heavier species (droplets) are difficult to divert from original direction. Figure 8.17 shows the different background pressures and visible dimensions of the plume for the ablated material using laser fluence of $4J/cm^2$. Initially, the plume is narrow and forward directed in $4x10^{-4}$mbar vacuum. Later, its broadening and brightness can be seen with the increase of oxygen partial pressure ($2x10^{-1}$mbar) due to ionisation, excitation and recombination effects.

Dyer et al.[31] have shown that E/P is the scaling factor for plume, where E is the laser-pulse energy, and P is the background pressure. The length of the plume, L, that determines the characteristics of front-deposition of plume, is given as:

$$L \propto (E/P)^{1/3\gamma} \qquad (8.3)$$

where γ is the ratio of the specific heats of the elements in the plume.

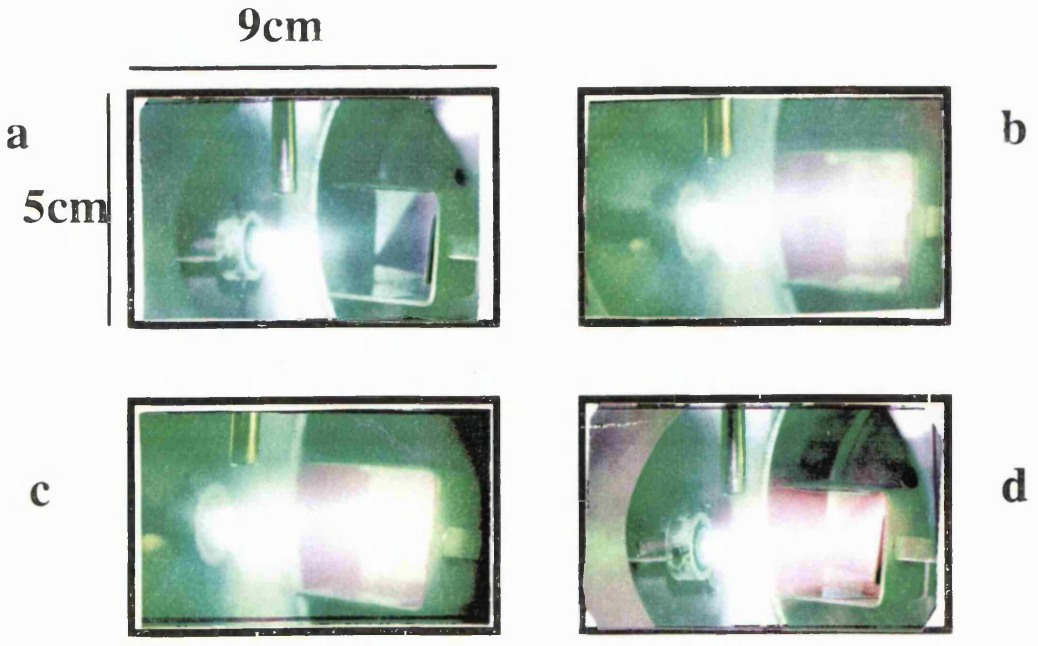

Figure 8.17. *Plume dimensions with different oxygen partial pressures*
a)$1x10^{-3}$mbar b) $8x10^{-3}$mbar c) $4x10^{-2}$mbar d) $2x10^{-1}$mbar.

To study the influence of oxygen partial pressure on droplet density and size, a set of experiment was carried out using Nd:YAG laser (532nm, $4J/cm^2$, 4ns, 10Hz) and melt

texture $Pb_{2.5}Sr_2(Y_{0.5}Ca_{0.5})Cu_3O_{8+\delta}$) target in different oxygen partial pressure, ranges from 0.08mbar to 3.0mbar. The deposition was performed only for 2 minute on heated MgO (001) single crystal substrates. The temperature was around 550°C during deposition, and heater was turned off just after turning off the laser, then thin layer was cooled down to room temperature in the same oxygen partial pressure.

A high resolution scanning electron microscope (type HITACHI S800) equipped with a field emission electron gun was used to analyse carbon coated thin layers. SEM micrographs were obtained under the same magnification during each thin layer analysis to observe the droplet density over the surface area. To find out the surface density and size distribution of the droplets and out growth, a modified computer program, initially written for the analysis of cloud pattern and later changed for counting and finding out the size of the droplets was used with granted permission of Dr. John Pollard. The number and size distribution of the analysis have been tabulated and presented in figure 8.18. The average droplet-density of various sizes is found maximum for 1.0mbar oxygen partial pressure whereas it is low enough for the same ablation-deposition parameters in the range of 0.08 to 0.5mbar oxygen partial pressure.

Table 8.3. *The number-density of droplets of different sizes found on the surface of thin layers after PLD at room temperature in various oxygen partial pressures.*

Number-density of droplets (number/μm^2)						
Radii of droplets / $P(O_2)$ (μm)↓ →	S1 1P 0.08mbar	S2 5P 0.2mbar	S3 2P 0.5mbar	S4 3P 1.0mbar	S5 6P 2.0mbar	S6 4P 3.0mbar
0.061-0.09155	0.098	0.113	0.32	0.33	0.0682	0.3
0.0946-0.122	0.0	0.0	0.046	0.219	0.091	0.0682
0.125-0.153	0.0	0.0	0.023	0.1093	0.0	0.1591
0.156-0.183	0.033	0.012	0.023	0.055	0.023	0.0455
0.186-0.214	0.0	0.0	0.0	0.0273	0.0455	0.0682
0.217-0.244	0.0	0.0	0.0	0.055	0.0	0.0227
0.247-0.275	0.0	0.0	0.0	0.0273	0.0	0.0455
0.278-0.307	0.0	0.0	0.0	0.0	0.0227	0.0455
>0.308	0.0682	0.023	0.0682	0.25	0.114	0.1591

The number density of droplets also decreases at or after 2.0mbar. It seems that the reason behind it is the size effects of plume with respect to the position of substrate. Other reasons could be the scattering of ablated lighter species due to the leakage of pressurised gas near the substrate, shock waves, cone formation and greater number of droplet emission.

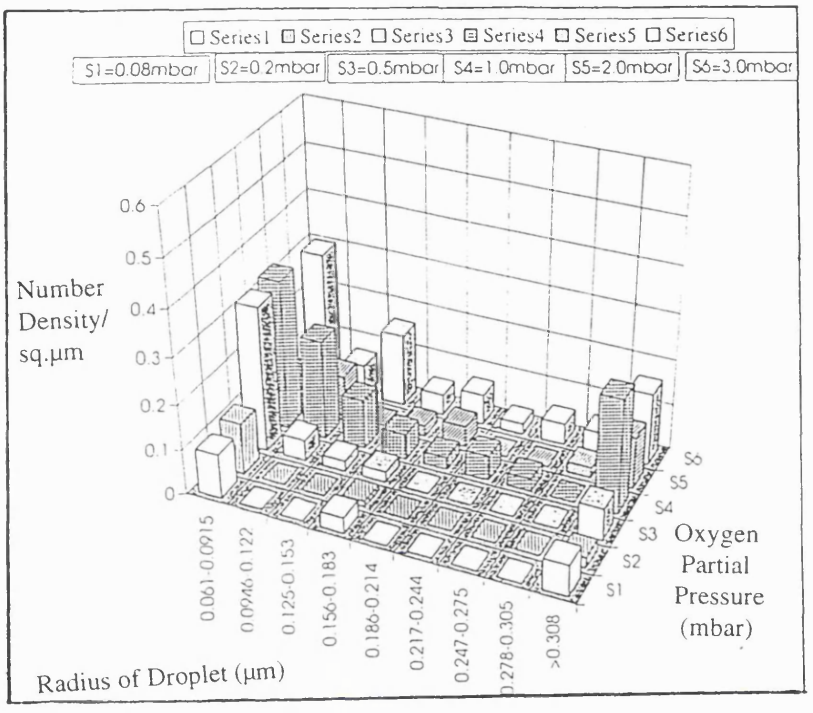

Figure 8.18-a) *Variations of droplet-size and distribution in various oxygen pressures.*

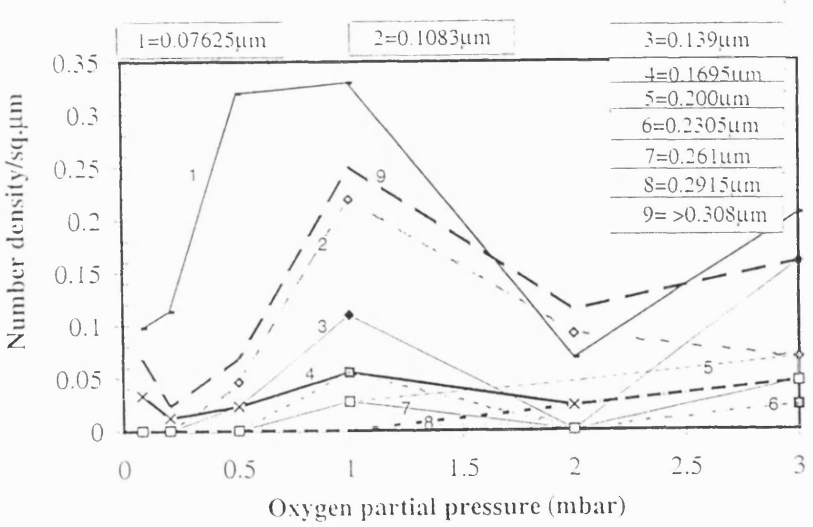

Figure 8.18-b) *Average droplet-size in different oxygen pressures.*

8.5 Rapid thermal annealing and smoothness

Using the same laser parameters, pellet, and deposition conditions described in section 8.4, with a constant oxygen partial pressure (0.05mbar), several thin layers were deposited on MgO (001) single crystal substrates. A rapid thermal annealing process has been adopted to observe the annealing effect on the size distribution of droplets. The deposited films on MgO(001) single crystal substrates were inserted within 5 minute into heated furnace at the required temperatures, left for 20 minutes and then quenched back to room temperature in flowing nitrogen. Using SEM, the films were analysed to observe the droplet distribution. The results are presented in figure 8.19 and 8.20 and tabulated in tables 8.4 and 8.5.

The smoothness is effected due to the presence of small crystallites and droplets on the surface of thin layers. As the annealing temperature increases the partial disintegration of droplets starts that can also increase the number density of small particles. This kind of recrystallisation and disintegration appear prominently at 800°C.

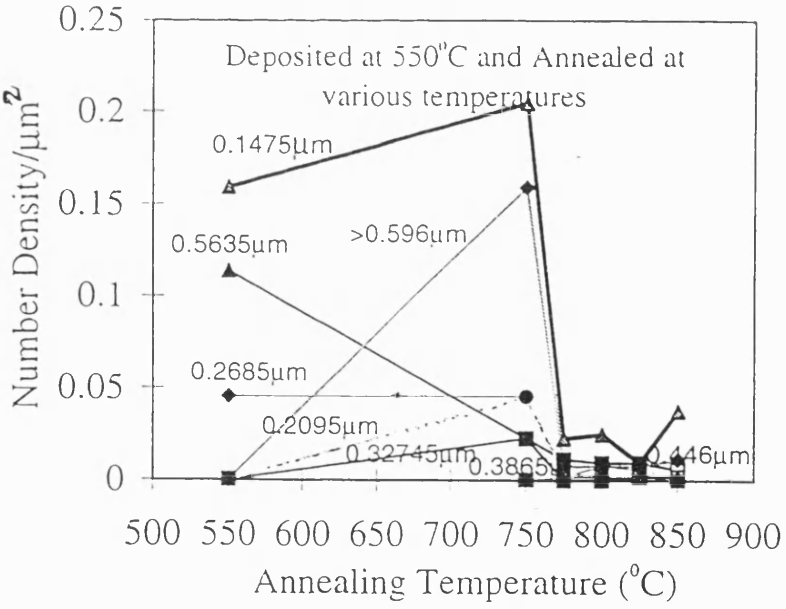

Figure 8.19. *Smoothness variations (droplets and out growth) with high temperature annealing.*

At 850°C, the droplets disappear but the roughness appears due to melting of droplets and during scanning of the SEM pictures, the dark spaces in between the crystals are considered as droplets by the computer programme. This is the reason the tables and figures are showing some particles above the annealing temperature of 825°C whereas

droplets were completely disintegrated. The situation is not different when the films were deposited at room temperature and annealed in nitrogen at various temperatures. Large sizes of out-growing crystals were appeared but decreased with annealing temperature and area found to be minimal at the annealing temperature of 850°C.

Table 8.4. *The number-density of droplets and out-growth of different radii found on the surface of thin layers annealed in nitrogen at various temperatures after PLD at 550°C in 0.05mbar oxygen.*

Number-density of droplets plus out-growth (number/μm^2)						
Radius of droplet (μm) ↓ Annealing → Temperature	0Ca4 S1 550°C	5Ca4 S2 750°C	2Ca4 S3 775°C	4Ca4 S4 800°C	3Ca4 S5 825°C	6Ca4 S6 850°C
0.118-0.177	0.1592	0.2046	0.0226	0.025	0.0094	0.0376
0.183-0.236	0.0	0.0227	0.0113	0.0094	0.0094	0.0057
0.242-0.295	0.0455	0.0454	0.002	0.0075	0.0056	0.0019
0.3009-0.354	0.0	0.0	0.0038	0.0	0.0019	0.0057
0.360-0.413	0.0	0.0454	0.0038	0.0019	0.0019	0.0019
0.420-0.472	0.0	0.0	0.0019	0.0	0.0056	0.0019
0.478-0.531	0.0	0.0	0.0019	0.0019	0.0019	0.00
0.537-0.590	0.1137	0.0227	0.0	0.0	0.0019	0.0019
>0.596	0.0	0.1591	0.0075	0.0076	0.0075	0.0113

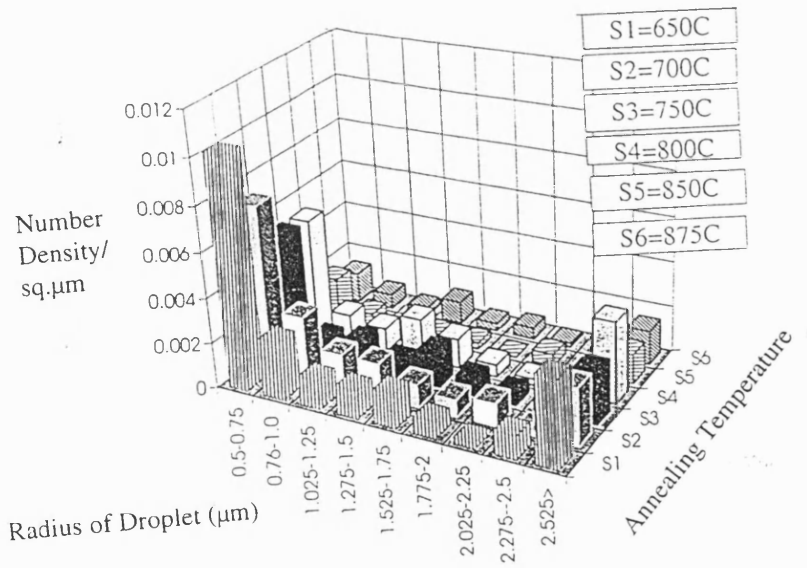

Figure 8.20. *Smoothness of room temperature deposited layers and annealed for 25 minute in N_2 at various temperatures.*

Table 8.5. *The number-density of droplets of different sizes found on the surface of thin layers annealed in nitrogen at various temperatures after PLD at room temperature.*

Number-density of droplets (number/μm^2)						
Radious of droplet (μm)↓ Annealing → Temperature	r1026 S1 650°C	r1025 S2 700°C	r1024 S3 750°C	r1023 S4 800°C	r1022 S5 850°C	r1021 S6 875°C
0.5-0.75	0.01021	0.00741	0.00536	0.0050	0.00179	0.00131
0.76-1.0	0.00265	0.00281	0.00102	0.00127	0.00051	0.00065
1.025-1.25	0.00128	0.00153	0.00128	0.00102	0.00	0.00033
1.275-1.5	0.00128	0.00153	0.00077	0.00179	0.00026	0.00098
1.525-1.75	0.00153	0.00102	0.00153	0.00128	0.00026	0.00033
1.775-2.0	0.00077	0.00077	0.00077	0.00051	0.00	0.00049
2.025-2.25	0.00256	0.00102	0.00051	0.00026	0.00051	0.00016
2.275-2.5	0.00102	0.00026	0.00051	0.00025	0.00	0.0
2.525>	0.00300	0.00256	0.00230	0.00200	0.0013	0.00147

8.6.1. Large area deposition

Another important factor is the large area deposition that is required for antennas, coplanar coils, filters where the dimensions are determined by wave lengths, and even for small devices like SQUIDs, large-size thin layers are desirable for commercial purpose. Stoichiometry and thickness uniformity are the problematic to get large area deposition due to forward nature of plume. Neifield et al.[32] have shown that the ejected particles, follow a profile of the form $\cos^n\phi$, where n can be large, typically 10 to 11 and ϕ is the angle between the surface normal and the direction of the ejected particles. The atomic mixture in $\cos^{10}\phi$ case is nearly identical to that in the bulk material and also insensitive to the incidence angle of the laser beam [33]. In PLD the working pressures for Y-Ba-Cu-O are in the range of 0.2-0.6mbar whereas for Pb-2213 material, it could be reduced (0.02-0.004mbar), forcing the use of a source-to-substrate distance of 3-10cm. If the pressures are reduced to enlarge the length of the plume that allows a large source-to-substrate distance, it still would not yield a uniformly stoichiometric film over a large area because of the directional nature of the plume [34].

A series of attempts has been made to obtain uniformly large-area deposition [35, 36, 37]. The synthesis of uniformly deposited area of 4 inch diameter of $YBa_2Cu_3O_7$ material on MgO substrate, using reactive co-evaporation process and spinning wafer technique has been

reported by P.Berberich et al.[37]. The reactive co-evaporation process has been well suited for large-area deposition, because of cosϕ profile of the evaporant where a large source-to-substrate distance (25 to 40cm) could be used. They obtained an average deposition rate 0.2nm/s, $T_{c,zero}$ of 86K and critical current density $2x10^6 A/cm^2$.

Recently, using the PLD technique, the limitations of processing ability to get uniform and stoichiometric layers over the larger areas have been considered by different research groups [35, 37, 38, 39, 40]. The deposition of the directional plume can be swept over a surface of arbitrary area by scanning the target, substrate or laser beam. V.M.Dubkov [40] has demonstrated the ability to scan the laser beam rapidly over a large area by means of external mirrors making it possible to synthesise multielemental compounds and to improve the thickness uniformity of a film over a large area.

J.A.Green [39] used computer programme of laser beam scanning over left or right-half of the major chord of a big pellet of 9cm diameter by decreasing or increasing the angle of incidence by 3.5°, made by the laser beam (248nm, KrF, 30Hz, $1J/cm^2$) with respect to the normal on the target surface, and deposited 3 square inch smoother area. Due to the large focal length of the lens and the large distance between the lens and target (~0.96cm), the spot-size and therefore the fluence could not vary by more than 5% as the beam is rastered from target centre to edge.

Scanning or rotating the substrate has allowed large-area deposition with good uniformity over the substrate larger than 2.5 inch diameter [39, 41]. Using a simple rotation of substrate mounted off-axis with respect to the centre of the plume, two inch diameter $LaAlO_3$ substrates were coated [42] with $YBa_2Cu_3O_7$. An excellent uniformity was claimed by the closeness of the transition temperature from 89 to 91K at four different places.

Simple target scanning has already been used by several authors just tilting the target so that the laser beam and hence the resulted plume can scan due to rotation of the target. In this technique, the pellet is mounted at a tilt angle (17° to 30°) with respect to the rotation axis. The plume wobbles during deposition and deposited area enlarges from 1 to $2.5cm^2$ [43, 44, 45]. Brown et al. [43] shown that due to wobbling plume, thickness 'd' is a function of the angle of tilt and the distance between the substrate and the target. They have demonstrated a large uniformity in area on the cost of thickness that came down from 1.0 to 0.25μm in $1x10^{-2}$mbar chamber pressure, measured by Talystep (resolution 10Å) covering $2.5cm^2$ central

region deposited by using the pellet mounted at a tilt angle of 30° with respect to the axis of rotation at 2.5cm away from the target.

8.6.2 Four sided deposition and uniformity

To increase the uniformity and larger area of deposition, a special geometry of substrate holder with four walls made of stainless steel was prepared (later it will be called as pigeon hole geometry, PG) and held in front of ablated target in such a manner that the plume enters into the container, where it touches the wall number 2 and 3 and facing wall number 1. The position of number 4 wall was adjustable by sliding it towards the plume or away from it. An important advantage of PG is the possibility of four-sided film preparation. The experimental set-up has been shown in figure 8.21.

The Si (111) substrates were cut and fitted on each wall nearly of the same dimensions. Initially, the deposition on each substrate at room temperature was obtained in different oxygen pressures, keeping all other parameters constant. The photographs presenting the uniformity of each film on silicon has been shown in figure 8.22, as well as simulation and measurements for four sided substrate.

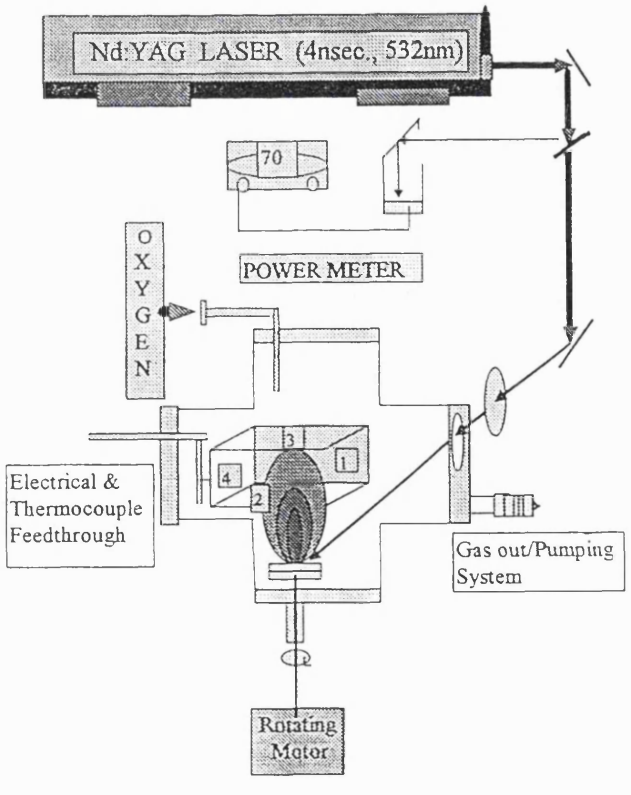

Figure 8.21. Experimental set-up shows the four sided deposition using PG substrate holder.

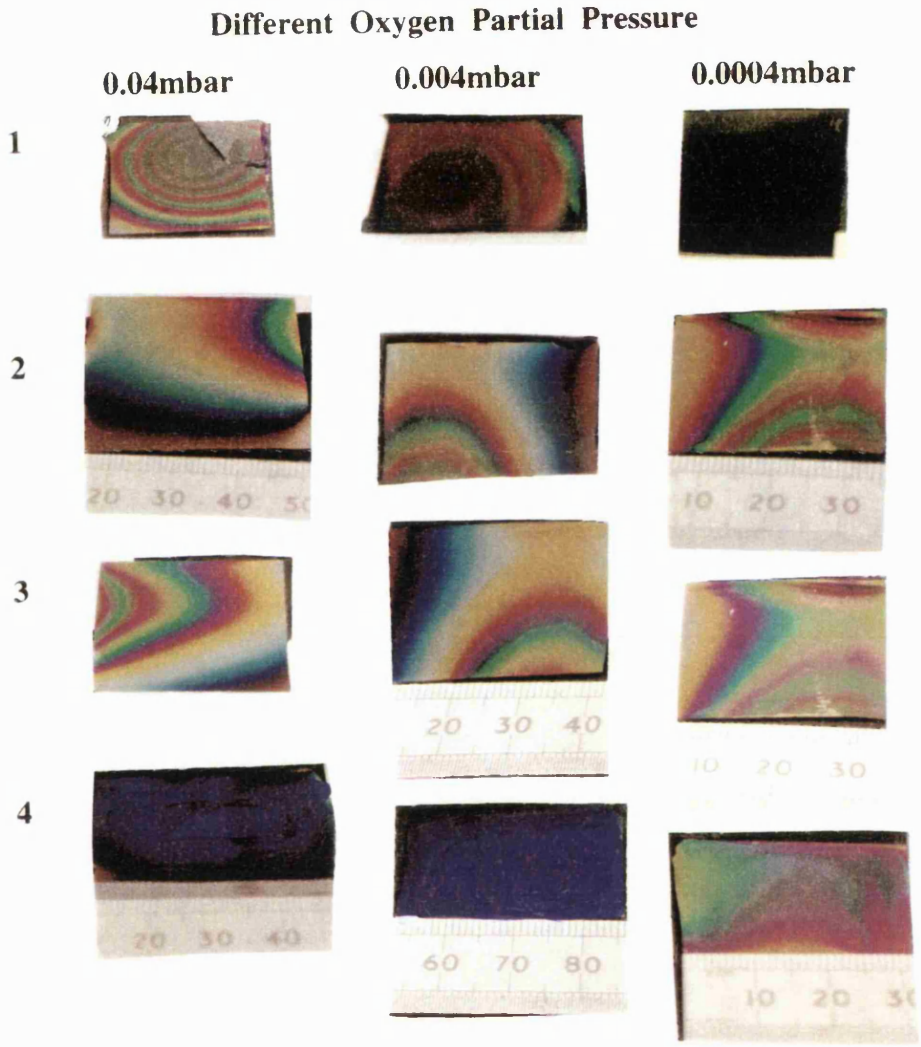

Figure 8.22-a. *Thickness uniformity along four sides of the plume in various oxygen partial pressures.*

Later, the information obtained from deposition on Si(111) substrate in $4x10^{-3}$mbar oxygen pressure was used to deposit thin layer on MgO(001) substrate by placing them at the thickest and stoichiometric parts on Si. The deposited layers on MgO(001) along four sides of PG were annealed in N_2 and characterised for resistive transition temperatures (figure 8.23). By adjusting the wall number 4 at different positions, for example out of the plume, by just touching the visible plume and inside mid of the plume, where the substrate cuts the plume into two parts along its direction of motion, several depositions were made first on Si and then on MgO(001) substrates and characterised. The thickness increases gradually when the substrate slides towards the mid of the plume.

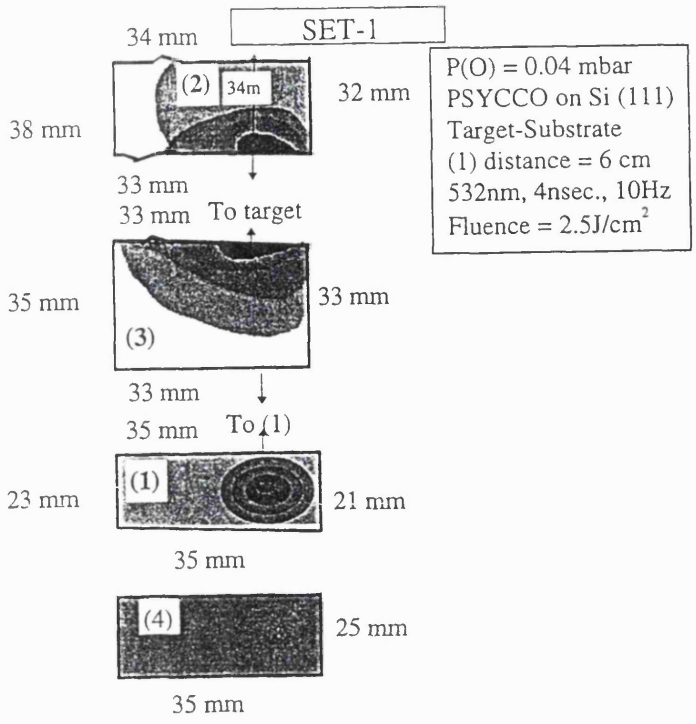

Figure 8.22-b. Thickness uniformity along four sides of the plume and dimension of substrates

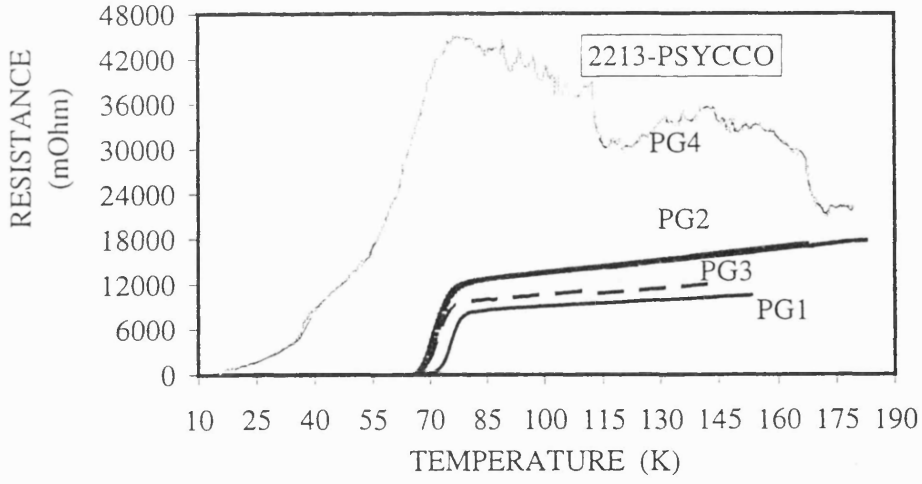

Figure 8.23. Resistance versus temperature of the films grown along the four sides of the plume.

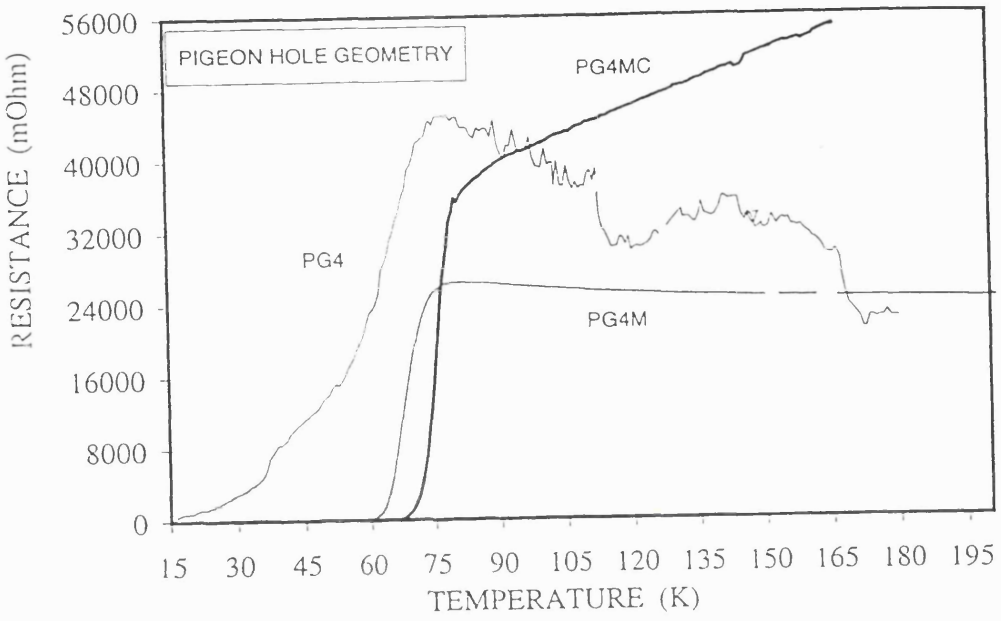

Figure 8.24. Resistance versus temperature of the films grown at different positions by adjusting the wall-four in PG substrate holder.

The deposited layer near the target was multi-coloured, but after few centimeters in length on the substrate, the deposition was found as dark bluish spreading over further 2 to 3cm in length. Figure 8.24 shows the transition temperatures of the films deposited at room temperature and then annealed in N_2 ambient.

Deposition of plume at an angle of 25°

Figure 8.25 shows the resistance versus temperature of the films deposited within the plume at various positions by cutting the forward directed plume at angle of 25°with respect to the normal on the target surface and parralell to incoming laser beam. This kind of front deposition gave an idea about the suitable place of stoichiometric transfer, and better superconducting properties. One MgO (001) substrate (1) was facing the central portion of the plume at an angle of 25° exhibited $T_{c,\ onset}$ around 75Kand $T_{c,\ zero}$ of 70K. 1cm above the centre and along the perpendicular direction of plume (4), the deposited thin layer has the

same onset transition temperature but $T_{c,\ zero}$ of 58K. The situation is similar in the case of placement of substrates 1cm right (3) or left side (2) of central-substrate along the horizontal line, where the $T_{c,\ zero}$ is of 54K and 62K respectively. This experiment shows that one can obtain a maximum superconducting transition temperature by depositing central portion of the plume, even at an angle of 25°, but the outer portions of the plume within 2cm range look non-stoichiometric.

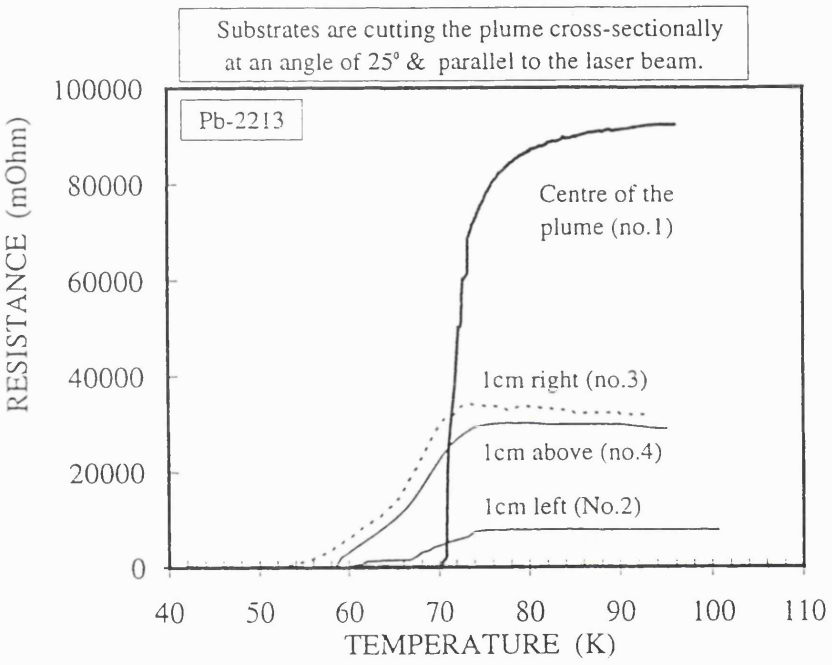

Figure 8.25. Resistance versus temperature of the films deposited within the plume at an angle of 25°.

8.6.3 Mid-plume deposition

Using the knowledge of previous experiment, a set of substrates of 7x7mm size was pasted at different distances on a 15cm flat substrate holder. The substrate holder was placed in such a way that it was cutting the plume in two parts in the forward direction, the one end of it was nearly touching the burn spot inside mid of the plume, and another end tilted out of the plume by 5-10°. A 3 cm long Si(111) substrate was placed to deposit central core of the plume before the MgO(001) substrates which were coated uniformly as inferred from the blue colour and the measured thickness using ellipsometry. The deposition on Si(111) substrate was found as multicolour and non-uniform. It is observed that inclined substrate holder outward by 5° from central portion of the plume, compensates the stoichiometric uniformity over a length of 12cm. However, the width of the deposited films was more than 0.7cm over the

substrate holder. The technique used to deposit uniform and larger area has also resulted a good control over the droplets just simply depositing the central core of plume over a Si-substrate, where most of the droplets of mid-plume and adjacent to the target were stopped. The droplet-density within a few centimetres away from the target also drops to nearly zero in this arrangement (figure 8.26). This set-up shows that a 12cm long tape (0.7cm wide) can be used to deposit uniformly without or a few droplets in minimum possible time that is not possible in front deposition even using more expensive techniques of droplet filtering.

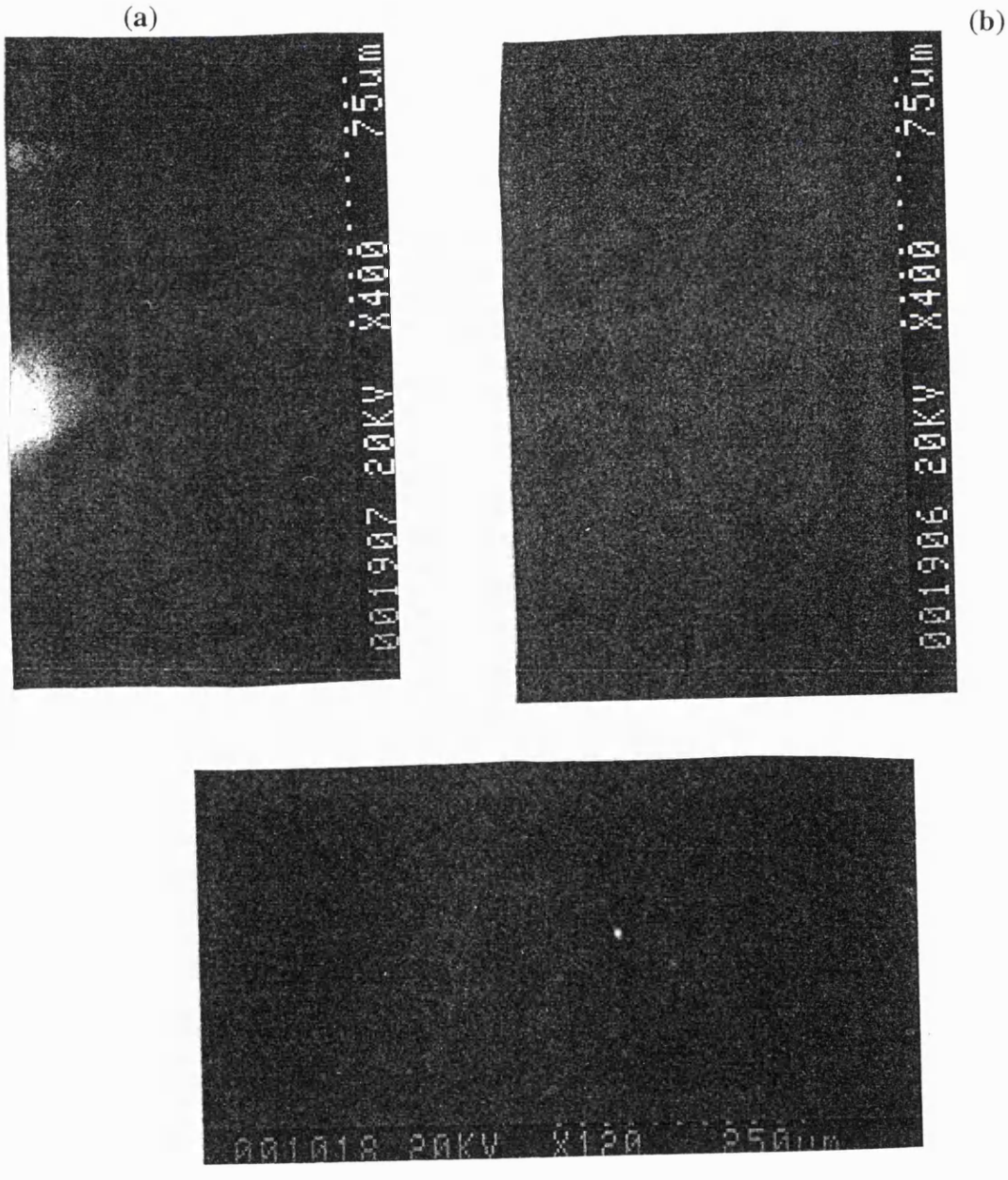

Figure 8.26. SEM micrograph of superconducting thin layers at different distances (a) 4cm (b) 9cm (d) 12cm inside mid of plume.

Figure 8.27 shows resistive transition versus temperature of the films deposited at various distances and inside-mid of the plume. Figure 8.28 shows the XRD pattern of one of the film deposited at 9cm away from the target and ex-situ annealed in nitrogen. The layer shows highly c-axis texturing and a lattice parameter, c=15.8Å.

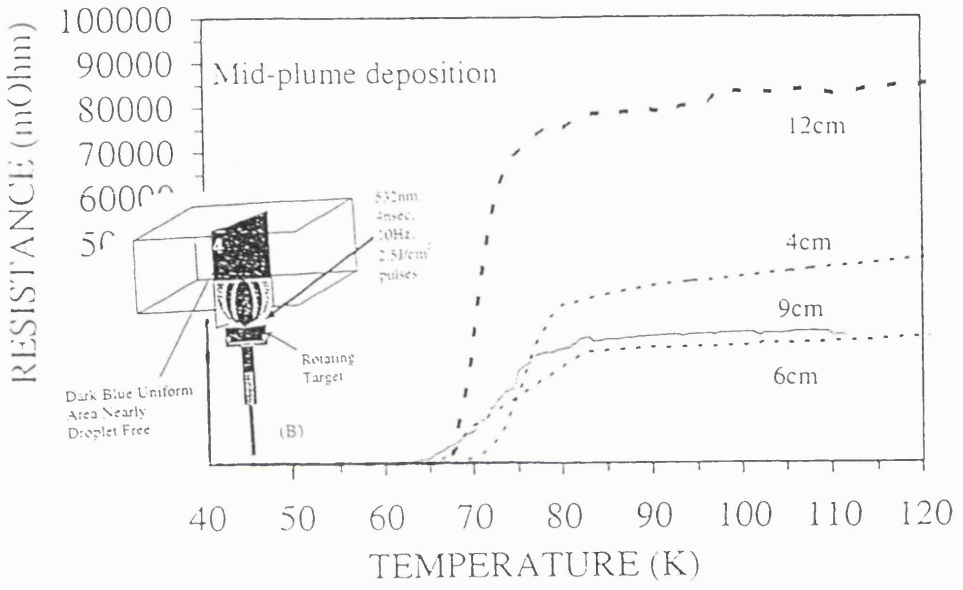

Figure 8.27. Resistance versus temperature of the films deposited inside-mid of the plume at different distances with minimum droplets.

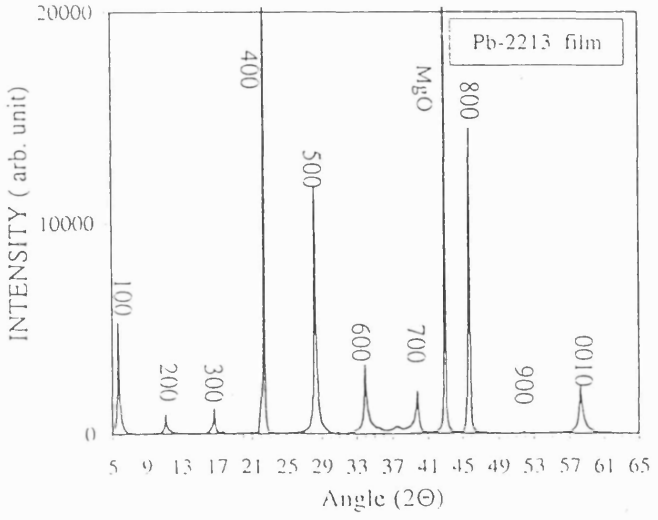

(a)

Figure 8.28. XRD pattern of the film grown at 9cm after ex-situ annealing.

Table 8.6. Thickness of the deposited layers on Si(111) substrates at various distances inside-mid of the plume.

Distance from the target to substrate placed inside mid of plume. (cm)	Thickness of the film (Å)
4	1063
6	1042
9	1038
12	1013

```
PR   210020
DE  =351.17  PSI=51.92

NL  1.8550
TL  1013  C
      TL  ORDERS:
#0  1013          #5=10904
#1  2991          #6=12882
#2  4969          #7=14861
#3  6948          #8=16839
#4  8926          #9=18817
OR  L=1978

PR   210020
DE  =332.46  PSI=44.58

NL  1.9130
TL  1042  C
      TL  ORDERS:
#0  1042          #5=10537
#1  2941          #6=12435
#2  4840          #7=14334
#3  6739          #8=16233
#4  8638          #9=18132
OR  L=1898

PRG 210020
DEL=305.25  PSI=25.08

NL  2.1650
TL  1063  C
      TL  ORDERS:
#0  1063          #5=9172
#1  2685          #6=10794
#2  4306          #7=12416
#3  5928          #8=14038
#4  7550          #9=15660
OR  L=1621

PR   210020
DE  =344.46  PSI=51.67

NL  1.8480
TL  1038  C
      TL  ORDERS:
#0  1038          #5=10982
#1  3027          #6=12971
#2  5015          #7=14960
#3  7005          #8=16949
#4  8993          #9=18938
OR  L=1988
```

Ellipsometeric results (computer print-out).

8.7 Summary

The possible mechanism of ablation and cone formation has been discussed in detail. The problem of droplet emission causes roughness on the surface of thin layers, and has been considered in terms of the effect of shock-waves, superheating and micro-explosions.

It is demonstrated that the ablated mass is strongly dependent on the physical and chemical nature of the targets. It is also found that the Pb-2213 material is more ablative compared with Y-Ba-Cu-O or Bi-Sr-Ca-Cu-O materials. The effect of laser energy and spot size on the amount of ablated mass has been demonstrated. The number density of droplets with the change in spot size was found different. It is also presented experimentally that for the constant laser energy, the bigger spot-size can reduce the number density of droplets, whereas the cone formation and their sizes are also related with the spot-sizes found during the ablation of Pb-Sr-(YCa)-Cu-O material.

It is also demonstrated that rotating targets are more ablative compared with a stationary target. The reason could be the possible segregation (that creates oxides of higher heat of sublimation) due to increase in number of ablating pulses per unit area in case of non-rotating target. The ionic species of the ablated materials from Pb-2213 target were detected and isolated using a modified cylindrical mirror analyser (CMA) and quadrupole mass spectrometer (QMS). An experimental set-up and various experimental parameters were described. The achieved results show that the atomic and molecular species of various isotopes, ions and neutrals and their energies were determined using a combination of modified CMA and QMS filters. It is also observed that the oxides of constituent elements of Pb-Sr-(YCa)-Cu-O material were not found in the plume. Low and high energy neutrals as well as singly and doubly charged ions of constituent elements of Pb-2213 phase were detected using CMA/QMS analysing system.

In this chapter, thickness and compositional uniformity, roughness due to large solid particles was addressed and attempted to solve these main problems in simple mode so that better large area deposition could be achieved using PLD in simple mode of deposition. The superconducting transition temperatures of the deposited thin layers at various positions within the plume show that the maximum values could be achieved for the deposition within the central portion of the plume. The smoothness of the thin layers varies with respect to the position of deposition. The droplet density can also be varied by changing the oxygen partial pressure other than laser parameters. The droplet sizes and densities can also be changed and better smoothness can be achieved by high temperature annealing for short durations (800°C/20minutes).

An unusual approach has been used for the smooth and large area deposition. The smooth and textured film has been grown using Nd:YAG laser and placing inclined substrate inside mid of the plume after stopping large sized droplets near the target. The films were ex-situ annealed in air and nitrogen shown high texturing but slight deviations in superconducting transition temperature were observed, could be a reason of small deviation over a long distance (3-12cm).

Reference

[1] C.C.chang, X.D.Wu, R.Ramesh, X.X.Xi, T.S.Ravi, T.Vankatesan, D.M.Hwang, R.E.Muenchausen, S.Foltyn, and N.S.Nogar, Appl. Phys.Lett. 57, 1814 (1990).

[2] G.Koren, R.J.Baseman, A.Gupta, M.I.Lutwyche, and R.B.Laibowitz, Appl. Phys.Lett. 56, 189 (1990).

[3] D.L.Lin, X.Li, Z.D.Lui, T.F.George, J.Appl.Phys. 72, 4227 (1992).

[4] D.H.A.Blank, R.P.J.Ijsselsteijn, P.G.Out, H.J.H.Kuiper, J.Flokstra and H.Rogalla, Mat.Sci.Eng. B, 13, 67(1992).

[5] R,K.Singh, D.Bhattacharya and J.Narayan, Appl.Phys.Lett. 57, 2022 (1990).

[6] J.F.Ready, "Effect of High Power Radiation", Academic Press, New York (1971).

[7] T.P.O'Brien, J.F.Lawler, J.G.Lunney and W.J.Blau, Mater.Sci.Eng. B13, 9(1992).

[8] D.Bhattacharya, R.Singh, and P.Holloway, J.Appl.Phys.70, 5438, (1991).

[9] O.Eryu, K.Murakami, K.Masuda, A.Kasuya and Y.Nishina, Appl.Phys.Lett. 54, (1989).

[10] H.Sankur, J.Denatale, W.Gunning, and J.G.Nelson, J.Vac.Sci.Technol., A5, 2869 (1987).

[11] P.E.Dyer, R.D.Greennough, A.Issa and P.H.Key, Appl.Phys.Lett 53, 534, (1988).

[12] M.Thompson, S.Chenery and L.Brett, J.Analytical Atomic Spectroscopy, 5, 49 (1990).

[13] S.Fujimori, T.Kasai, and T.Inamura, Thin Solid Films 92, 71 (1982).

[14] S.Kuper and J.Brannon, Appl.Phys.Lett. 60, 1633 (1992).

[15] J.T.Cheung and H.Sankur,, CRC Critical Review in Solid State and Material Science, 15, 63 (1988).

[16] D.S.Misra and S.B.Palmer, Physica C 176, 43 (1991).

[17] C.C.Chang, X.D.Wu, R.Ramesh, X.X.Xi, and T.S.Ravi, Appl. Phys. Lett. 57, 1814 (1990).

[18] C.Scarfone, M.G.Norton, C.B.Carter, J.Li, J.W.Mayer, MRS Symp.Proc.,191, 181 (1991).

[19] H.J.Schiebe, A.A.Gorbunov, G.K.Baranova, N.V.Klassen, V,I,Konov, M.P.Kulanov, W.Rompe, A.M.Prokhorov, H.J.Weiss, Thin Solid Films, 189, 283 (1990).

[20] B. Holzapfel, B.Roas, L.Schultz, P.Bauer and G.Saemann-Ischenko, Appl.Phys.Lett. 61, 3179 (1992).

[21] R.J.Kennedy, Thin Solid Films 214, 223 (1992)

[22] S.V.Gaponov, A.A.Gudkov, and A.A.Fraerman, Sov.Phys.Tech.Phys. 27, 1130, (1982).

[23] M.D.Strikovsky, E.B.Klyuenkov, J.Schubert, C.A.Copetti and S.V.Gaponov, Appl.Phys.Lett. 63, (1993).

[24] G.Koren, R.J.Baseman, A.Gupta, M.I.Lutwyche and R.B.Laibowitz, Appl.Phys.Lett.56, 2144 (1990).

[25] W.P.Barr, J.Sci.Instrum., 2, 1112(1969).

[26] J.J.Dubowski, Pro.Soc.Photo-Opt.Instrum.Eng., 668, 97 (1986).

[27] D.Lubben, S.A.Barnett, K.Suzuki, S.Gorbatkin, and J.E.Greene, J.Vac.Sci.Technol., B3, 968 (1985).

[28] T.Venkatesan, X.D.Wu, R.Muenchausen, and A.Pique, MRS Bulletin, XVII, 54 (Feb, 1992).

[29] O.Auciello, S.Athavale, O.E.Hankins, M.Sito, A.F.Schreiner and N.Biunno, Appl.Phys.Lett. 53, 72(1988).

30] L.Shi, H.J.Frankena and H.Mulder, Rev.Sci.Instrum. 60, 332 (1989

[31] P.E.Dyer, A.Issa and P.H.Key. Appl.Phys.Lett. 57, 186 (1990).

[32] R.A.Neifield, S.Gunapala, C.Liang, S.A.Shaheen, M.Croft, J.Price, D.Simons, and W.T.Hill, Appl. Phys. Letter 53, 703 (1988).

[33] J.Perrierre, E.Fogarassy, G.Hauchecorne, C.Fuchs, F.Kerherve, F.Rochet, R.M.Defourneau, C.Simon, I.Rosenman, J.P.Enard and A.Laurent, Solid

State Commun. 67, 975 (1988).

[34] T.Venkatesan, X.D.Wu, A.Inam, and J.B.Watchman, Appli.Phys.Letters 52, 1193 (1988).

[35] S.T. Foltyn, R.E.Muenchausen, R.C.Dye, X.D.Wu, L.Luo, D.W.Cooke, R.C.Taber, Appl.Phys.Lett. 59, 1374 (1991).

[36] J.A.Green, J.Vac.Sci.Technol. A10, 1821(1992).

[37] P.Berberich, B.Utz, W.Prusseit and H.Kinder, Physica C, 497 (1994).

[38] M.F.Davis, J.Wosik, K.Forster, S.C.Deshmukh, H.R.Rampersad, S.Shah, P.Siemsen, J.C.Wolfe, and D.J.Economou, J.Appl.Phys. 69, 7182 (1991).

[39] J.A.Green, J.Vac.Sci.Technol. A10, 1821 (1992).

[40] V.M.Dubkov, Sov. J. Opt. Techn. 49, 168 (1982).

[41] J.A.Greer and J.B.Hook, SPIE proceedings, 79, 1377 (1990).

[42] R.E.Muenchausen, R.C.Dye, X.D.Wu, L.Luo and D.W.Cook, Appl.Phys.Lett. 59,1374 (1991).

[43] M.Brown, M.Shiloh, R.B.Jackman and I.W.Boyd, Appl. Surf. Sci. 43, 382 (1989).

[44] P.V.Kolinsky, P.May, M.R.Harrison, P.Miller and D.Jedamzik, Supercond. Sci. Technol.1, 333 (1989).

[45] D.B.Chrisey, J.S.Horwitz, K.S.Grabowski, M.E.Reeves, M.S.Dsofsky and C. R.Gossett, Appl.Surf.Sci.43, (1989).

Chapter 9

Critical currents and lead cuprates

One of the most technological important parameters of bulk, single crystal or film superconductors is the critical current density, J_C, usually obtained through irreversible magnetisation measurements. This convenient method eliminates contact problems often made using silver paste for measuring transport critical current density. Magnetic measurements provide an average over all closed current loops within a superconducting sample, while transport measurements follow the easiest and strongest current paths between the voltage contacts. Therefore, magnetic measurements are useful with samples that show a large degree of inhomogeneity such as granular superconductors. In this chapter, the estimated critical current densities through magnetisation measurements of different bulk compositions and thin films have been included.

The magnetic measurements were made using a Vibrating Sample Magnetometer (VSM). The basis of these experiments is that the variations in circulating screening currents are induced in superconductors by the change in applied magnetic fields. These screening currents have a dipole moment 'm' that can be detected by the VSM. For a single current loop, 'm' is defined as

$$m = I\,a \qquad (9.1)$$

Where 'I' is the current flowing in the loop and 'a' is the area enclosed by the loop. The magnetic dipole moment of the sample will be due to the sum of all current loops in the sample. The magnetisation 'M' of a sample is the magnetic dipole moment normalised by the volume 'V' of the sample, so that

$$M = m/V \qquad (9.2)$$

9.1.1 The Bean Model

Type II superconductors are distinguished by the penetration of an applied magnetic flux in the form of magnetic vortices or flux lines above a certain

applied field 'H'>H_{c1}. Any change in the density of these flux lines can result in a net current density, J, flow according to Ampere's Law:

$$\nabla xH=J. \qquad (9.3)$$

The flux lines feel a Lorentz force, F_L, where

$$F_L=JxB \qquad (9.4)$$

that drives them to a uniform density profile and tends towards an equilibrium state in which no macroscopic screening currents are present. However, if the flux lines are pinned they can resist the Lorentz force and the flux density decreases towards the sample and a net macroscopic screening current can be set up. At some point the magnetic field becomes large enough that the Lorentz force can be depinned the flux lines. At this point the magnetisation in the hysteresis loop becomes reversible and provides irreversibility line.

In order to explain the irreversibility of the magnetisation of type II superconductors, C.P.Bean proposed a simple model that allows one to estimate the critical current of the superconducting sample [1]. He assumed that there is a maximum $J_c(H)$ or critical current density that any electromotive force (e.m.f.), however small, will induce a full current density to flow locally. There are possible states of current flow for a given axis of magnetic field: zero current in those regions which have not experienced the magnetic field; and full current flow perpendicular to the applied field axis in those that have the sense, depending on the e.m.f. resulting from the last local change of the field. In the simplest form the Bean model assumes that for any value of e.m.f., current density, J= $\pm J_c$ or 0 and is independent of H. Upon increasing the applied magnetic field a point is reached where the magnetic flux density becomes non-zero at the centre of the sample and the sample is said to be fully penetrated. For example consider a flat superconducting disc, of radius, R and thickness, t, as shown in figure 9.1.a, a screening current flows within a thickness δr from the edge of the sample as the flux penetrates δr into the sample. The process of flux penetration is shown in figure 9.1.b. As the field direction is reversed the process reverses the direction of circulating currents.

The circulating currents are set up in a ring δr from the edge, and grow towards the centre wiping out the existing memory. From this simple model the entire magnetisation loop can be predicted.

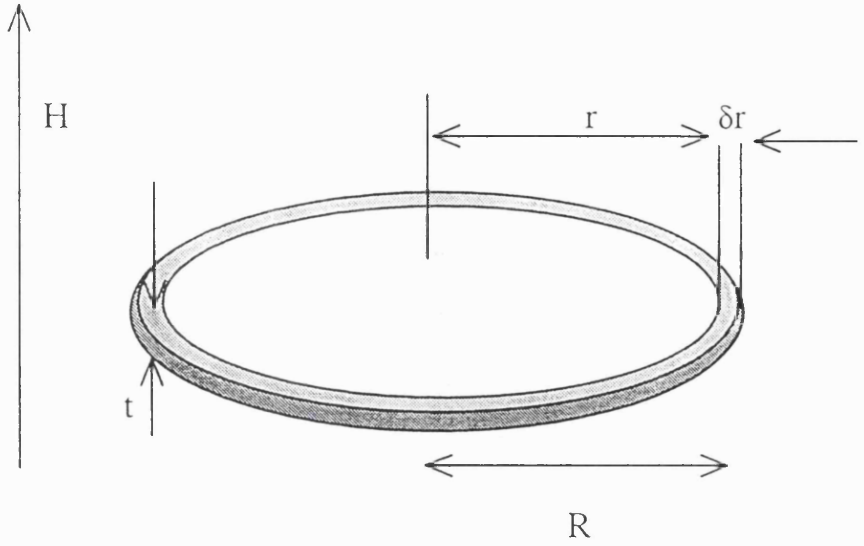

Figure 9.1. *A) A superconducting disc with flux to penetrate. The screening currents flow in a ring δr from the edge.*

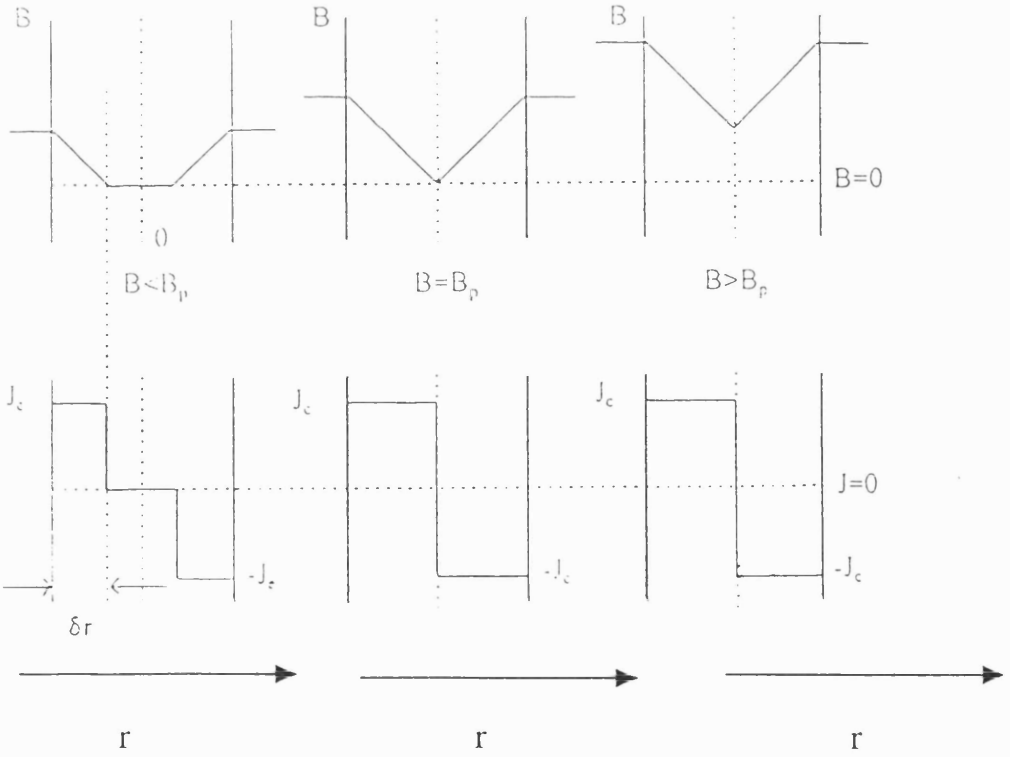

Figure 9.1. *B) Current and field for a superconducting disc as the field penetrates the sample.*

The existence of flux pinning in a material sets up screening currents and a magnetic moment, m, develops. By integrating over a series of current loops within the sample one obtains:

$$m = \int_0^R \pi r^2 J t dr \qquad (9.5)$$

or

$$m = \pi t J R^3/3. \qquad (9.6)$$

J is the parameter one is generally interested in and its behaviour depends on the electric field, temperature and magnetic fields. Once fully penetrated the sample can be considered to have concentric current loops and said to be in the Bean Critical State. The hysteresis in m, Δm, can thus be written as:

$$\Delta m = 2/3\ JVR \qquad (9.7)$$

Usually, the change in normalised magnetisation, $\Delta M(H)$, is taken between the magnetisation measured in increasing $M\uparrow$ and decreasing $M\downarrow$ fields, $\Delta M = (M\uparrow - M\downarrow)$. The J_c is assumed to be uniform over the sample, so that the sample volume, V, change in irreversible magnetisation, ΔM, are related as:

$$J_c = 3\ \Delta M/2R \qquad (9.8)$$

while for a thin layer or slab of thickness, D,

$$J_c = 2\ \Delta M/D \qquad (9.9)$$

9.1.2 Vibrating sample magnetometer

The vibrating sample magnetometer (VSM) is in principle a simple instrument. It operates by vibrating a sample in a uniform magnetic field, and measuring the e.m.f. induced in a pick-up coil that is a set of two differentially, antisymmetrically wound coils close to the sample [2]. The e.m.f. is caused by the magnetic flux variations inside the coil (Faraday's Law), and hence can only be due to the motion of the magnetic sample and not to the applied field. The noise level of the system can be greatly reduced by filtering out signals away from the vibration frequency. Typical noise level are 10^{-8} to $10^{-9} Am^2$. It is important that the pick-up coil does not move relative to the magnet,

otherwise the applied field will then contribute directly to the e.m.f. Reducing the vibration coupling between the sample vibrator and the rest of the mechanical assembly is therefore an important aspect of VSM design. Another important area of design is the pick-up coil arrangement, where the inductive coupling between the sample and the coils needs to be maximised [3, 4,5].

9.1.3 Squid magnetometers

Other types of magnetometer such as SQUID magnetometer are also available. The SQUID magnetometer measures the total flux inside a detection coil. A magnetisation measurement is achieved by measuring the flux density both with and without a sample inside the coil. The scan length is the distance that the sample is moved between these two settings. In some commercial systems this scan length can be as much as 13 cm. The SQUID is in fact a much more sensitive device than the VSM (typical noise level ~10^{-12} Am^2) but the sample has to be moved in and out of the coil for each measurement. This reduces the speed of measurement, and can cause problems if the field is not homogeneous over the distance that the sample is moved since then the sample will be swept through a small field cycle on every scan.

9.1.4 Vortex pinning

In the range of an applied magnetic field $H_{c1}<H<H_{c2}$, a tube of flux-bearing normal state material occurs in the superconductor. A tube of material is called a vortex or filament, and at its centre the superconducting order parameter ($K= \lambda/\xi \rightarrow 0$) reaches zero. The current circulating around a vortex makes each vortex act like a tiny bar magnet. Repulsion occurs between vortices according to the Lorentz force, JxH, on the magnetic field of another vortex. The vortex-vortex repulsion can arrange vortices in the form of a hexagonal or triangular shape called a flux lattice or an Abrikosov lattice. If there is no pattern of vortices then the randomness of the vortices is called a flux glass. The repulsive vortex-vortex forces oppose independent vortex motion and below a

certain temperature $T_g(H)$, the system remains frozen in cuprate superconductors where the resistance of the sample, R'=0. If the vortices can move freely, it is not possible to pass a current without dissipation. Therefore, to achieve a finite critical current the vortices are pinned or prevented from moving within the superconductor. Resistanceless superconductors for $H_{c1}<H<H_{c2}$, can be achieved only if the vortices are strongly pinned and techniques that pin the vortices are important for high field and current applications. The pinning of vortices usually occurs due to inhomogeneities of the material, such as impurities, grain boundaries, voids, dislocations, non-superconducting precipitates etc.,. In order to be efficient, pinning the inhomogeneities has to be of the order of ξ or λ where a local variation of the parameters and the energy of the flux tube changes accordingly and the vortices become pinned to the energetically more favourable sites that stops the flux motion and decrease in critical current density.

9.1.5 Experimental procedure

All the measurements were carried out on bulk or thin PSYCCO layers to trace m-H loops using a commercial vibrating sample magnetometer (Model 3001), supplied by Oxford instruments Ltd. The applied magnetic field, H, was always perpendicular to bulk sample or parallel to the c-axis of oriented films.

9.2.1 Pb-2213 phase films and critical currents

Excellent thin layers of different materials can be grown by several deposition techniques onto various substrates. It has already been described (in chapter three and six) that the lead based materials have complexities of different phase formation, impurities as well as sensitive transitional behaviour towards the oxygen content. Thin superconducting layers grown on MgO (001) substrate using the PLD and ex-situ N_2 annealing procedure described earlier (chapter) provided highly c-axis oriented texturing with $T_{c,onset}$ of 78K and $T_{c,zero}$ of

65K. This is the highest reported superconducting transition temperature for Pb-2213 single phase layers so far by any technique.

An excess of oxygen defects plays an important role in lead based materials. For example, in the Pb-2213 phase, the oxygen content can be raised from 8 to 9.9 and vary the superconducting behaviour, eventually turning the material into an insulating antiferromagnetic state at maximum oxygen levels. This is opposite to what happens with the $YBa_2Cu_3O_{7-\delta}$ material. Therefore, oxygen rich defects can behave as pinning centres similar to the oxygen deficient defects in $YBa_2Cu_3O_{7-\delta}$.

Figure 9.2 (a and b) shows the m-H hysteresis loops and current density obtained at various temperatures. For applied fields in the 0-0.5 tesla range, J_c decays exponentially for fixed temperatures of 15K and 35K, and then becomes nearly constant with the slope (dJ_c/dH) being very minute at fields > |0.5| tesla. At 55K J_c initially decays exponentially for 0-0.1T and upon increasing the applied field it decays linearly to zero around 1.3 tesla. This field dependence of J_c is similar to that of the single crystal Pb-2213 phase reported by Metlushko et al. [6], except that the thin layer has J_c values one order higher than have the single crystals. Oxygen related defects could be responsible for the enhancement of the vortex pinning and J_c at various temperatures. Figure 9.3 shows the zero field cooled J_c behaviour with temperature for PSYCCO films, values for which tabulated in table 9.2.

The magnetisation measurements exhibit reversible behaviour over a range of magnetic fields and temperatures where flux pinning and critical currents become immeasurably small. To determine the effect of excessive oxygen on critical current density and flux pinning, another set of experiments was performed.

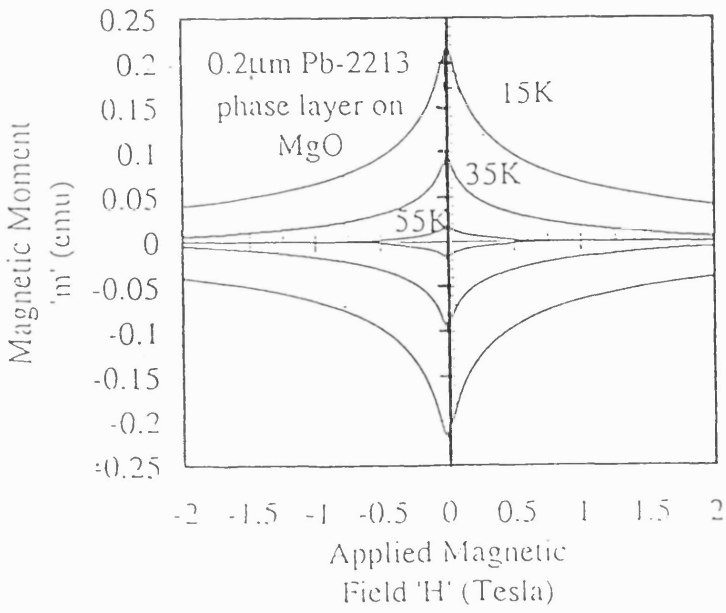

Figure 9.2. *(a) Hysteresis loops of c-axis oriented Pb-1213 phase layer on MgO (001) substrate at various temperatures.*

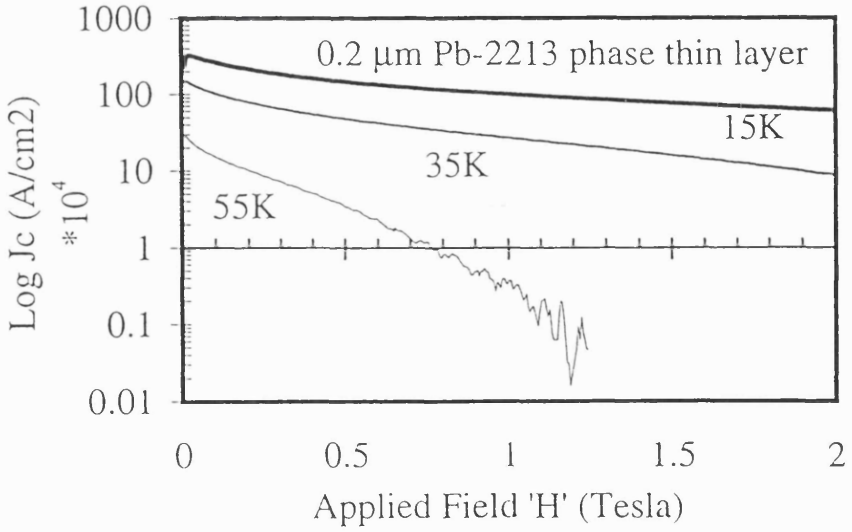

Figure 9.2. *(b) Field dependence of the critical current of Pb-2213 phase film at various temperatures.*

Table 9.1. Estimated critical current density at various fields.

Temperature (K)	J_c(zero field) A/cm^2	J_c(H=0.5tesla) A/cm^2	J_c(H=1tesla) A/cm^2
15	3.25×10^6	1.50×10^6	1.05×10^6
35	1.50×10^6	0.55×10^6	0.28×10^6
55	0.32×10^6	0.025×10^6	0.005×10^6

The Pb-2213 phase film used in experiment described above was oxidised in flowing oxygen at 700°C and converted to an insulating layer, then further annealed in nitrogen for half of the period that is required to achieve maximum $T_{c,\,zero}$. This film (with an excessive oxygen content) was characterised for J_c at various temperatures and plotted in figure 9.3 (with data presented in table 9.2 for zero field cooled).

Table 9.2. Critical current J_c (zero field) at various temperatures.

Temperature (K)	J_c(zero field) A/cm^2
10	0.90×10^4
30	0.40×10^4
60	0.09×10^4

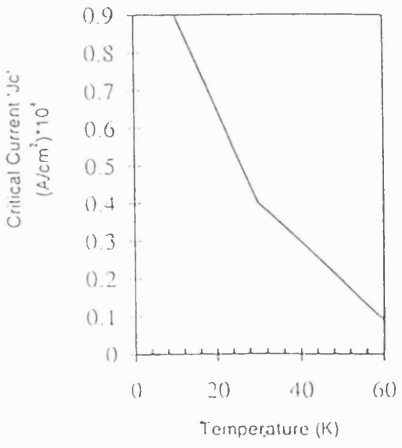

Figure 9.3. *Zero field cooled J_c versus temperature for a 0.2 μm thin layer of Pb-2213 phase material.*

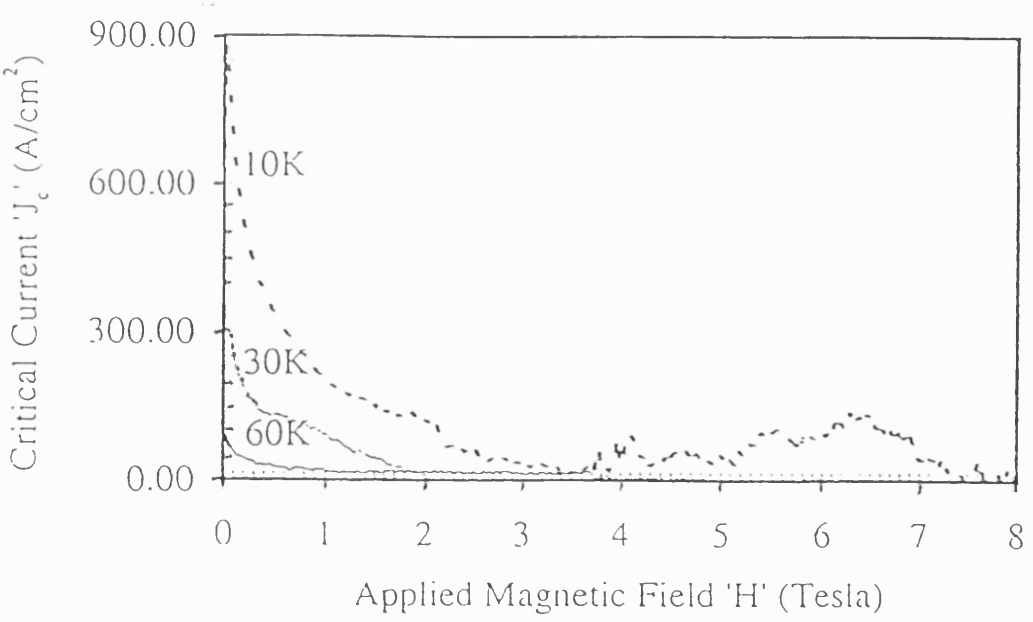

Figure 9.4. Variations in J_C with applied field at various temperatures for 0.2 μm layer after partial reduction.

From figure 9.4, it is obvious that J_C has decreased with excess oxygen content that is achieved by partial reduction of Pb-2213 layer in nitrogen. It falls sharply from 0→0.2 tesla, then a small plateau is observed before it decreases to 10A/cm^2 between 1 and 2 tesla for 30K and 60K. At 10K, the J_C varies quasi-exponentially down to 3 tesla, after a sharp fall from 0→0.2 tesla. As the field increases from 3 to 8 tesla, the J_C values increase gradually from 10A/cm^2 to 115A/cm^2 at 6.4 tesla then finally form a tail that vanishes at 8 tesla. This anomaly may be due to excessive oxygen defects that are pinned and enhance the magnetisation and the corresponding J_C values. When the applied field exceeds a certain limit, the weakest superconducting grains are driven normal, providing additional pinning centres to those already existing. This increases the magnetisation of the sample. As the field is increased, the number of normal regions is increased. At higher fields the vortex core size becomes appreciably larger than the coherence length and the order parameters are

suppressed and are unable to pin the flux. In these processes the peak in the magnetisation anomaly is created in the certain magnetic field region.

9.2.2 Pb-2213 phase bulk and critical currents

One of the superconducting bulk $Pb_2Sr_2(Y_{0.5}Ca_{0.5})Cu_3O_{8+\delta}$ samples was characterised by using VSM for magnetisation measurements to estimate J_c at various applied fields and temperatures. These results are shown in figure 9.4 and in table 9.3. The critical current density shows an exponential decay in the range of applied magnetic field from 0→0.3 tesla. Between 1 and 7.5 tesla it remains constant before decaying to zero at 8 tesla. Similarly, drastic variations in J_c in the low field regions are observed at 35K and 15K. At lower temperature (15K), the J_c values remains nearly constant as low as 50A/cm^2 from 1→8 tesla whereas at 35K, after the low field region, J_c decays linearly from 1 to 4 tesla in logarithmic scale then it achieves constant value as 1A/cm^2. The low values of J_c in the bulk with respect to the thin layers could be considered in terms of grain boundaries and oxygen non-stoichiometric effects.

Usually, low J_c values in ceramic samples of other cuprate superconductors are limited by large angle grain boundaries that can be eliminated by the melt-quenched processing technique, by forming oriented tapes or thin films. However, this material has already been synthesised above the melting point using melt assisted processing technique and bu forming a 1mm thick pellet to get better superconducting transition temperatures using shortened reduction period. It seems that it is not easy to obtain samples of single phase, weak-link free and homogeneous in composition. These J_c values for the bulk Pb-2213 phase are even higher at 65K and 2→8 tesla than the values reported by Koike et al.[7] where the maximum critical current density is 1A/cm^2 at 4.2K between 0→1 tesla fields and then it achieves 0.1A/cm^2 for 1→13 tesla fields.

Table 9.3. Critical current density of the Pb-2213 phase bulk at various fields and temperature.

Temperature (K)	J_c(zero field) A/cm^2	J_c(H=1Tesla) A/cm^2	J_c(H=2Tesla) A/cm^2
15	420	150	70
35	100	15	6
65	5.5	0.6	0.6

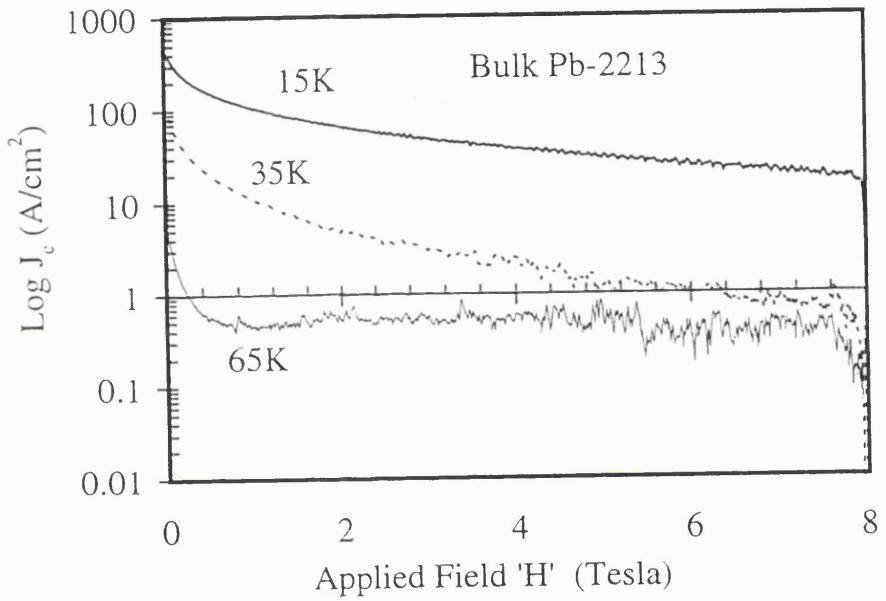

Figure 9.5. *Critical current density of Pb-2213 phase bulk at various fields and temperatures.*

9.3.1 Pb-1212 phase bulk and critical currents

One of the bulk $(Pb_{0.75}Cu_{0.25})Sr_2(Y_{0.3}Ca_{0.7})Cu_2O_{7-\delta}$ sample was synthesised at high temperature (already described in chapter 6) and characterised for J_c. The sample bearing highest superconducting transition temperature does not show any single phase. The hysteresis in magnetisation was obtained and shown in figure 9.6 (a). The m-H loop-1 remains open up to

maximum applied field, 8 tesla at 20K, at 30K the loop-2 closes at 4 tesla and at 50K it closes at 2 tesla fields only.

Some of the J_c values are included in table 9.4 and presented in figure 9.6 (b). It can be seen that the Pb-1212 phase bulk has better J_c than the Pb-2213 phase that could be due to inhomogeneity in terms of oxygen and lead stoichiometry that are more difficult to control in the Pb-2213 phase. The inset in figure 9.6(b) shows the J_c variations with low applied fields below the onset transition temperature at 77K. The J_c decays inversely from 2.8A/cm^2 to zero at 0.007 tesla. These values are typically lower than the other ceramic cuprates such as YBCCO, BSCCO or TBCCO materials at liquid nitrogen temperature. The J_c values come down drastically from 130 to 60A/cm^2 at 50K with 0→0.2 tesla applied field, 300 to 110A/cm^2 at 30K with 0→0.3 tesla and from 450 to 200A/cm^2 with the applied field 0→0.45 tesla, then variations are slow down and achieves nearly constant values after 1 tesla up to 2, 4 and 7 tesla.

Table 9.4. *Critical current density at various fields and temperatures.*

Temperature (K)	J_c(zero field) A/cm^2	J_c(H=0.004Tesla) A/cm^2	J_c(H=0.006Tesla) A/cm^2
77	2.8	0.8	0.2
	H=0	H=1Tesla	H=2Tesla
20	450	115	95
30	300	68.75	56
50	130	31.25	25

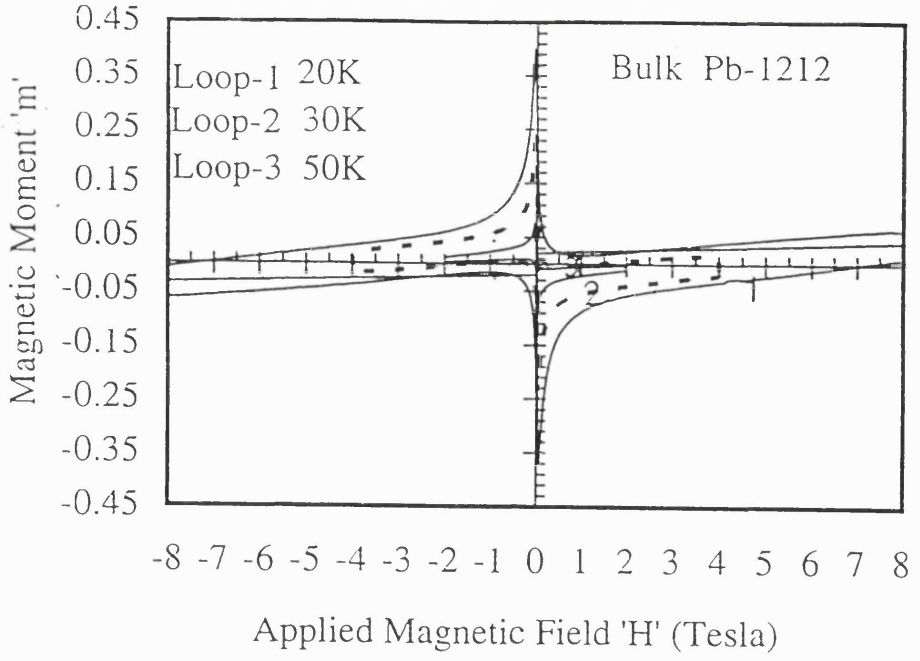

(a)

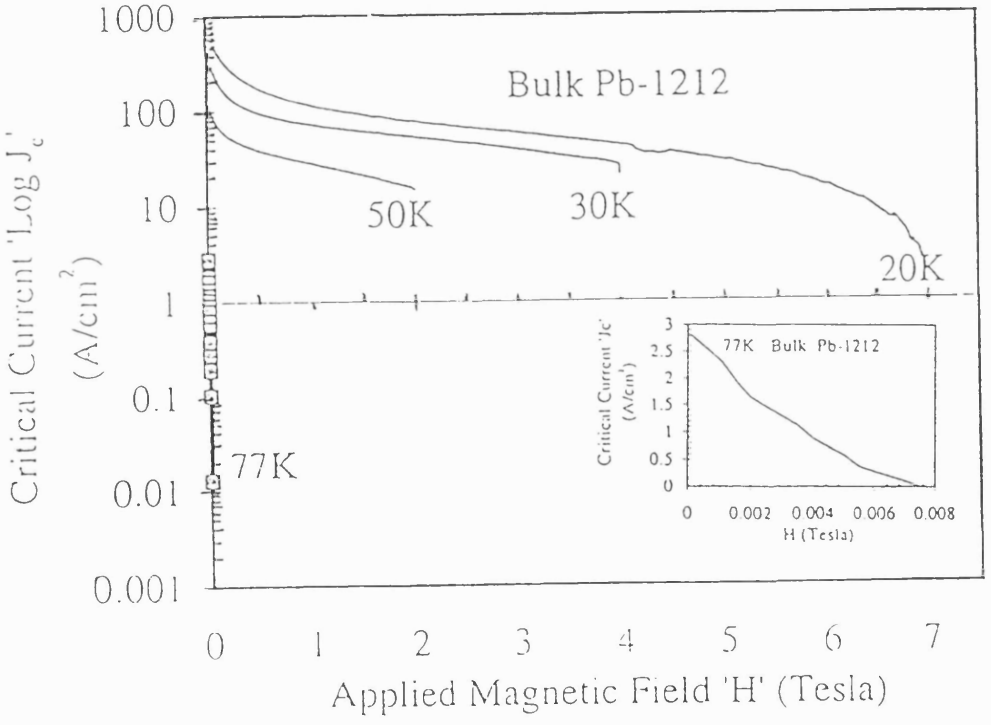

(b)

Figure 9.6. (A) Hysteresis loops at different temperature of bulk (Pb,Cu)-1212 sample (b) estimated J_c versus applied field at various temperatures.

9.4.1 Pb-3324 (Ca=1, Y=1) composition and critical currents

The composition $Pb_3Sr_3(Y_{0.5}Ca_{0.5})_2Cu_4O_z$ with $T_{c,\ zero}$~74K was also checked for J_c with the variation of applied magnetic field and temperatures. The J_c values have been plotted in figure 9.7 and few are tabulated in table

9.5. Just above the $T_{c,zero}$ and after the $T_{c,onset}$, the J_c values are very small but better than the other bulk compositions that have been included in the above text. The variation in J_c values with applied field up to 1 tesla are drastic but onward the J_c is nearly constant with the sweeping field up to 8 for 10K and 30K that shows the strong pinning effect, could be due to inhomogeneous oxygen non-stoichiometry or defects on atomic scale. For 60K fixed temperature, the J_c decays inversely in logarithmic scale around 2 tesla, then dies off nearly 3 tesla after achieving 0.1A/cm^2 value.

Table 9.5. Ccritical current density at various fields and temperature.

Temperature (K)	J_c(zero field) A/cm^2	J_c(0.2tesla) A/cm^2	J_c(0.4tesla) A/cm^2	J_c(0.44tesla) A/cm^2
75	13.5	8.5	2.0	1.0
	H=0	H=0.5Tesla	H=1Tesla	H=1.5Tesla
10	720	300	185	140
30	340	60	35	30
60	75	4.5	1.2	0

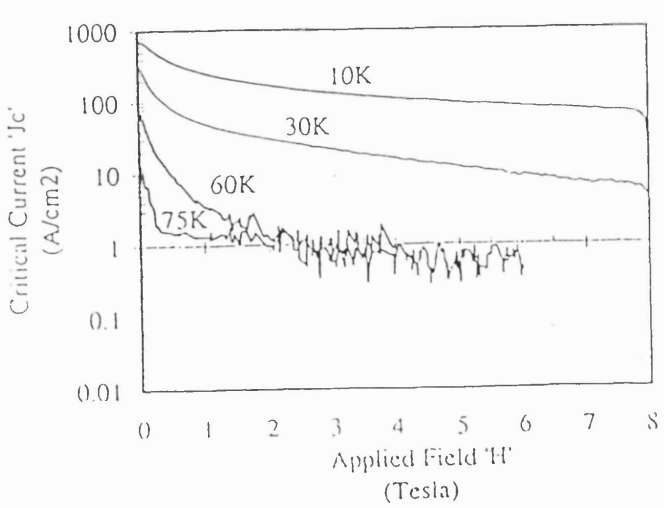

Figure 9.7. The J_c versus applied field of the bulk Pb-3324 composition at various temperatures.

Summary

The critical current density of lead cuprates was determined through irreversible magnetization measurements. The bulk Pb-2213 phase composition shows lower values as compared with thin layers. The maximum obtained values of J_c for bulk and thin layers of Pb-2213 phases synthesised using PLD are 420A/cm^2 and 3.25x10^{6}A/cm^2 respectively in zero applied magnetic field at 15 K. It is also observed that by increasing oxygen content the critical current density decreases. To enhance the current density and orientation it is observed that melt processing and texturing are suitable for other HTSC materials. However, the material was synthesised using partial melt processing, the values of J_c for the bulk Pb-1212 phase is low enough even at 50K in zero field (130A/cm^2). The J_c value for the composition of Pb-3324 phase has also been obtained which are 720 A/cm^2 at 10K and 75A/cm^2 at 60K. The values of critical currents are found better than the values reported by other authors in present literature.

Reference:

[1] C.P.Bean, Rev. Mod. Phys. 36, 31 (1964).

[2] S.R.Hoon, Eur.J.Phys.4, 614 (1983).

[3] J.Mallinson, J.Appl.Phys. 37, 2514 (1966).

[4] C.N.Guy, J.Phys.E, 19, 433 (1976).

[5] C.N.Guy, J.Phys.E, 19, 790(1976).

[6] V.V.Metlushko, G.Guntherodt, V.V.Moshchalkov, Y.Bruynseraede and M.M.Lukina, Phys. Rev. B, 47, 8212 (1993).

[7] Y.Koike, M.Masuzawa, H.Sunagawa, T.Noji, H.Kawabe, N.Kobayashi and Y.Saito, Jpn.J.Appl.Phys., 29, L408 (1990).

Chapter 10

Conclusion and suggestion for further work

In this chapter the general conclusions and key results achieved during the course of research project are highlighted.

10.1 Conclusions

In first few chapters, a brief discussion has been included on the techniques used to synthesise bulk and thin layers of high temperature superconducting materials. Most of the important properties of superconductors depend fundamentally on different processing routes and techniques. To maximize critical current density, Jc, the large grained and textured materials are required. Melt texture processing of bulk, using directional crystallisation of the cuprate material has provided better results. The use of shock-waves as an ultrafast synthesising technique for cuprates without any use of temperature rise above ambient has been successful only for $La_{1.75}Sr_{0.15}CuO_4$ and $Tl_2Ba_2CuO_6$ material. The shock-wave technique may therefore provide a relative cheap and fast means to safely produce single CuO_2 layered ceramics. The lead based materials need a reduced oxygen ambient for the synthesis and could be successful to synthesise using shock-wave technique. The common properties of low temperature superconductors and HTSC cuprates along with an introduction of lead based cuprate superconductor has been described.

In the chapter six, the bulk synthesis of lead based HTSC material using common ceramic method in two steps has been described and the results are included. A modification in synthesising procedure was developed in which the synthesis and annealing in air at high temperatures (>880°C) and later, low temperature (<850°C) annealing in pure nitrogen was performed and better results were achieved. There are various lead based superconducting cuprates. Among all the known phases, the Pb-2213 and Pb-1212 phases are more interesting due to their higher superconducting transition temperatures.

Various annealing conditions for Pb-1212 phase have been investigated by several authors. It includes high pressure oxygen annealing or simple high temperature annealing in gaseous mixture reported by several authors. A short period processing technique has been developed and presented. The results achieved during the course of research by the adjustment of oxygen are better than any other reports present in the recent literature.

Pulsed-laser deposition is one of the techniques that has been welcomed in the present decade to grow multicationic materials due to its easy control over the stoichiometric transfer of target material to substrate. In chapter four, various deposition techniques were described and comparison of PLD technique with advantages and disadvantages were highlighted. The processing during laser target interaction and deposition were briefly described.

Both in-situ and ex-situ thin film's growth of Pb-2213 phase material using PLD has been investigated. In the in-situ, growth parameters such as substrate temperature and oxygen pressure are very important factors to achieve superconducting layers. Lead loss with the deposition temperatures becomes serious around the growth temperature of lead based superconducting thin layer. To overcome this situation, low temperature deposition in oxygen and high temperature annealing in nitrogen ambient has been performed to achieve better superconducting transition temperature. Ex-situ processing was used after low temperature deposition of Pb-2213 phase material on MgO(001) substrates. A set of annealing conditions in nitrogen ambient was developed that has resulted highly c-axis oriented thin layers.

A method measuring energy and mass of various species (ions and neutrals) was described using a combination of energy and mass analysing technique (QMS/CMS). The energy distributions of various species created during the ablation as a result of interaction of laser fluence of $1.5J/cm^2$ value with Pb-2213 material. A broad spectrum from low to high energy singly or doubly charged particles (20 to 160eV) were observed at $1.5J/cm^2$ fluence. The pulses of neutral species of Pb, Sr, Y, Ca, Cu atoms and atomic or molecular oxygen(O_2, O^0) were detected. The intensities of the neutral species depend upon the source voltages

A different approach has been utilized to grow stoichiometric, uniformly thick and large area deposition. The smooth and highly textured film has been grown using Nd:YAG laser (532nm, 4ns, 10Hz, 470mJ) and placing inclined substrate inside mid of the plume after stopping large sized droplets near the target. The films were ex-situ annealed in air and nitrogen shown high texturing but slight deviations in superconducting transition temperature were observed, could be a reason of minute oxygen or any cation stoichiometric deviation over a long distance (3-12cm). The in-situ growth of Pb-2213 phase film can also be tried using different oxidising agents such as N_2O. It is also interesting to monitor growth mechanism in a reducing atmosphere and in-situ XPS can be used to monitor oxidation states of Cu and Pb. The SEM investigations have revealed that very few droplets are present within several mm lengths in the mid plume deposition.

A detailed study can be performed to grow multilayered structure of Bi-Sr-Ca-Cu-O and Pb-Sr-(Y,Ca)-Cu-O materials using MgO(001) and Si-substrates. The optimised growth conditions can be used to fabricate electronic devices and could be compared with the layers grown using some other techniques.

10.2 Further work

The surface uniformity of deposited layers was found to be better for short laser wave length, low oxygen partial pressure (0.01mbar) and high temperatures(>750°C) annealing for short durations (20-35 minutes). A heated system can be designed to deposit superconducting layers on long metallic substrates can be used as a long superconducting tape with thickness uniformity, compositional smooth and minimum droplets that can provide better superconducting properties such as critical current and high magnetic fields.

The critical current density of a few compositions either it is bulk or thin films have been estimated using VSM. It is found that the thin layers exhibit critical currents as high as --A/cm^2 in zero field at 50K, is better than any recent reports. The bulk materials have very low critical current either in zero field or at around 8Tesla. The flux flow and pinning can be studied by combining the techniques of bulk synthesis and PLD. In this project the grown bulk can be crushed, grains of similar size can be separated, and then uniformly coated by any magnetic material using PLD technique. Again after forming

pellet and sintering at low temperature, the flux pinning effects can be studied and a possible better critical currents could be achieved.